SYNTHESIS AND CHARACTERIZATION OF NOVEL QUINOXALINE-BASED AND THIENO[3,4-C]PYRROLE-4,6-DIONE-BASED CONJUGATED POLYMERS AND THEIR APPLICATIONS IN ORGANIC ELECTRONICS

A THESIS SUBMITTED TO
THE GRADUATE SCHOOL OF NATURAL AND APPLIED SCIENCES
OF
MIDDLE EAST TECHNICAL UNIVERSITY

BY

ALİEKBER KARABAĞ

IN PARTIAL FULFILLMENT OF THE REQUIREMENTS
FOR
THE DEGREE OF MASTER OF SCIENCE
IN
POLYMER SCIENCE & TECHNOLOGY

SEPTEMBER 2017

Approval of the thesis:

SYNTHESIS AND CHARACTERIZATION OF NOVEL QUINOXALINE-BASED AND THIENO[3,4-C]PYRROLE-4,6-DIONE-BASED CONJUGATED POLYMERS AND THEIR APPLICATIONS IN ORGANIC ELECTRONICS

submitted by **ALİEKBER KARABAĞ** in partial fulfillment of the requirements for the degree of **Master of Science in Polymer Science & Technology Department, Middle East Technical University** by,

Prof. Dr. Gülbin Dural Ünver _____
Dean, Graduate School of **Natural and Applied Sciences**

Prof. Dr. Necati Özkan _____
Head of Department, **Polymer Science & Technology**

Assist. Prof. Dr. Görkem Günbaş _____
Supervisor, **Department of Chemistry, METU**

Examining Committee Members:

Prof. Dr. Levent Toppare _____
Department of Chemistry, METU

Assist. Prof. Dr. Görkem Günbaş _____
Department of Chemistry, METU

Prof. Dr. Ali Çırpan _____
Department of Chemistry, METU

Assist. Prof. Dr. Salih Özçubukçu _____
Department of Chemistry, METU

Assist. Prof. Dr. Safacan Kölemen _____
Department of Chemistry, Koc University

Date: 08.09.2017

I hereby declare that all information in this document has been obtained and presented in accordance with academic rules and ethical conduct. I also declare that, as required by these rules and conduct, I have fully cited and referenced all material and results that are not original to this work.

Name, Last name: Aliekber KARABAĞ

Signature:

ABSTRACT

SYNTHESIS AND CHARACTERIZATION OF NOVEL QUINOXALINE-BASED AND THIENO[3,4-C]PYRROLE-4,6-DIONE-BASED CONJUGATED POLYMERS AND THEIR APPLICATIONS IN ORGANIC ELECTRONICS

Karabağ, Aliekber

M. Sc., Department of Polymer Science and Technology

Supervisor: Assist. Prof. Dr. Görkem Günbaş

September 2017, 168 pages

In this thesis novel quinoxaline-based and thieno[3,4-c]pyrrole-4,6-dione (TPD)-based monomers were firstly synthesized. Structural analysis of each material synthesized was performed with Nuclear Magnetic Resonance (NMR) Spectroscopy and High-Resolution Mass Spectroscopy (HRMS). Two novel quinoxaline-based monomers were polymerized with electrochemical and/or chemical polymerization whereas TPD-based monomer was polymerized with benzodithiophene-based acceptor via Stille coupling polycondensation reaction. Molecular weight of the polymers was determined by Gel Permeation Chromatography (GPC). The electrochemical behaviors of monomers were studied with Cyclic Voltammetry (CV); on the other hand, the electrochromic properties of polymers were studied with spectroelectrochemical, colorimetric and kinetic studies.

ELEC-PQUIN-12C-TH showed both n-dopable/p-dopable and multi-chromic characteristics. In literature, the polymers having such property is rare; therefore, they are used for special purposes such as display systems and smart windows. On the other

hand, ELEC-PQUIN-2OD-ED and CHEM-PQUIN-2OD-ED showed just p-dopable characteristics. Although such properties were common for almost all conjugated polymers, the polymers showing green color in their neutral state and transmissive grey color in their oxidized state are rare in literature. This kind of polymers having one of the complementary colors (RGB colors) in their neutral states and transmissive grey in their oxidized states are interested in many applications like simple display devices. In addition, both ELEC-PQUIN-2OD-ED and CHEM-PQUIN-2OD-ED displayed greater optical contrasts in the visible region (43% at 728 nm and 45% at 730 nm) compared to the state of the art polymer, PDOPEQ. Furthermore, chemically synthesized quinoxaline-based homopolymer with EDOT side units showed excellent solubility in common organic solvents, especially in CHCl3. To make CHEM-PQUIN-2OD-ED soluble in such solvents, it was designed with a long-branched alkyl chain. Since ELEC-QUIN-12C-TH, ELEC-PQUIN-2OD-ED and CHEM-PQUIN-2OD-ED have promising electrochemical and electrochromic characteristics, they can be easily integrated into today's electrochromic technology even the new generation electrochromic devices.

An acceptor unit containing TPD was designed with selenophene building blocks since polymers that utilizes with selenophene side units result in polymers with low band gap energy (<2.0 eV) and broad absorptions with covering NIR region. There is only one report of selenophene attached TPD unit being used in organic solar cells. A number of possible novel polymers can be synthesized using this material. Therefore, selenophene was integrated into TPD central unit as a side unit. In literature, BTA and BDT are also known as promising materials for preparing organic solar cells with a high efficiency. Therefore, novel random copolymer including TPD, BTA and BDT materials were designed and synthesized via Stille coupling. This polymer was then used as donor whereas PCBM, the common and soluble derivative of fullerene was used as acceptor in preparation of organic solar cells. Thickness and morphological properties of poly(TPD-BTA-BDT):$PC_{71}BM$ were investigated and based on these results suitable solar cell devices (ITO/PEDOT:PSS/poly(TPD-BTA-BDT):$PC_{71}BM$/LiF/Al) were prepared. Current-Voltage (I-V) properties of each cell were also examined. All solar cell studies were done by using solar simulators in a nitrogen-filled glovebox system (moisture <0.1 ppm; oxygen <0.1 ppm). Data

obtained from photovoltaic device was used to calculate Power Conversion Efficiency (PCE) measured under standard AM1.5 G illumination (100mW.cm^{-2}). Without going through the optimization process which has significant effect on PCEs, the material showed 3.0% efficiency. This is a highly promising result and the optimizations are currently underway in our laboratories.

Keywords: electrochromism, quinoxaline, thieno[3,4-c]pyrrole-4,6-dione, conjugated polymers, organic solar cells

ÖZ

ÖZGÜN KİNOKSALİN TABANLI VE TİYENO[3,4-C]PİROL-4,6-DİYON TABANLI KONJUGE POLİMERLERİN SENTEZİ, KARAKTERİZASYONU VE ORGANİK ELEKTRONİKTEKİ UYGULAMALARI

Karabağ, Aliekber
Yüksek Lisans, Polimer Bilim ve Teknolojisi
Tez Yöneticisi: Yrd. Doç. Görkem Günbaş

Eylül 2017, 168 sayfa

Bu tezde ilk olarak özgün kinoksalin tabanlı ve özgün tiyeno[3,4-c]pirol-4,6-diyon (TPD) tabanlı monomerler sentezlenmiştir. Sentezlenen her bir malzemenin yapısal analizi Nükleer Manyetik Rezonans Spektroskopisi (NMR) ve Yüksek Çözünürlüklü Kütle Spektroskopisi (HRMS) yöntemleri ile yapılmıştır. İki yeni kinoksalin tabanlı monomer elektrokimyasal ve/veya kimyasal polimerleşme ile polimerleştirilmişken, TPD tabanlı monomer benzoditiyofen tabanlı akseptör ile Stille kenetlenme reaksiyonu sayesinde polimerleştirilmiştir. Polimerlerin kütlesel ağırlıkları Jel Geçirgenlik Kromatografisi (GPC) ile tayin edilmiştir. Monomerlerin elektrokimyasal davranışları Dönüşümlü Voltametri (CV) ile incelenirken, polimerlerin elektrokromik özellikleri spektroelektrokimyasal, kolorimetrik ve kinetik analizler ile incelenmiştir.

ELEC-PQUIN-12C-TH hem n-tipi/p-tipi katkılanabilen hem de multikromik özellik sergilemiştir. Literatürde bu tip özelliklere sahip polimerler nadirdir; bundan dolayı, bu polimerler görüntü sistemleri ve akıllı camlar gibi özel amaçlar için kullanılırlar.

Öte yandan, ELECT-PQUIN-2OD-ED ve CHEM-PQUIN-2OD-ED polimerlerin yalnızca p-katkılanma özelliği göstermiştir. Bu özellikler neredeyse tüm konjuge polimerler için yaygın olmasına rağmen, nötr halinde yeşil ve oksitlenme halinde geçirgen gri rengi gösteren polimerler literatürde nadirdir. Nötr halinde tamamlayıcı renklerden (RGB rengi) birisine sahip ve oksitlenme halinde geçirgen gri rengine sahip olan bu tip polimerler, basit görüntü cihazları gibi birçok elektrokromik uygulamalarda ilgilenilmektedir. Dahası, görünür bölgede ELECT-PQUIN-2OD-ED ve CHEM-PQUIN-2OD-ED polimerlerin (728 nm'de %43 ve 730 nm'de %45), geçirgen bir oksitlenme halindeyken en gelişmiş polimere (PDOPEQ) göre daha fazla optik kontrast sergilemişlerdir. Ayrıca, çözünür alkoksi grupları ile akıllıca dizayn edilen monomer sayesinde, kimyasal yöntemle sentezlenen yapısında EDOT ünitesini bulunduran kinoksalin içerikli homopolimer yaygın organik çözücüler içerisinde mükemmel bir çözünürlük göstermiştir. CHEM-PQUIN-2OD-ED polimerini bahsi geçen çözücülerde çözünür yapmak için uzun dallanmış alkil zinciri ile dizayn edilmiştir. ELEC-QUIN-12C-TH, ELEC-PQUIN-2OD-ED ve CHEM-PQUIN-2OD-ED polimerlerin ümit veren elektrokimyasal ve elektrokromik sonuçları sayesinde, bu polimerler hem şimdiki hem de yeni nesil elektrokromik teknolojisine kolayca entegre edilebilirler.

Selenofen yan ünitesi ile birlikte kullanılan polimerler düşük enerji bant aralığı (<2.0 eV) ve NIR bölgesini de kapsayan geniş absorpsiyonlar sergilediğinden, TPD içeren bir akseptör ünitesi selenofen yapı taşı ile birlikte dizayn edilmiştir. Organik güneş pillerinde kullanılmış, selenofenin TPD ünitesine bağlı olduğu yalnızca bir makale vardır. Bu malzemeyi kullanarak birçok olası özgün polimerler sentezlenebilir. Bundan dolayı, selenofen ünitesi TPD merkezi ünitesine yan ünite olarak entegre edildi. Aynı zamanda, literatürde BTA ve BDT yüksek verime sahip organik güneş pili hücreleri hazırlamak için de umut vaat eden malzemelerdir. Bu nedenden dolayı, TPD, BTA ve BDT malzemelerini içeren özgün random kopolimerler tasarlanmıştır ve Stille kenetlenme reaksiyonu ile sentezlenmiştir. Organik güneş hücresinde bu polimer donör olarak kullanılmıştır. Aynı zamanda PCBM fullerenin yaygın ve çözünür bir türevi olan PCBM ise akseptör olarak bu organik güneş pilinin hazırlanmasında kullanılmıştır. Kalınlık ve morfolojik özelleri araştırıldıktan sonra, bu çalışmaların sonuçlarına dayanarak uygun güneş hücresi aygıtları

(ITO/PEDOT:PSS/poli(TPD-BTA-BDT):$PC_{71}BM$/LiF/Al) hazırlanmıştır. Ayrıca her bir hücrenin akım-gerilim (I-V) özellikleri incelenmiştir. Tüm güneş pili çalışmaları azot dolu eldivenli bir kabin sistemin içinde güneş simülatörleri kullanılarak yapılmıştır (nem <0.1 nm; oksijen <0.1 ppm). Fotovoltaik cihazdan alınan veri, AM 1.5 G aydınlatma (100 $mW.cm^{-2}$) sayesinde ölçümü yapılan güç çevirim verimini (PCE) hesaplamak için kullanılmıştır. Kullanılan farklı sistemlerin hazırlanan güneş hücrelerin verimine katkı sağladığı bilinmektedir. Bu çalışmada herhangi bir optimizasyon yapılmadan %3 verimin elde edilmesi umut vaat edici bir sonuçtur. Elde edilen bu ilk veri göz önüne alındığında laboratuvarda hazırlanacak, optimizasyonu yapılacak fotovoltaik hücrelerin verimliliğinin bir hayli yüksek olması beklenmektedir.

Anahtar Sözcükler: elektrokromizm, kinoksalin, tiyeno[3,4-c]pirol-4,6-diyon, konjuge polimerler, organik güneş pilleri

ACKNOWLEDGEMENTS

I would like to express my gratitude to my supervisor, Assist. Prof. Dr. Görkem Günbaş for giving me a chance to work with him. After I joined his successful group, dealing with any problem in the shortest time and running any project in the best way become easy. Whenever I had a problem related to any synthesis, he always shared his valuable time to solve this problem together and sometimes it took hours. Due to such a great attitude, I could learn a lot of tricks about my syntheses. Therefore, I could increase my laboratory skills in a very short time. Also, he always found a way to support me during my academic career. This meant a lot for me because I could focus my projects without feeling the pressure of money problem too much. Even my concentration decreased, he always talked with me as a friend and tried to find the best way to keep me harmonious. I could say that if I succeeded on any project, that was because of his excellent guidance and his extraordinary knowledge on syntheses.

I would like to greatest thanks to Prof. Dr. Levent Toppare for joining me in working ECOPIX project, encouraging me by sharing his outstanding experience and trying to support me continuously throughout the entire project. Also, I was too grateful to him because of giving access to his all laboratories and research facilities and letting me to use everything in them freely. I always remembered the days of working with him as one of the best feelings and one of the greatest successes in my whole life.

I would like to thank Prof. Dr. Ali Çırpan for sharing all chemicals and all instruments in his lab before and after ECOPIX project. He always motivated me solving any problem in a very funny way. I could say that he had a very spectacular style.

It is a great pleasure to thank Assist. Prof. Dr. Salih Özçubukçu. Although he was not my official supervisor in the past, he taught me a lot of greatest things that were not only related to chemistry but also associated with the life itself. Due to his great

attitude towards everyone and his knowledge in chemistry, I can easily say that he is more than a teacher.

I would like to special thanks to Assoc. Prof. Dr. Yasemin Arslan Udum, Şerife Özdemir Hacıoğlu and Duygu Keleş for listening to me friendly, sharing their excellent knowledge kindly and helping me for electrochemical, spectroelectrochemical and kinetic studies willingly all the time.

Words are intimately meaningless to express my feelings, pleasure and gratefulness to my first chemistry teacher, Derya Ekincikli who still teaches chemistry at the highest level in Darica Aslan Çimento Technical and Industrial Vocational High School. Her endless guidance increased my interest, knowledge and motivation towards chemistry. I was so lucky to take chemistry courses from her because I could not have imagined having a better high school chemistry teacher during my high school life. Her priceless advices, and worthful encouragements made me today's researcher.

I would like to thank Mustafa Yaşa for being with me all the time, listening to me heartedly, and trying to solve my all issues logically. I could say that he played a very big role in my most of successions.

Special thanks go to my dear assistants, Melek Parlak, Seda Okumuş, Halil İpek and Ali Fatih Şeybek for their kind friendship, giving valuable recommendations, providing intimate encouragement and sharing their valuable chemistry knowledge with me. Whenever I need a hand, they always helped me just at the right time. That's why, I was so grateful to them for their assistance and support.

I would like to express my sincere gratitude to Figen Varlıoğlu, Gizem Atakan, Cansu İğci, Gülce Öklem, Osman Karaman, Dilay Kepil, Begüm Özbakış, Sultan Çetin, Betül Şeker, Merve Erkan, Kia Ghasemi, and Pelin Yuşan for the stimulating discussions, for the sleepless nights we were working together before deadlines, and for all the fun we have had in the last three years. I would always remember each day sharing with them as the most interesting and the funniest day in my life. No matter

how I tried to express my eternal gratitude to each GÜNBAŞ Research Group member, words will fail.

I would like to special thanks to Janset Turan and Sultan Taşkaya for sharing their great experience with me and creating a very effective collaborative work environment throughout the ECOPIX project. I really wanted to say that running any big project while working with them could always turn to an easy project.

I would like to thank Seza Göker for her priceless assistance about theoretical information on syntheses and the related experimental procedures. Even she was far away from me, she could always find a way to help me and make me motivated.

I would like to special thanks to Esra Bağ for helping me too much in preparing solar cells by using the random copolymer synthesized in this thesis and characterizing each cell in the fastest way. Also, I would like to thank Gönül Hızalan, Eda Bolayır and Mert Can Erer for willingly sharing their photovoltaic knowledge with me and being ready for any solar cell study.

I would like to special thanks to all TOPPARE and ÇIRPAN Research Group members for their excellent guidance, caring, patience, and providing me with an excellent atmosphere for doing research. Because of their intimate collaboration and partnership, I could be successful on research projects with great memories.

I would like to thank Majid Akbar, Yusuf Samet Aytekin, Şevki Can Cevher, Ismailov Kadyrbek Aniverovich, Osman Karaman, Mustafa Yaşa, Alim Yolalmaz, Gencay Çelik, Hakan Ünay, Shaukat Ali Changezi, Ali Farid for doing my academic life funny. I could never forget the Friday nights, watermelon parties and ice-cream breaks.

I would like to express my gratitude to Beksultanova Nurzhan Kanatbekovna and her funny and sincere friends for creating an entertaining environment with interesting games and giving me a chance to carry various plastic jerrycans filled with acetone, distilled water, hexane, etc. I will never forget these memories.

I would like to special thanks to Halil Memiş for supplying almost all chemicals and equipment needed for my experiments. Due to his endless chemical source, most of the time I could continue to my experiments without waiting the chemicals from chemical companies. Even I waited the chemicals from chemical companies, I could also have a chance to apply alternative experimental procedures with his chemical support.

I would like to express my sincere gratitude to glassmakers for creating any target glassware in a shortest time. Without their precious support, it would not be possible to finish my researches on the time.

To Şahin Akbaba and Erkan Aktaş for always believing in me and making me feel strong enough to achieve everything. Because of their intimate friendship, my life become always handleable and enjoyable, especially while walking together for hours and giving tea and potato breaks while sitting on any café with sea view.

Last but not the least, I would like to express my deepest gratitude to my parents and to my brother and sisters for providing me with endless support and continuous encouragement throughout my years of study and through the process of researching and writing this thesis. This accomplishment would not have been possible without them. Thank you, my precious family.

TO SCIENCE

TABLE OF CONTENTS

LIST OF FIGURES

FIGURES

LIST OF ABBREVIATIONS

ACN	Acetonitrile
BDT	Benzo[1,2-b:4,5-b′]dithiophene
BHJ	Bulk Heterojunction Cell
BTA	Benzo[d][1,2,3]triazole
$CHCl_3$	Chloroform
CIE	Commission Internationale de l'Eclairage
CV	Cyclic Voltammetry
D-A	Donor-Acceptor
D-A-D	Donor-Acceptor-Donor
DCM	Dichloromethane
DMF	Dimethyl Formamide
DMSO	Dimethyl Sulfoxide
EDOT	3,4-Ethylenedioxythiophene
E_g	Band Gap
E_g^{ec}	Electronic Band Gap
E_g^{op}	Optical Band Gap
EtOH	Ethanol
GPC	Gel Permeation Chromatography
HRMS	High Resolution Mass Spectrometer
HOMO	Highest Occupied Molecular Orbital

ITO	Indium Tin Oxide
I-V	Current Density-Voltage
J_{sc}	Short-Circuit Current Density
L, a, b	Luminance, Hue, Saturation
$LiClO_4$	Lithium Perchlorate
LUMO	Lowest Unoccupied Molecular Orbital
n-BuLi	n-Butyl Lithium
$NaClO_4$	Sodium Perchlorate
NBS	N-Bromosuccinimide
NHE	Normal Hydrogen Electrode
NIR	Near-Infrared
NMR	Nuclear Magnetic Resonance Spectrometer
OSC	Organic Solar Cell
$PC_{71}BM$	[6,6]-Phenyl C_{71} Butyric Acid Methyl Ester
PCE	Power Conversion Efficiency
PSS	Polystyrene Sulfonate
Pt	Platinum
p-TSA	*p*-Toluene Sulfonic Acid
$TBAPF_6$	Tetrabutylammonium Hexafluorophosphate
THF	Tetrahydrofuran
TLC	Thin Layer Chromatography
TPD	Thieno[3,4-c]pyrrole-4,6-dione
VIS	Visible
V_{oc}	Open-Circuit Voltage

CHAPTERS

1. SYNTHESIS AND CHARACTERIZATION OF NOVEL QUINOXALINE-BASED CONJUGATED POLYMERS AND THEIR APPLICATIONS IN ORGANIC ELECTRONICS

1.1. INTRODUCTION

1.1.1. Electrochromism

Electrochromism is defined as the reversible and visible changes in optical characteristics of electroactive materials applied at specific voltage intervals [1]. When the voltage is introduced to such materials, two types of electron transfers can occur. These possible transfers can be achieved either by taking electron (reduction) or by losing electron (oxidation). In each case the generation of different redox states occur, followed by formation of new electronic absorption bands in the spectrum. Because of such changes, the electroactive materials change color(s) while switching [2]. The possible color changes are described as follows:

i. from a color state to a transmissive state;
ii. from a color state to a new colored state;
iii. from a color state to several colored states (multichromic) [2].

These properties of electrochromic materials mentioned above attract outstanding attention in both academia and industry, which resulted in further research and investigation on electrochromic conjugated polymers [3].

There are several materials showing electrochromic characteristics in literature. The most famous examples from main classes of electrochromics are shown as follows:

i. transition metal oxides;
ii. phthalocyanines;
iii. Prussian blue viologens;
iv. conducting polymers [2], [4], [5].

The most well-studied metal oxide films known in history of electrochromism were tungsten trioxide (WO_3) and iridium dioxide (IrO_2) [4]. Over the past years, conducting polymers become more popular since they have advantages over inorganic counterparts. Higher coloration efficiency, better UV stability, higher optical contrast, and faster switching time are several advantages of such polymers [6]. In addition to these benefits, conducting polymers can be easily modified with almost limitless number of both alkyl chains and side units [7]. Combining all these advantages of conducting polymers together, they become very popular for fabrication of various electrochromic devices such as smart windows [8] and e-papers [9].

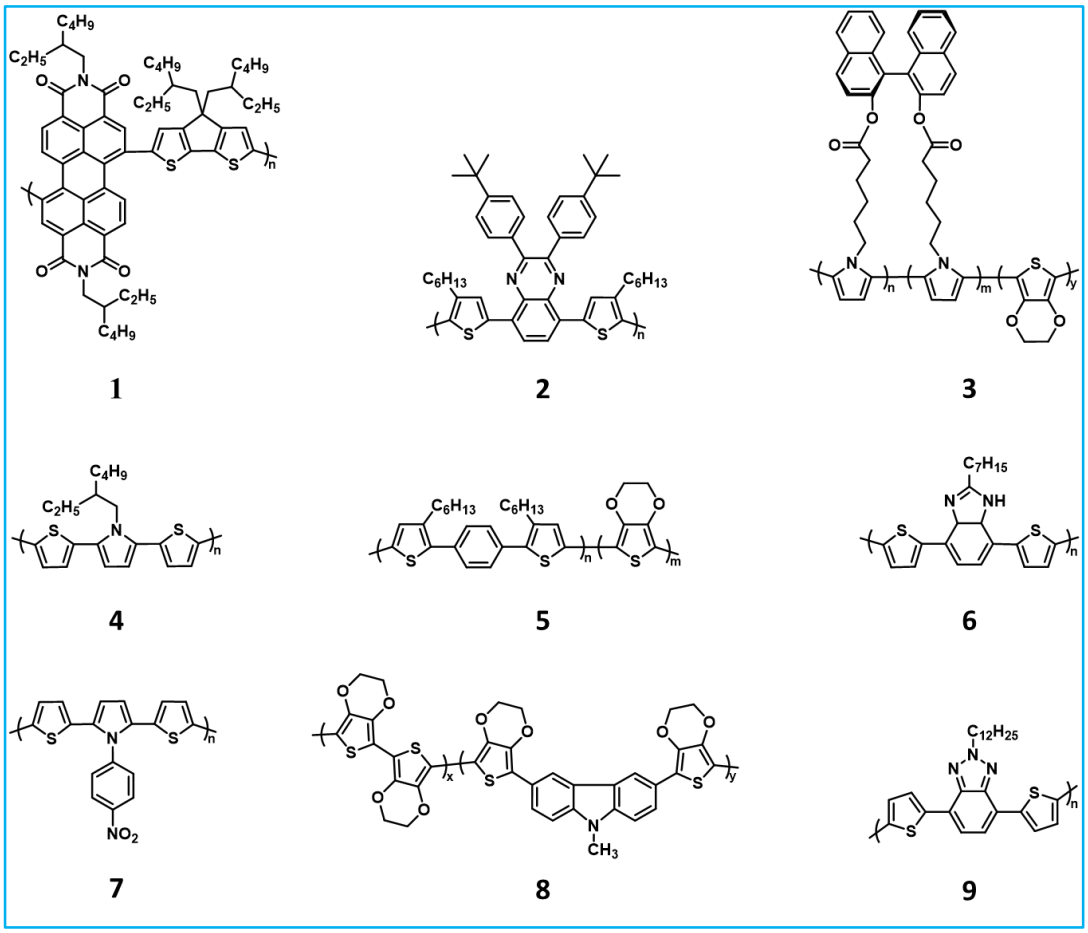

Figure 1.1. Various electrochromic polymers in literature [10]–[17].

1.1.2. Importance of Conducting Polymers

A variety of electroactive monomers, for instance, pyrrole-based [18], quinoxaline-based [19], and thiophene-based [20] are known in literature. After the discovery of conducting polymers, most of them have been polymerized with different polymerization methods such as electrochemical polymerization [21] and chemical polymerization [22] to prove whether they show electrochromic characteristics. The studies showed that a lot of them show promising electrochromic characteristics such as high contrast ratio, long-term stability, fast switching times, and ease of processability [23]. In addition, the studies proved that conducting polymers can be synthesized as either homopolymer or copolymer and modified alkyl chains and side units depending on the application [18]. Because of these great opportunities, many novel monomers have been synthesized and characterized via electrochemical,

spectroelectrochemical, and kinetic studies. An immense number of articles on electrochromic conducting polymers have been published by academia. Electrochromic devices are making their way to the market [8].

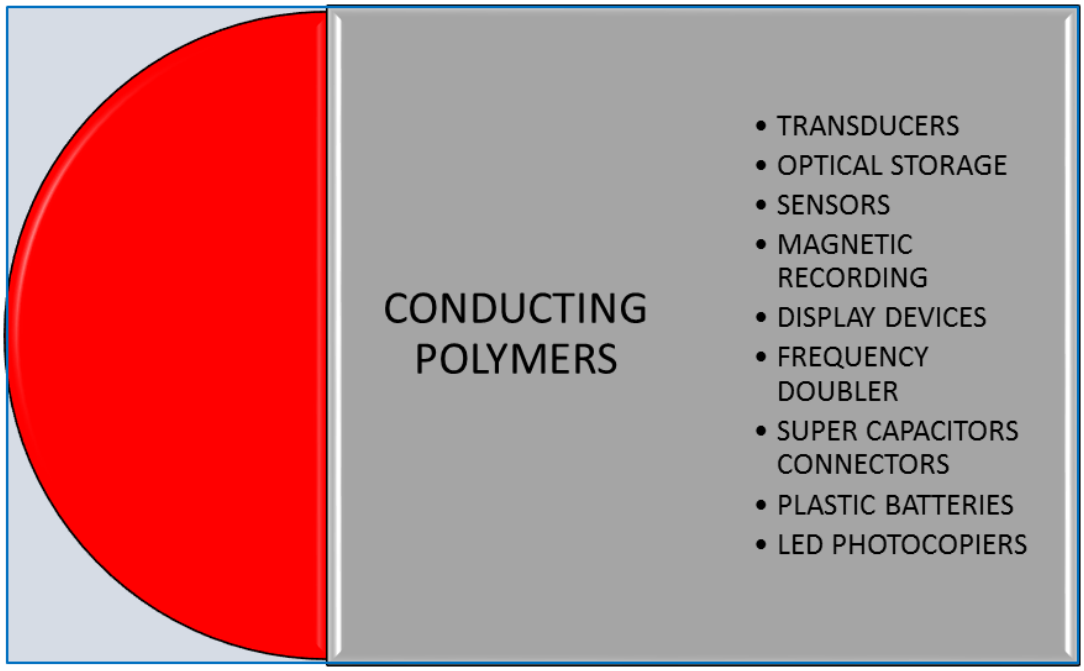

Figure 1.2. Some application areas of conductive polymers [24].

1.1.3. RGB Colors in Conducting Polymers

RGB colors consist of red, green, and blue colors and known as three additive main colors or three complementary colors [25]. The syntheses of conducting polymers having one of three complementary colors in their neutral state have been a crucial problem for the fabrication of colorful and high-quality electrochromic devices. Since only one absorption band centered at visible region was needed to obtain blue and red color, such colored polymers have been discovered firstly [26]. On the other hand, two absorption bands (red and blue) centered at visible region was needed to obtain green color [26]. Thus, the discovery of green colored polymers had taken longer time than the red and blue counterparts. After the missing part in RGB color space was completed by Wudl et al. [27] and later by Toppare et al. [28] in 2008, obtaining any kind of color become possible by applying the color-mixing theory.

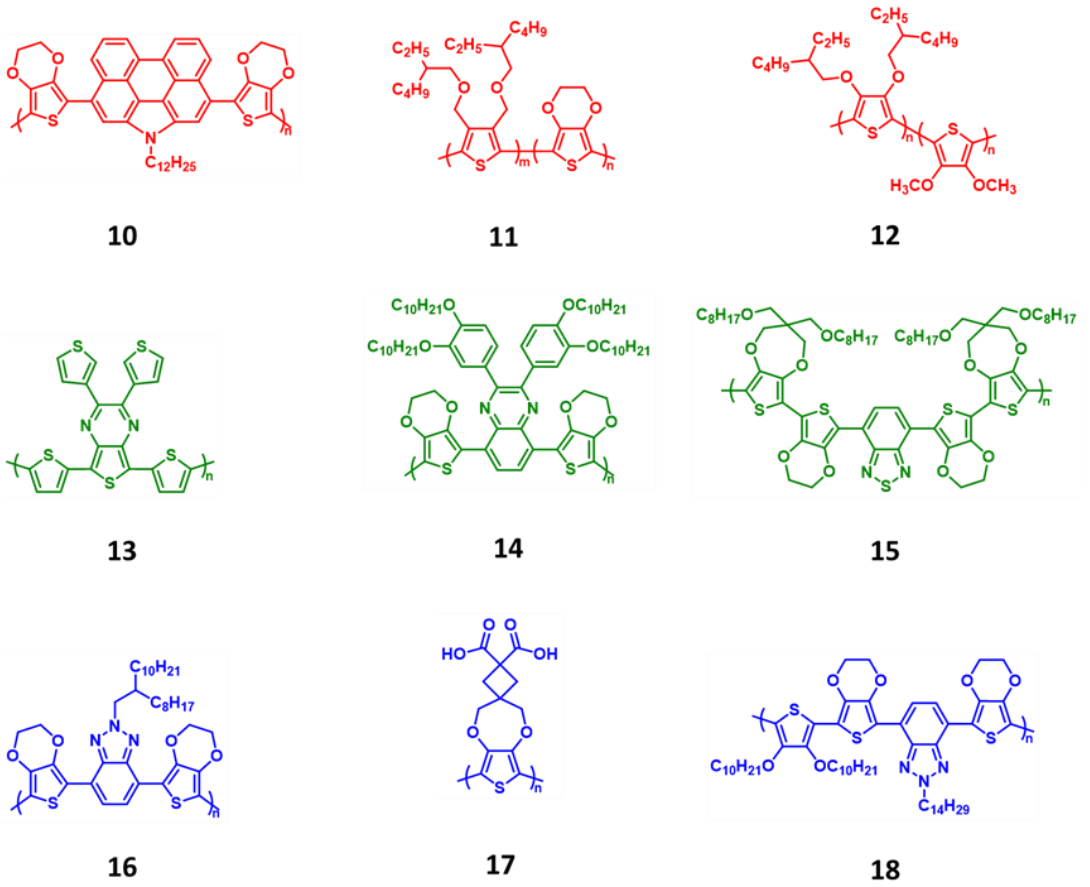

Figure 1.3. Several RGB-based conjugated polymers in literature [27]–[35].

1.1.4. Importance of Green to Transmissive Electrochromic Polymers

In history of electrochromics, both blue to transmissive and red to transmissive conducting polymers were quickly discovered. However, the synthesis of green colored conjugated polymer in its neutral state was still a crucial need for completing the last missing part in RGB color space. In 2004, the first green to transmissive conducting polymer defined as PDDTP was discovered by Sonmez et al. [27]. Even the first green polymer was switching between a green and brown state, it played a key role for attracting researchers' attention on this area. Just four years later, quinoxaline-based homopolymer with linear alkyl chain defined as PDOPEQ was synthesized by Toppare and coworkers [28]. This time green polymer could be switching between a green and transmissive oxidized state. It was noted as the world's first green to transmissive switching polymer.

Polymers in a desired color have been generally obtained by synthesizing of polymers including Donor-Acceptor-Donor (D-A-D) type materials. In addition to the color optimization, D-A-D type acceptors also lower the band gap energy and widen the absorption spectra of the resulting homopolymer and/or copolymer. Therefore, D-A-D type acceptors increase their popularity in organic electronics.

1.1.5. Acceptor Units

Designing acceptor units are very important to not only increase the quality of electrochromic properties but also to enhance the efficiency of photovoltaic devices. Since each application requires polymers with tuned band gap, designing novel acceptor units and their use in design and synthesis of novel materials is a crucially important. There are several factors affecting band gap of conjugated polymers. Some of these factors are shown below:

i. bond length alternation;
ii. donor-acceptor choice;
iii. substituent effect;
iv. resonance effect;
v. planarity effect [36]–[40].

The most powerful method mentioned above is donor-acceptor (D-A) choice since suitable combination of D-A units not only lowers the band gap but also enhances many distinct parameters. For example, the combination of D-A units affects the color and conductivity of resulting polymers. By a proper combination of these units in an electrochromic device design, polymers with high conductivity and desired colors can be achieved [41]. On the other hand, D-A units affects the range of solar energy absorption, hole mobility, planarity and the amount of harvesting solar energy of resulting polymers. By a suitable match of D-A units in a PV device design, broad solar energy absorption, high hole mobility, high planarity and significant amounts of harvesting sun light can be obtained. Moreover, by structural modifications of D-A units, the soluble and processable polymers can be synthesized.

1.1.5.1. Quinoxaline-Based Central Units

Quinoxaline-based conjugated polymers have been studied for many years since the importance of conducting polymers were revealed. Quinoxaline is known as strong electron-accepting unit. Because quinoxaline central unit has two symmetric sp^2 hybridized nitrogen atoms in its structure, it shows high electron affinity [42]. Any poly(quinoxaline) derivative also provides strong electron transporting due to ease of switching to its quinoid form [43].

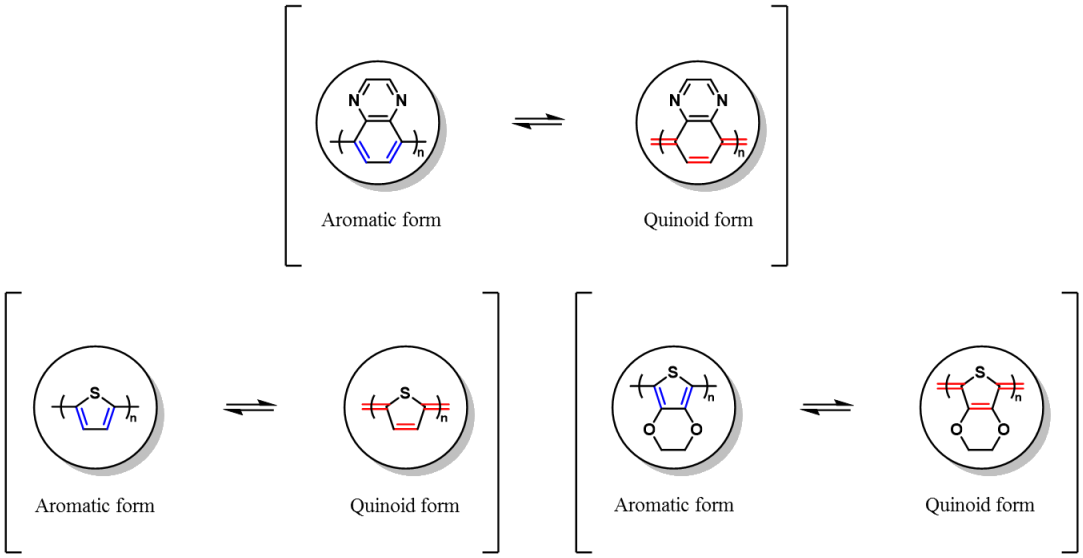

Figure 1.4. Aromatic and quinoid forms of poly(quinoxaline), poly(thiophene), and poly(EDOT) [43].

There are also other benefits of quinoxaline central unit. One of the most impressive benefits of such unit is that it can effectively tune the energy level, followed by lowering the band gap of the resulting poly(quinoxaline) derivatives [42]. Additionally, quinoxaline central unit enables to make a lot of modifications on its structure [23]. For example, thiophene and EDOT derivatives have been connected to the quinoxaline central unit and electrochemical, optical, and photovoltaic characteristics of resulting poly(quinoxaline) derivatives have been studied. According to the results it was confirmed that quinoxaline-based polymers with either thiophene or EDOT side units provide broad absorptions and display great charge-transfer properties, fast switching times, and high air stabilities for electrochromic device [44]-[45]. Besides, soluble and processable polymers are very important to

fabricate electrochromic devices in industrial level. Combining these significant advantages together, designing and synthesizing poly(quinoxaline) derivatives become one of the best solutions for fabrication of high-quality electrochromic devices.

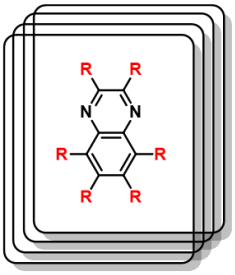

Figure 1.5. Quinoxaline central unit.

1.1.6. ECOPIX Project

To attract audiences' attention, advertising agencies have tried to find the best, easiest, cheapest, and the most effective ways and used many significant media tools for these purposes. For instance, such agencies have benefited from the power of billboards, internet, print medias, televisions, and radios for many years. Nowadays, outdoor advertising, known as "out-of-home" advertising (OOH) affects audiences much more than the other forms of media such as print media, radio, and television. One of the sub-branch of OHH is known as digital OHH (DOOH). In developing advertising market, such displays have played a key role to determine customers' habits. Digital billboards integrated with either LCD or LED technology are therefore installed everywhere. Since they provide easier and faster updating of advertisements by a remote computer control, many advertising agencies prefer to announce their products and messages by using such billboards rather than the traditional billboards. However, besides several advantages of DOOH displays, they also create many problems. For example, a great number of electrical power and a lot of money are needed to operate such digital displays. Furthermore, DOOH pollutes the environment with the significant amount of electronic wastes. When such drawbacks are considered, some serious projects are needed to take a big step forward of DOOH technology. For this purpose, ECOPIX project has been organized by joining 8 European pioneering

academic and industrial organizations from 4 various countries and funded by the European Union, in the 7th Framework Programme between the years of 2014-2017.

ECOPIX project is mainly based on the development of environmentally-friendly new generation of reflective color displays by using innovative printable polymers showing electrochromic characteristics. The aim of this project is to create a new technology with sustainable, flexible power-saved, light-weight, and color-controlled DOOH displays. The role of METU in this project is to synthesize soluble and processable red to transparent, green to transparent and blue to transparent electrochromic polymers in very high quantity and characterized each of them by building pilot devices.

1.1.7. Polymerization Methods

A lot of techniques have been developed after the importance of conducting polymers was clear. The main techniques are described as follows:

- electrochemical polymerization;
- photochemical polymerization;
- metathesis polymerization;
- solid-state polymerization;
- chemical polymerization;
- inclusion polymerization;
- plasma polymerization [24].

When all methods mentioned above are compared with each other, electrochemical and chemical polymerization methods become the most preferable methods in both academia and industry. For instance, polymerization of conjugated monomers and characterization of resulting polymers can be achieved rapidly by electrochemical polymerization method [21] On the other hand, there is no need for an electrochemical setup for chemical polymerization; thus, polymers both in high quantity and in high molecular weight can be synthesized easily by applying such method [46].

1.1.7.1. Importance of Electrochemical Polymerization Method

Electrochemical polymerization is performed by CV and mainly defined as the self-coupling reaction of an aromatic compound like thiophene under an inert atmosphere [21]. Three-electrode system, supporting electrolyte(s) and solvent(s) are needed in such polymerization. These electrodes are mainly ITO-coated glass slide as working electrode, Pt wire as counter electrode, and Ag wire as reference electrode [47].

The solubility of both conjugated monomers and supporting electrolyte(s) determine the choice of solvent(s) [47]. In other words, the monomer and supporting electrolyte(s) should be dissolved in solvent or solvent couples completely. In literature, $TBAPF_6$, $LiClO_4$, and $NaClO_4$ are some of the most popular supporting electrolytes used in CV. On the other hand, ACN and PC are known as the most common solvents due to having high relative permittivity and large potential range.

Electrochemical polymerization method is one of the best choices for production and characterization of electrochromic materials since this kind of method provides many advantages [48]. For instance, either homopolymer or copolymer films can be obtained and the thickness of resulting polymer films can be controlled by using such method. Furthermore, conjugated monomers can be polymerized on electrode very rapidly and generally it takes a few seconds. The fast electrochemical and optical characterizations of the polymer films are also possible. Moreover, there is no need to make further purification in such polymerization method.

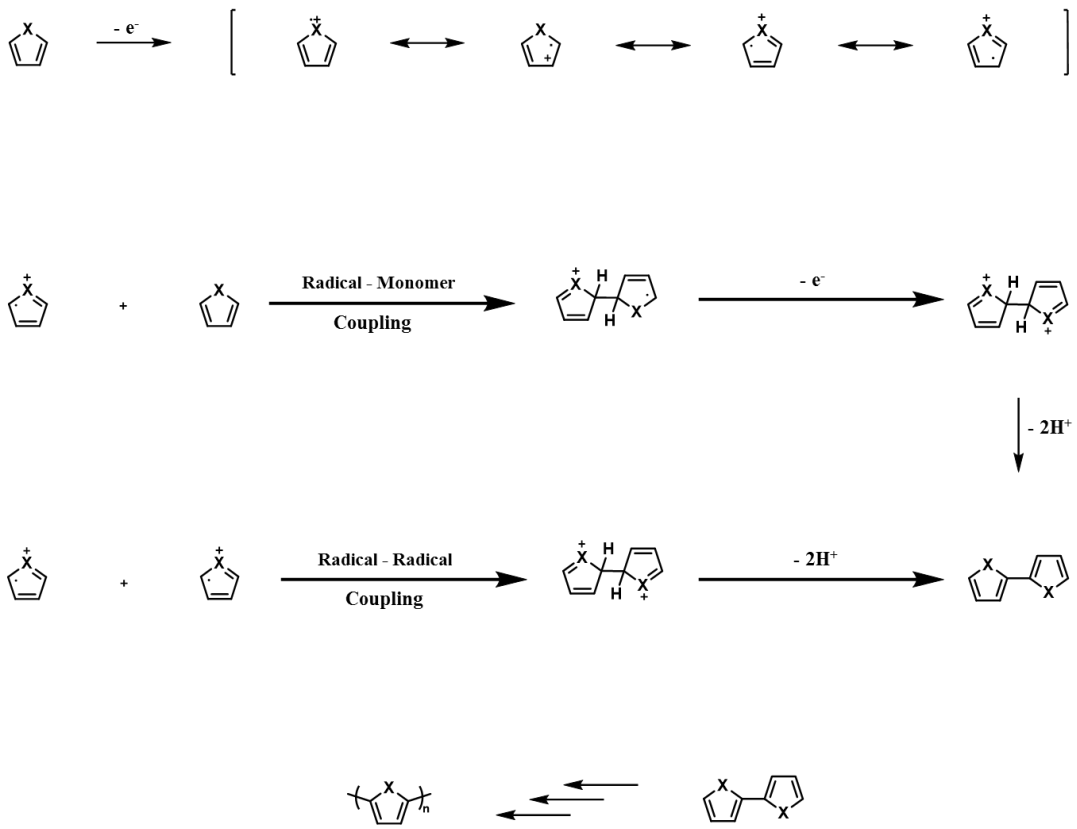

Figure 1.6. General mechanism of electrochemical polymerization where X = N-H, O, S, and Se [21].

1.1.7.2. Importance of Oxidative Chemical Polymerization

Oxidative chemical polymerization is known as the coupling reaction of an aromatic compound like EDOT with a Lewis acid catalyst under an inert atmosphere [49]. $FeCl_3$. $MoCl_5$, $Fe(OTs)_3$, and $RuCl_3$ are some of the catalysts used in this method; however, the most commonly used catalyst is $FeCl_3$. In addition, this kind of polymerization can be easily achieved in common organic solvents such as $CHCl_3$, EtOAc, and dioxane.

There are many benefits of oxidative chemical polymerization [50]. One of the beauties of such polymerization is that conjugated monomers can be polymerized easily and the corresponding polymer can be obtained both in high quantity and in high molecular weight. Additionally, solution processable polymers can be obtained with applying such polymerization method. This means that the polymers can be

coated no matter how much the size of ITO-coated glass. Based on these reasons, oxidative chemical polymerization method become one of the most promising methods to satisfy the needs for industrial processes.

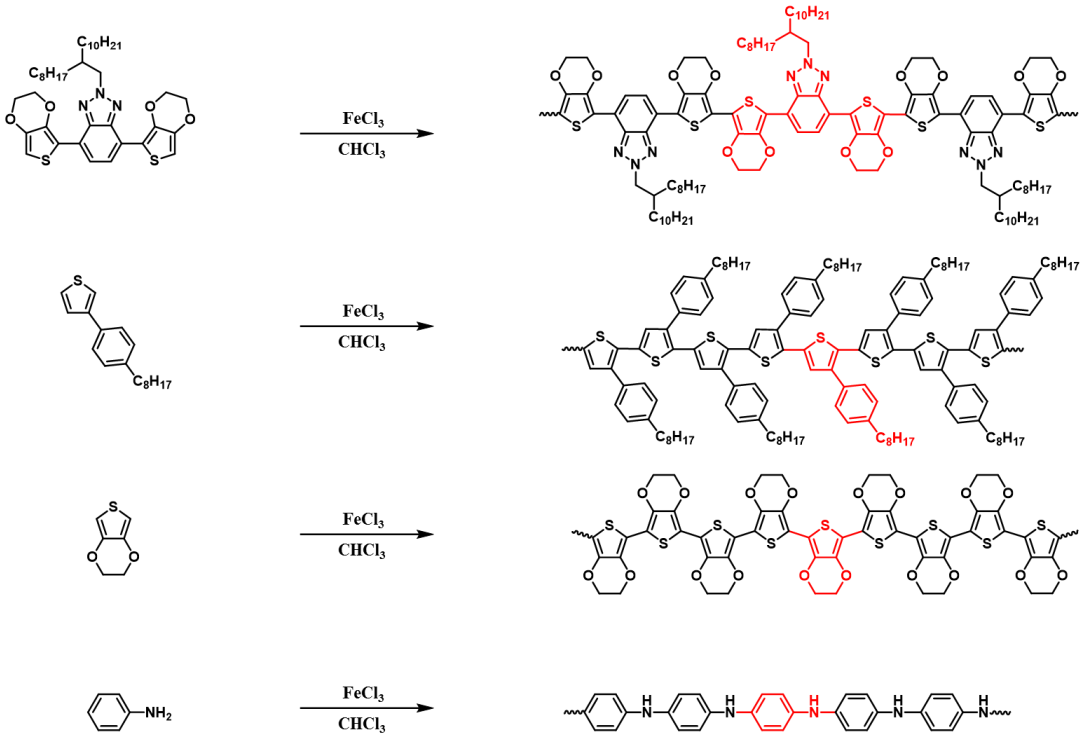

Figure 1.7. Various examples of oxidative chemical polymerization in literature [22], [33], [51], [52].

1.1.8. Characterization of Conducting Polymers

There are various methods to characterize the conducting polymers synthesized via electrochemical and/or chemical methods. For example, CV is a significant characterization method to get information about reduction and oxidation behaviors, color changes, the HOMO/LUMO energy levels and E_g^{ec} of polymers. Furthermore, conducting polymers are characterized by spectroelectrochemical studies to learn E_g^{op}, λ_{max}, polaron and bipolaron states upon oxidation of electrochromic materials by applying stepwise potentials. In addition, kinetic studies are used to characterize the optical contrast(s) (% transmittance(s)) and the switching time(s) of conducting polymers by applying potentials switching between neutral and oxidized states.

Moreover, NMR spectroscopy is mainly used for proving the structures of the polymers and also gain idea about the degree of polymerization. On the other hand, GPC is used for determination of molecular weight and the PDI of the polymers.

1.1.9. Aim of This Work

The aim of this work was to synthesize two novel Donor-Acceptor-Donor (D-A-D) type monomers (QUIN-12C-TH and QUIN-2OD-ED) with Stille coupling and polymerized them with chemical polymerization and/or electrochemical polymerization. Each monomer included quinoxaline core unit but they differed from each other with donor side units and alkoxy groups in their structure.

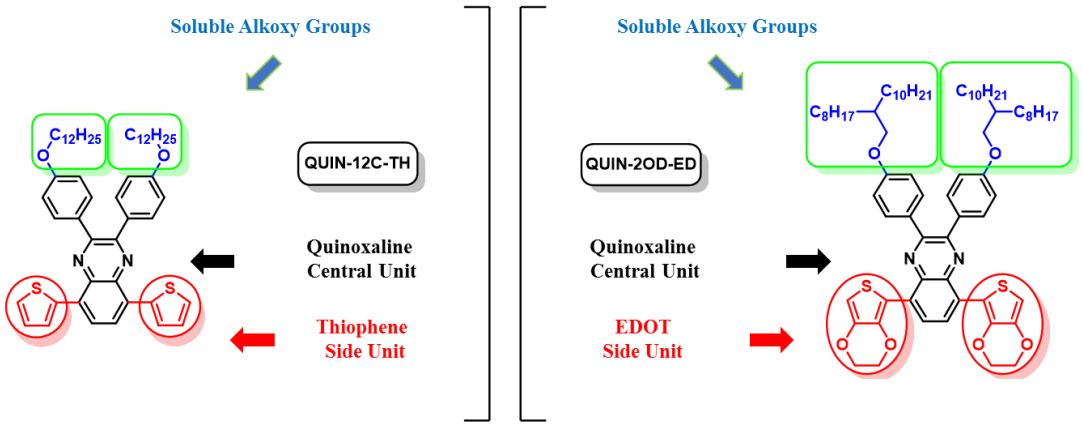

Figure 1.8. Quinoxaline-based monomers designed for electrochromic devices.

Since it was proved that quinoxaline-based polymers with thiophene side units show great charge-transfer properties, broad absorptions, fast switching times, and enhanced air stability for electrochromic devices, the first monomer (QUIN-12C-TH) was designed with thiophene building blocks in the main chain. Moreover, alkoxy groups with linear alkyl chains was linked to the quinoxaline side units to make resulting polymer (PQUIN-12C-TH) soluble and processable. QUIN-12C-TH was then electrochemically polymerized and the electrochromic characteristics of homopolymer films of PQUIN-12C-TH were investigated in detail. On the other hand, the second monomer was designed for ECOPIX project as an alternative green to transparent polymer to the first green to transparent polymer (PDOPEQ) previously

synthesized by Toppare and coworkers in 2008. Here the main aim was to synthesize a polymer with highly saturated green color in the neutral state. The electrochromic characteristics of PDOPEQ was not quite suitable for the ambitious aim of the ECOPIX project. During our studies on blue to transmissive polymers, we discovered that changing a linear alkyl chain on polymer backbone to a branched one not only improved the solubility but also resulted in better electrochromic properties [33]. Hence, in the context of the ECOPIX project we decided to change the linear alkyl chain of the original PDOPEQ with branched ones to be able to find out if similar enhancements will be observed. Since PDOPEQ was synthesized with EDOT side units, second quinoxaline-based monomer (QUIN-2OD-ED) was also designed with such side units to increase the probability of getting green to transparent polymer. However, this time the branched alkyl chains rather than linear ones were connected to the quinoxaline side units to make the corresponding polymer (PQUIN-2OD-ED) soluble and processable. Then, QUIN-2OD-ED was electrochemically and chemically polymerized and compared the electrochemical results with each other and PDOPEQ as well.

1.2. EXPERIMENTAL

1.2.1. Materials & Methods

All commercially available reagents were purchased from Sigma-Aldrich, Across, Tokyo Chemical Industry Co., Ltd. (TCI), and Merck. All reactions were performed under Ar unless otherwise noted. All anhydrous solvents such as THF, DMF, and toluene were either distilled over Na/benzophenone or supplied from a solvent purification system. The electrochemical properties of each monomer were investigated by using a Voltalab 50 potentiostat in a three-electrode system including Indium Tin Oxide (ITO) coated glass slide as the working electrode, platinum wire as the counter electrode, and Ag wire as the pseudo reference electrode calibrated against Fc/Fc^{+}. All cyclic voltammetry measurements of polymers were made by using GAMRY Reference 600 potentiostat and such measurements were performed under argon atmosphere at room temperature. The spectroelectrochemical properties of each polymer were analyzed by using Varian Cary 5000 UV-Vis spectrophotometer. HOMO and LUMO energy values were determined by taking NHE value as -4.75 eV in the formula of $HOMO = -(4.75 + 0.3 + E_{onset}^{ox})$ and $LUMO = -(4.75 + 0.3 + E_{onset}^{red})$. ^{1}H and ^{13}C NMR spectra of each product were identified by using Bruker Spectrospin Avance DPX-400 Spectrometer with using either $CDCl_3$ or DMSO as solvent. To make such analysis chemical shifts (δ / ppm) were reported relative to TMS as an internal reference. The accurate mass measurements for each novel product were made by HRMS by using Waters Synapt MS System. Silica Gel Column Chromatography with silica gel (Acros, 35–70 μm) filled in a suitable glass column was used to purify most of the products. TLC on glass plates coated with EMD silica gel 50 F254 was used to determine the best solvent system to make Silica Gel Column Chromatography and to confirm the identity of each product by either looking under ultraviolet light or staining $KMnO_4$ stain by exposing mild heating.

1.2.2. Synthesis of Two Novel Quinoxaline-Based Monomers

1.2.2.1. Synthetic Route for QUIN-12C-TH

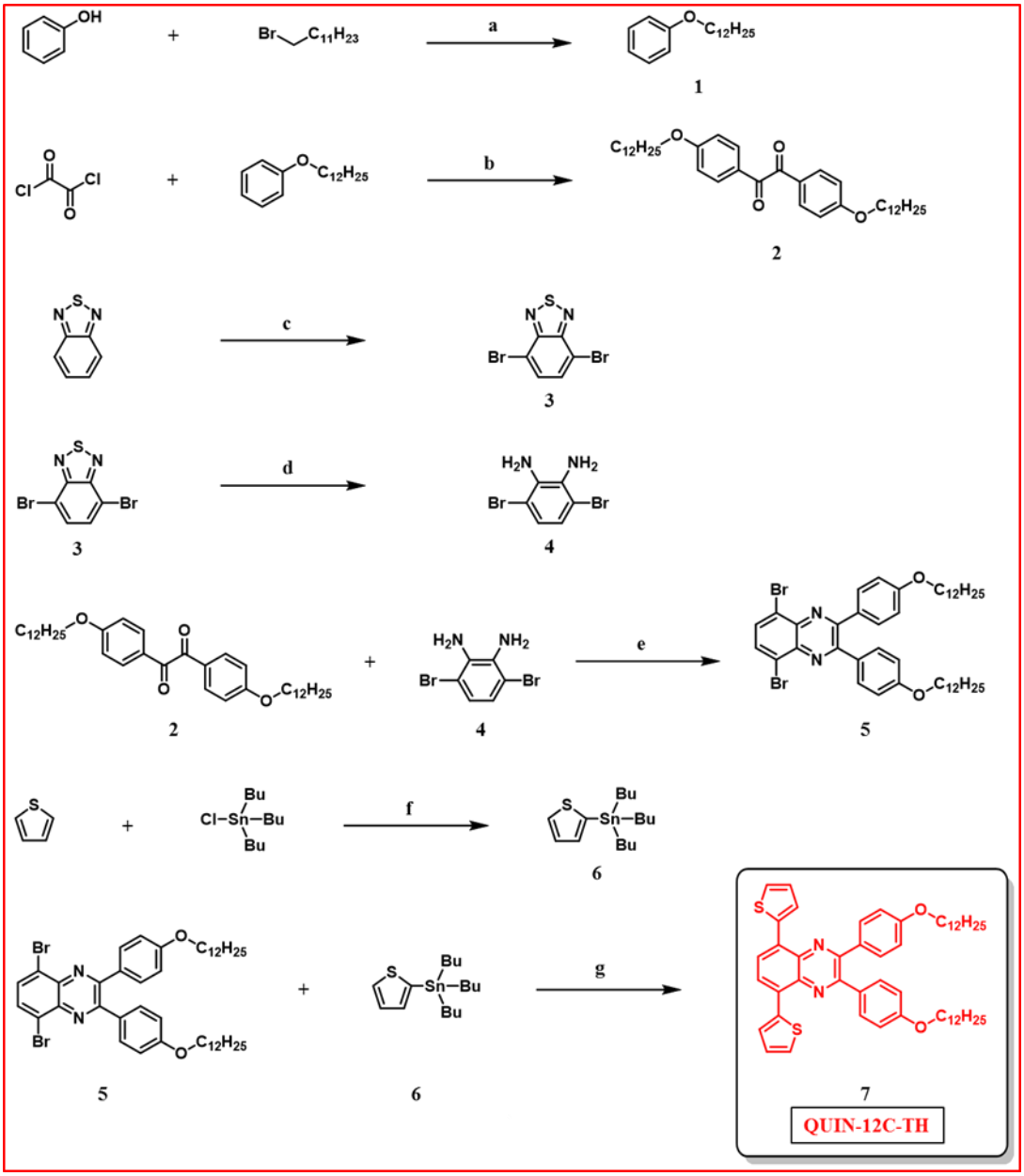

Figure 1.9. Reagents and conditions: ***a.*** K_2CO_3, DMF, 80 °C, 91%; ***b***. urea, $AlCl_3$, DCM, 0 °C → rt, 85%; ***c.*** HBr, Br_2, 130 °C, 90%; ***d.*** EtOH, $NaBH_4$, 0 °C → rt, 89%; ***e.*** EtOH, *p*-TSA, 85 °C, 73%; ***f.*** THF, n-BuLi, -78 °C → rt, 97%; ***g.*** PhMe, $Pd(PPh_3)_4$, 115 °C, 84%.

1.2.2.2. Synthetic Route for QUIN-2OD-ED

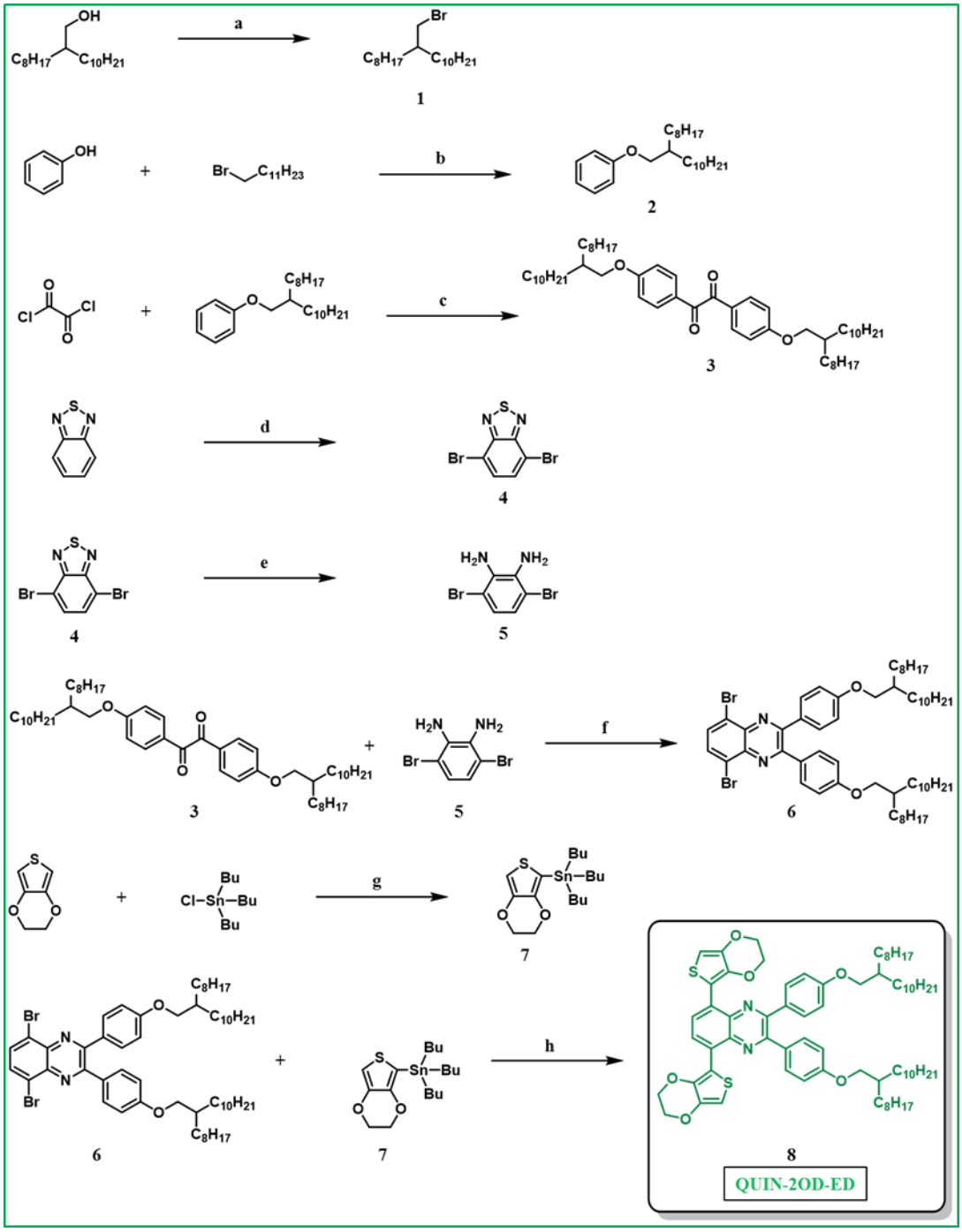

Figure 1.10. Reagents and conditions: ***a.*** DCM, PPh_3, NBS, 0 °C → rt, 82%; ***b.*** K_2CO_3, DMF, 80 °C, 85%; ***c***. urea, $AlCl_3$, DCM, 0 °C → rt, 56%; ***d.*** HBr, Br_2, 130 °C, 90%; ***e.*** EtOH, $NaBH_4$, 0 °C → rt, 89%; ***f.*** EtOH, *p*-TSA, 85 °C, 82%; ***g.*** THF, n-BuLi, -78 °C → rt, 99%; ***h.*** PhMe, $Pd_2(dba)_3$, $P(o\text{-}tol)_3$, 115 °C, 90%.

1.2.3. Experimental Procedures for Synthesis of QUIN-12C-TH

1.2.3.1. (Dodecyloxy)benzene

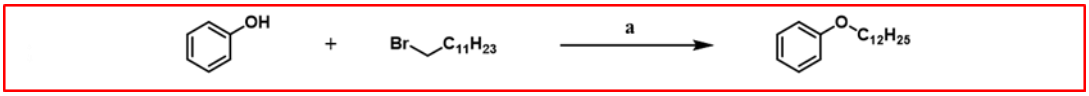

Figure 1.11. Reagents and conditions: ***a.*** K_2CO_3, DMF, 80 °C, 91%.

(Dodecyloxy)benzene was prepared according to the literature [53]. Under an argon atmosphere phenol (3.8 g, 40 mmol) and K_2CO_3 (6.6 g, 49 mmol) were added into the reaction flask and dissolved in anhydrous DMF (25 mL). 1-bromododecane (10 g, 40 mmol) was added to the solution dropwise at 80 °C. The reaction mixture was stirred at this temperature overnight and then cooled to the room temperature. H_2O was introduced to the reaction flask and aqueous layer was extracted with DCM several times. The combined organic layers were dried over anhydrous Na_2SO_4. After filtration, the solvent was removed under reduced pressure. The resulting light brown oil was then purified by column chromatography (SiO_2, Hexane).The target product was obtained as a colorless oil (9.5 g, 91%): ^{1}H NMR (400 MHz, $CDCl_3$): δ 7.33 – 7.27 (m, 2H), 6.98 – 6.90 (m, 3H), 3.97 (t, *J* = 6.6 Hz, 2H), 1.81 (quin, *J* = 6.2 Hz, 2H), 1.48 (quin, *J* = 6.4 Hz, 2H), 1.38 – 1.27 (m, 16H), 0.92 (t, *J* = 6.7 Hz, 3H); ^{13}C NMR (101 MHz, $CDCl_3$): δ 159.24, 129.42, 120.47, 114.54, 67.89, 32.05, 29.80, 29.77, 29.73, 29.54, 29.48, 29.43, 26.19, 22.81, 14.20.

1.2.3.2. 1,2-Bis(4-(dodecyloxy)phenyl)ethane-1,2-dione

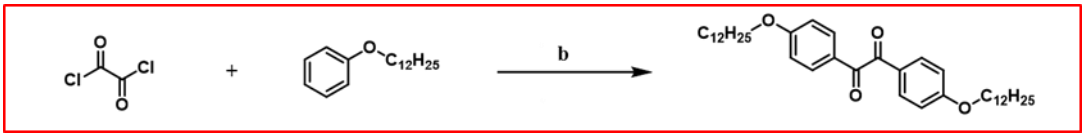

Figure 1.12. Reagents and conditions: ***b.*** urea, $AlCl_3$, DCM, 0 °C → rt, 85%.

1,2-Bis(4-(dodecyloxy)phenyl)ethane-1,2-dione was prepared according to the literature [54]. Under an argon atmosphere (dodecyloxy)benzene (5.9 g, 22 mmol), urea (1.4 g, 23 mmol) and $AlCl_3$ (4.5 g, 34 mmol) were added into the reaction flask.

The reaction temperature was decreased to 0 °C with an ice/H_2O bath. At this temperature DCM was added until the mixture was completely dissolved. Oxalyl chloride (1.3 g, 10 mmol) was added dropwise over 30 min at 0 °C. Then, the reaction mixture was warmed to room temperature and stirred overnight. Resulting brown mixture was poured into cold H_2O and aqueous phase was then extracted with DCM several times. The combined organic layers were washed with aqueous 15% $NaHCO_3$ solution and dried over anhydrous Na_2SO_4. After filtration, the solvent was removed under reduced pressure. The resulting reddish-brown oil was then purified by column chromatography (SiO_2, Hexane 20:1 EtOAc). The target product was obtained as a yellow oil (5.1 g, 85%): ^{1}H NMR (400 MHz, $CDCl_3$): δ 7.95 – 7.90 (m, 4H), 6.96 – 6.92 (m, 4H), 4.02 (t, *J* = 6.5 Hz, 4H), 1.79 (quin, *J* = 6.7 Hz, 4H), 1.45 (quin, *J* = 8.1 Hz, 4H), 1.31 – 1.24 (m, 32H), 0.88 (t, *J* = 6.7 Hz, 6H); ^{13}C NMR (100 MHz, $CDCl_3$): δ 193.54, 164.48, 132.34, 126.10, 114.70, 68.47, 31.92, 29.65, 29.63, 29.58, 29.54, 29.34, 29.32, 29.01, 25.94, 22.69, 14.12.

1.2.3.3. 4,7-Dibromobenzo[c][1,2,5]thiadiazole

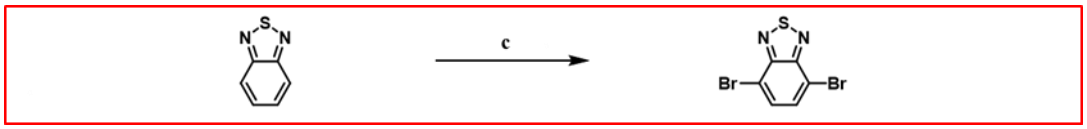

Figure 1.13. Reagents and conditions: ***c.*** HBr, Br_2, 130 °C, 90%.

4,7-Dibromobenzothiadiazole was prepared according to the literature [55]. Under an argon atmosphere benzothiadiazole (4.0 g, 29 mmol) was added into the reaction flask and dissolved in HBr (72 mL, 48% in water). The solution of Br_2 (3.2 mL) and HBr (32 mL, 48% in water) was added dropwise to the mixture. The mixture was stirred at reflux temperature for 6 h and then cooled to the room temperature. Precipitate formed in the reaction flask was filtered by suction filtration and washed with saturated solution of $NaHSO_3$ to remove excess bromine. The resulting solid was dissolved in DCM. Organic phase was washed with saturated solution of $NaHSO_3$ and H_2O several times. The combined organic layers were then dried over anhydrous Na_2SO_4. After filtration, the solvent was removed under reduced pressure. The target product was

obtained purely as a yellow solid (7.8 g, 90%): ^{1}H NMR (400 MHz, $CDCl_3$): δ 7.71 (s, 2H); ^{13}C NMR (100 MHz, $CDCl_3$): δ 152.95, 132.35, 113.91.

1.2.3.4. 3,6-Dibromobenzene-1,2-diamine

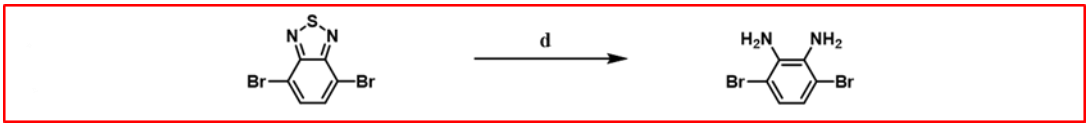

Figure 1.14. Reagents and conditions: ***d.*** EtOH, $NaBH_4$, 0 °C → rt, 89%.

3,6-Dibromobenzene-1,2-diamine was prepared according to the literature [56]. Under an argon atmosphere 4,7-dibromobenzothiadiazole (5.10 g, 17.4 mmol) was added into the reaction flask and dissolved in EtOH (170 mL). The reaction temperature was then decreased to 0 °C with an ice/H_2O bath. At this temperature $NaBH_4$ (12.2 g, 322 mmol) was added portionwise over 30 min and the mixture was stirred at room temperature overnight. Then, EtOH was removed under reduced pressure. The crude product was washed with brine followed by extraction with diethyl ether. The combined organic layers were dried over anhydrous Na_2SO_4. After filtration, the solvent was removed under reduced pressure. The resulting yellow solid was purified by column chromatography (SiO_2, Hexane 5:1 EtOAc). The target product was obtained as a pale-yellow solid (4.1 g, 89%): ^{1}H NMR (400 MHz, $CDCl_3$): δ 6.84 (s, 2H), 3.89 (s, 4H); ^{13}C NMR (100 MHz, $CDCl_3$): δ 133.74, 123.27, 109.70.

1.2.3.5. 5,8-Dibromo-2,3-bis(4-(dodecyloxy)phenyl)quinoxaline

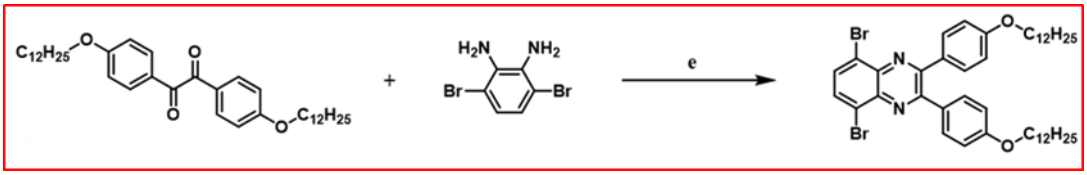

Figure 1.15. Reagents and conditions: ***e.*** EtOH, *p*-TSA, 85 °C, 73%.

5,8-Dibromo-2,3-bis(4-(dodecyloxy)phenyl)quinoxaline was prepared according to the literature [56]. Under an argon atmosphere 1,2-bis(4-(dodecyloxy)phenyl)ethane-1,2-dione (2.17 g, 3.75 mmol), 3,6-dibromobenzene-1,2-diamine (1.00 g, 3.75 mmol) and catalytic p-TSA (32 mg, 0.19 mmol) were dissolved in EtOH (50 mL). The reaction mixture was stirred at reflux temperature overnight and then cooled to the room temperature. H_2O was added to the resulting yellow mixture. This aqueous phase was extracted with DCM several times. The combined organic layers were washed with brine and dried over anhydrous Na_2SO_4. After filtration, the solvent was removed under reduced pressure. The resulting greenish yellow solid was then purified by column chromatography (SiO_2, Hexane 50:1 EtOAc). The target product was obtained as a yellow solid (2.2 g, 73%): ^{1}H NMR (400 MHz, $CDCl_3$): δ 7.82 (d, *J* = 3.0 Hz, 2H), 7.66 (d, *J* = 8.4 Hz, 4H), 6.88 (d, *J* = 8.5 Hz, 4H), 3.99 (t, *J* = 6.6 Hz, 4H), 1.81 (q, *J* = 7.1 Hz, 4H), 1.48 – 1.23 (m, 36H), 0.90 (t, *J* = 6.4 Hz, 6H); ^{13}C NMR (100 MHz, $CDCl_3$): δ 160.48, 153.55, 139.01, 132.47, 131.69, 130.35, 123.46, 114.36, 68.11, 31.96, 29.71, 29.69, 29.65, 29.62, 29.45, 29.40, 29.25, 26.08, 22.73, 14.17.

1.2.3.6. Tributyl(thiophen-2-yl)stannane

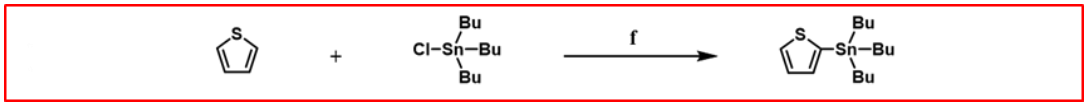

Figure 1.16. Reagents and conditions: ***f.*** THF, n-BuLi, -78 °C → rt, 97%.

Tributyl(thiophen-2-yl)stannane was prepared according to the literature [57]. Under an argon atmosphere thiophene (1.0 g, 12 mmol) was added into the reaction flask and dissolved in anhydrous THF (25 mL). Then, the reaction mixture was cooled to -78 °C and n-BuLi (5.1 mL, 13 mmol; 2.5 M in hexane) was added dropwise over 30 min. The reaction mixture was stirred at -78 °C for 1.5 h. Tributyltin chloride (4.2 g, 13 mmol) was then added dropwise at -78 °C. The reaction mixture was warmed to the room temperature and stirred at this temperature overnight. H_2O was added into the reaction mixture. This aqueous phase was extracted with Et_2O three times. The combined organic layers were washed with brine and dried over anhydrous Na_2SO_4. After filtration, the solvent was removed under reduced pressure. The target product

was obtained as a yellow oil (4.3 g, 97%) and used without making any further purification.

1.2.3.7. 2,3-Bis(4-(dodecyloxy)phenyl)-5,8-di(thiophen-2-yl)quinoxaline

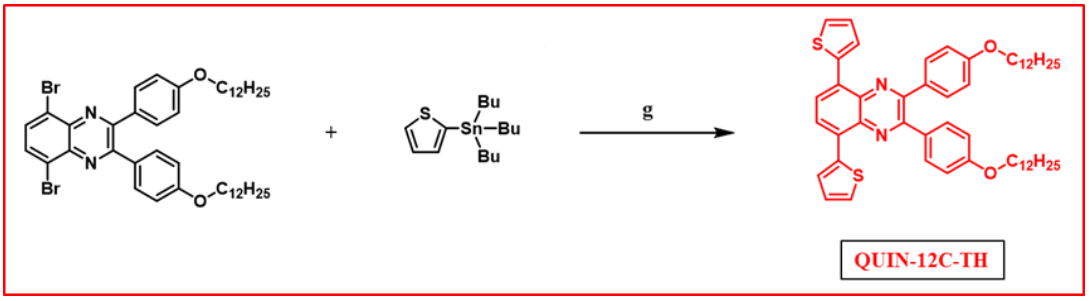

Figure 1.17. Reagents and conditions: ***g.*** PhMe, $Pd(PPh_3)_4$, 115 °C, 84%.

QUIN-12C-TH was prepared according to the literature [58]. Under an argon atmosphere 5,8-dibromo-2,3-bis(4-(dodecyloxy)phenyl)quinoxaline (2.0 g, 2.5 mmol) and tributyl(thiophen-2-yl)stannane (2.3 g, 6.2 mmol) were added to the reaction flask and dissolved in anhydrous toluene (50 mL). Then, $Pd(PPh_3)_4$ (0.11 g, 0.10 mmol) were introduced to the reaction mixture. This mixture was stirred at 115 °C for 24 h and then cooled to the room temperature. H_2O was then added to resulting reddish-brown solid and the aqueous layer was extracted with DCM several times. The combined organic layers were washed with brine and dried over anhydrous Na_2SO_4. After filtration, the solvent was removed under reduced pressure. The resulting reddish yellow solid was then purified by column chromatography (SiO_2, Hexane 30:1 EtOAc). The target product was obtained as an orange solid (1.7 g, 84%): ^{1}H NMR (400 MHz, $CDCl_3$): δ 8.04 (s, 2H), 7.83 (d, *J* = 3.7 Hz, 2H), 7.73 (d, *J* = 8.5 Hz, 4H), 7.51 (d, *J* = 5.1 Hz, 2H), 7.17 (t, *J* = 4.4 Hz, 2H), 6.92 (d, *J* = 8.5 Hz, 4H), 4.01 (t, *J* = 6.6 Hz, 4H), 1.82 (quin, J = 6.8 Hz, 4H), 1.49 – 1.29 (m, 36H), 0.93 (t, *J* = 6.7 Hz, 6H); ^{13}C NMR (100 MHz, $CDCl_3$): δ 160.29, 147.78, 141.39, 137.88, 133.41, 130.86, 128.61, 128.41, 128.37, 126.64, 126.19, 116.09, 68.42, 31.84, 29.98, 29.87, 29.78, 29.73, 29.51, 29.44, 26.09, 22.75, 14.10.

1.2.4. Experimental Procedures for Synthesis of QUIN-2OD-ED

1.2.4.1. 9-(Bromomethyl)nonadecane

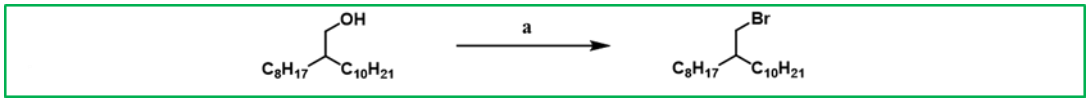

Figure 1.18. Reagents and conditions: ***a.*** DCM, PPh_3, NBS, 0 °C → rt, 82%.

9-(Bromomethyl)nonadecane was prepared according to the literature [59]**.** Under an argon atmosphere 2-octyldodecanol (35.3 g, 118 mmol) was added into the reaction flask and dissolved in DCM (110 mL). Then, the reaction mixture was placed in an ice/H_2O bath. When the temperature become 0 °C, PPh_3 (44.6 g, 170 mmol) was added in one portion and the mixture was stirred for 30 min at 0 °C. NBS (28.8 g, 162 mmol) was added portionwise over 30 min. Then, ice/H_2O bath was removed and the reaction was stirred at room temperature overnight. The solvent was removed under reduced pressure and hexane was added into the resulting sticky brown oil followed by filtration of this mixture. Hexane was then removed under reduced pressure and the residue was purified by column chromatography (SiO_2, Hexane). The target product was obtained as a colorless oil (35 g, 82%): ^{1}H NMR (400 MHz, $CDCl_3$): δ 3.44 (d, *J* = 4.7 Hz, 2H), 1.59 (hept, *J* = 5.7 Hz, 1H), 1.41 – 1.22 (m, 32H), 0.89 (t, *J* = 6.6 Hz, 6H); ^{13}C NMR (100 MHz, $CDCl_3$): δ 39.50, 32.60, 31.97, 31.66, 29.86, 29.72, 29.68, 29.63, 29.43, 29.38, 26.61, 22.74, 14.13.

1.2.4.2. ((2-Octyldodecyl)oxy)benzene

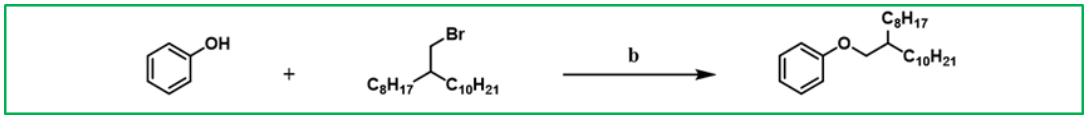

Figure 1.19. Reagents and conditions: ***b.*** K_2CO_3, DMF, 80 °C, 85%.

((2-Octyldodecyl)oxy)benzene was prepared according to the literature [53]. Under an argon atmosphere phenol (6.60 g, 70.1 mmol) and K_2CO_3 (12.3 g, 89.0 mmol) were

added into the reaction flask and dissolved in anhydrous DMF (40 mL). Then, 2-octyldodecyl bromide (25.5 g, 70.6 mmol) was added to the solution dropwise at 80 °C. The reaction mixture was stirred at this temperature overnight and then cooled to the room temperature. H_2O was introduced to the reaction flask and aqueous layer was then extracted with DCM several times. The combined organic layers were dried over anhydrous Na_2SO_4. After filtration, the solvent was removed under reduced pressure. The target product was obtained as a colorless oil (22 g, 85%): ^{1}H NMR (400 MHz, $CDCl_3$): δ 7.34 – 7.27 (m, 2H), 6.98 – 6.91 (m, 3H), 3.88 (d, *J* = 5.9 Hz, 2H)), 1.84 (hept, *J* = 7.0 Hz, 1H), 1.42 – 1.25 (m, 32H), 0.97 (t, *J* = 6.7 Hz, 6H); ^{13}C NMR (100 MHz, $CDCl_3$): δ 159.53, 129.38, 120.40, 114.59, 70.78, 38.15, 38.07, 32.09, 31.76, 31.56, 31.49, 30.20, 30.14, 29.82, 29.77, 29.52, 27.03, 26.96, 22.84, 14.20.

1.2.4.3. 1,2-Bis(4-((2-octyldodecyl)oxy)phenyl)ethane-1,2-dione

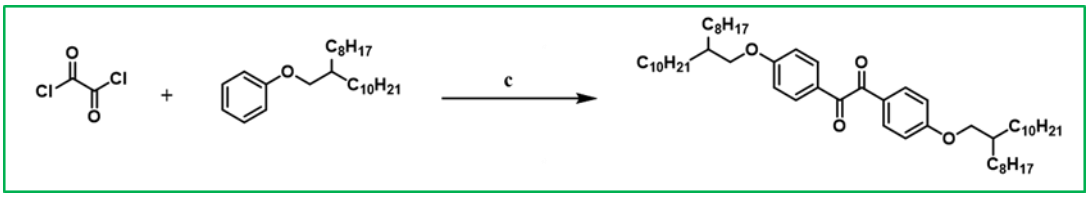

Figure 1.20. Reagents and conditions: ***c.*** urea, $AlCl_3$, DCM, 0 °C → rt, 56%.

1,2-Bis(4-((2-octyldodecyl)oxy)phenyl)ethane-1,2-dione was prepared according to the literature [54]. Under an argon atmosphere ((2-octyldodecyl)oxy)benzene (15 g, 40 mmol), urea (2.4 g, 40 mmol) and $AlCl_3$ (8.0 g, 60 mmol) were added into the reaction flask. The reaction was then cooled to 0 °C with an ice/H_2O bath. At this temperature DCM was added until the mixture was completely dissolved. Oxalyl chloride (2.5 g, 20 mmol) was added dropwise over 30 min at 0 °C. Then, the reaction mixture was warmed to room temperature and stirred overnight. Resulting brown mixture was poured into cold H_2O and aqueous phase was then extracted with DCM several times. The combined organic layers were washed with aqueous 15% $NaHCO_3$ solution and dried over anhydrous Na_2SO_4. After filtration, the solvent was removed under reduced pressure. The resulting reddish-brown oil was then purified by column chromatography (SiO_2, Hexane 1:1 DCM). The target product was obtained as a

yellow oil (9.0 g, 56%): ^{1}H NMR (400 MHz, $CDCl_3$): δ 7.93 (d, *J* = 8.9 Hz, 4H), 6.95 (d, *J* = 8.8 Hz, 4H), 3.90 (d, *J* = 5.6 Hz, 4H), 1.79 (hept, *J* = 5.9 Hz, 2H), 1.41 – 1.23 (m, 64H), 0.87 (t, *J* = 6.6 Hz, 12H); ^{13}C NMR (100 MHz, $CDCl_3$): δ 193.58, 164.73, 132.34, 126.07, 114.74, 71.33, 37.81, 31.92, 31.89, 31.26, 29.97, 29.65, 29.56, 29.34, 29.31, 26.81, 22.68, 14.11.

1.2.4.4. 5,8-Dibromo-2,3-bis(4-((2-octyldodecyl)oxy)phenyl)quinoxaline

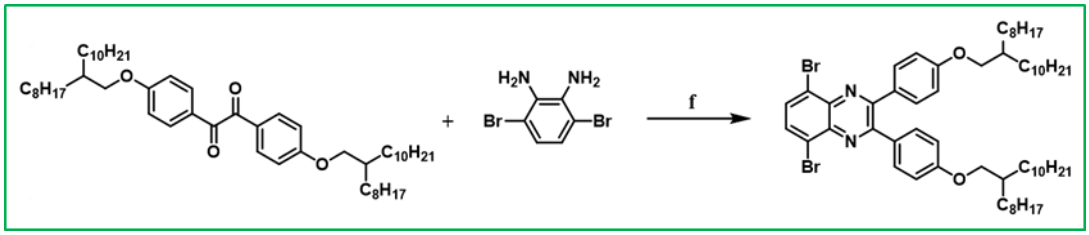

Figure 1.21. Reagents and conditions: ***f.*** EtOH, *p*-TSA, 85 °C, 82%.

5,8-Dibromo-2,3-bis(4-((2-octyldodecyl)oxy)phenyl)quinoxaline was prepared according to the literature [56]. 1,2-Bis(4-((2-octyldodecyl)oxy)phenyl)ethane-1,2-dione (4.1 g, 5.1 mmol), 3,6-dibromobenzene-1,2-diamine (1.5 g, 5.6 mmol) and catalytic p-TSA (88 mg, 0.51 mmol) were added to the reaction flask and dissolved this mixture with EtOH (50 ml). The reaction mixture was stirred at reflux temperature overnight and then cooled to the room temperature. H_2O was added to the resulting yellow mixture. This aqueous phase was extracted with DCM several times. The combined organic layers were washed with brine and dried over anhydrous Na_2SO_4. After filtration, the solvent was removed under reduced pressure. The resulting yellow brown solid was then purified by column chromatography (SiO_2, Hexane 2:1 DCM). The target product was obtained as a yellow solid (4.3 g, 82%): ^{1}H NMR (400 MHz, $CDCl_3$): δ 7.82 (s, 2H), 7.69 (d, *J* = 8.1 Hz, 4H), 6.90 (d, *J* = 8.0 Hz, 4H), 3.89 (d, *J* = 5.3 Hz, 4H), 1.81 (hept, *J* = 5.1 Hz, 2H), 1.48 – 1.13 (m, 64H), 0.91 (t, *J* = 6.7 Hz, 12H); ^{13}C NMR (100 MHz, $CDCl_3$): δ 160.77, 153.56, 139.03, 132.44, 131.67, 130.34, 123.49, 114.43, 71.03, 37.97, 31.98, 31.40, 30.08, 29.74, 29.71, 29.65, 29.41, 26.92, 22.74, 14.17.

1.2.4.5. Tributyl(2,3-dihydrothieno[3,4-b][1,4]dioxin-5-yl)stannane

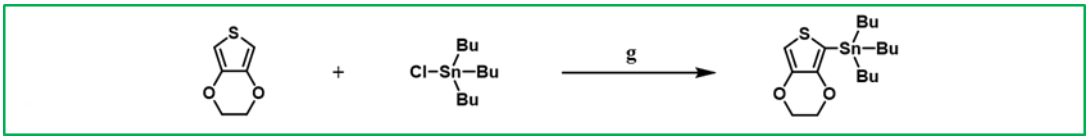

Figure 1.22. Reagents and conditions: ***g.*** THF, n-BuLi, -78 °C → rt, 99%.

Tributyl(2,3-dihydrothieno[3,4-b][1,4]dioxin-5-yl)stannane was prepared according to the literature [60]. Under an argon atmosphere 3,4-ethylenedioxythiophene (3.0 g, 21 mmol) was added into the reaction flask and dissolved in anhydrous THF (60 mL). Then, the reaction mixture was cooled to -78 °C and n-BuLi (9.3 mL, 23 mmol; 2.5 M in hexane) was added dropwise over 30 min. The reaction mixture was stirred at -78 °C for 1.5 h. Tributyltin chloride (8.2 g, 25 mmol) was then added dropwise at -78 °C. The reaction mixture was warmed to room temperature and stirred at this temperature overnight. H_2O was added into the reaction mixture. This aqueous phase was extracted with Et_2O three times. The combined organic layers were washed with brine and dried over anhydrous Na_2SO_4. After filtration, the solvent was removed under reduced pressure. The target product was obtained as a yellow oil (9.0 g, 99%) and used without making any further purification.

1.2.4.6. 5,8-Bis(2,3-dihydrothieno[3,4-b][1,4]dioxin-5-yl)-2,3-bis(4-((2-octyldodecyl)oxy)phenyl)quinoxaline

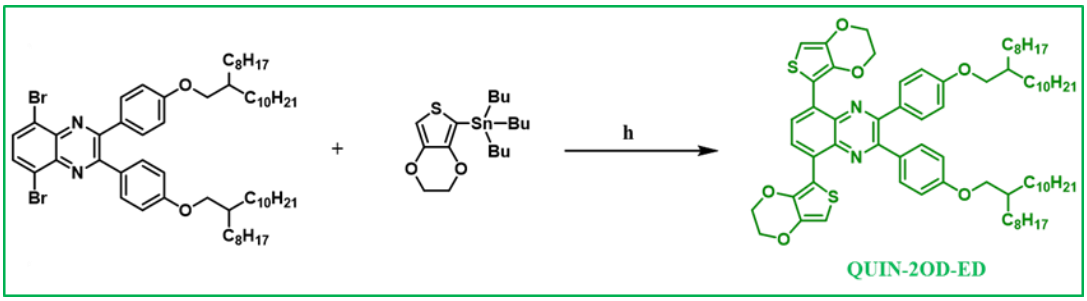

Figure 1.23. Reagents and conditions: ***h.*** PhMe, $Pd_2(dba)_3$, $P(o\text{-}tol)_3$, 115 °C, 90%.

QUIN-2OD-ED was prepared according to the literature [58]. 5,8-Dibromo-2,3-bis(4-((2-octyldodecyl)oxy)phenyl)quinoxaline (2.0 g, 1.9 mmol), 2-(tributylstannyl)-3,4-ethylenedioxythiophene (2.1 g, 4.8 mmol), $Pd_2(dba)_3$ (88 mg, 97 μmol), and $P(o\text{-}tol)_3$ (88.4 mg, 290 μmol) were added to the reaction flask under an argon atmosphere and dissolved in anhydrous toluene (50 mL). This mixture was stirred at 115 °C for 24 h and then cooled to the room temperature. H_2O was added to the resulting reddish-brown sticky oil and the aqueous layer was extracted with DCM several times. The combined organic layers were washed with brine and dried over anhydrous Na_2SO_4. After filtration, the solvent was removed under reduced pressure. The resulting reddish-brown sticky oil was then purified by column chromatography (SiO_2, Petroleum Ether 1:1 DCM). The target product was obtained as a red sticky oil (2.0 g, 90%): ^{1}H NMR (400 MHz, $CDCl_3$): δ 8.58 (s, 2H), 7.74 (d, *J* = 8.8 Hz, 4H), 6.90 (d, *J* = 8.8 Hz, 4H), 6.55 (s, 2H), 4.49 – 4.23 (m, 8H), 3.88 (d, *J* = 5.6 Hz, 4H), 1.74 (hept, *J* = 6.8 Hz, 2H) 1.60 – 1.15 (m, 64H), 0.98 – 0.81 (t, *J* = 6.9 Hz, 12H); ^{13}C NMR (100 MHz, $CDCl_3$): 160.08, 150.34, 141.35, 140.19, 136.87, 131.96, 131.93, 131.07, 128.46, 127.56, 123.42, 114.20, 113.55, 102.94, 71.01, 64.95, 64.37, 38.01, 31.95, 31.40, 30.06, 29.71, 29.68, 29.63, 29.38, 26.90, 22.72, 14.15.

1.3. RESULTS AND DISCUSSION

1.3.1. Quinoxaline-Based Polymer Syntheses

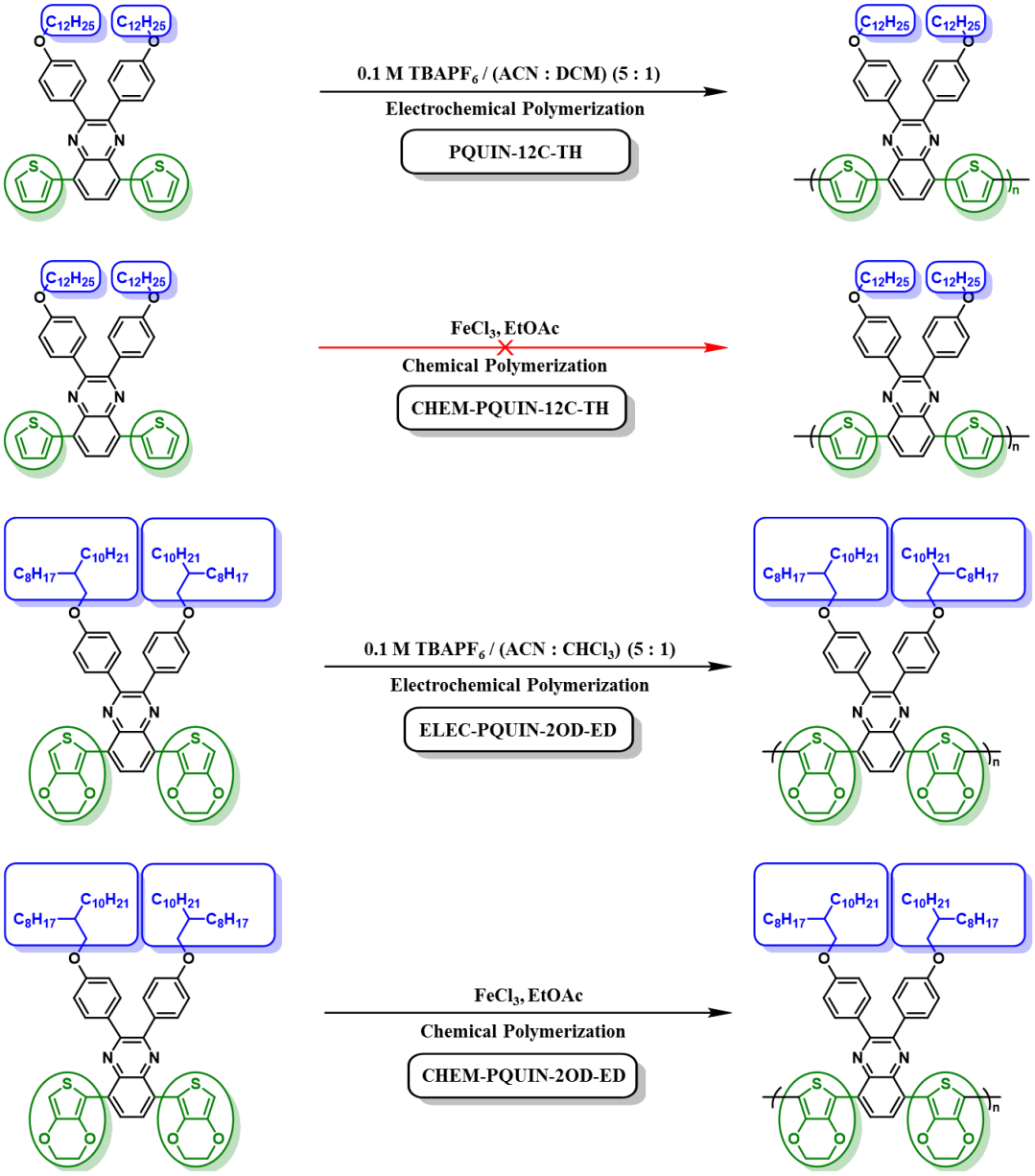

Figure 1.24. Polymerizations of QUIN-12C-TH and QUIN-2OD-ED.

Quinoxaline acceptor with both a linear alkyl chain and a branched alkyl chain were known in the literature. Both stannylated EDOT and stannylated thiophene were also

known in literature. QUIN-12C-TH and QUIN-2OD-ED monomers were synthesized via Stille coupling with using several Pd catalysts. Homopolymer films of QUIN-12C-TH could be just produced by electrochemical polymerization (ELEC-PQUIN-12C-TH) although QUIN-12C-TH was tried to be polymerized electrochemically and chemically. On the other hand, homopolymer films of QUIN-2OD-ED could be synthesized by both electrochemical polymerization (ELEC-PQUIN-2OD-ED) and oxidative chemical polymerization (CHEM-PQUIN-2OD-ED). After that, electrochemical, spectroelectrochemical and kinetic characteristics of each polymer were investigated.

1.3.1.1. Chemical Polymerization of QUIN-12C-TH

Under an argon atmosphere QUIN-12C-TH was tried to be polymerized via oxidative chemical polymerization with anhydrous $FeCl_3$ at different conditions. In other words, the parameters such as the amount of anhydrous $FeCl_3$, the time interval and the type of solvent were changed one by one after each unsuccessful attempt. For instance, QUIN-12C-TH was tried to be polymerized with both 3.5 and 7.0 equivalents of anhydrous $FeCl_3$ by using the same organic solvent ($CHCl_3$) at same time interval (24h). However, extremely sticky precipitates were obtained after the reaction mixture was added into a beaker filled with cold MeOH. Because this resulting residue could not be isolated for characterization, the polymerization of QUIN-12C-TH was repeated by changing $CHCl_3$ with EtOAc. The same extremely sticky residue was again obtained. After all trials at different conditions, the desired homopolymer could not be attained.

1.3.1.2. Chemical Polymerization of QUIN-2OD-ED

Under an argon atmosphere anhydrous $FeCl_3$ (49.1 mg, 303 μmol; 3.5 eq.) was added to the reaction flask and dissolved in a minimum amount of EtOAc. At the same time, QUIN-2OD-ED (100 mg, 86.5 μmol) was added to a vial filled with argon and dissolved in a minimum amount of EtOAc. This solution was then introduced to the

$FeCl_3$ solution dropwise under dark environment. After the addition was completed, the reaction mixture was stirred at room temperature for 24h. The resulting polymer solution was transferred into a beaker including cold MeOH; therefore, the fast precipitation of polymer (CHEM-PQUIN-2OD-ED) was achieved. Then, the poly(CHEM-PQUIN-2OD-ED) were excessively washed with MeOH. To dedope the polymer, 5% hydrazine monohydrate solution (100 mL in CHC_3) and the resulting mixture was stirred at room temperature for 45 min. After that, the solvent was removed under reduced pressure. The polymer was then excessively washed with MeOH, followed by washing with acetone. This washing procedure was done until the polymer films did not give any color to the filtrate. The residue was dried in vacuum oven at 100 °C. CHEM-PQUIN-2OD-ED were obtained as dark blue films (100 mg, 98%); GPC: M_n (Da): 33,453, M_w (Da): 44.908, PDI: 1.3.

1.3.2. General Procedure of Electrochemical Studies

For each electrochemical polymerization, the most suitable voltage interval where fully neutral and oxidized states of polymers can be observed in a three-electrode system. The electrodes used in this system were shown as follows:

1. ITO-coated glass slide as working electrode;
2. Pt wire as counter electrode;
3. Ag wire as reference electrode.

The most suitable solvent and supporting electrolyte(s) couples were chosen to make homogeneous homopolymer films on ITO by scanning appropriate potential range. Since CHEM- PQUIN-2OD-ED was obtained with chemical polymerization, the polymer films of it were coated on ITO by spray coating. Then, polymerization CVs and single scan voltammograms for each polymer were analyzed. By using the data obtained, the electroactivity of each monomer and the formation of corresponding polymers were proved. Additionally, the monomer oxidation peak for each polymer was detected by looking the first cycle represented as red line in such voltammogram throughout this thesis. By using the data obtained from single scan voltammogram, p-

doping/p-dedoping and/or n-doping/n-dedoping potentials, the HOMO/LUMO energy levels and the electronic band gaps of ELEC-PQUIN-12C-TH, ELEC-PQUIN-2OD-ED and CHEM-PQUIN-2OD-ED were determined respectively. To calculate the HOMO and LUMO energy levels of each polymer, the onset of the corresponding p-doping/p-dedoping peaks and n-doping/n-dedoping peaks were determined and then the following equations were used:

- $HOMO = -(4.75 + 0.3 + E_{ox}^{onset})$;
- $LUMO = -(4.75 + 0.3 + E_{red}^{onset})$.

4.75 referred to NHE value as -4.75 eV vs vacuum whereas 0.3 referred to the calibration of reference electrode wrt Fc/Fc+ as 0.3 eV. If there was no n-doping and n-dedoping peaks at single scan voltammogram, optical band gap data obtained from Spectroelectrochemistry was used to determine the LUMO energy level. Moreover, the color characteristics of corresponding polymers upon positive and/or negative doping were investigated.

1.3.2.1. Electrochemical Studies of ELEC-PQUIN-12C-TH

Electrochemical polymerization of QUIN-12C-TH was carried out in 0.1 M $TBAPF_6$/(ACN : DCM)(5 : 1) and 0.01 M monomer (QUIN-12C-TH) solutions with repeated scanning between -0.2 and 1.2 V. Multiple scan voltammogram for polymerization of QUIN-12C-TH proved the electroactivity of this monomer and the formation of corresponding polymer films. By looking to the first cycle shown with red line in Figure 3.2, the monomer oxidation peak for QUIN-12C-TH was determined as 1.10 V. This polymer showed multi-color characteristic at its oxidized state.

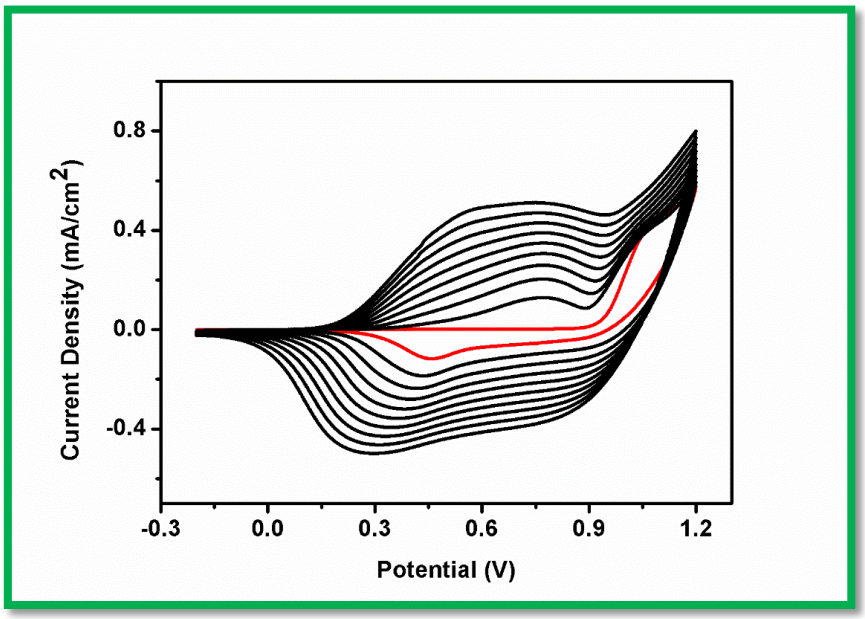

Figure 1.25. Multiple scan voltammogram for polymerization of QUIN-12C-TH at 100 mV/s in 0.1 M $TBAPF_6$/(ACN : DCM)(5 : 1) solution on ITO.

By looking to Figure 3.3, p-doping and p-dedoping peaks of ELEC-PQUIN-12C-TH were detected at 0.59 and 0.37 V. Also, two different n-doping and n-dedoping peaks were observed in this figure. This type of conjugated polymers are rare polymers having both p-doped and n-doped properties are valuable for fabrication of ambipolar transistors. In Figure 3.3, the first n-doping and n-dedoping peaks were detected at -1.39 and -1.27 V whereas the second n-doping and n-dedoping peaks were found at -2.10 and -1.76 V. The HOMO and LUMO energy levels of ELEC-PQUIN-12C-TH were calculated as -4.95 and -3.52 eV, respectively. By using these two values, the electronic band gap of ELEC-PQUIN-12C-TH was calculated as 1.43 eV.

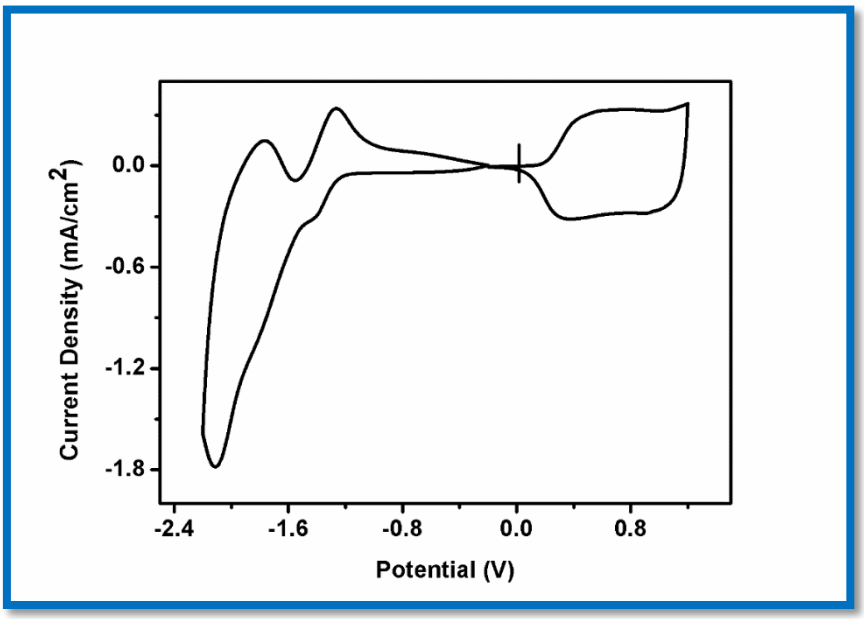

Figure 1.26. Single scan cyclic voltammogram of ELEC-PQUIN-12C-TH in a monomer free 0.1 M $TBAPF_6$/ACN solution on ITO.

1.3.2.2. Electrochemical Studies of ELEC-PQUIN-2OD-ED

Electrochemical polymerization of QUIN-2OD-ED was carried out in 0.1 M $TBAPF_6$/(ACN : $CHCl_3$)(5 : 1) and 0.01 M monomer (QUIN-2OD-ED) solutions with repeated scanning between -0.6 and 1.1 V. Multiple scan voltammogram for polymerization of QUIN-2OD-ED proved the electroactivity of this monomer and the formation of corresponding polymer films. By looking to the first cycle shown with red line in Figure 3.4, the monomer oxidation peak for QUIN-2OD-ED was detected at 0.72 V. This polymer had saturated green color at its neutral state and transmissive grey color at its oxidized state.

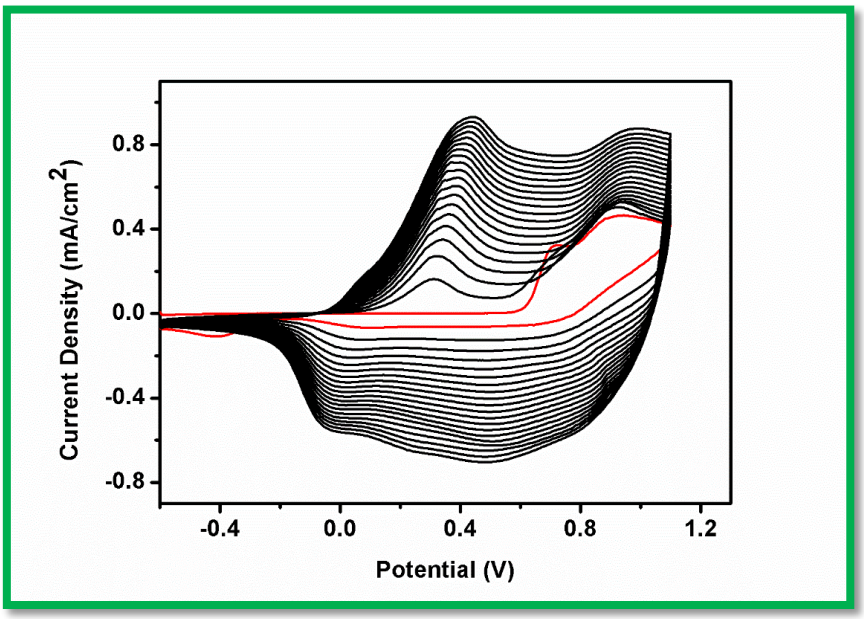

Figure 1.27. Multiple scan voltammogram for polymerization of QUIN-2OD-ED at 100 mV/s in 0.1 M $TBAPF_6$/(ACN : $CHCl_3$)(5 : 1) solution on ITO.

Two different p-doping and p-dedoping peaks belonging to ELEC-PQUIN-2OD-ED were detected in Figure 3.5. The first p-doping and p-dedoping peaks were determined at 0.49 and 0.00 V whereas the second p-doping and p-dedoping peaks were found at 0.76 and 0.50 V. In literature, the similar homopolymer with linear alkyl chain known as PDOPEQ was synthesized by Toppare and coworkers in 2008. Based on the results in this paper, the monomer oxidation potential of ELEC-PQUIN-2OD-ED (0.72 V) was significantly lower than the oxidation potential of PDOPEQ (0.80 V). In addition, the oxidation and reduction potentials of ELEC-PQUIN-2OD-ED (0.49 V and 0.01 V) were quite similar with PDOPEQ (0.50 V and 0.07 V). The HOMO energy level of ELEC-PQUIN-2OD-ED was calculated as -4.85 eV. Since ELEC-PQUIN-2OD-ED did not show n-doping and n-dedoping characteristics, the LUMO energy level was determined by using the band gap values shown in the spectroelectrochemical study of this polymer. The LUMO energy level was noted as -3.37 eV.

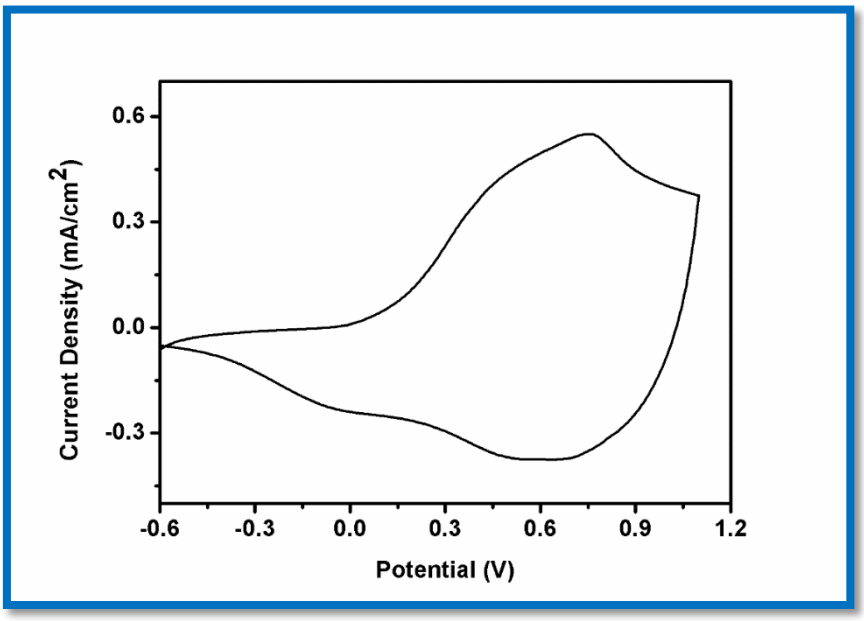

Figure 1.28. Single scan cyclic voltammogram of ELEC-PQUIN-2OD-ED in a monomer free 0.1 M $TBAPF_6$/ACN solution on ITO.

1.3.2.3. Electrochemical Studies of CHEM-PQUIN-2OD-ED

CHEM-PQUIN-2OD-ED was spray coated onto ITO coated glass electrode and cyclic voltammetry studies were performed in 0.1 M $TBAPF_6$/ACN monomer free solution. Two different p-doping and p-dedoping peaks belonging to CHEM-PQUIN-2OD-ED were detected in Figure 3.6. The first p-doping and p-dedoping peaks were determined at 0.39 and 0.00 V whereas the second p-doping and p-dedoping peaks were found at 0.70 and 0.52 V. The HOMO energy level of CHEM-PQUIN-2OD-ED was calculated as -4.78 eV. Since CHEM-PQUIN-2OD-ED did not show n-doping and n-dedoping characteristics, the LUMO energy level was determined by using the band gap values shown in the spectroelectrochemical study of this polymer. The LUMO energy level was noted as -3.23 eV. This polymer had saturated green color at its neutral state and transmissive grey color at its oxidized state.

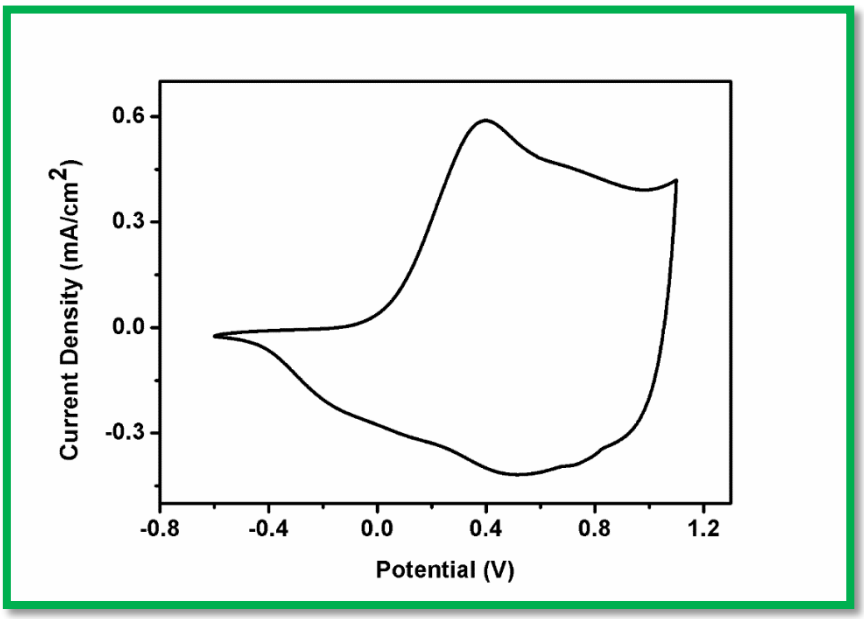

Figure 1.29. Single scan cyclic voltammogram of CHEM-PQUIN-2OD-ED in a monomer free 0.1 M $TBAPF_6$/ACN solution on ITO.

1.3.3. General Procedure of Spectroelectrochemical Studies

Polymer films of ELEC-PQUIN-12C-TH, ELEC-PQUIN-2OD-ED were obtained by growing on ITO potentiodynamically whereas polymer films of CHEM-PQUIN-2OD-ED were formed on ITO by spray coating. After that, each ITO was put in a monomer free 0.1 M $TBAPF_6$/ACN solution after thoroughly washed with ACN to eliminate residual monomers and/or small oligomers. Then, the changes in both the electronic structure and the optical characteristics (λ_{max} and E_g^{op}) upon doping-dedoping processes of corresponding polymers were analyzed at a specific voltage interval with Varian Cary 5000 UV-Vis spectrophotometer. By looking the electronic absorption spectra, λ_{max} and the formation of polaronic states were determined. Furthermore, to calculate E_g^{op} of each polymer, the onset of the lower energy transition was firstly detected and then the following equation was used:

- $E = \frac{h \times c}{\lambda}$ or $E = \frac{1240 \frac{eV}{nm}}{\lambda_{let}^{onset}}$ (De Broglie equation)

To emphasize the scientific color of polymers with respect to CIE (Commission Internationale de l'Eclairage) coordinates, colorimetric measurements were also done. Based on each color changing at different voltages, L, a, b values of each polymer were determined. In CIE coordinates, L is referred to as Luminance, a is referred to as hue and b is referred to as saturation.

1.3.3.1. Spectroelectrochemical Studies of ELEC-PQUIN-12C-TH

The homopolymer films of ELEC-PQUIN-12C-TH were obtained via electrochemical polymerization. To eliminate the monomer and small molecules on ITO, a monomer free 0.1 M $TBAPF_6$/ACN solution was used. To investigate the optical characteristic of ELEC-PQUIN-12C-TH, the potentials between - 0.3 and 1.2 V were applied with 0.05 increments. As seen in Figure 3.7, ELEC-PQUIN-12C-TH showed two λ_{max} centered at 396 nm and 622 nm. Additionally, the first polaronic band centered at 895 nm upon oxidation. E_g^{op} of this polymer was calculated as 1.57 eV. Furthermore, this polymer had turquois color at its neutral state and transmissive grey color upon positive doping. These colors of ELEC-PQUIN-12C-TH and its L, a, and b values were shown in Figure 3.8.

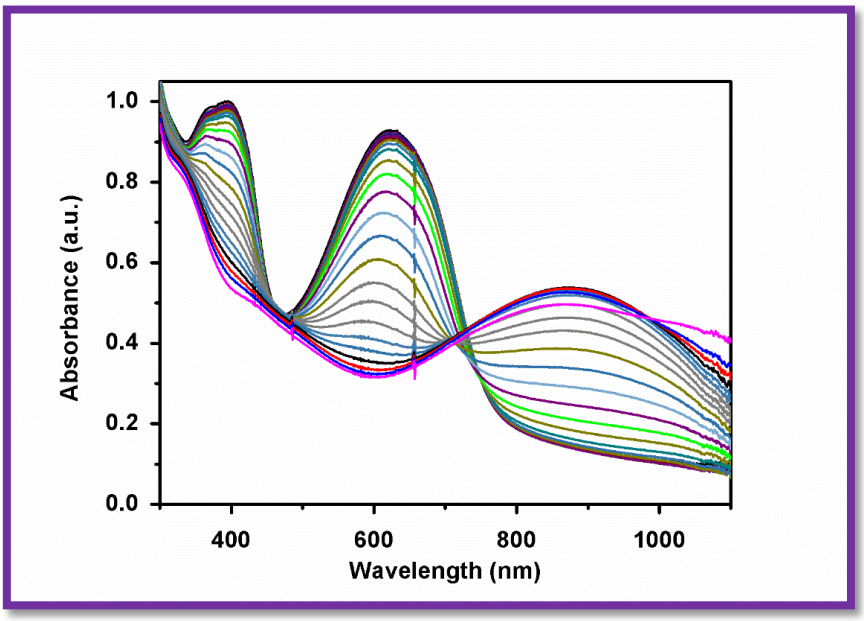

Figure 1.30. Electronic absorption spectra of ELEC-PQUIN-12C-TH upon p-doping between -0.3 V and 1.2 V in a monomer free 0.1 M $TBAPF_6$/ACN solution on ITO.

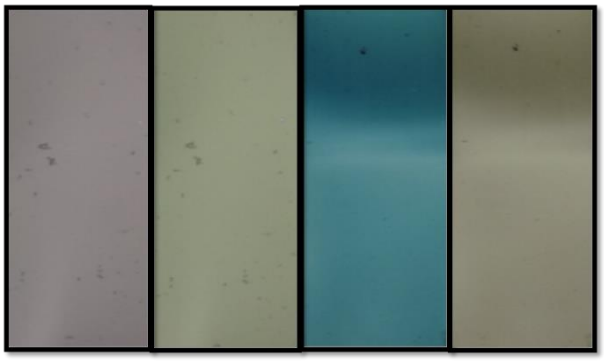

Figure 1.31. Colors of PQUIN-12C-TH and its L, a, and b values.

1.3.3.2. Spectroelectrochemical Studies of ELEC-PQUIN-2OD-ED

The homopolymer films of ELEC-PQUIN-2OD-ED were obtained via electrochemical polymerization. To eliminate the monomer and small molecules on ITO, a monomer free 0.1 M $TBAPF_6$/ACN solution was used. To investigate the optical characteristic of ELEC-PQUIN-2OD-ED, the potentials between -0.6 V to 1.1

V were applied stepwise. As seen in Figure 3.9, ELEC-PQUIN-2OD-ED films showed two λ_{max} centered at 405 nm and 728 nm. In literature, it is known that if any material has two absorption maxima at around 400 nm and 700 nm, it shows the true green color in its neutral state. Additionally, the first polaronic band centered at 930 nm upon oxidation. E_g^{op} of ELEC-PQUIN-2OD-ED was calculated as 1.48 eV. Furthermore, this polymer had saturated green color at its neutral state and transmissive grey color upon positive doping. These colors of ELEC-PQUIN-2OD-ED and its L, a, and b values were shown in Figure 3.10.

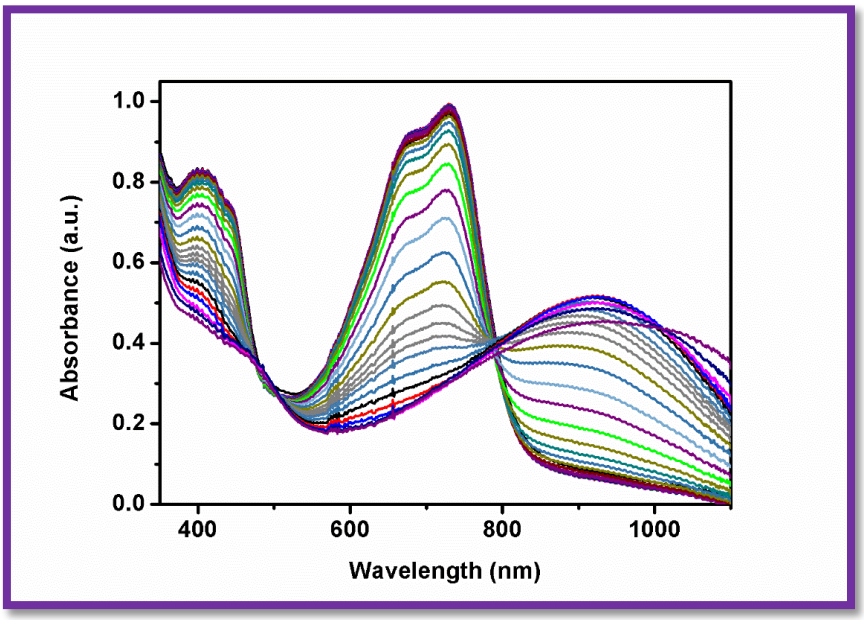

Figure 1.32. Electronic absorption spectra of ELEC-PQUIN-2OD-ED upon p-doping between -0.3 V to 0.95 V in a monomer free 0.1 M $TBAPF_6$/ACN solution on ITO.

-0.3 V	1.1 V
L: 35	L: 41
a: -25	a: -2
b: 13	b: 12

Figure 1.33. The colors of ELEC-PQUIN-12C-TH and its L, a, and b values.

1.3.3.3. Spectroelectrochemical Studies of CHEM-PQUIN-2OD-ED

The polymer films of CHEM- PQUIN-2OD-ED were grown by spray coating on ITO. To eliminate the monomer and small molecules on ITO, a monomer free 0.1 M $TBAPF_6$/ACN solution was used. To investigate the optical characteristic of CHEM-PQUIN-2OD-ED, the potentials between -0.6 V to 1.1 V were applied stepwise. As seen in Figure 3.11, CHEM-PQUIN-2OD-ED films showed two λ_{max} centered at 417 nm and 730 nm. In literature, it is known that if any material has two absorption maxima at around 400 nm and 700 nm, it shows the true green color in its neutral state. Additionally, the first polaronic band centered at 935 nm upon oxidation. E_g^{op} of CHEM-PQUIN-2OD-ED was calculated as 1.55 eV. Furthermore, this polymer had green color at its neutral state and transmissive grey color upon positive doping. These colors of CHEM-PQUIN-2OD-ED and its L, a, and b values were shown in Figure 3.12. We were pleased to see that the new polymer CHEM-PQUIN-2OD-ED showed brighter more saturated green color in its neutral state compared to PDOPEQ. This makes CHEM-PQUIN-2OD-ED a better candidate for electrochromic device applications.

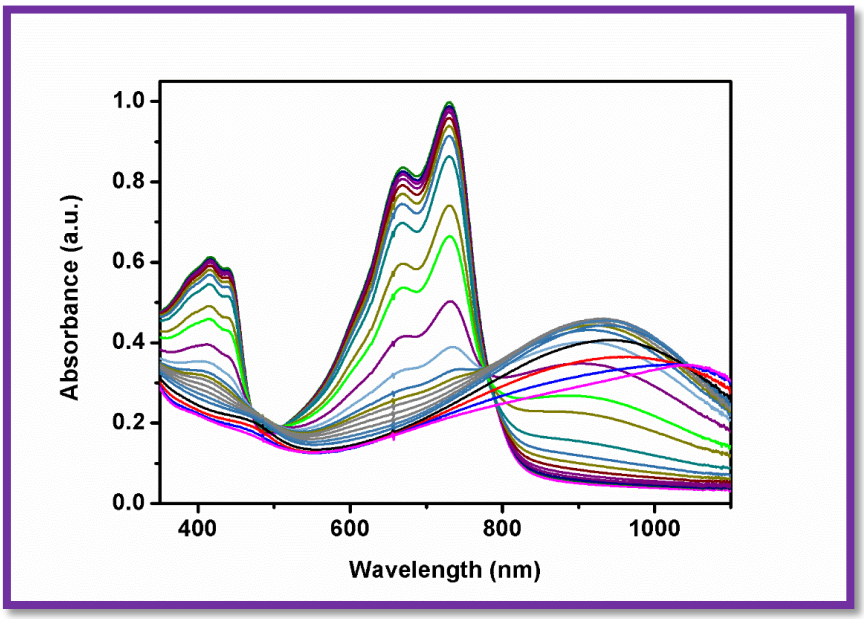

Figure 1.34. Electronic absorption spectra of CHEM-PQUIN-2OD-ED upon p-doping between -0.3 V to 0.95 V in a monomer free 0.1 M $TBAPF_6$/ACN solution on ITO.

Figure 1.35. The colors of CHEM-PQUIN-2OD-ED and its L, a, and b values.

1.3.4. General Procedure of Kinetic Studies

The polymer films on ITO were obtained as mentioned above. Then, the optical contrasts (% transmittance) and the switching times of PQUIN-12C-TH, ELEC-PQUIN-2OD-ED and CHEM-PQUIN-2OD-ED were analyzed by probing the

changes in transmittance with respect to applied potentials and these analyses were made by Varian Cary 5000 UV-Vis spectrophotometer.

1.3.4.1. Kinetic Studies of ELEC-PQUIN-12C-TH

The optical contrasts (% transmittances) of PQUIN-12C-TH were found as 16% at 400 nm and 31% at 625 nm. Moreover, the switching times of this polymer were determined as 1.3 s at 400 nm and 2.0 s at 625 nm.

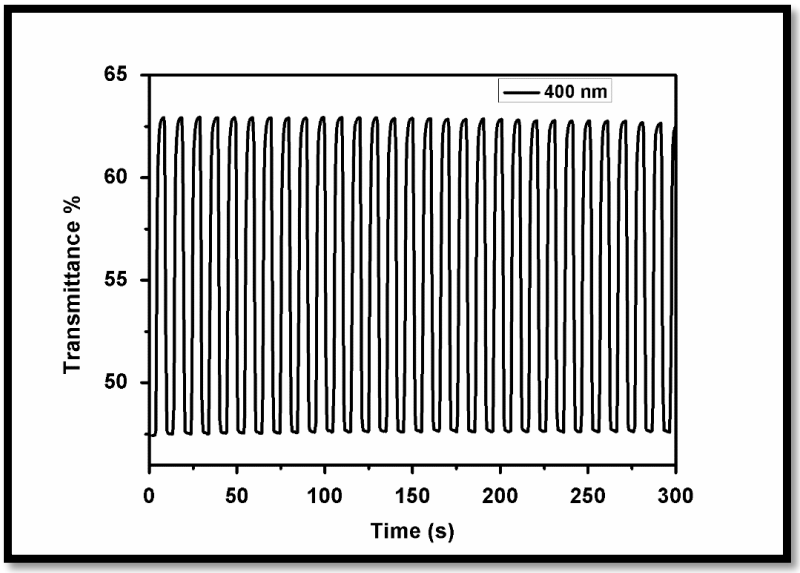

Figure 1.36. The optical contrasts of PQUIN-12C-TH in a monomer free 0.1 M $TBAPF_6$/ACN solution at 400 nm.

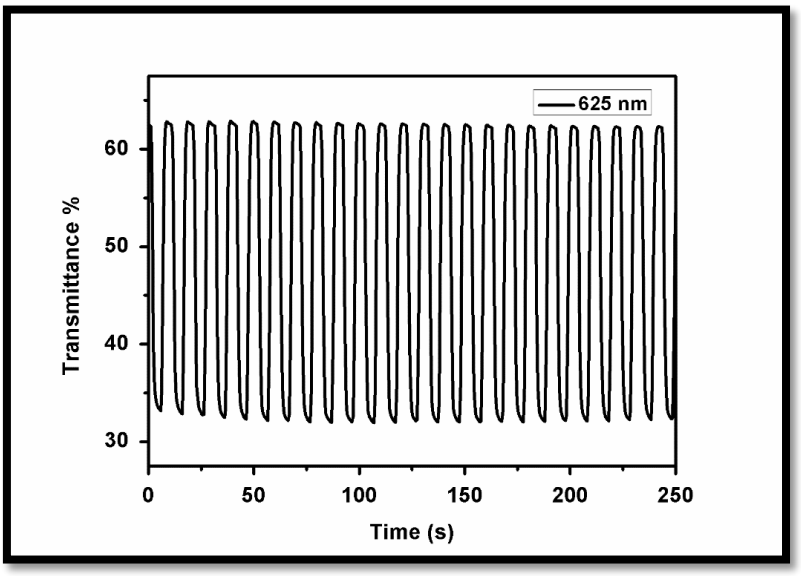

Figure 1.37. The optical contrasts of PQUIN-12C-TH in a monomer free 0.1 M $TBAPF_6$/ACN solution at 625 nm.

1.3.4.2. Kinetic Studies of ELEC-PQUIN-2OD-ED

The optical contrast (% transmittance) of ELEC-PQUIN-2OD-ED were found as 43% which was relatively high optical contrast at 728 nm. Moreover, the switching times of this polymer were determined as 2 s at 728 nm.

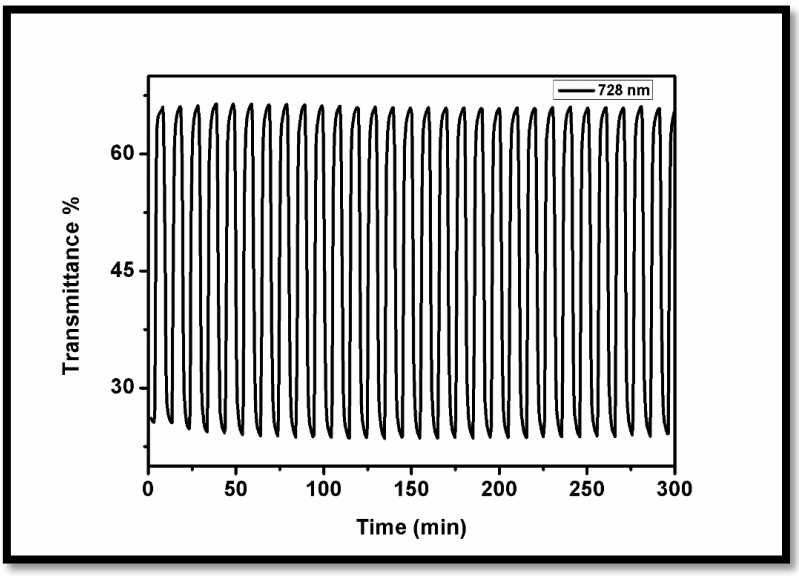

Figure 1.38. The optical contrast of ELEC-PQUIN-2OD-ED in a monomer free 0.1 M $TBAPF_6$/ACN solution at 728 nm.

1.3.4.3. Kinetic Studies of CHEM-PQUIN-2OD-ED

The optical contrast (% transmittance) of CHEM-PQUIN-2OD-ED were found as 45% which was relatively high optical contrast at 730 nm. Moreover, the switching times of this polymer were determined as 1.9 s at 730 nm. This optical contrast value was higher than what was achieved with PDOPEQ (42%). However, switching times were faster for PDOPEQ compared to CHEM-PQUIN-2OD-ED.

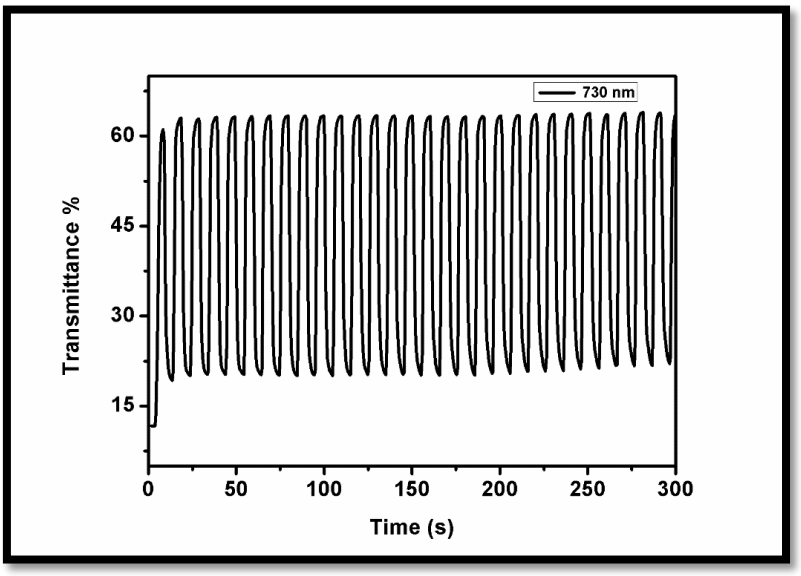

Figure 1.39. The optical contrast of CHEM-PQUIN-2OD-ED in a monomer free 0.1 M $TBAPF_6$/ACN solution at 730 nm.

	ELEC-PQUIN-12C-TH	ELEC-PQUIN-2OD-ED	CHEM-PQUIN-2OD-ED
E_m^{ox} (V)	1.10	0.72	-
$E_{p\text{-doping}}$ (V)	0.59	0.49 / 0.76	0.39 / 0.70
$E_{p\text{-dedoping}}$ (V)	0.37	0.00 / 0.50	0.00 / 0.52
$E_{n\text{-doping}}$ (V)	-1.39 / -2.10	-	-
$E_{n\text{-dedoping}}$ (V)	-1.27 / -1.76	-	-
HOMO (eV)	-4.95	-4.85	-4.78
LUMO (eV)	-3.52	-3.37	-3.23
E_g^{ec} (eV)	1.43	1.45	1.50
λ_{max} (nm)	396 / 622	728 / 683	730 / 668
E_g^{op} (eV)	1.57	1.48	1.55
Optical contrast (ΔT %)	16% (400 nm) 31% (625 nm)	43 (728 nm)	45 (730 nm)
Switching times (s)	1.3 (400 nm) 2.0 (625 nm)	2.0 (728 nm)	1.9 (730 nm)

Figure 1.40. Summary of electrochemical, spectroelectrochemical and kinetic studies of ELEC-PQUIN-12C-TH, ELEC-PQUIN-2OD-ED and CHEM-PQUIN-2OD-ED.

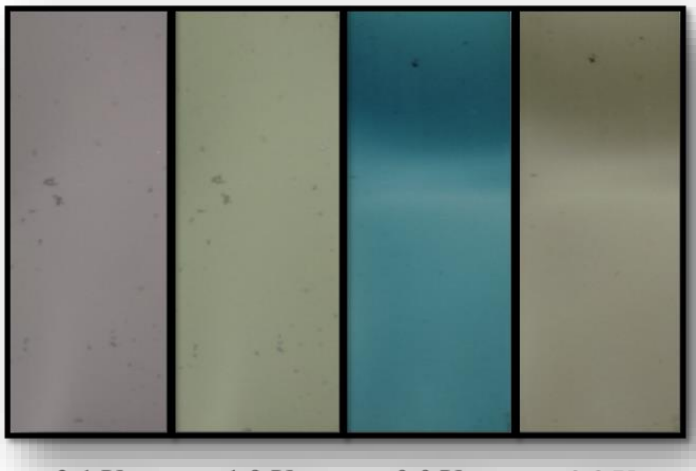

(ELEC-PQUIN-12C-TH)

(ELEC-PQUIN-2OD-ED)

(CHEM-PQUIN-2OD-ED)

Figure 1.41. Summary of colorimetric studies of ELEC-PQUIN-12C-TH, ELEC-PQUIN-2OD-ED and CHEM-PQUIN-2OD-ED.

1.4. CONCLUSION

In this thesis two novel quinoxaline-based monomers with thiophene and EDOT side units were designed and synthesized via Stille coupling reactions. Each synthesized product was characterized with NMR spectroscopy. Quinoxaline-based homopolymer films (ELEC-PQUIN-12C-TH) with a linear alkyl chain and thiophene side units were synthesized via electrochemical polymerization. On the other hand, quinoxaline-based homopolymer films with a branched alkyl chain and EDOT side units were synthesized with both electrochemical polymerization (ELEC-PQUIN-2OD-ED) and oxidative chemical polymerization (CHEM-PQUIN-2OD-ED). Electrochemical, spectroelectrochemical and kinetic properties of PQUIN-12C-TH, ELEC-PQUIN-2OD-ED and CHEM-PQUIN-2OD-ED were investigated respectively.

The electrochemical studies showed that both ELECT-PQUIN-2OD-ED and CHEM-PQUIN-2OD-ED are p-dopable polymers. Both polymers revealed a rare characteristic of electrochromic polymers which is switching between green and transmissive grey color during doping/dedoping. Since ELECT-PQUIN-2OD-ED and CHEM-PQUIN-2OD-ED have one of the complementary colors (RGB color) in their neutral states, they are promising candidates for many electrochromic applications like simple display devices. In literature, there are also few polymers that display both n-doping/p-doping and multichromic. The electrochemical study results proved that ELEC-PQUIN-12C-TH was the member of this group of multifunctional polymers. Due to such unique characteristics, this polymer can be used for special optoelectronic applications such as display systems and smart windows. Furthermore, the kinetic studies proved that in the visible region, ELECT-PQUIN-2OD-ED and CHEM-PQUIN-2OD-ED had higher optical contrasts (43% at 728 nm and 45% at 730 nm) than the first green polymer with a transmissive oxidized state (PDOPEQ). Moreover, chemically produced quinoxaline-including homopolymer with EDOT side unit had great solubility in common organic solvent due to the logical design of monomer with solubilizing alkoxy groups. The promising electrochemical and electrochromic results

make ELEC-QUIN-12C-TH, ELEC-PQUIN-2OD-ED and CHEM-PQUIN-2OD-ED excellent candidates for both current and next generation electrochromic device applications.

2. SYNTHESIS AND CHARACTERIZATION OF NOVEL THIENO[3,4-C]PYRROLE-4,6-DIONE-BASED CONJUGATED POLYMERS AND THEIR APPLICATIONS IN ORGANIC ELECTRONICS

2.1. INTRODUCTION

2.1.1. The Need for Photovoltaics

With the continuous developments in both science and technology over the last decades and with increasing population, the energy consumption on Earth increases steadily. However, such energy consumptions become a worldwide problem day by day since there is a limitation of almost all sources used for energy in today's society. In other words, the problem is that all energy sources are not renewable sources such as crude oil, natural gas, and coal [61]. Because of this reason, in near future they will have been exhausted completely. That's why the usage of renewable and sustainable energy sources such as wind and sunlight is needed to replace non-renewable ones before the energy crisis is evolved. For such purpose, solar cells converting sunlight into electricity become one of the most powerful solutions to meet the energy demands of world and over the years they have proved their importance with the development of various solar cell devices [61].

2.1.2. The History of Photovoltaics

The development of solar energy started with the discovery of photovoltaic effect by the French physicist Alexandre Edmond Becquerel in 1839 [62]. He realized the generation of photocurrent on the Pt electrodes placed into the electrolytes while working on illumination of various metal halides such as AgCl and AgBr in an acidic

solution [62]. In 1873, the first photoconductivity in solid Se was discovered by English electrical engineer Willoughby Smith [63]. In 1876, the first report on the formation of electricity from light was published by William Grylls Adams and his student Richard Evans Day [62]. They inspired by Willoughby Smith and made a lot of experiments with Se. At the end of their experiments they realized that when Se is exposed to sunlight, it can produce electricity. Because of these two discoveries on photoconductivity in Se, the first thin-film Se-based PV cell was created by an American inventor Charles Fritts in 1883 [62]. Although PCE of this cell was lower than 1%, it provided for considerable increase in the researches on this area. In 1905, the article related with the theory of photoelectric effect was published by Albert Einstein [62]. In this paper, he mentioned how the electrons could be released on a metal surface by the help of light. In 1916, this theory was proven by American physicist Robert Andrews Millikan; therefore, Einstein was granted a Nobel Prize with his study in 1922 [62]. In 1906, the photoconductivity in solid anthracene was discovered by Pochettino [63]. His discovery was crucial because anthracene was the first organic compound displays photoconductivity. Until 1918, any Si-based PV cell was not constructed. Luckily when the time was 1918, a method for production of monocrystalline silicon was developed by a Polish scientist Jan Czochralski [64]. His study enabled for preparation monocrystalline PV cells; however, the first monocrystalline Si-based PV cell could be produced in 1941. In 1932, the photovoltaic effect in cadmium-selenide was discovered [65]. In 1946, the modern junction semiconductor PV cell was patented by an American engineer Russell Shoemaker Ohl [62]. In 1951, the first germanium-based PV cell was made whereas in 1954 the first efficient Si-based PV cell was created at Bell Laboratories [66]. Even though this cell had 6% efficiency, the governments started to support PV researches significantly because they believed that limitless and eco-friendly energy of the sun will be converted into electricity in the near future. Because of such support and investment, PCE of PV cells were increased to 14% in 1960s. The first crucial application in PV world was made by USA for space explorations and in 1958 the US satellite known as ‘’Vanguard I’’ was launched to the space which was the world's first solar-powered satellite [62]. In the beginning of 1960s different types of PV materials such as GaAs, methylene blue, and carotenes were found due to the significant researchers in PV field and PV cells were prepared by using them [63].

However, the price of PV cells was expensive for public. That's why they could be mainly used in small area applications like calculators. In the years between 1980 and 2000, a number of important discoveries and developments were realized. For example, the first heterojunction PV device based on small organic molecules was made by Tang in 1986 whereas the first dye/dye bulk heterojunction device was reported by Hiramoto in 1991 [63]. Just two years later, the first polymer/C_{60} heterojunction PV device was published by Sariciftci [63]. Furthermore, within two consecutive years, the first bulk polymer/C_{60} heterojunction PV cell and the first bulk polymer/polymer heterojunction cell were made by Yu and Yu/Hall corporations, respectively [63]. Because of such revolutions in PV field, polymer solar cells (PSC) become a new field for the development of PV applications. Other than silicon based technologies, since the high-cost, low stability, and short lifetime were significant issues for mass production, innovative low-cost techniques, discovery of novel inorganic, organic and polymeric materials have been addressing these problems over the last decades [67].

2.1.3. Parts of Photovoltaic Solar Energy System

There are four major parts in a typical PV solar system. They are shown as below:

1. photovoltaic module;
2. charge controller;
3. battery bank;
4. inverter [68].

The first part consists of many small photovoltaic cells. The electricity is firstly generated on the surfaces of these cells when they are exposed to the solar energy. The efficiency of these cells determines the amount of electricity produced. The main significant advantages of PV cells are shown as follows:

i. They do not need any fuel to work;
ii. They do not create any noise while working;

iii. They do not harm the environment with any waste [68].

The second part, the charge controller is used for checking the batteries whether they are either overcharged or discharged. The third part is responsible for storing the surplus produced by the modulus to be used later. The last part of PV solar system, inverter is needed to convert the direct current (DC) generated by PV panels to alternating current (AC) [68].

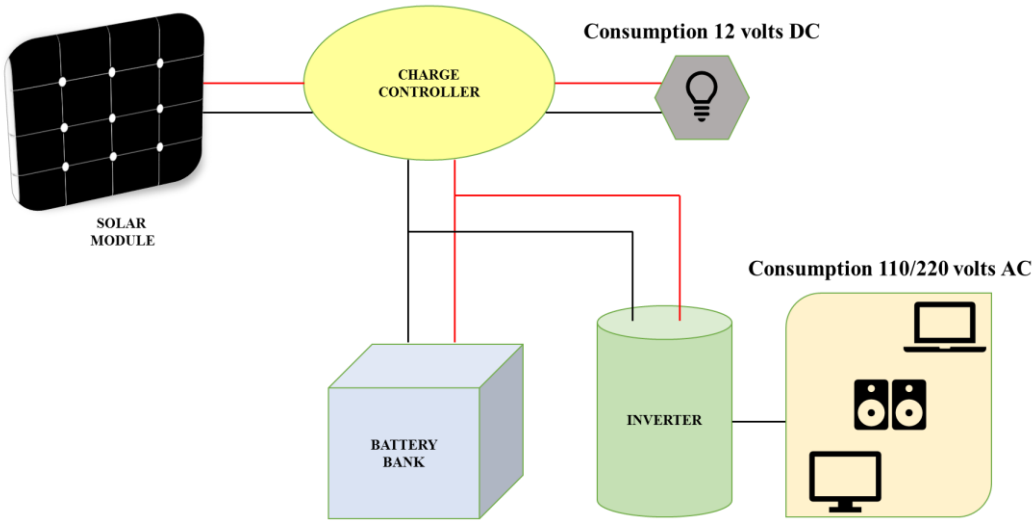

Figure 2.1. Parts of photovoltaic solar energy system [68].

2.1.4. Working Principle of Photovoltaics

PV cells works based on the junction principle effect. In a typical PV cell, semiconducting materials such as Ge and Si are firstly doped with the elements in Group 3 and Group 5, respectively. Then, these materials are used as p-type and n-type materials in PV cells. Doping process is therefore known as inserting another atom into the bulk crystal to modify the conductivity. To obtain p-typed material with a free positive charge (hole), silicon is doped with one of the elements in Group 3 like B or Ga. On the other hand, to produce n-type material with an extra electron, silicon is doped with any element in Group 5 such as P and As. After the end of doping process, p-type material tends to receive electrons whereas n-type material has a tendency to share their electrons. When these two materials are placed in contact with

each other, diffusion takes place on the surface between p-type and n-type materials. Due to the random motions of the free electrons, electrons in the n-type side start to diffuse across into the p-type side. Similarly, holes start to diffuse from the p-type side into the n-type side [69]. A space charge region, an area around the junction is generated due to such diffusions. When electrons fill each hole in the p-type side of the space charge region, negatively charged ions are generated in this side. On the other hand, positively charged ions are produced in the n-type side of the space charge region. An internal electric field is then created due to the existence of these oppositely charged ions and pushes an electron to enter the space charge zone [70]. Electrons produced by solar energy in the vicinity of the space charge zone can easily move to the n-type side. By making a connection with a metallic wire between n-type and p-type layers, the flow of these electrons from n-type side to the p-type side is obtained by crossing the space charge region [70]. Then, these electrons move to the external wire back to complete the circuit and a flow of electricity is generated.

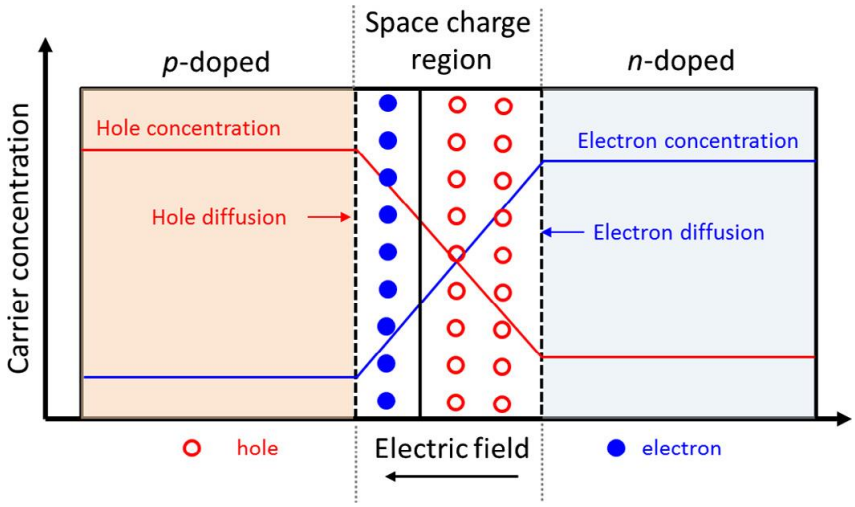

Figure 2.2. Working principle of a typical p-n junction [70].

2.1.5. Generations of Photovoltaics

In recent years, the energy need of society and the industry have been one of the major problems with developing and emerging technologies. To meet such a significant amount of energy need, the renewable and sustainable energy sources have been investigated as a permanent solution. Like wind energy, hydro energy or geothermal

energy, solar energy has played a key role to produce clean, sustainable, renewable and eco-friendly energy over the last two decades [68]. Although a lot of different types of PV devices have been designed and released to the market, the PV cell technologies are mainly divided into three generations. These generations are shown below:

1. 1st Generation PV cells;
2. 2nd Generation PV cells;
3. 3th Generation PV cell [61].

2.1.5.1. 1st Generation PV Cells

The production of the first generation of PV cells are dominated by single-junction PV cells based on silicon (Si) wafers and such PV cells can be produced from 100 to 200 μm thick wafers [71]. Since crystalline forms of Si is used as a main material, two type of PV cells are fabricated in such generation. These PV cells are shown below:

1. single-crystalline Si-based (sc-Si-based) PV cells;
2. multi-crystalline Si-based (mc-Si-based) PV cells [71].

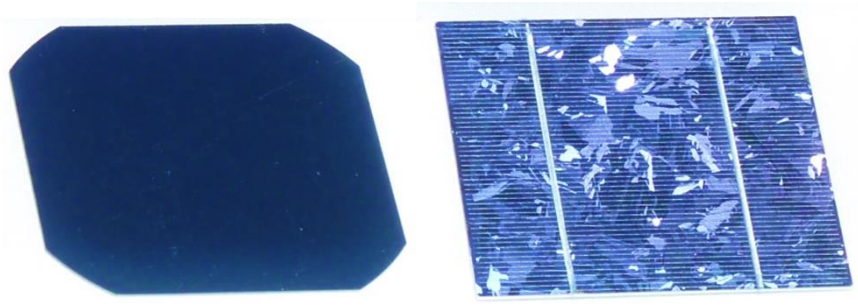

a **b**

Figure 2.3. ***a.*** Single-crystalline Si-based PV cell; ***b.*** Multi-crystalline Si-based PV cell [71].

Since Si is an inorganic material, the first-generation PV cells is also known as inorganic-based PV cells. The main source of Si is silica (SiO_2) which is the most

abundant mineral in the earth's crust; therefore, Si is primarily obtained by using silica.

There are several benefits of such generation. For instance, since Si is the second most abundant element in the earth's crust, it can easily meet the world's energy needs in the long term [68]. Also, eco-friendly solar cells can be utilized since crystalline Si shows non-toxic characteristic [72]. In addition, Si-based PV cells have high stability so that they can be used for many years without decreasing in their performance [68]. However, there are also some drawbacks of such PV cells. For example, the performance of the first-generation PV cells decreases by almost 20% at high temperatures [71]. Furthermore, the fabrication of flexible Si-based PV cells is not possible due to the crystalline form Si; therefore, they are fabricated in rigid forms. This flexibility drawback also affects the installation of such cells and they are generally built at restricted places like building roofs.

2.1.5.1.1. Single-Crystalline Si-Based (sc-Si-Based) PV Cells

Single-crystalline Si-based PV cells dominate the global PV cell market with a market share of 30%. This type of cells is generated by slicing wafer from a single extreme purity cylindrical crystal ingot. These wafers are sliced with octagonal shape in order to optimize the cell density. The purity of single-crystalline Si-based PV cells are crucial. Since their purity should be extremely high, suitable methods have been investigated. For this purpose, Czochralski process has been developed and used as the best method for many years [64]. The pure single-crystalline Si has a uniform blue black color [71].

The manufacturing cost of this type of PV cells is higher than the other PV cells since more expensive and more sophisticated procedures are needed to generate such cells. Single-crystalline Si possesses a band gap energy of 1.1 eV. After a lot of studies and trials, PCE of them have been increased to 25.3%. Moreover, the energy payback time (EPBT) of such cells is recorded as 4 years. Also, the average operational lifetime of them is measured as 30 years and this makes sc-Si-based PV cells viable. However, the performance of these PV cells decreases by 15% at high temperatures because the

temperature coefficient of power output (P_{max}) used to measure the percentage decrease in PCE with each degree rise in temperature from standard test condition (STC) is -0.5% [71]. Due to high energy needs in their life cycle, high manufacturing costs, long energy return time, and extreme ultra-purity material requirements with the perfect crystal structure, further studies have been investigated to eliminate these drawbacks and create better PV cells.

2.1.5.1.2. Multi-Crystalline Si-Based (mc-Si-Based) PV Cells

The need of manufacturing low cost PV cells in mass production scale led to the enhancement of new crystallization methods. In such case, the PV cells based on multi-crystalline Si appeared in the literature. Such cells include small crystals known as crystallites with visible crystal grain; therefore, they gain a metal-flake appearance [73]. Multi-crystalline Si-based PV cells are generated by sawing a square cast block of Si into bars and wafers respectively. Due to the production of the wafers in square shape, the minimum amount of Si is wasted during fabrication compared to the manufacturing of single-crystalline Si-based cells [71].

This new PV devices become more attractive since it provides more cost effective and less sophisticated manufacturing processes. Multi-crystalline Si-based PV cells dominate the PV cell market with a market share of 54%. Since this type of PV cells experienced rapid growth in PCE and decrease in cell cost, such cells reached the highest market share. Multi-crystalline Si has a band gap energy of 1.1 eV. After many investigations, PCE of them have been up to 21.9%. Moreover, EPBT of these cells is recorded as 3 years. Furthermore, the average operational lifetime of them is measured as 30 years and this makes sc-Si-based PV cells salable. However, the performance of these PV cells decreases by 20% at elevated temperatures since the temperature coefficient of power output (P_{max}) is -0.5% [71]. Given these realities, both scientists and manufacturers have looked for alternative materials and different device fabrications for producing lower cost PV cells.

2.1.5.2. 2nd Generation PV Cells

Second generation PV cells are resulted from the need of the production of cost effective PV cells. For such purpose, thin film PV technology based on the single junction device principle is developed by minimizing the material and energy usage. To obtain cost effective PV cell, these cells are also deposited on low cost substrates such as glass, plastic, and metal. There are several types of PV cells in this generation. These PV cells dominating the PV market are shown below:

1. Amorphous-Si (a-Si);
2. Gallium Arsenide (GaAs);
3. Cadmium Telluride (CdTe);
4. Copper Indium Gallium Selenide (CIGS) [71].

Since PV devices in this generation are manufactured in thin film form, they are also known as either thin film PV cells or thin film solar cells. The thickness of such film layers can be achieved in both a few micrometer (μm) and even in nanometer (nm) scale [74].

In recent years, the use of second generation PV cells has increased because they provide significant advantages compared to first generation PV cells. For example, by using the thin film PV cells, much smaller amount of active material compared to crystalline Si-based PV cells can be used to be able to absorb same amount of solar energy. Such PV technology also enables to fabricate highly flexible and light-weight PV cells [74]. Since less material is enough to manufacture of such PV cells, this generation cells are generally cheaper than the first-generation PV cells. Furthermore, there is no installation problem so that they can be easily integrated into many surfaces [74]. In addition, the performance of thin film PV cells is unaffected by high temperatures and shading as well. On the contrary, these cells show their best performance at high temperatures since the temperature coefficient of power output (P_{max}) is less than -0.25% [71].

2.1.5.2.1. Amorphous-Si (a-Si) PV Cells

In 1965, the first amorphous Si (a-Si) layer obtained by chemical vapor deposition was reported by Sterling and Swann [75]. However, the first amorphous Si-based PV cell was reported by Carlson 11 years later [72]. A very thin PV solar cells can be achieved by using 1 μm thick of a-Si in such cells and these cells can absorb 90% of the solar energy. When a-Si is compared with the crystalline counterparts, it is proven that a-Si shows higher solar energy absorption characteristic. Since Si atoms are placed randomly in their atomic structure, a-Si shows higher band gap energy of 1.7 eV than the crystalline-Si (1.1 eV). Furthermore, a-Si-based PV cells have good heat resistance; therefore, their performance does not decrease under both high temperature and shaded conditions. On the contrary, PV cells based on amorphous Si shows better performance at these conditions since the temperature coefficient of power output (-0.25%) is higher than the crystalline-based PV cells (-0.5%). After significant amount of trials, PCE of them have been increased to 13.6%. In addition, EPBT of these cells is recorded as 2 years and the average operational lifetime of them is measured as 25 years [71]. Although such PV cells provides a number of advantages than the crystalline counterparts, the modules produced by using a-Si-based PV cells become more fragile, heavier and larger than the modules generated by using the first-generation PV cells. In addition, such PV cells show less popularity in the global PV market when they are compared to the crystalline counterparts due to their lower power conversion efficiencies [72].

2.1.5.2.2. Gallium Arsenide (GaAs) PV Cells

GaAs PV cells are primarily made from gallium and arsenic. Gallium is obtained as a byproduct of Al and Zn refining exists rarely in the earth crust whereas As is common however highly toxic [71]. Luckily, GaAs shows stable and non-toxic characteristics. GaAs has a band gap energy ranging from 1.43 to 1.7 eV; therefore, they can absorb higher energy sunlight compared to crystalline Si-based PV cells. Moreover, each GaAs PV cell needs a few microns thick cell to absorb higher amount of solar energy than the first-generation PV cells since GaAs possesses high absorptivity. After many

studies, PCE of this type of cells has been increased to 29% and this is recorded as the highest PCE for any single junction PV cell. These cells demonstrate good heat and radiation resistivity. Furthermore, the temperature coefficient of power output (P_{max}) is measured as 0%. This value means that no performance loss is not observed at temperature rises. Moreover, EPBT of these cells is recorded as 18 months. Despite these advantages, GaAs PV cells share the global PV market with 1%. The main reason is due to their significantly high cost. Thus, they have been used for satellites and solar power cars applications [68].

2.1.5.2.3. Cadmium Telluride (CdTe) PV Cells

Cadmium obtained as a byproduct of industrial metals commonly exists in earth crust and shows extremely carcinogen properties. It is known as one of the six deadliest toxic materials in nature. Due to its fatal nature, there are strict rules established by Restriction of Hazardous Substances (ROHS) directive to prevent Cd and similar material usage [68]. Despite an extremely toxic nature of Cd, CdTe shows much more eco-friendly characteristics. Furthermore, CdTe demonstrates more stable and less soluble properties than Cd. On the other hand, Te is a very rare element; therefore, it causes an increase in the price of CdTe-based PV cells. CdTe-based PV cells exist in the global PV cell market with a market share of 6%. Such PV cells provides cheaper and simpler production than any Si-based PV cells, and other thin PV cells as well. CdTe shows a band gap energy of 1.5 eV. After significant research efforts, PCE of such cells has been increased to 21%. Moreover, EPBT of these cells is recorded as 8 months which is the lowest EPBT among any PV cell. The temperature coefficient of power output (P_{max}) is measured as 0%; therefore, they show very good performance at high temperatures. In addition, the average operational lifetime of GaTe-based PV cells is recorded as 20 years [71].

2.1.5.2.4. Copper Indium Gallium Selenide (CIGS) PV Cells

The CIGS PV cells are made by using vacuuming manufacturing method to deposit a thin layer (2 μm) Cu, In, Ga and Se on either glass or plastic connecting to electrodes on the front and back sides [71]. Ga-free variants of the semiconductor material are abbreviated as CIS. The generation cost is lower than the crystalline Si-based PV cells but higher than any other second generation PV cells [76]. CIGS-based PV cells have increased popularity due to introduction of number of promising PV cells to the market. CIGS possess a band gap energy of 1.45 eV [71]. Like in the CdTe-based PV cells, the temperature coefficient of power output (P_{max}) is measured as 0%. Thus, such solar cells can still show excellent performance at high temperatures but shading causes a slight decrease in their performance. Furthermore, EPBT of such cells is noted as 1 year. Because of these benefits, a lot of companies and research centers took special interest in them and they have worked to develop the lifecycle reliability and PCE of CIGS-based PV cells. They also have aimed to decrease the cost of these solar cells. However, the investments on these cells were seriously decreased after a number of major companies supporting the production of CIGS-based solar cells like Nanosolar and Solyndra pull out of the PV market. Due to the support of Solar Frontier, CIGS-based thin film solar cells continued to maintain their existence in the global PV market. Highest PCE recorded for CIGS materials is 20% [77].

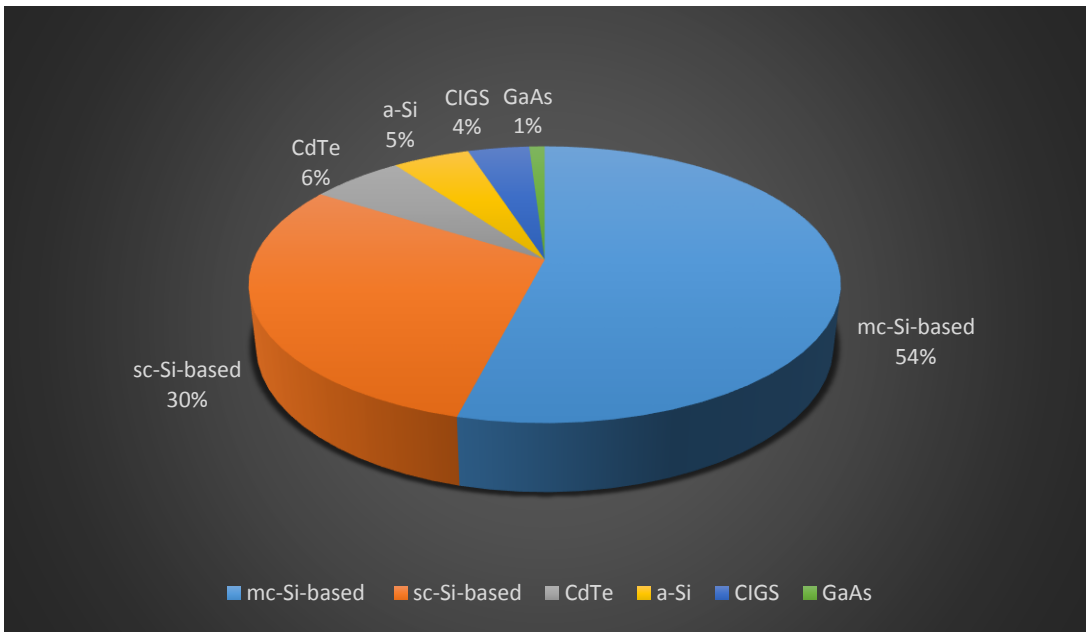

Figure 2.4. Market share of first/second generation PV cells (%) [71].

2.1.5.3. 3th Generation PV Cells

The manufacturing of any PV module requires developments in device with high PCE and good stability while using eco-friendly and cost-effective materials. Despite many advantages of previous generations, they release expensive solar cells to the market due to the needs to high temperature and vacuum conditions to manufacture these cells. Therefore, realization of a new generation of materials and devices were pursued. This generation of solar cells termed as emerging technology since it is still at experimental stage with little or no global PV market share. Third generation PV cells are manufactured by using solution processable materials such as organic small molecules, dye sensitized materials, polymers, perovskite materials and quantum dots [78]. There are various PV cells in this generation. The main PV cells are shown below:

1. dye-sensitized solar cells (DSCs);
2. quantum dot-sensitized solar cells (QDSC);
3. perovskite solar cells (PSCs);
4. organic solar cells (OSCs).

2.1.5.3.1. Dye-Sensitized Solar Cells (DSCs)

The first DSC was proposed by O'Regan and Grätzel in 1991; thus, such cells are also known as Grätzel cells [79]. In DSCs, ruthenium-based dyes, porphyrin-based dyes and non-metallic organic dyes are the most popular type of materials used as sensitizers. DSCs have been investigated to optimize the issues related to PCE, cost of production and environmental problems.

Dye-sensitized solar modules are produced with thin film cells [80]. The dyes show photovoltaic characteristics and the fabrication procedure does not need elaborate equipment. On the contrary, easy and simple procedure is used for manufacturing; therefore, DSCs have low cost. In addition, these cells provide a production with do-it-yourself (DIY) technique. The primary difference of DSCs compared to other solar cells is that the functional element (dye), responsible for the absorption of light is separated from the transport mechanism of the charge carriers. Therefore, there is no need to use pure material in fabrication so that it also leads to reduce the price of dye-sensitized solar devices. Because DSC materials like TiO_2 are abundant, cheap, eco-friendly and processable, a roll-to-roll (R2R) method can be applied to print DSCs on flexible substrates with a large amount of production [79]. Moreover, such PV cells show better performance under lower light intensities so that they DSCs are greatly suitable for indoor applications.

Besides increasing the efficiency of DSCs, the stability improvement has been also crucial need for manufacturing. For example, leakage of liquid electrolyte and degradation of Pt catalyst cause a significant decrease in stability [78]. To overcome these problems, liquid electrolyte was replaced with solid state hole transport material (HTM) whereas Pt catalyst was replaced with graphene materials possessing good electrochemical stability. However, DSCs are sensitive to air and moisture; therefore, the lifetime of DSCs could only be increased to 10 years [71]. Furthermore, the performance of such cells lowers at elevated temperatures. Because of this reason, DSCs are used for low temperature applications.

2.1.5.3.2. Quantum Dot-Sensitized Solar Cells (QDSCs)

As improvements in DSCs continue, an idea to replace organic dyes with any inorganic sensitizer leads to the emergence of QDSCs. Quantum dots are also defined as nano-sized semiconductor crystals with a narrow band gap and a high extinction coefficient [78]. Due to the low band gaps, QDSCs can absorb solar energy in the visible region. Also, because of the high extinction coefficient, the improvement in the performance of QDSCs is possible.

There are various benefits for QDSCs. One of these powerful advantages is that quantum dots are generated easily and resulting QDs show durable characteristics. Moreover, the optical band gaps of QDs can be adjusted. Furthermore, the generation of multiple electron-hole pairs per photon via hot electrons is possible because of the impact of ionization in the quantum dots. Due to the production of multiple charge carriers, at least two excitons can be produced by a single photon of energy higher than the band gap [81]. In addition, since QDs reduce the amount of possible dark currents, better performance of QDSCs can be obtained [78]. However, there are also some disadvantages of these type of cells. The primary drawbacks of QDSCs are the high recombination rate and the low charge collection efficiency. After making a lot of investigations, PCE of QDSCs has been increased to 13%. To increase the efficiency and overcome the drawbacks mentioned above, new studies like finding alternative QDs are being pursued.

2.1.5.3.3. Perovskite Solar Cells (PSCs)

Perovskite PV cells have emerged as an economically viable, new generation PV cells that have showed promising stability and efficiencies. These cells are prepared by thin film technology with a thickness of 1 μm [71]. Since few simple fabrication steps without including complex equipment are needed to manufacture PSCs, PV cells are quite cheap. Perovskite was originally named after the discovery of the mineral $CaTiO_3$ by Russian mineralogist L.A. Perovski [82]. Therefore, perovskites are also known as organometal halides abbreviated as ABX_3 and used as sensitizers in PSC

technology. A and B represent cations whereas X refers to an anion. A and B occupy the corner position. On the other hand, X stays at the face center of pseudo cubic unit cell.

The perovskite materials have several benefits; for instance, these materials provide minimal recombination losses [83]. With the usage of different anions and cations, the band gap can also be tuned. In addition, the perovskite active materials can be generated from cheap commonly available starting materials and they have high optical absorption. However, there are also some disadvantages of using perovskite materials. For example, they have a tendency to react with both moisture and oxygen; therefore, the resulting undesired products affect the stability of PSCs negatively. Also, the energy payback time (EPBT) of such cells is recorded as almost 3 months. Moreover, the usage of lead as one of the ingredients of perovskite materials causes serious environmental hazards.

Between the years of 2012 and 2015, significant amount of research performed on PSCs. The incredible increase in PCE from 9.8% to 20.2% has been observed. Such tremendous results obtained in just three years make them highly popular and promising solar cells. Nowadays, PCE of these solar cells has been increased to 22.1%.

2.1.5.3.4. Organic Solar Cells (OSCs)

Organic PV cells have emerged from the needs of manufacturing cost-effective, highly efficient and innovative thin film solar cells [74]. Either small organic molecules or conducting polymers are used as an active material [68]. Such conjugated molecules show excellent conductivity characteristics due to the delocalization of π-electrons on their backbones; therefore, these electrons provide easy movement through both intramolecular and intermolecular bonds [84]. Although conjugated molecules are obtained by complex and multi-step syntheses, OSC technology has benefitted from the unique properties of such molecules [85]. For example, the fabrication process is cheaper than the traditional silicon-based PV cells

since it needs low cost materials and simple technical challenges without requiring high temperature and vacuum conditions. Moreover, a significant amount of different conjugating molecules showing either similar or completely different solar cell characteristics can be produced by modifying just unit in the corresponding monomer structure. In other words, the band gap energy, the absorption spectra, the color, the processability, and the solubility of the resulting conjugated molecules can be changed by structural modifications [84]. Therefore, many parameters such as efficiency, stability and lifetime will be affected by OSCs prepared by these molecules. Besides the fabrication of thin PV cells (generally 100 nm), the OSC technology enables the production flexible, light weight and semitransparent solar cells [68]. These cells can be easily integrated into various devices such as field-effect transistors and electroluminescent diodes. However, such cells have a limited durability and polymeric materials short exciton diffusion length. In addition, the capability of converting solar energy into electricity is lower than the other solar cells. Although fullerene acceptors used in OSC as electron-accepting materials possess high electron mobilities, great tendency to accept electrons, and an ability to create a favorable nanoscale morphological network with electron-donating materials, they have some drawbacks such as crystallization tendency, difficulty in tuning the band gap, high cost, inflexible characteristics and poor absorption in the visible region [86]. Therefore, alternative acceptors to the fullerene-based acceptors have been investigated to overcome such these issues. By the discovery of small molecule and polymer non-fullerene acceptors, OSCs have been prepared based on these acceptors and the results of non-fullerene-based OSCs have shown encouraging PCEs of over 4%. Over the past decade, PCE of OSCs have been increased to 11.5%.

2.1.6. Working Principle of OSCs

Most of the organic PV cells have a planar-layered structure. Two electrodes are needed to complete the circuit. One of the electrodes must be either semi-transparent or transparent whereas the other electrode should be metal electrode. ITO-coated glass substrate has been used for many years as an optically transparent and electrically conductive anode electrode. Various metals such as Al, Ca, Au, and Mg are used as a

cathode in organic PV cells electrode but Al is more commonly used due to its low-cost price. Between these two different electrodes, the active layer is sandwiched. To obtain an efficient charge transfer, there should be a match between the work function of organic materials and the work function of commercial ITO (4.5-4.8 eV) [87].

When the sunlight is absorbed by a PV cell, an electron is firstly promoted from the HOMO to the LUMO of the organic-based donor to generate an exciton [84]. Such exciton is then diffused to the D/A interfaces with an electric field, followed by dissociation into free charge carriers including an electron and a hole. However, excitons have a limited lifetime; thus, this situation affects the efficiency of PV cells. The electron is then transported to the LUMO of the either fullerene-based or non-fullerene-based acceptor, followed by collection of the electron and the hole at metal and ITO-coated glass substrate electrodes, respectively.

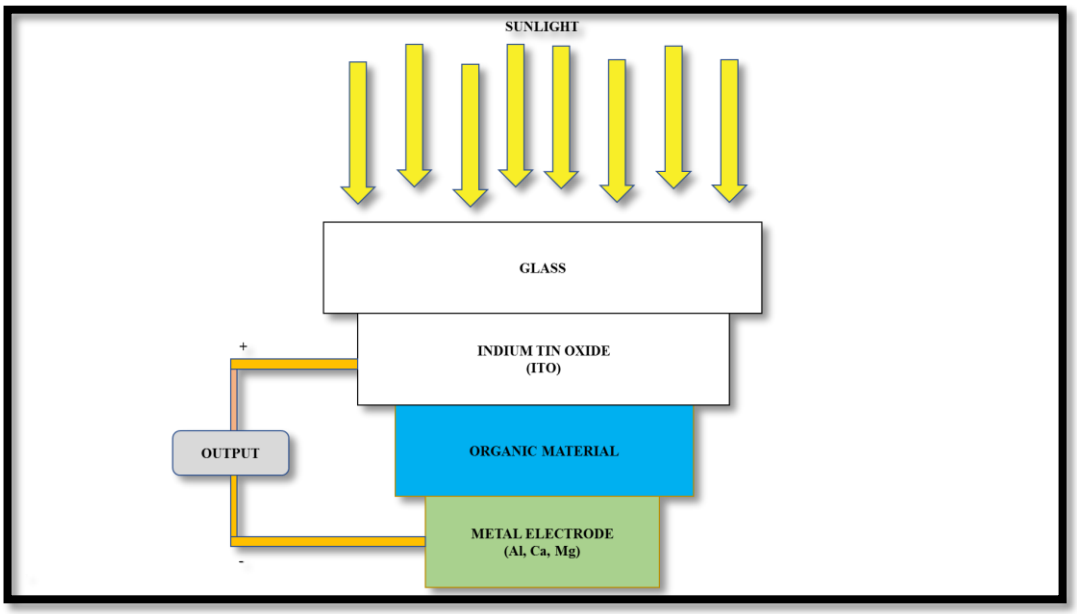

Figure 2.5. Working principle of a typical OSC [63].

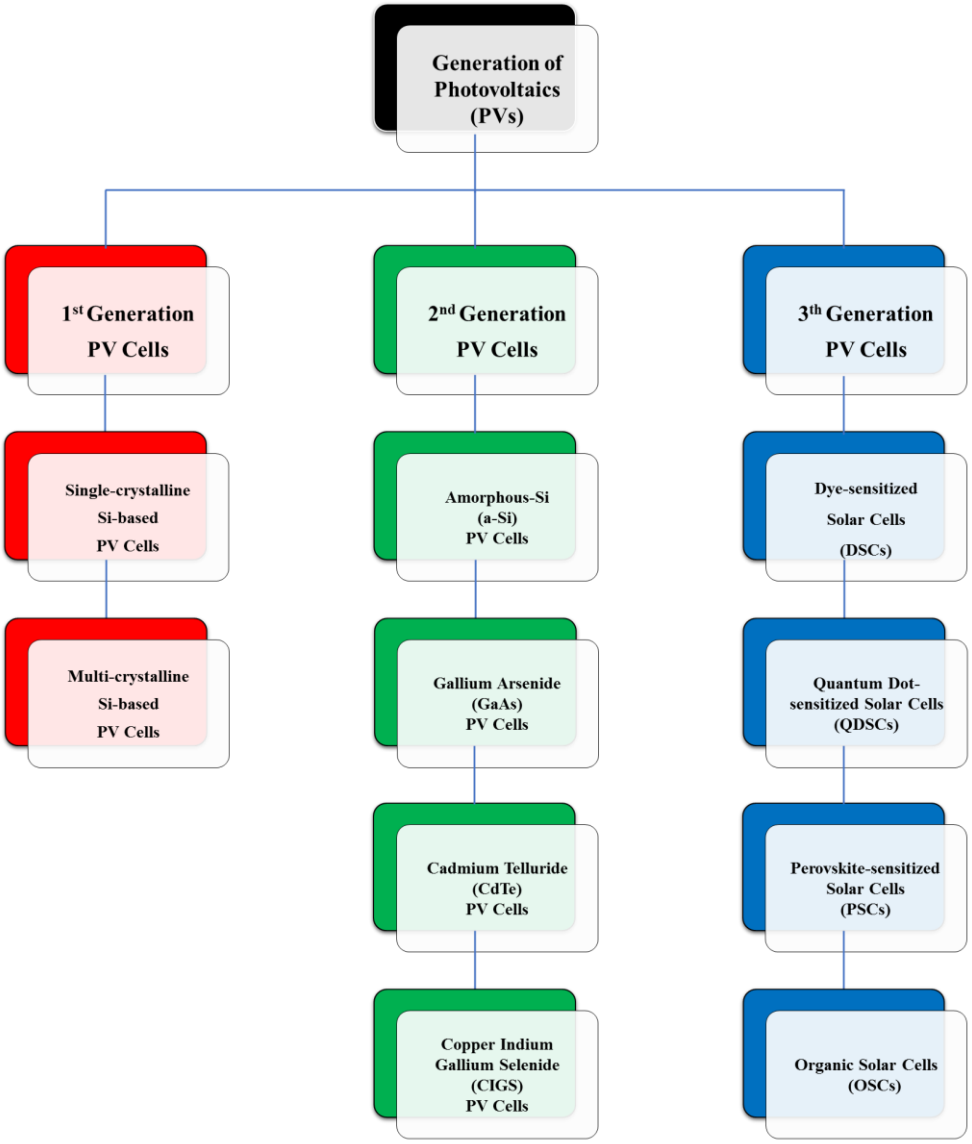

Figure 2.6. Classifications of solar cell generations.

2.1.7. Block Copolymerization, Tandem and Ternary Methods

Solar cells based on polymers still needs to be developed since the efficiency of PV cells has not caught the inorganic counterparts. The main reason is that a lot of materials utilized for PV cells absorb between 400 and 700 nm; therefore, a great amount of energy in the NIR portion of the solar energy could not be converted to electricity [88]. To extend the limited absorption spectra of organic semiconductors into the NIR region, some smart approaches have been developed. These approaches

not only enable to enhance the light harvesting properties but also increase the PV cell performances. The most common novel and promising approaches in organic solar cells are shown below:

i. block copolymerization [89];
ii. tandem method [90];
iii. ternary method [91].

2.1.7.1. Block Copolymerization

Block copolymers are known as macromolecules consisting of at least two homopolymer chains, or blocks, covalently connected to each other [92]. For example, when two polymer blocks (A and B) linked on one end, the resulting block copolymer is called as diblock copolymer. Between these two blocks, covalent bonds occur and these bonds prevent the bulk phase separation; therefore, polymer chains self-assemble into nanoscopic domains with a morphology depending on the ratio of A and B block lengths. Some of the most commonly observed diblock morphologies are body-centered, hexagonally packed cylinders and lamellae.

In a global PV market, clean, efficient, low-cost and stable solar cell production is very important [89]. Therefore, inexpensive materials usually are preferred for mass production. However, the PV cells based on these materials show low efficiencies. Because of this reason, some significant developments are still required to control the morphology on nanoscale. Designing and production of block copolymers can meet such need and several methodologies have been created. Although there are some promising theories covering the important role of block copolymerization in PV device, this is a new-born research area. Thus, a significant amount of works is needed to prove the power of block copolymerization in photovoltaic cells with high efficiencies.

2.1.7.2. Tandem Method

A typical organic tandem PV cell consists of at least two different individual single cells including donor-acceptor composites and one intermediate layer existing between these two devices [90]. The bottom sub-cell includes an acceptor and a donor that are either mixed or stacked on each other. On the other hand, although the intermediate layer was primarily based on a thin metallic layer, recent organic tandem PV cells have been designed with fully solution-processed interlayers. These layers are used as a recombination center. In other words, intermediate layer provides the recombination of electrons arriving from one sub-cell with holes arriving from the other cell. Tandem approach is aimed to solve two problems related to π-conjugated organic semiconductors. These problems resulted from the poor charge carrier mobility and the narrow absorption. After all trials with a combination of many different materials and intermediate layers, the efficiency of tandem PV cell has been increased to 12.8%. By achieving different kinds of functional intermediate layers, more efficient novel materials and much better matching of these materials with complimentary absorption spectra, more efficient tandem solar cells will be developed in near future.

2.1.7.3. Ternary Method

Initially, ternary PV cells were developed by preparing donor:multi-acceptor blends [85]. Later, it was realized that there was a mixing problem of polymers resulted from the powerful intermolecular attractions between multi-polymer chains and lack of entropic driving force for mixing them. Therefore, initial strategy has been changed with a new strategy and this time donor:multi-acceptor blends have been used to overcome the complexity of polymer mixing and create an optimal phase morphology. These renewable ternary PV cells include a wide bandgap polymer used as a host donor, a NIR sensitizer and either a fullerene or non-fullerene derivative used a host acceptor. In ternary PV cells, not only photon absorption range is improved but also charge transfer is facilitated while reducing recombination [91]. The highest

efficiency of ternary PV cell has been achieved as 12.1% with a wide range absorption.

2.1.8. Importance of NIR Absorption

The solar spectrum covers a highly broad wavelength centered between ultraviolet and near-IR (NIR) regions. In theory, the ideal band gap of conducting polymers should be close to 1.5 eV but the results indicate that many semiconducting polymers show optical band gap (E_g^{op}) either larger or around 2.0 eV [88]. Because of this reason, only visible light can be harvested. Due to such mismatch of the absorption to the solar spectrum, PV devices cannot work in full performance. One of the greatest strategies to lower E_g^{op} is to synthesize of novel NIR-absorbing polymers but it is possible with a logical design [93]. For example, polymers with a selenophene unit show stronger and broader absorption in the vis-NIR region rather than the polymers with other aromatic units such as EDOT, furan and thiophene. Therefore, designing light absorbing materials with the selenophene units is one of the logical approaches. Moreover, widening the absorption spectra of the polymers is possible by using one of three powerful methods mentioned above. When these are achieved, more efficient PV devices can be obtained so that more solar energy can be converted into electricity.

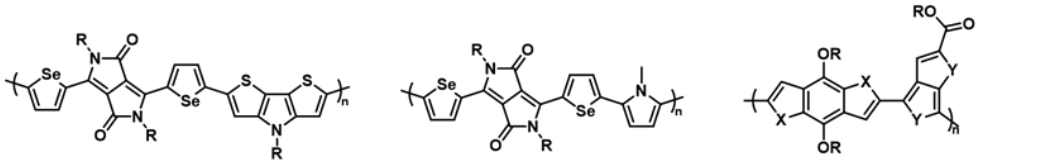

19

PDPPSPyS: PCE = 3.5
R = 2-ethylhexyl

20

PDPPSDTPS: PCE = 2.9
R = 2-ethylhexyl

21

PTB9: X = Y= S; PCE = 5.66
PSeB1: X = S, Y = Se; PCE = 5.47
PSeB2: X = Y = Se; PCE = 6.87
PSeB3: X = Se, Y = S; PCE = 6.13
R = 2-ethylhexyl

Figure 2.7. NIR-absorbing conjugated polymers in literature [93], [94].

2.1.9. Design Principle of TPD-Based Acceptor

Thieno[3,4-c]pyrrole-4,6-dione (TPD) is known as one of the promising electron-accepting unit (acceptor). This acceptor provides strong electron transporting due to ease of switching to its quinoid form and enables structural modifications. Since TPD is a symmetric molecule, the resulting D-A copolymer enhances the charge carrier mobility.

TPD-including acceptors have been polymerized with the common donor materials such as dithienogermole (DTG) and benzodithophene (BDT)-based materials. The results related to organic solar cell studies show that when TPD-containing polymers are blended with various fullerene derivatives, these cells show promising efficiencies (PCE>6%).

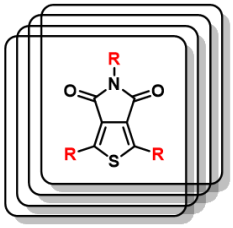

Figure 2.8. Thieno[3,4-c]pyrrole-4,6-dione (TPD) central unit.

There are several benefits of the usage of TPD acceptor unit. This unit excellently tunes the energy level, lowers the band gap of the resulting poly(TPD) derivatives and allows structural modifications at three positions.

Design principle of our work is to not only synthesize near-IR-absorbing random polymer including TPD, BTA and BDT units on the polymer backbone but also obtain high efficient bulk heterojunction solar cells with blending the resulting polymer with $PC_{71}BM$ on the active layer. In our design principle, TPD acceptor unit played the crucial role to shift the absorption spectrum of corresponding polymer to NIR region. Since it is known that selenophene has an effect to enable broad absorption centered at near-IR, we designed the TPD unit with selenophene unit. Also, to overcome the

solubility problem of random polymer, we made further design including the attachment of solubilizing group on TPD structure.

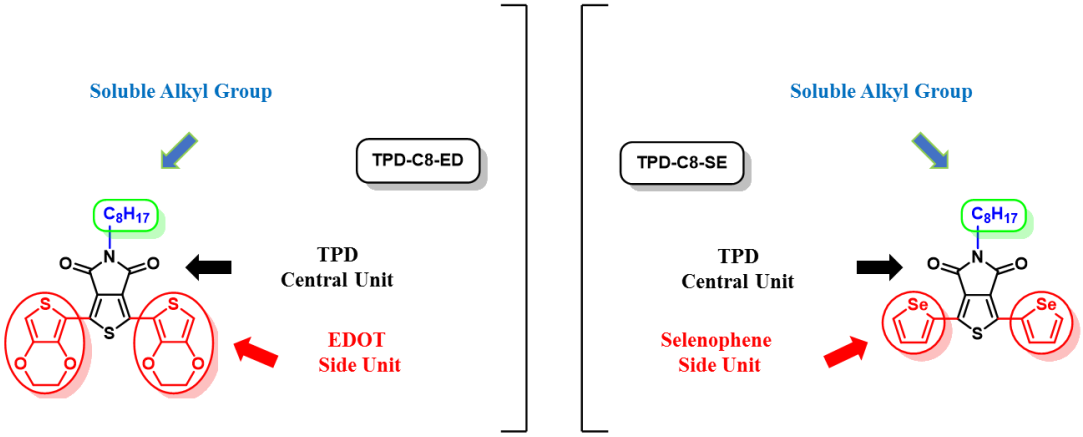

Figure 2.9. TPD-based monomers designed for organic electronics.

Higher performing TPD-based polymers usually have an TPD moiety with a linear alkyl chain and a donor moiety with a branched alkyl chain. Such TPD moiety provides sterically accessible interactions with the fullerene derivative. Unlike acceptor moiety, donor moiety sterically prevents the interactions with the fullerene derivatives. Based on this reality, we designed TPD-including acceptor moiety with a linear alkyl chain and purchased BDT-including donor moiety with a branched alkyl.

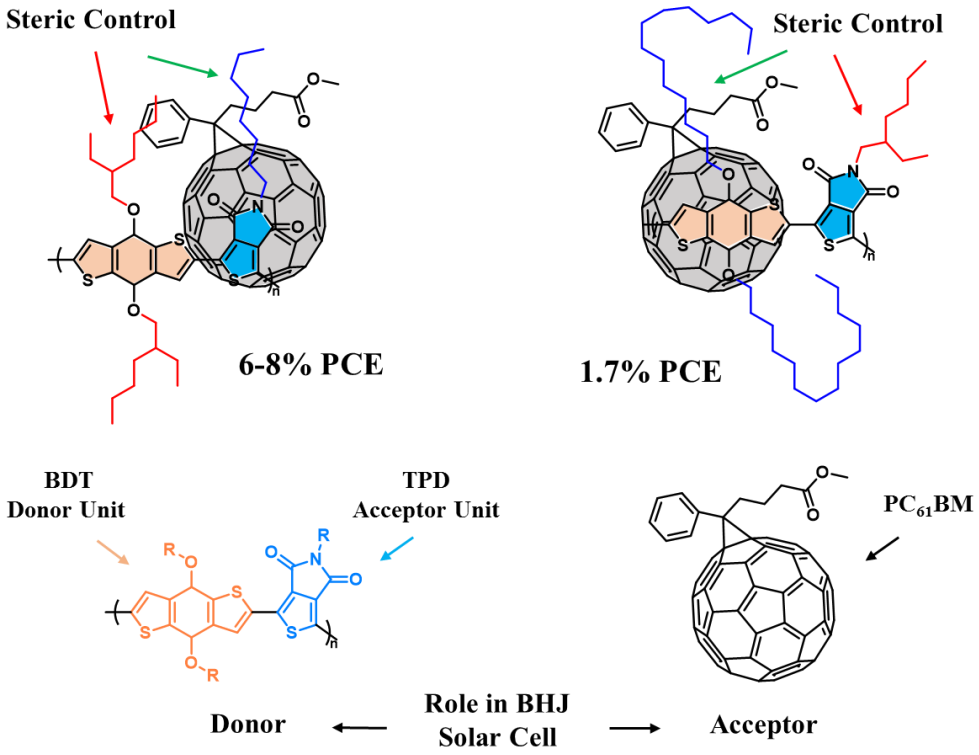

Figure 2.10. TPD-BDT-based polymers in literature [95].

2.1.10. Aim of This Work

Solubilizing groups such as alkyl and alkoxy groups and aromatic units such as furan and thiophene units can be linked to TPD central unit. The aim of this work was to synthesize two novel D-A-D type monomers (TPD-C8-ED and TPD-C8-SE) with Stille coupling and polymerized them with electrochemical polymerization and/or random copolymerization. Each monomer included thieno[3,4-c]pyrrole-4,6-dione (TPD) core unit having the same linear alkyl chains but they differed from each other with donor side units in their structure.

Since it was proved that EDOT unit show great charge-transfer properties, broad absorptions, fast switching times, and high air stabilities for electrochromic devices, the first monomer (TPD-C8-ED) was designed with EDOT building blocks in main chain. Moreover, linear alkyl chain was linked to the TPD side units to make resulting polymer soluble and processable. TPD-C8-ED was then electrochemically

polymerized and the electrochromic characteristics of homopolymer films of ELEC-PTPD-C8-ED were investigated in detail. On the other hand, the second monomer was designed with selenophene building blocks in main chain (TPD-C8-SE) because monomers with Se side units are promising materials for showing low band gap energy (<2.0 eV) and broad absorptions with covering NIR region. There is only one report of selenophene attached TPD unit being used in organic solar cells. A number of possible novel polymers can be synthesized using this material. Therefore, selenophene was integrated into TPD central unit as a side unit. In literature, BTA and BDT are also known as promising materials for preparing organic solar cells with a high efficiency. Therefore, random copolymer including TPD, BTA and BDT materials were designed and synthesized via Stille coupling in the presence of $Pd_2(dba)_3$ and $P(o\text{-}tol)_3$ catalysts. It was aimed to produce soluble and processable random copolymer films. This polymer was then used as donor whereas PCBM, the common and soluble derivative of fullerene was used as acceptor in preparation of organic solar cells. It was envisioned that PV cells prepared will show high efficiencies due to broad absorption that could be attained by incorporation of TPD-C8-SE in the polymer backbone.

2.2. EXPERIMENTAL

2.2.1. Materials & Methods

All commercially available reagents were purchased from Sigma-Aldrich, Across, Tokyo Chemical Industry Co., Ltd. (TCI), Merck and Solarmer, Energy Ink. At each stage argon was continuously given to the reaction flask unless otherwise specified. In addition, magnetic stirrer was always used. All anhydrous solvents such as THF, DMF, and toluene were either distilled over Na/benzophenone or supplied from a solvent purification system. The electrochemical properties of each monomer were investigated by using a Voltalab 50 potentiostat in a three-electrode system including Indium Tin Oxide (ITO) coated glass slide as the working electrode, platinum wire as the counter electrode, and Ag wire as the pseudo reference electrode calibrated against Fc/Fc+. Cyclic voltammetry measurements of TPD-based homopolymer and TPD-based random copolymer were made by using GAMRY Reference 600 potentiostat and such measurements were performed under argon atmosphere at room temperature. The spectroelectrochemical properties of TPD-based homopolymer was just analyzed by using Varian Cary 5000 UV-Vis spectrophotometer. HOMO and LUMO energy values were determined by taking NHE value as -4.75 eV in the formula of $HOMO = -(4.75 + 0.3 + E_{onset}^{ox})$ and $LUMO = -(4.75 + 0.3 + E_{onset}^{red})$. ^{1}H and ^{13}C NMR spectra of each product were identified by using Bruker Spectrospin Avance DPX-400 Spectrometer with using either $CDCl_3$ or DMSO as solvent. To make such analysis chemical shifts (δ / ppm) were reported relative to TMS as an internal reference. The accurate mass measurements for each novel product were made by HRMS by using Waters Synapt MS System. Silica Gel Column Chromatography with silica gel (Acros, 35–70 μm) filled in a suitable glass column was used to purify most of the products. TLC on glass plates coated with EMD silica gel 50 F254 was used to determine the best solvent system to make Silica Gel Column Chromatography and to confirm the identity of each product by either looking under ultraviolet light or staining $KMnO_4$ stain by exposing mild heating.

2.2.2. Synthesis of Two Novel TPD-Based Monomers

2.2.2.1. Synthetic Route for TPD-C8-ED

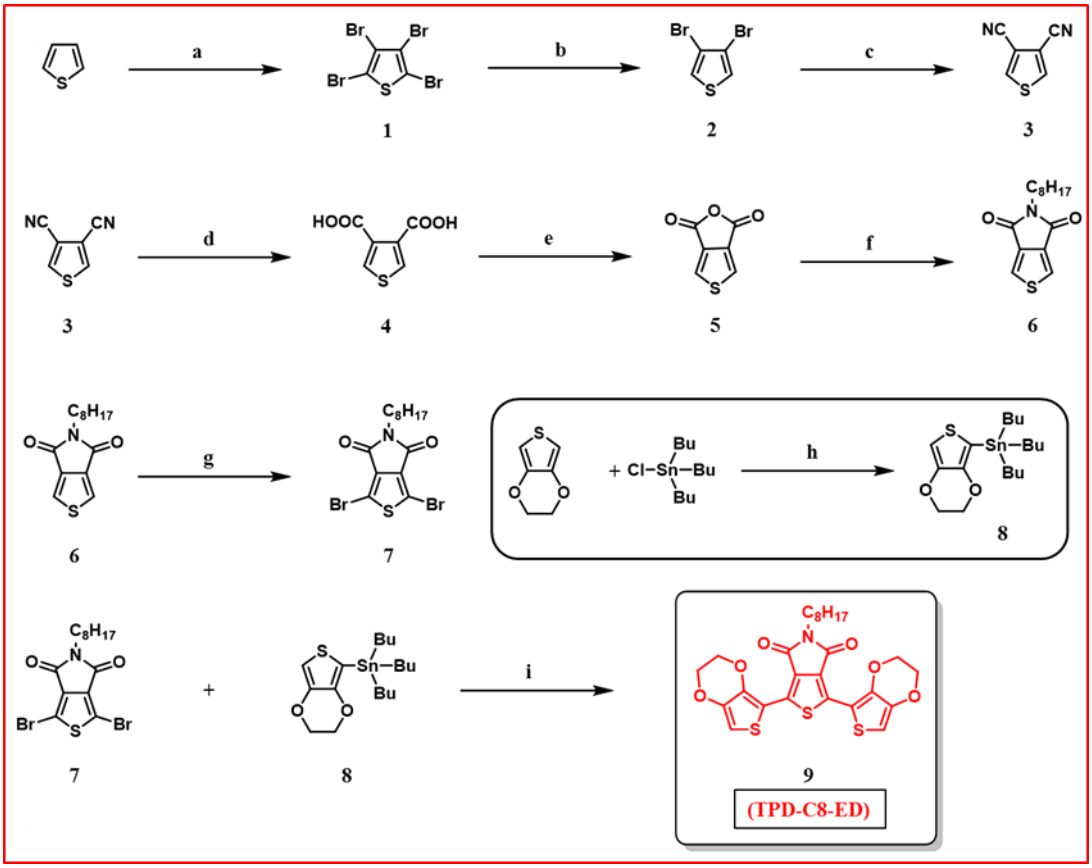

Figure 2.11. Reagents and conditions: ***a.*** HBr, Br_2, $CHCl_3$, 0 °C → 70 °C, 97%; ***b.*** AcOH-H_2O (v/v, 1:2), Zn, 120 °C, 87%; ***c.*** CuCN, DMF, 70 °C, 22%; ***d.*** 1) KOH, $(EtOH)_2$, 220 °C; 2) H_3O^+, 40%; ***e.*** A_2O, 140 °C, 97%; ***f.*** 1) $C_8H_{17}NH_2$, PhMe, 120 °C; 2) $SOCl_2$, 77 °C → rt, 80%; ***g.*** CF_3COOH, H_2SO_4, NBS, 0 °C → rt, 80%; ***h.*** THF, *n*-BuLi, -78 °C → rt, 97%; ***i.*** PhMe, $Pd(PPh_3)_4$, 115 °C, 75%.

2.2.2.2. Synthetic Route for TPD-C8-SE-BR

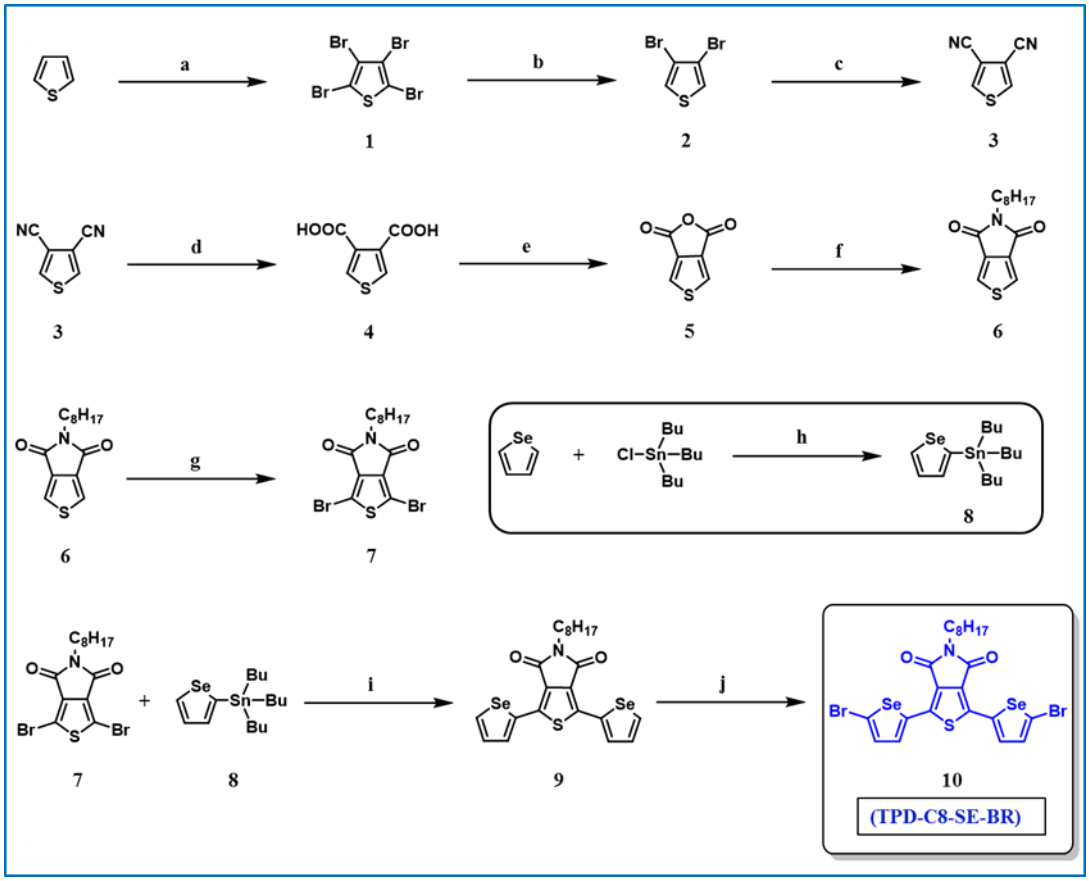

Figure 2.12. Reagents and conditions: ***a.*** HBr, Br_2, $CHCl_3$, 0 °C → 70 °C, 97%; ***b.*** AcOH-H_2O (v/v, 1:2), Zn, 120 °C, 87%; ***c.*** CuCN, DMF, 70 °C, 22%; ***d.*** 1) KOH, $(EtOH)_2$, 220 °C; 2) H_3O^+, 40%; ***e.*** A_2O, 140 °C, 97%; ***f.*** 1) $C_8H_{17}NH_2$, PhMe, 120 °C; 2) $SOCl_2$, 77 °C → rt, 80%; ***g.*** CF_3COOH, H_2SO_4, NBS, 0 °C → rt, 80%; ***h.*** THF, *n*-BuLi, -78 °C → rt, 97%; ***i.*** PhMe, $Pd(PPh_3)_4$, 115 °C, 97%; ***j.*** AcOH-$CHCl_3$ (v/v, 1:15), NBS, 0 °C → rt, 85%.

2.2.3. Experimental Procedures for Synthesis of TPD-C8-ED

2.2.3.1. 2,3,4,5-Tetrabromothiophene

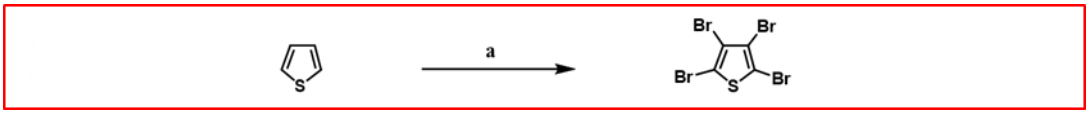

Figure 2.13. Reagents and conditions: ***a.*** HBr, Br_2, $CHCl_3$, 0 °C → 70 °C, 97%.

2,3,4,5-Tetrabromothiophene was prepared according to the literature [53]. Thiophene (10 g, 0.12 mol) was added into the reaction flask and dissolved in $CHCl_3$ (10 mL). To turn the toxic gas of HBr into the harmless NaBr salt, a trap filled with saturated NaOH solution was connected to the condenser. Then, the reaction mixture was placed in an ice/H_2O bath. When the temperature become 0 °C, $CHCl_3$ (40 mL) and Br_2 (37 mL, 0.71 mol) were introduced to the reaction flask dropwise with a dropping funnel and this mixture was stirred at 0 °C for 3 h. After that, the reaction mixture was warmed to room temperature and additional amount of Br_2 (5 mL) was added. The mixture was stirred at reflux temperature for 3 h and then cooled to room temperature. At this temperature, saturated solution of NaOH (150 mL) was poured to the reaction mixture dropwise to eliminate the excess amount of Br_2. The reaction mixture was stirred at 95 °C for 1 h and then cooled to room temperature. Precipitation of yellow crystals was observed. These crystals were filtered and added into the separatory funnel with H_2O. The aqueous phase was extracted with DCM several times. The combined organic layers were then dried over anhydrous Na_2SO_4. After filtration, the solvent was removed under reduced pressure. The product was recrystallized from methanol and the crystals were washed with cold MeOH several times. The target product was obtained purely as white crystals (46 g, 97%): ^{3}C-NMR (100 MHz, $CDCl_3$): δ (ppm) 116.97, 110.31.

2.2.3.2. 3,4-Dibromothiophene

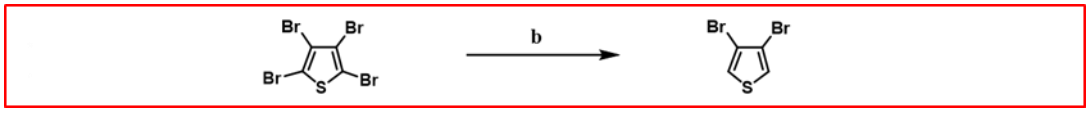

Figure 2.14. Reagents and conditions: ***b.*** AcOH-H_2O (v/v, 1:2), Zn, 120 °C, 87%.

3,4-Dibromothiophene was prepared according to the literature [53]. Under argon atmosphere AcOH (20 mL) and H_2O (40 mL) were added into the reaction flask which was equipped with Dean-Stark trap. At a different flask 2,3,4,5-tetrabromothiophene (25 g, 0.063 mmol) and Zn dust (13 g, 0.20 mol) were mixed homogenously. This solid mixture was added into the reaction flask portionwise over 45 minutes. Then, the reaction mixture was stirred at 120 °C for 24 h. The target product was purely collected in the trap as colorless liquid (13 g, 87%): ^{1}H-NMR (400 MHz, $CDCl_3$): δ (ppm) 7.31 (s, 2H); ^{13}C-NMR (100 MHz, $CDCl_3$): δ (ppm) 123.80, 113.99.

2.2.3.3. 3,4-Dicyanothiophene

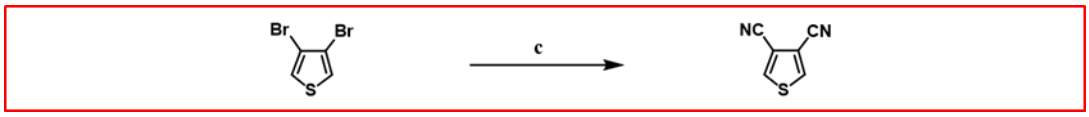

Figure 2.15. Reagents and conditions: ***c.*** CuCN, DMF, 70 °C, 22%.

3,4-Dicyanothiophene was prepared according to the literature [53]. Under argon atmosphere 3,4-dibromothiophene (5.04 g, 20.8 mmol) and CuCN (5.38 g, 60.1 mmol) were added to the reaction flask and dissolved in DMF (8 mL). This mixture was stirred at 160 °C for 24 h and then cooled to room temperature. Anhydrous $FeCl_3$ (33.5 g, 207 mmol) in HCl (2 M) was added to the reaction flask dropwise with a dropping funnel. This mixture was stirred at 70 °C for 1 h and then cooled to room temperature. Reddish-brown sticky mixture was filtered. H_2O was then added to the residue and the aqueous layer was extracted with DCM several times. The combined organic layers were washed with HCl (6 M) two times. At this stage, it was observed that the reddish-brown color passed to the acid layer and the color of organic layer become yellow. Then, the combined organic layers were washed with Na_2CO_3 and

H_2O two times respectively. All organic layers were dried over anhydrous Na_2SO_4. After filtration, the volatiles were removed under reduced pressure. The resulting yellow solid was then purified by column chromatography (SiO_2, Hexane 1:1 DCM). The target product was obtained as white solid (0.60 g, 22%): ^{1}H NMR (400 MHz, $CDCl_3$): δ (ppm) 8.08 (s, 2H); ^{13}C NMR (400 MHz, $CDCl_3$): δ (ppm) 136.93, 113.13, 111.71.

2.2.3.4. Thiophene-3,4-dicarboxylic acid

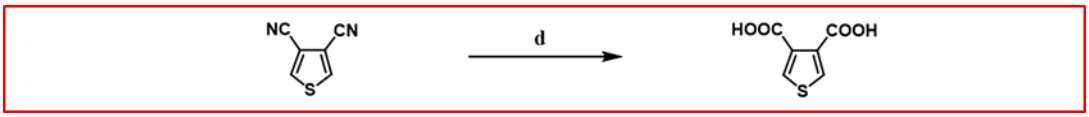

Figure 2.16. Reagents and conditions: ***d.*** 1) KOH, $(EtOH)_2$, 220 °C; 2) H_3O^+, 40%.

Thiophene-3,4-dicarboxylic acid was prepared according to the literature [53]. Under argon atmosphere 3,4-dicyanothiophene (600 mg, 4.47 mmol), KOH (1.63 g, 29.1 mmol) and ethylene glycol (7.2 mL) were added into the reaction flask. This mixture was stirred at 220 °C for 24 h and then cooled to room temperature. H_2O was added to the residue and the aqueous layer was extracted with diethyl ether three times. Then, the water layer was separated and poured in a cold H_2O. At this temperature HCl (12M) was added into the same beaker. The acidified layer was extracted with diethyl ether three times. The combined organic layers were dried over anhydrous Na_2SO_4 and filtered. After that, the solvent was removed under reduced pressure. The resulting bright brown solid was recrystallized from water. The target product was obtained as white crystals (0.30 g, 40%): ^{1}H NMR (400 MHz, $CDCl_3$): δ (ppm) 10.48 (s, 2H), 8.22 (s, 2H); ^{13}C NMR (400 MHz, $CDCl_3$): δ (ppm) 164.41, 133.83, 133.64.

2.2.3.5. 1H,3H-Thieno[3,4-c]furan-1,3-dione

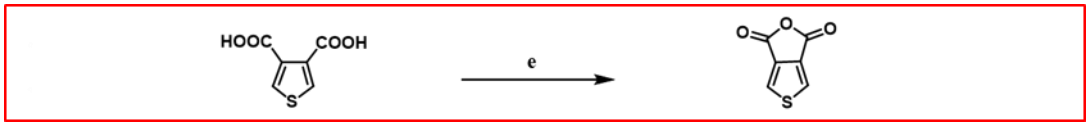

Figure 2.17. Reagents and conditions: ***e.*** A_2O, 140 °C, 97%.

1H,3H-Thieno[3,4-c]furan-1,3-dione was prepared according to the literature [96]. Thiophene-3,4-dicarboxylic acid (1.5 g, 8.7 mmol) was added into the reaction flask filled with argon and dissolved in acetic anhydride (45 mL). The reaction mixture was stirred at 140 °C for 24 h and then cooled to room temperature. Acetic anhydride was removed under reduced pressure. The product was recrystallized from toluene several times. The target product was obtained as brown crystals (1.3 g, 97%): ^{1}H NMR (400 MHz, $CDCl_3$): δ 8.10 (s, 2H); ^{13}C NMR (100 MHz, $CDCl_3$): δ 156.36, 135.16, 129.39.

2.2.3.6. 5-Octyl-4H-thieno[3,4-c]pyrrole-4,6(5H)-dione

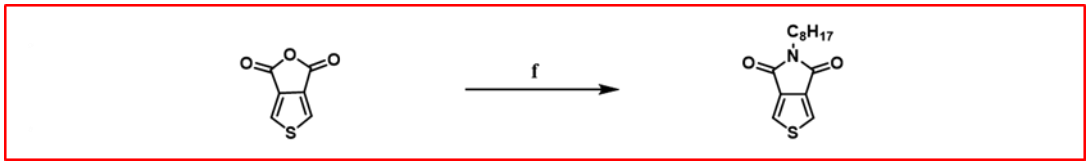

Figure 2.18. Reagents and conditions: ***f.*** 1) $C_8H_{17}NH_2$, PhMe, 120 °C; 2) $SOCl_2$, 77 °C → rt, 80%.

5-Octyl-4H-thieno[3,4-c]pyrrole-4,6(5H)-dione was prepared according to the literature [97]. Under argon atmosphere 1H,3H-thieno[3,4-c]furan-1,3-dione (1.3 g, 8.5 mmol) was added into the reaction flask and dissolved in anhydrous toluene (90 mL). Then, n-octylamine (2.0 mL, 12 mmol) was introduced to the same reaction flask. The reaction mixture was stirred at 115 °C for 24 h and then cooled to room temperature. Toluene was removed under reduced pressure. 4-(octylcarbamoyl)thiophene-3-carboxylic acid was obtained as brown solid and used freshly for the next stage without making any further purification. Under argon atmosphere it was dissolved in $SOCl_2$ (60 mL). The reaction mixture was stirred at 77 °C for 3 h and then cooled to room temperature. $SOCl_2$ was removed under reduced

pressure carefully since it was a very toxic liquid. The crude product was then purified by column chromatography (SiO_2, Hexane 2:1 DCM). The target product was obtained as white crystals (1.8 g, 80%): ^{1}H NMR (400 MHz, $CDCl_3$): δ 7.79 (s, 2H), 3.57 (t, *J* = 7.4 Hz, 2H), 1.61 (quin, J = 7.1 Hz, 2H), 1.32 – 1.20 (m, 10H), 0.83 (t, *J* = 6.6 Hz, 3H); ^{13}C NMR (100 MHz, $CDCl_3$): δ 162.64, 136.69, 125.43, 38.49, 31.76, 29.15, 28.47, 26.86, 22.61, 14.07.

2.2.3.7. 1,3-Dibromo-5-octyl-4H-thieno[3,4-c]pyrrole-4,6(5H)-dione

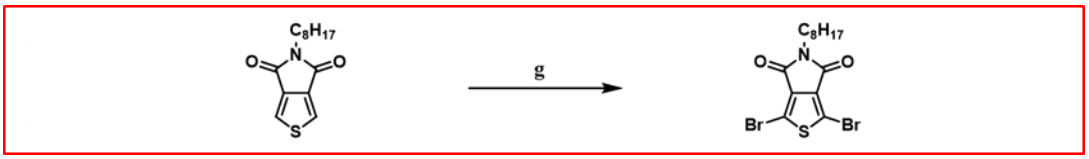

Figure 2.19. Reagents and conditions: ***g.*** CF_3COOH, H_2SO_4, NBS, 0 °C → rt, 80%.

1,3-Dibromo-5-octyl-4H-thieno[3,4-c]pyrrole-4,6(5H)-dione was prepared according to the literature . Under argon atmosphere 5-octyl-4H-thieno[3,4-c]pyrrole-4,6(5H)-dione (700 mg, 264 mmol) was added into the reaction flask and dissolved in TFA (9 mL) and H_2SO_4 (3 mL). Then, NBS (1.41 g, 7.91 mmol) was added portionwise and the reaction mixture was stirred at room temperature for 24 h. H_2O was poured into the reddish orange residue and the mixture was extracted with DCM several times. The combined organic layers were dried over anhydrous Na_2SO_4 and filtered. The residue was then purified by column chromatography (SiO_2, Hexane 1:1 DCM). The target product was obtained as white crystals (1.8 g, 80%): ^{1}H NMR (400 MHz, $CDCl_3$): δ 3.55 (t, *J* = 7.3 Hz, 2H), 1.59 (quin, J = 7.2 Hz, 2H), 1.24 (dd, *J* = 8.1 Hz, 10H), 0.83 (t, *J* = 6.6 Hz, 3H); ^{13}C NMR (101 MHz, $CDCl_3$) δ 162.63, 136.66, 125.46, 38.47, 31.75, 29.15, 28.46, 26.86, 22.61, 14.07.

2.2.3.8. Tributyl(2,3-dihydrothieno[3,4-b][1,4]dioxin-5-yl)stannane

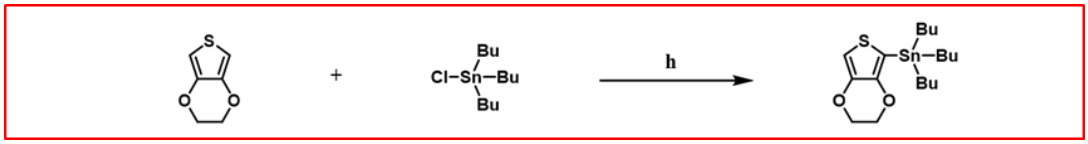

Figure 2.20. Reagents and conditions: ***h.*** THF, *n*-BuLi, -78 °C → rt, 99%.

For experimental procedure of stannylated EDOT, see Chapter 1 Section 2.4.5.

2.2.3.9. 1,3-Bis(2,3-dihydrothieno[3,4-b][1,4]dioxin-5-yl)-5-octyl-4H-thieno[3,4-c]pyrrole-4,6(5H)-dione

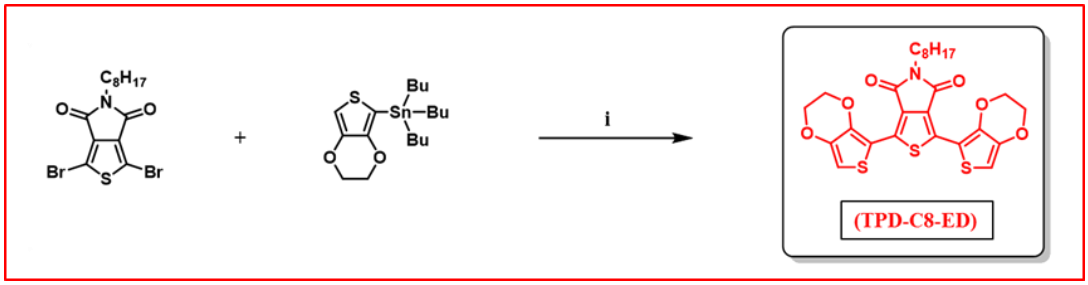

Figure 2.21. Reagents and conditions: ***i.*** PhMe, $Pd(PPh_3)_4$, 115 °C, 75%.

TPD-C8-ED was prepared according to the literature [98]. Under argon atmosphere 1,3-dibromo-5-octyl-4H-thieno[3,4-c]pyrrole-4,6(5H)-dione (300 mg, 0.71 mmol), 2-(tributylstannyl)-3,4-ethylenedioxythiophene (900 mg, 2.09 mmol) and tetrakis(triphenylphosphine)palladium(0) (82 mg, 0.071 mmol) were added to the reaction flask and dissolved in anhydrous toluene (20 mL). This mixture was stirred at 115 °C for 24 h and then cooled to room temperature. Toluene was removed under reduced pressure. H_2O was added to the resulting solid mixture and the aqueous layer was extracted with DCM several times. The combined organic layers were washed with brine and dried over anhydrous Na_2SO_4. After filtration, the solvent was removed under reduced pressure. Then, the unpurified solid mixture was purified by column chromatography (SiO_2, Hexane 1:2 DCM). The target product was obtained as yellow crystals (0.29 g, 75%): ^{1}H NMR (400 MHz, $CDCl_3$): δ 6.52 (s, 2H), 4.41 - 4.16 (m, 8H), 3.57 (t, *J* = 7.4 Hz, 3H), 1.62 (quin, J = 7.2 Hz, 2H), 1.31 (dd, *J* = 8.2 Hz, 10H),

0.90 (t, *J* = 6.6 Hz, 3H): ^{13}C NMR (100 MHz, $CDCl_3$): δ 162.88, 141.04, 140.93, 134.42, 126.48, 109.56, 103.05, 65.47, 64.23, 38.36, 31.79.

2.2.4. Experimental Procedures for Synthesis of TPD-C8-SE-BR

The first seven reaction covered the same synthetic pathway including same products. By considering this situation, each product was synthesized in a large amount. After 1,3-dibromo-5-octyl-4H-thieno[3,4-c]pyrrole-4,6(5H)-dione was synthesized, the similar reaction route was followed as mentioned in the literature to obtain the desired 1,3-bis(5-bromoselenophen-2-yl)-5-octyl-4H-thieno[3,4-c]pyrrole-4,6(5H)-dione.

2.2.4.1. Tributyl(selenophen-2-yl)stannane

Figure 2.22. Reagents and conditions: ***h.*** THF, *n*-BuLi, -78 °C → rt, 97%.

Tributyl(selenophen-2-yl)stannane was prepared according to the literature [99]. Under an argon atmosphere selenophene (1.00 g, 7.63 mmol) was added into the reaction flask and dissolved in anhydrous THF (25 mL). Then, the reaction mixture was cooled to -78 °C and *n*-BuLi (3.4 mL, 8.5 mmol; 2.5 M in hexane) was added dropwise over 30 minutes. The reaction mixture was stirred at -78 °C for 1.5 h. Tributyltin chloride (2.5 mL, 9.2 mmol) was poured into the reaction flask dropwise at -78 °C. The reaction mixture was warmed to the room temperature and stirred overnight. Then, H_2O was added into the reaction mixture and the aqueous phase was extracted with DCM three times. The combined organic layers were dried over anhydrous Na_2SO_4 and filtered. The target was removed under reduced pressure. The crude product was obtained as brown liquid (3.1 g, 97%) and used without making any further purification.: ^{1}H NMR (400 MHz, $CDCl_3$): δ 8.62 – 8.24 (m, 1H), 7.66 – 7.47 (m, 2H), 1.73 – 1.54 (m, 6H), 1.46 – 1.31 (m, 6H), 1.29 – 1.06 (m, 6H), 0.98 –

0.88 (m, 9H); ^{13}C NMR (100 MHz, $CDCl_3$): δ 143.58, 137.90, 135.30, 130.54, 29.00, 27.30, 13.68, 11.14.

2.2.4.2. 5-Octyl-1,3-di(selenophen-2-yl)-4H-thieno[3,4-c]pyrrole-4,6(5H)-dione

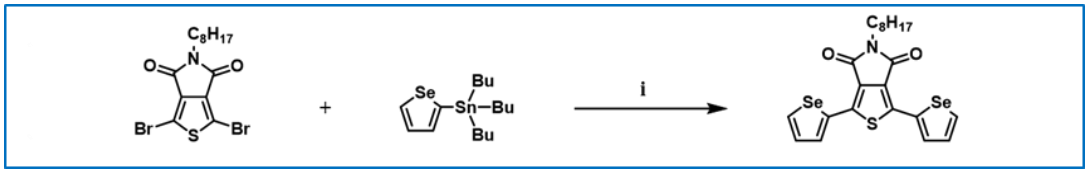

Figure 2.23. Reagents and conditions: ***i.*** PhMe, $Pd(PPh_3)_4$, 115 °C, 97%.

5-Octyl-1,3-di(selenophen-2-yl)-4H-thieno[3,4-c]pyrrole-4,6(5H)-dione was prepared according to the literature [98]. Under argon atmosphere 1,3-dibromo-5-octyl-4H-thieno[3,4-c]pyrrole-4,6(5H)-dione (300 mg, 0.71 mmol), tributyl(selenophen-2-yl)stannane (900 mg, 2.14 mmol) and tetrakis(triphenylphosphine)palladium(0) (82.0 mg, 0.071 mmol) were added into the reaction flask and dissolved in anhydrous toluene (20 mL). The reaction mixture was stirred at 115 °C for 24 h and then cooled to room temperature. Toluene was removed under reduced pressure. The target was then directly purified by column chromatography (SiO_2, Hexane 1:1 DCM). The crude product was obtained as yellow crystals (0.36 g, 97%): ^{1}H NMR (400 MHz, $CDCl_3$): δ 8.11 (d, *J* = 5.6 Hz, 2H), 7.76 (d, *J* = 3.9 Hz, 2H), 7.21 (dd, *J* = 5.7, 3.9 Hz, 2H), 3.54 (t, *J* = 7.5 Hz, 2H), 1.63 (quin, J = 7.3 Hz, 2H), 1.35 – 1.21 (m, 10H), 0.86 (t, *J* = 6.5 Hz, 3H); ^{13}C NMR (100 MHz, $CDCl_3$): δ 162.52, 138.70, 136.48, 135.73, 131.50, 130.15, 127.72, 38.49, 31.84, 29.25, 28.57, 27.05, 22.69, 14.17.

2.2.4.3. 1,3-Bis(5-bromoselenophen-2-yl)-5-octyl-4H-thieno[3,4-c]pyrrole-4,6(5H)-dione

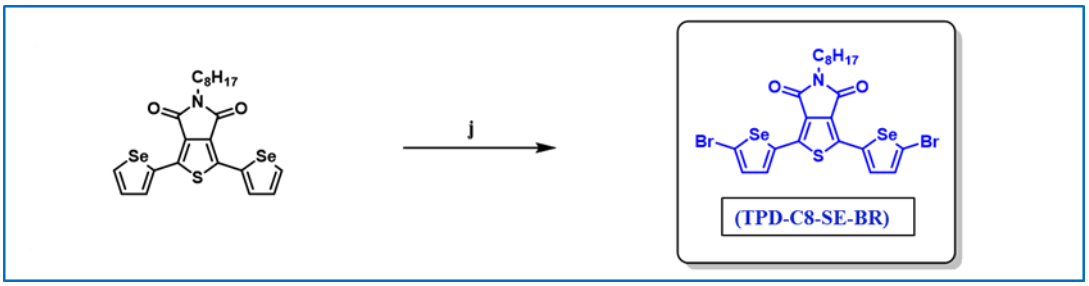

Figure 2.24. Reagents and conditions: ***j.*** AcOH-$CHCl_3$ (v/v, 1:15), NBS, 0 °C → rt, 85%.

TPD-C8-SE-BR was prepared according to the literature [98]. Under argon atmosphere 5-octyl-1,3-di(selenophen-2-yl)-4H-thieno[3,4-c]pyrrole-4,6(5H)-dione (0.20 g, 0.38 mmol) was added into the reaction flask and dissolved in $CHCl_3$ (10 mL) and glacial acetic acid (0.2 mL). Then, the reaction mixture was placed in an ice/H_2O bath. When the temperature become 0 °C, NBS (0.14 g, 0.80 mmol) was introduced to the reaction flask portionwise over 30 min. The reaction mixture was stirred at 0 °C for 4 h. Ice/H_2O bath was then removed and the reaction was warmed to room temperature. $CHCl_3$ and glacial acetic acid were removed under reduced pressure. H_2O was added into the reaction mixture and the aqueous phase was extracted with DCM several times. The combined organic layers were dried over anhydrous Na_2SO_4 and filtered. The target was then purified by column chromatography (SiO_2, Hexane 2:1 DCM). The crude product was obtained as white crystals (0.22 g, 85%): ^{1}H NMR (400 MHz, $CDCl_3$): δ 7.37 (d, *J* = 4.2 Hz, 2H), 7.17 (d, *J* = 4.3 Hz, 2H), 3.55 (t, *J* = 7.4 Hz, 2H), 1.62 (quin, J = 7.2 Hz, 2H), 1.35 – 1.24 (m, 10H), 0.86 (t, *J* = 6.4 Hz, 3H); ^{13}C NMR (100 MHz, $CDCl_3$) δ 162.50, 138.12, 137.62, 133.37, 130.74, 127.91, 122.64, 38.62, 31.80, 29.20, 28.49, 26.99, 22.65, 14.12.

2.3. RESULTS AND DISCUSSION

2.3.1. TPD-Based Polymer Syntheses

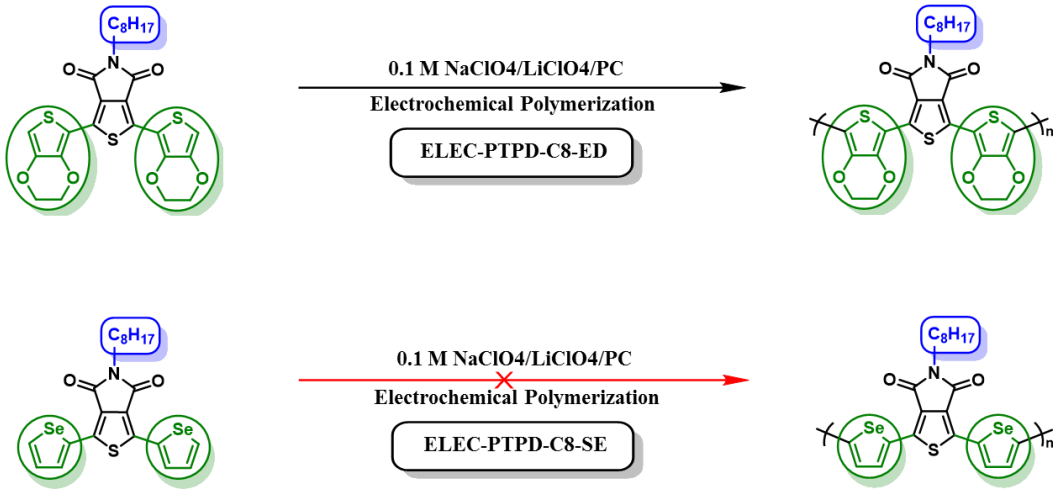

Figure 2.25. Electropolymerization pathway of TPD-C8-ED and TPD-C8-SE.

Brominated TPD a linear alkyl chain, stannylated EDOT and stannylated selenophene were known in literature. TPD-C8-ED and TPD-C8-SE monomers were synthesized via Stille coupling with using tetrakis(triphenylphosphine)palladium(0) catalyst. Homopolymer films of TPD-C8-ED and TPD-C8-SE tried to be produced by electrochemical polymerization and then electrochemical, spectroelectrochemical and kinetic characteristics of each polymer were aimed to be studied. However, only TPD-C8-ED showed electrochromic properties; therefore, just ELEC-PTPD-C8-ED was characterized with related electrochromic studies. On the other hand, TPD-C8-SE was used for further random copolymerization with benzo[d][1,2,3]triazole-based (BTA-based) acceptor and benzo[1,2-b:4,5-b′]dithiophene-based (BDT-based) donor. The aim of designing this random copolymer was to produce random copolymers with strong absorption in visible and NIR region, solubility and processability for PV cell applications.

2.3.2. Random Copolymerization of TPD-C8-SE-BR with BTA-Based Acceptor and BDT-Based Donor

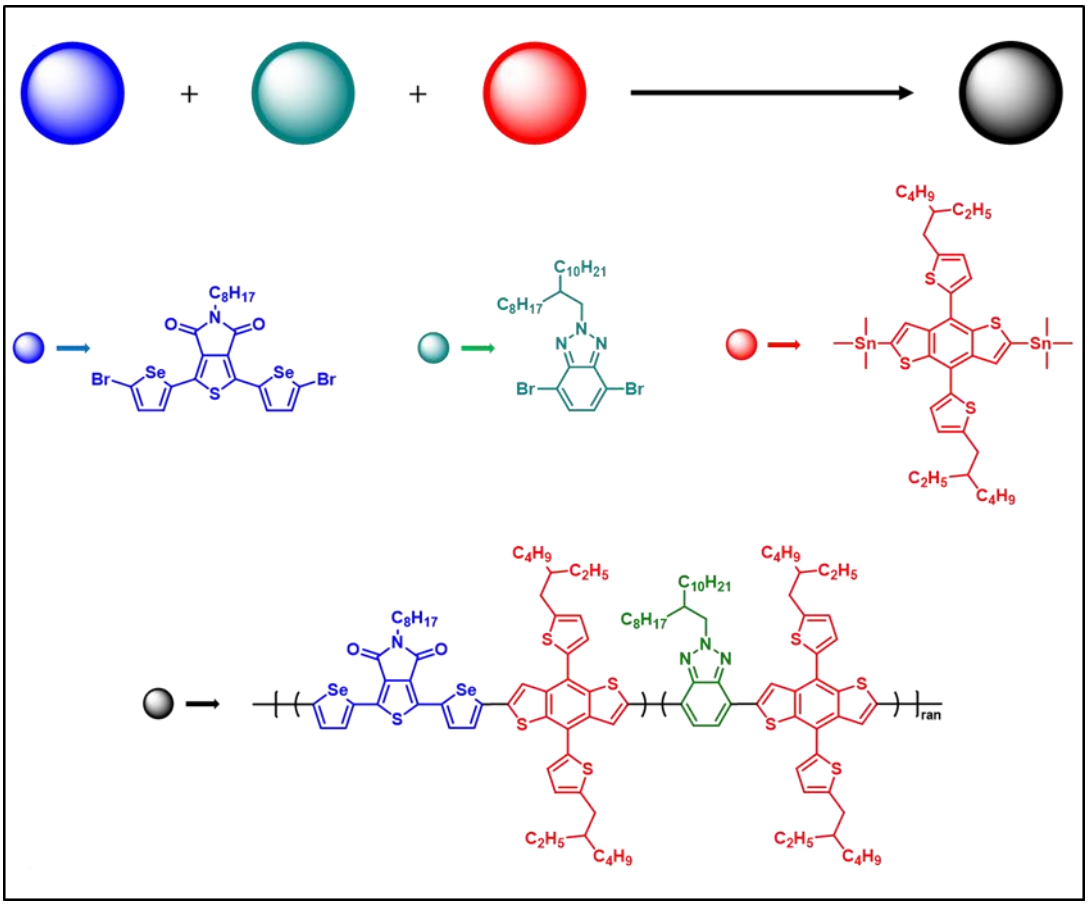

Figure 2.26. Reagents and conditions: chlorobenzene, $Pd_2(dba)_3$, $P(o\text{-}tol)_3$, 115 °C, 12h, 52%.

1,3-Bis(5-bromoselenophen-2-yl)-5-octyl-4H-thieno[3,4-c]pyrrole-4,6(5H)-dione (75 mg, 0.11 mmol), 4,7-dibromo-2-(2-octyldodecyl)-2H-benzo[d][1,2,3]triazole (61 mg, 0.11 mmol), (4,8-bis(5-(2-ethylhexyl)thiophen-2-yl)benzo[1,2-b:4,5-b']dithiophene-2,6-diyl)bis(trimethylstannane) (199 mg, 0.22 mmol), $Pd_2(dba)_3$ (4.0 mg, 4,4 µmol) and $P(o\text{-}tol)_3$ (4.0 mg, 13 µmol) were added to the reaction flask filled with Ar and dissolved in chlorobenzene (10 mL) waited in sieves for one day. This mixture was stirred at 115 °C for 12 h and then cooled to room temperature. Chlorobenzene was then removed under reduced pressure. Cold MeOH was added into the resulting random copolymer films. Then, the homopolymer films of TPD-BTA-BDT-based random copolymer were excessively washed with MeOH to get rid

of all Pd catalysts, followed by washing with acetone. This washing procedure was done until the polymer films did not give any color to the filtrate. Then, the pure polymer films without having any kind of impurities such as Pd catalysts, small molecules and oligomers were dried under reduced pressure. At the end of these procedures, TPD-BTA-BDT-based random copolymer films were obtained as shiny brown films (120 mg, 52%).

2.3.3. Electrochemical Studies of ELEC-PTPD-C8-ED

For general consideration please see Chapter 1 Section 3.2. Electrochemical polymerization of TPD-C8-ED was carried out in 0.1 M $NaClO_4$/$LiClO_4$/PC and 0.01 M monomer (TPD-C8-ED) solutions with repeated scanning between 0.0 and 1.0 V. Multiple scan voltammogram for polymerization of TPD-C8-ED proved the electroactivity of this monomer and the formation of corresponding polymer films. By looking to the first cycle shown with red line in figure 3.2, the monomer oxidation peak for TPD-C8-ED was determined as 0.77 V. This polymer had a pale blue color at its neutral state and transmissive grey color at its oxidized state.

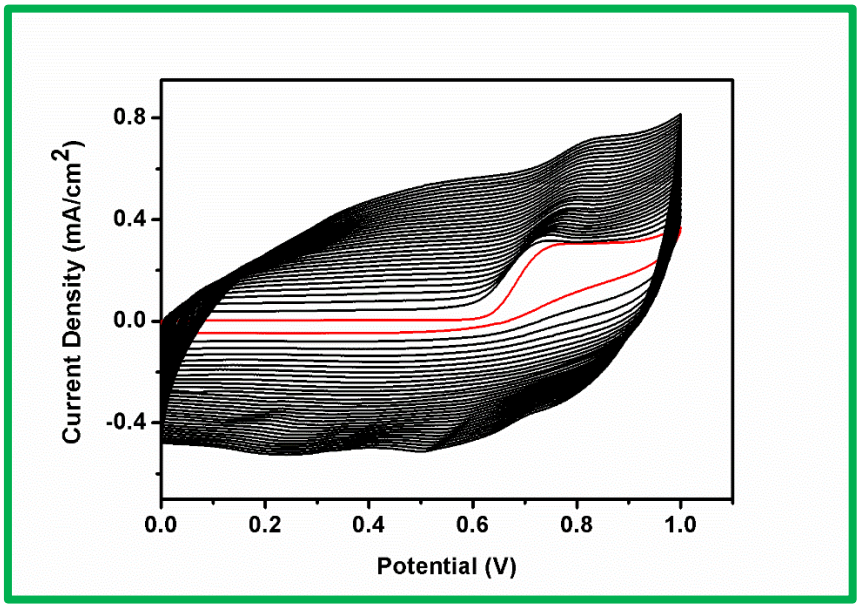

Figure 2.27. Multiple scan voltammogram for polymerization of TPD-C8-ED at 100 mV/s in 0.1 M $NaClO_4$/$LiClO_4$/PC solution on ITO.

In figure 3.4, just p-doping peak belonging to ELEC-PTPD-C8-ED was detected. The p-doping peak was observed at 0.12. The p-dedoping peak was not clearly observed. The reason behind such a significant property is that this polymer acts as a capacitor material. This polymer also did not show n-doping and n-dedoping characteristics.

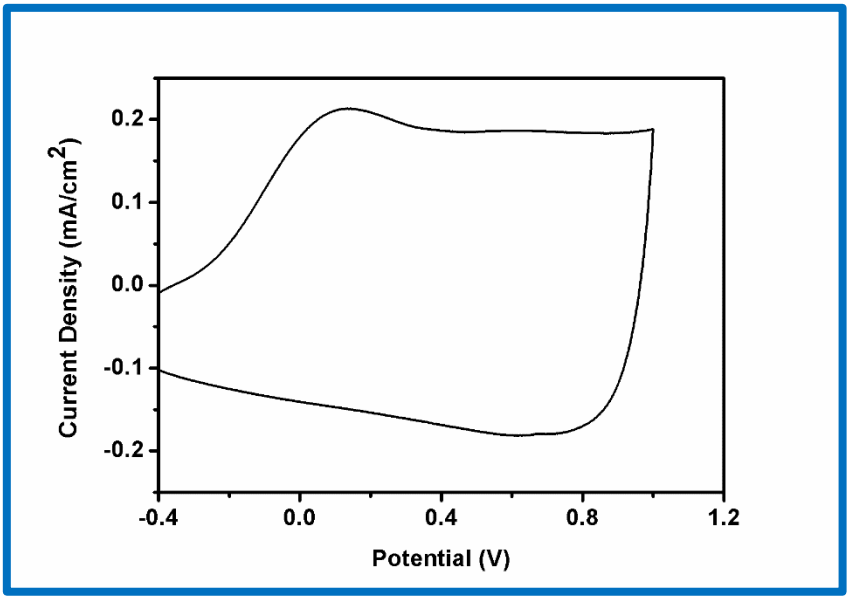

Figure 2.28. Single scan voltammogram of ELEC-PTPD-C8-ED in a monomer free 0.1 M $TBAPF_6$/ACN solution on ITO.

2.3.4. Spectroelectrochemical Studies of ELEC-PTPD-C8-ED

Polymer films of ELEC-PTPD-C8-ED were obtained via electrochemical polymerization. Then, this ITO was put in a monomer free 0.1 M $TBAPF_6$/ACN solution after thoroughly washed with ACN to eliminate residual monomers and/or small oligomers. To investigate the optical characteristic of ELEC-PTPD-C8-ED, the potentials between 0.0 V to 1.0 V were applied stepwise. As seen in figure 3.4, ELEC-PTPD-C8-ED films showed one λ_{max} centered at 625 nm. In literature, most of the polymers possesses one λ_{max} centered at visible region Additionally, the first polaronic band centered at 865 nm upon oxidation. E_g^{op} of ELEC-PTPD-C8-ED was calculated as 1.54 eV. Furthermore, this polymer had a pale blue color at its neutral state and transmissive grey color upon positive doping. These colors of ELEC-PTPD-C8-ED and the resulting L, a, and b values were shown in figure 3.5.

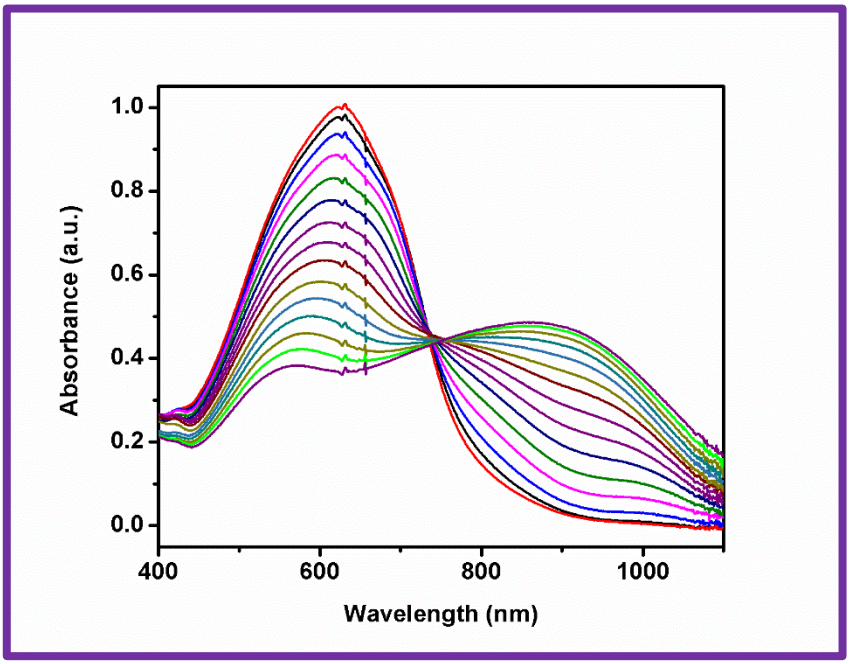

Figure 2.29. Electronic absorption spectra of ELEC-PTPD-C8-ED upon p-doping between 0.0 V and 1.0 V in a monomer free 0.1 M $TBAPF_6$/ACN solution on ITO.

0.0 V	1.0 V
L: 45	L: 53
a: 1	a: -2
b: -15	b: -7

Figure 2.30. The colors of ELEC-PTPD-C8-ED and related L, a, and b values.

2.3.5. Kinetic Studies of ELEC-PQUIN-12C-TH

For general consideration please see Chapter 1 Section 3.4. The optical contrasts (% transmittances) of ELEC-PTPD-C8-ED were found as 26% at 625 nm and 13% at 865

nm. Moreover, the switching times of this polymer were determined as 0.9 s at 625 nm and 1.2 s at 865 nm.

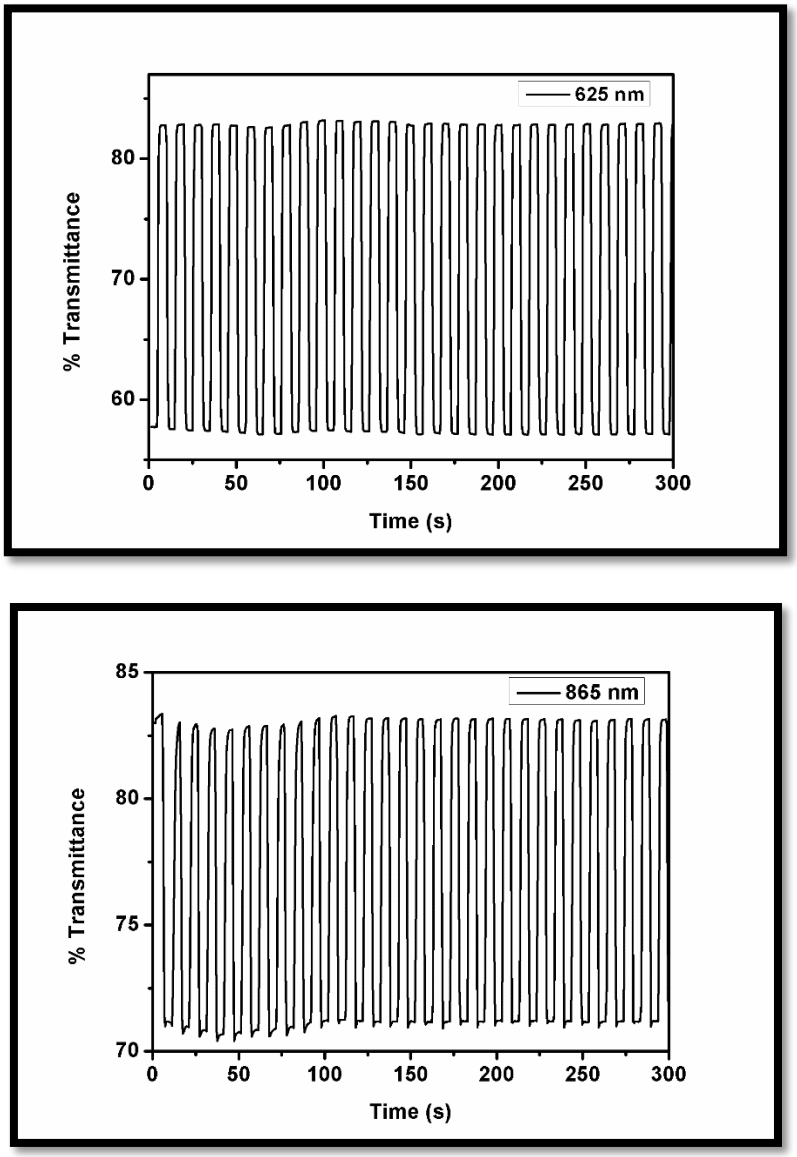

Figure 2.31. The optical contrasts of ELEC-PTPD-C8-ED in a monomer free 0.1 M $TBAPF_6$/ACN solution at 625 nm and 865 nm.

	E_m^{ox} (V)	$E_{p\text{-doping}}$ (V)	$E_{p\text{-dedoping}}$ (V)	HOMO (eV)	LUMO (eV)	λ_{max} (nm)	E_g^{op} (eV)
ELEC-PTPD-C8-ED	0.77	0.12	-	-4.48	-	625 865	1.54

	Optical contrast (ΔT %)		Switching times (s)
ELEC-PTPD-C8-ED	26	625 nm	0.9
	13	865 nm	1.2

Figure 2.32. Summary of electrochemical, spectroelectrochemical and kinetic studies of ELEC-PTPD-C8-ED.

2.3.6. Organic Solar Cell Fabrication

The bulk heterojunction organic solar cell devices were fabricated through the structure of ITO/PEDOT:PSS/poly(TPD-BTA-BDT):$PC_{71}BM$/LiF/Al. Firstly, ITO-coated glass substrates (15 Ω sq^{-1}) were etched using dilute HCl. Then, glass substrates were cleaned with acetone, isopropyl alcohol, detergent and water for 10 minutes in ultrasonic bath, respectively and blow-dried with N_2 gun. Following the cleaning procedure, oxygen plasma treatment was performed in Harrick Plasma Cleaner for 5 minutes. After that, PEDOT: PSS was filtered with PVDF syringe filter (0.45 µm) and deposited onto pre-cleaned ITO-coated glass substrate at 3500 rpm for 45 secs and 4500 rpm for 15 secs. Then, substrates were transferred to the hot plate for annealing at 130^o C for 20 min to remove water residue. poly(TPD-BTA-BDT):$PC_{71}BM$ mixture were dissolved in chlorobenzene at 1:3 ratio and filtered through PTFE syringe filter (0.20 µm). Active layer was spin coated on top of PEDOT: PSS layer at 1500 rpm for 45 secs and 2000 rpm for 15 secs. Lastly, LiF (0.6 nm) and aluminum (100 nm) were evaporated with thermal deposition techniques. Current density-voltage (J-V) characteristics were measured by using Keithley 2400 under illumination of Atlas Material Testing Solutions solar simulator (AM 1.5 G).

2.3.7. Electrochemical Studies of Poly(TPD-BTA-BDT)

Poly(TPD-BTA-BDT) was spray coated onto Pt and cyclic voltammetry studies were performed in 0.1 M $TBAPF_6$/ACN monomer free solution. The p-doping and p-dedoping peaks belonging to poly(TPD-BTA-BDT) were detected at 1.1 and 1.1 V in Figure 2.33. Same figure also illustrates the existing of n-doping and n-dedoping peaks. These peaks were found at -1.4 and -1.7 V, respectively. The HOMO and LUMO levels of poly(TPD-BTA-BDT) from the onset of oxidation and reduction potentials were observed at -3.85 eV and -5.65 eV respectively. Then, E_g^{el} of poly(TPD-BTA-BDT) was calculated as 1.8 eV.

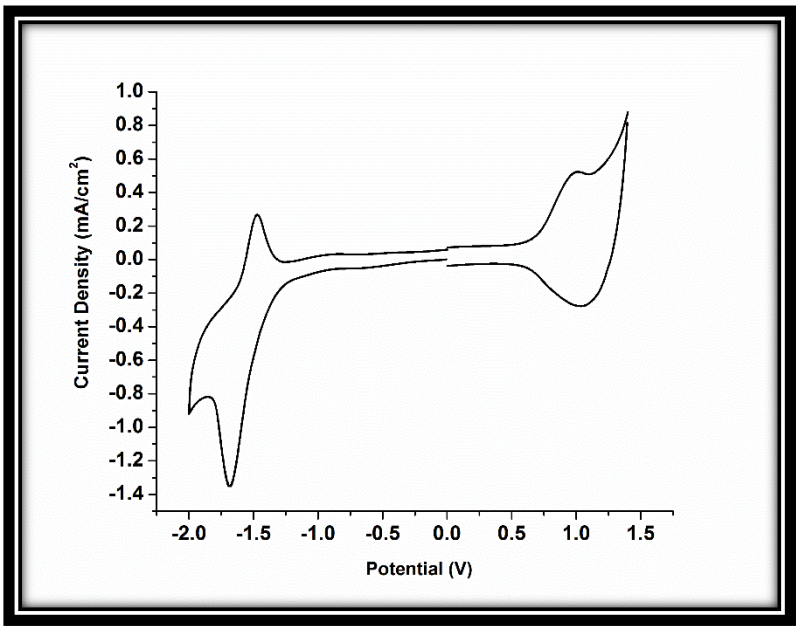

Figure 2.33. Thin film UV-Vis spectrum of poly(TPD-BTA-BDT).

2.3.8. Spectroelectrochemical Studies of Poly(TPD-BTA-BDT)

A thin film of poly(TPD-BTA-BDT) was spray coated on to ITO glass slides and the UV-Vis spectrum was recorded. The lower energy absorption maximum for poly(TPD-BTA-BDT) was reported to be 615 nm. Additionally, the first polaronic band centered at 860 nm upon oxidation. E_g^{op} of poly(TPD-BTA-BDT) was calculated from the onset and was found to be 1.7 eV.

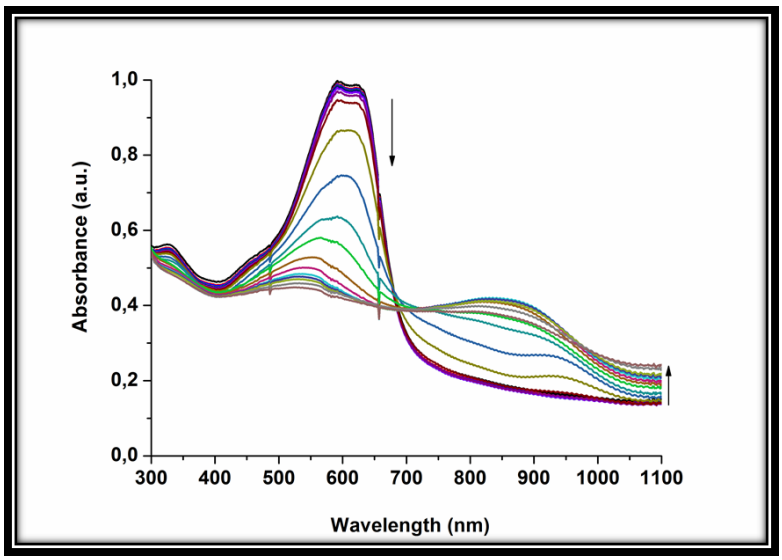

Figure 2.34. Cyclic voltammogram of poly(TPD-BTA-BDT).

2.3.9. Organic Solar Cell Studies of Poly(TPD-BTA-BDT)

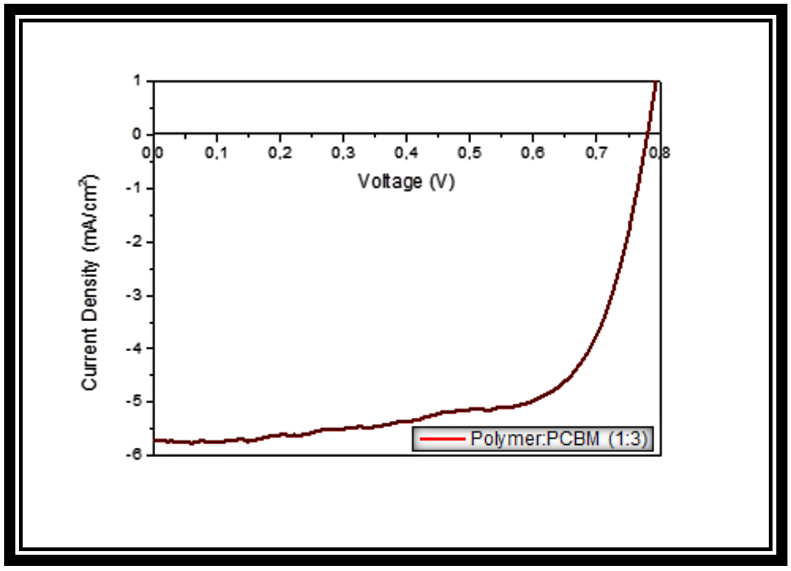

Figure 2.35. J-V curve for poly(TPD-BTA-BDT).

The efficiency of the first PV cell prepared based on poly(TPD-BTA-BDT):$PC_{71}BM$ was calculated as 3.0%. This result was highly promising because this is the first trial and further improvement studies will be made to enhance the efficiency of BHJ solar cells. In literature, there are some promising optimization methods. The most common methods to enhance the efficiency of solar cells are shown as follows:

i. optimization of active layer morphology
ii. solvent and/or thermal annealing
iii. optimization of film thickness
iv. usage of fullerene derivatives
v. usage of several additives

It is aimed that the efficiency of PV cells will significantly increase by applying these methods.

Poly(TPD-BTA-BDT):$PC_{71}BM$ Ratio	V_{oc} (V)	J_{sc} (mA/cm^2)	V_{mp} (V)	I_{mp} (mA/cm^2)	FF (%)	PCE (%)
1:3	0.783	5.76	0.638	4.73	67.0	3.02

Figure 2.36. Solar cell performance of poly(TPD-BTA-BDT):$PC_{71}BM$ blend

2.4. CONCLUSION

In this thesis two novel thieno[3,4-c]pyrrole-4,6-dione (TPD)-based monomers with EDOT (TPD-C8-ED) and selenophene (TPD-C8-SE) side units were designed and synthesized with Stille coupling reactions. Each synthesized product was characterized with NMR spectroscopy. Then, TPD-based homopolymer film with a linear alkyl chain ($-C_8H_{17}$) and EDOT side units (ELEC-PTPD-C8-ED) were synthesized via electrochemical polymerization. Electrochemical, spectroelectrochemical and kinetic properties of ELEC-PTPD-C8-ED were studied respectively. Despite it was certain that there were p-doping, p-dedoping peak was not clearly observed. The reason was due to highly broad peaks, and CV was square like. In literature, the homopolymer having such property is rare; therefore, such polymers are used for capacitor applications. In addition, ELEC-PTPD-C8-ED displayed good optical contrast in the visible region (26% at 625 nm and 13% at 865 nm). ELEC-PTPD-C8-ED have rare electrochromic and capacitor properties. This material can be utilized in electrochromic capacitors. Work along this way will be conducted in the near future. TPD-C8-SE was also tried to be polymerized electrochemically but the polymer films did not grow on ITO coated glass. The same core unit with selenophene side units (TPD-C8-SE) were used for further random copolymerization after it was brominated with NBS (TPD-C8-SE-BR). TPD-BTA-BDT-based random copolymer was then successfully produced by using Stille coupling polymerization in the presence of $Pd_2(dba)_3$, $P(o\text{-}tol)_3$ catalysts. Furthermore, TPD-BTA-BDT-based random copolymer showed excellent solubility in common organic solvents like $CHCl_3$. This property is also crucial because the conjugated polymers should be processable to fabricate any electrochromic devices in high quantity. By using this soluble and processable random copolymer, organic solar cells were prepared and preliminary studies were performed. The efficiency of the preliminary solar cells prepared were calculated as 3.0%. Based on such promising result, it is expected that the efficiency of the optimized PV cells that will be prepared in our laboratories will be significantly higher.

REFERENCES

[1] W. Liptay, "Electrochromism and solvatochromism," *Angew. Chemie Int. Ed.*, vol. 8, no. 3, pp. 177-188, 1969.

[2] R. J. Mortimer, "Organic electrochromic materials," *Electrochim. Acta*, vol. 44, no. 18, pp. 2971-2981, 1999.

[3] D. R. Rosseinsky and R. J. Mortimer, "Electrochromic systems and the prospects for devices," *Adv. Mater.*, vol. 13, no. 11, pp. 783-793, 2001.

[4] R. J. Mortimer, "Electrochromic materials," *Chem. Soc. Rev.*, vol. 26, no. 3, pp. 147-156, 1997.

[5] J. M. Green and L. R. Faulkner, "Reversible oxidation and rereduction of entire thin films of transition-metal phthalocyanines," *J. Am. Chem. Soc.*, vol. 105, no. 10, pp. 2950-2955, 1983.

[6] A. A. Argun, P. H. Aubert, B. C. Thompson, I. Schwendeman, C. L. Gaupp, J. Hwang, N. J. Pinto, D. B. Tanner, A. G. Macdiarmid, and J. R. Reynolds, "Multicolored electrochromism in polymers: structures and devices," *Chem. Mater.*, vol. 16, no. 23, pp. 4401-4412, 2004.

[7] J. Mei and Z. Bao, "Side chain engineering in solution-processible conjugated polymers for organic solar cells and field-effect transistors," *Chem. Mater.*, vol. 26, no. 1, pp. 604-615, 2013.

[8] K. Bange and T. Gambke, "Electrochromic materials for optical switching devices," *Adv. Mater.*, vol. 2, no. 1, pp. 10-16, 1990.

[9] P. M. Beaujuge and J. R. Reynolds, "Color control in π-conjugated organic polymers for use in electrochromic devices," *Chem. Rev.*, vol. 110, no. 1, pp. 268-320, 2010.

[10] J. Hou, S. Zhang, T. L. Chen, and Y. Yang, "A new n-type low bandgap conjugated polymer P-co-CDT: synthesis and excellent reversible electrochemical and electrochromic properties," *Chem. Commun.*, no. 45, pp. 6034-6036, 2008.

[11] F. Ozyurt, E. G. Gunbas, A. Durmus, and L. Toppare, "Processable and multichromic polymer of bis-3-hexylthiophene substituted 4-tert-butylphenyl quinoxaline," *Org. Electron.*, vol. 9, no. 3, pp. 296-302, 2008.

[12] A. Balan, D. Baran, G. Gunbas, A. Durmus, F. Ozyurt, and L. Toppare, "One polymer for all: benzotriazole containing donor-acceptor type polymer as a multi-purpose material," *Chem. Commun.*, vol. 60, no. 44, pp. 6768-6770, 2009.

[13] S. Varis, M. Ak, C. Tanyeli, I. M. Akhmedov, and L. Toppare, "A soluble and multichromic conducting polythiophene derivative," *Eur. Polym. J.*, vol. 42, no. 10, pp. 2352-2360, 2006.

[14] P. Camurlu, C. Gultekin, and Z. Bicil, "Fast switching, high contrast multichromic polymers from alkyl-derivatized dithienylpyrrole and 3,4-ethylenedioxythiophene," *Electrochim. Acta*, vol. 61, pp. 50-56, 2012.

[15] C. Zhang, C. Hua, G. Wang, M. Ouyang, and C. Ma, "A novel multichromic copolymer via electrochemical copolymerization of (S)-1, 1′-binaphthyl-2, 2′-diyl bis (N-(6-hexanoic acid-1-yl) pyrrole) and 3, 4-ethylenedioxythiophene," *Electrochim. Acta*, vol. 55, no. 13, pp. 4103-4111, 2010.

[16] M. İcli-Ozkut, H. İpek, B. Karabay, A. Cihaner, and A. M. Önal, "Furan and benzochalcogenodiazole based multichromic polymers via a donor–acceptor approach," *Polym. Chem.*, vol. 4, no. 8, pp. 2457-2463, 2013.

[17] C. Zhang, C. Hua, G. Wang, M. Ouyang, and C. Ma, "A novel multichromic copolymer of 1,4-bis(3-hexylthiophen-2-yl)benzene and 3,4-ethylenedioxythiophene prepared via electrocopolymerization," *J. Electroanal. Chem.*, vol. 645, no. 1, pp. 50-57, 2010.

[18] S. C. Rasmussen and S. J. Evenson, "Dithieno [3, 2-b: 2′, 3′-d] pyrrole-based materials: synthesis and application to organic electronics," *Prog. Polym. Sci.*,

vol. 38, no. 12, pp. 1773-1804, 2013.

[19] M. Sendur, A. Balan, D. Baran, and L. Toppare, "Syntheses and optoelectronic properties of quinoxaline polymers: the effect of donor unit," *J. Polym. Sci. Part A Polym. Chem.*, vol. 49, no. 18, pp. 4065-4070, 2011.

[20] H. S. O. Chan and S. C. Ng, "Synthesis, characterization and applications of thiophene-based functional polymers," *Prog. Polym. Sci.*, vol. 23, no. 7, pp. 1167-1231, 1998.

[21] S. Sadki, P. Schottland, N. Brodie, and G. Sabouraud, "The mechanisms of pyrrole electropolymerization," *Chem. Soc. Rev.*, vol. 29, no. 5, pp. 283-293, 2000.

[22] N. Y. Abu-Thabit, "Chemical oxidative polymerization of polyaniline: a practical approach for preparation of smart conductive textiles," *J. Chem. Educ.*, vol. 93, no. 9, pp. 1606-1611, 2016.

[23] S. Goker, G. Hizalan, Y. A. Udum, and L. Toppare, "Electrochemical and optical properties of 5,6-bis(octyloxy)-2,1,3 benzooxadiazole containing low band gap polymers," *Synth. Met.*, vol. 191, pp. 19-27, 2014.

[24] D. Kumar and R. C. Sharma, "Advances in conductive polymers," *Eur. Polym. J.*, vol. 34, no. 8, pp. 1053-1060, 1998.

[25] G. Sonmez, H. B. Sonmez, C. K. F. Shen, and F. Wudl, "Red, green, and blue colors in polymeric electrochromics," *Adv. Mater.*, vol. 16, no. 21, pp. 1905-1908, 2004.

[26] G. Sonmez, "Polymeric electrochromics," *Chem. Commun.*, no. 42, pp. 5251-5259, 2005.

[27] G. Sonmez, C. K. F. Shen, Y. Rubin, and F. Wudl, "A red, green, and blue (RGB) polymeric electrochromic device (PECD): the dawning of the PECD era," *Angew. Chemie*, vol. 116, no. 12, pp. 1524-1528, 2004.

[28] G. E. Gunbas, A. Durmus, and L. Toppare, "A unique processable green polymer with a transmissive oxidized state for realization of potential RGB-based electrochromic device applications," *Adv. Funct. Mater.*, vol. 18, no. 14,

pp. 2026-2030, 2008.

[29] G. Atakan, and G. Gunbas, "A novel red to transmissive electrochromic polymer based on phenanthrocarbazole," *RSC Adv.*, vol. 6, no. 30, pp. 25620-25623, 2016.

[30] Z. Xu, X. Chen, S. Mi, J. Zheng, and C. Xu, "Solution-processable electrochromic red-to-transmissive polymers with tunable neutral state colors, high contrast and enhanced stability," *Org. Electron.*, vol. 26, pp. 129-136, 2015.

[31] A. L. Dyer, M. R. Craig, J. E. Babiarz, K. Kiyak, and J. R. Reynolds, "Orange and red to transmissive electrochromic polymers based on electron-rich dioxythiophenes," *Macromolecules*, vol. 43, no. 10, pp. 4460-4467, 2010.

[32] P. M. Beaujuge, S. Ellinger, and J. R. Reynolds, "Spray processable green to highly transmissive electrochromics via chemically polymerizable donor-acceptor heterocyclic pentamers," *Adv. Mater.*, vol. 20, no. 14, pp. 2772-2776, 2008.

[33] R. Yuksel, E. Ataoglu, J. Turan, E. Alpugan, S. H. Ozdemir, L. Toppare, A. Cirpan, H. E. Unalan, and G. Gunbas, "A new high-performance blue to transmissive electrochromic material and use of silver nanowire network electrodes as substrates," *J. Polym. Sci. Part A Polym. Chem.*, vol. 55, no. 10, pp. 1680-1686, 2017.

[34] W. T. Neo, L. M. Loo, J. Song, X. Wang, C. M. Cho, H. S. On Chan, Y. Zong, and J. Xu, "Solution-processable blue-to-transmissive electrochromic benzotriazole-containing conjugated polymers," *Polym. Chem.*, vol. 4, no. 17, pp. 4663-4675, 2013.

[35] X. Chen, H. Liu, Z. Xu, S. Mi, J. Zheng, and C. Xu, "Highly regiosymmetric homopolymer based on dioxythiophene for realizing water-processable blue-to-transmissive electrochrome," *ACS Appl. Mater. Interfaces*, vol. 7, no. 21, pp. 11387-11392, 2015.

[36] S. R. Marder, L. T. Cheng, B. G. Tiemann, A. C. Friedli, M. Blanchard-Desce, J. W. Perry, and J. Skindhøj, "Large first hyperpolarizabilities in push-pull

polyenes by tuning of the bond length alternation and aromaticity mireille blanchard-desce," *Science,* vol. 263, pp. 511-514, 1994.

[37] A. Ajayaghosh, "Donor-acceptor type low band gap polymers: polysquaraines and related systems," *Chem. Soc. Rev.*, vol. 32, no. 4, pp. 181-191, 2003.

[38] R. Kroon, M. Lenes, J. C. Hummelen, P. W. M. Blom, and B. De Boer, "Small bandgap polymers for organic solar cells (polymer material development in the last 5 years)," *Polym. Rev.*, vol. 48, no. 3, pp. 531-582, 2008.

[39] E. Bundgaard and F. C. Krebs, "Low band gap polymers for organic photovoltaics," *Sol. Energy Mater. Sol. Cells,* vol. 91, no. 11, pp. 954-985, 2007.

[40] M. Chen, E. Perzon, M. R. Andersson, S. Marcinkevicius, S. K. M. Jönsson, M. Fahlman, and M. Berggren, "1 micron wavelength photo-and electroluminescence from a conjugated polymer," *Appl. Phys. Lett.*, vol. 84, no. 18, pp. 3570-3572, 2004.

[41] G. L. Gibson, T. M. Mccormick, and D. S. Seferos, "Atomistic band gap engineering in donor-acceptor polymers," *J. Am. Chem. Soc.*, vol. 134, no. 1, pp. 539-547, 2011.

[42] L. Huo, Z. A. Tan, X. Wang, Y. Zhou, M. Han, and Y. Li, "Novel two-dimensional donor-acceptor conjugated polymers containing quinoxaline units: synthesis, characterization, and photovoltaic properties," *J. Polym. Sci. Part A Polym. Chem.*, vol. 46, no. 12, pp. 4038-4049, 2008.

[43] J. Yuan, J. Ouyang, V. Cimrová, M. Leclerc, A. Najari, and Y. Zou, "Development of quinoxaline based polymers for photovoltaic applications," *J. Mater. Chem. C,* vol. 5, no. 8, pp. 1858-1879, 2017.

[44] F. Zhang, D. Wu, Y. Xu, and X. Feng, "Thiophene-based conjugated oligomers for organic solar cells," *J. Mater. Chem.*, vol. 21, no. 44, pp. 17590-17600, 2011.

[45] J. Roncali, P. Blanchard, and P. Frère, "3, 4-Ethylenedioxythiophene (EDOT) as a versatile building block for advanced functional π-conjugated systems," *J.*

Mater. Chem., vol. 15, no. 16, pp. 1589-1610, 2005.

[46] S. Amou, O. Haba, K. Shirato, T. Hayakawa, M. Ueda, K. Takeuchi, and M. Asai, "Head-to-tail regioregularity of poly(3-hexylthiophene) in oxidative coupling polymerization with $FeCl_3$," *J. Polym. Sci. Part A Polym. Chem.*, vol. 37, no. 13, pp. 1943-1948, 1999.

[47] J. Heinze, "Cyclic voltammetry-'electrochemical spectroscopy'. New analytical methods (25)," *Angew. Chemie Int. Ed.*, vol. 23, no. 11, pp. 831-847, 1984.

[48] M. Gerard, A. Chaubey, and B. D. Malhotra, "Application of conducting polymers to biosensors," *Biosens. Bioelectron.*, vol. 17, no. 5, pp. 345-359, 2002.

[49] K. Yoshino, S. Hayashi, and R. I. Sugimoto, "Preparation and properties of conducting heterocyclic polymer films by chemical method," *Jpn. J. Appl. Phys.*, vol. 23, no. 12A, pp. L899-L900, 1984.

[50] T. Okada, T. Ogata, and M. Ueda, "Synthesis and characterization of regiocontrolled poly(2,5-di-n-butoxy-1,4-phenylene) by oxovanadium-catalyzed oxidative coupling polymerization," *Macromolecules*, vol. 29, no. 24, pp. 7645-7650, 1996.

[51] M. R. Anderssonl, D. Selse, M. Berggren, H. Jarvinen, T. Hjertberg, O. Inganäs, and J. Osterholmil, "Regioselective polymerization of 3-(4-octylphenyl) thiophene with $FeCl_3$," *Macromolecules*, vol. 27, no. 22, pp. 6503-6506, 1994.

[52] W. Baik, W. Luan, R. H. Zhao, S. Koo, and K. S. Kim, "Synthesis of highly conductive poly(3,4-ethylenedioxythiophene) fiber by simple chemical polymerization," *Synth. Met.*, vol. 159, no. 13, pp. 1244-1246, 2009.

[53] X. Chen, B. Liu, Y. Zou, W. Tang, Y. Li, and D. Xiao, "Copolymers from naphtho[2,3-c]thiophene-4,9-dione derivatives and benzodithiophene: synthesis and photovoltaic applications," *RSC Adv.*, vol. 2, no. 19, pp. 7439-7448, 2012.

[54] B. Mohr, V. Enkelmann, and G. Wegner, “Synthesis of alkyl-and alkoxy-substituted benzils and oxidative coupling to tetraalkoxyphenanthrene-9,10-diones,” *J. Org. Chem.*, vol. 59, no. 3, pp. 635-638, 1994.

[55] J. H. Kim, H. U. Kim, D. Mi, S. H. Jin, W. S. Shin, S. C. Yoon, and D. H. Hwang, “Introduction of perylene units for enhanced interchain interaction in conjugated polymers for organic photovoltaic devices,” *Macromolecules*, vol. 45, no. 5, pp. 2367-2376, 2012.

[56] P. I. Lee, S. L. C. Hsu, and P. Lin, “White-light-emitting diodes from single polymer systems based on polyfluorene copolymers with quinoxaline derivatives,” *Macromolecules*, vol. 43, no. 19, pp. 8051-8057, 2010.

[57] C. Istanbulluoglu, S. Goker, G. Hizalan, S. O. Hacioglu, Y. A. Udum, E. D. Yildiz, and L. Toppare, “Synthesis of a benzotriazole bearing alternatingcopolymer for organic photovoltaic applications,” *New J. Chem.*, vol. 39, no. 8, pp. 6623-6630, 2015.

[58] A. V. Patil, W. H. Lee, E. Lee, K. Kim, I. N. Kang, and S. H. Lee, “Synthesis and photovoltaic properties of a low-band-gap copolymer of dithieno[3, 2-b: 2′, 3′-d]thiophene and dithienylquinoxaline,” *Macromolecules*, vol. 44, no. 6, pp. 1238-1241, 2011.

[59] T. T. Steckler, P. Henriksson, S. Mollinger, A. Lundin, A. Salleo, and M. R. Andersson, “Very low band gap thiadiazoloquinoxaline donor-acceptor polymers as multi-tool conjugated polymers,” *J. Am. Chem. Soc.*, vol. 136, no. 4, pp. 1190-1193, 2014.

[60] B. Jousselme, P. Blanchard, E. Levillain, R. de Bettignies, and J. Roncali, “Electrochemical synthesis of C_{60}-derivatized poly(thiophene)s from tailored precursors,” *Macromolecules*, vol. 36, no. 9, pp. 3020-3025, 2003.

[61] S. Sharma, Bulkesh Siwach, S. K. Ghoshal, and D. Mohan, “Dye sensitized solar cells: From genesis to recent drifts,” *Renew. Sustain. Energy Rev.*, vol. 70, no. July 2015, pp. 529-537, 2017.

[62] L. Szabó, “The history of using solar energy,” *Int. Conf. Mod. Power Syst. (MPS)*, pp. 1-8, 2017.

[63] H. Spanggaard and F. C. Krebs, “A brief history of the development of organic and polymeric photovoltaics,” *Sol. Energy Mater. Sol. Cells*, vol. 83, no. 2, pp. 125-146, 2004.

[64] P. E. Tomaszewski, “Jan Czochralski-father of the Czochralski method,” *J. Cryst. Growth*, vol. 236, no. 1, pp. 1-4, 2002.

[65] L. L. Tobin, T. O’Reilly, D. Zerulla, and J. T. Sheridan, “Characterising dye-sensitised solar cells,” *Opt.-Int. J. Light Electron Opt.*, vol. 122, no. 14, pp. 1225-1230, 2011.

[66] M. Riordan, “The lost history of the transistor,” *IEEE Spectr.*, vol. 41, no. 5, pp. 44-46, 2004.

[67] G. Li, W. H. Chang, and Y. Yang, “Low-bandgap conjugated polymers enabling solution-processable tandem solar cells,” *Nat. Rev. Mater.*, vol. 2, no. 8, p. 201743, 2017.

[68] P. G. V. Sampaio and M. O. A. González, “Photovoltaic solar energy: Conceptual framework,” *Renew. Sustain. Energy Rev.*, vol. 74, no. June 2016, pp. 590-601, 2017.

[69] K. K. Ng, “p- n junction diode,” *Complet. Guid. to Semicond. Devices, Second Ed.*, pp. 11-23, 2002.

[70] G. Han, S. Zhang, P. P. Boix, L. H. Wong, L. Sun, and S. Y. Lien, “Towards high efficiency thin film solar cells,” *Prog. Mater. Sci.*, vol. 87, pp. 246-291, 2017.

[71] O. O. Ogbomo, E. H. Amalu, N. N. Ekere, and P. O. Olagbegi, “A review of photovoltaic module technologies for increased performance in tropical climate,” *Renew. Sustain. Energy Rev.*, vol. 75, pp. 1225-1238, 2017.

[72] T. D. Lee and A. U. Ebong, “A review of thin film solar cell technologies and challenges,” *Renew. Sustain. Energy Rev.*, vol. 70, pp. 1286-1297, 2017.

[73] S. R. Wenham and M. A. Green, “Silicon solar cells,” *Prog. Photovoltaics: Res. Appl.*, vol. 4, no. 1, pp. 3-33, 1996.

[74] A. V. Shah, H. Schade, M. Vanecek, J. Meier, E. Vallat- Sauvain, N. Wyrsch, and J. Bailat, "Thin-film silicon solar cell technology," *Prog. Photovoltaics: Res. Appl.*, vol. 12, no. 2-3, pp. 113-142, 2004.

[75] A. G. Aberle, "Overview on SiN surface passivation of crystalline silicon solar cells," *Sol. Energy Mater. Sol. Cells*, vol. 65, no. 1, pp. 239-248, 2001.

[76] F. Kessler, D. Herrmann, and M. Powalla, "Approaches to flexible CIGS thin-film solar cells," *Thin Solid Films*, vol. 480, pp. 491-498, 2005.

[77] P. Jackson, D. Hariskos, E. Lotter, S. Paetel, R. Wuerz, R. Menner, and M. Powalla, "New world record efficiency for Cu(In,Ga)Se_2 thin- film solar cells beyond 20%," *Prog. Photovoltaics Res. Appl.*, vol. 19, no. 7, pp. 894-897, 2011.

[78] M. A. Mingsukang, M. H. Buraidah, and A. K. Arof, "Third-generation-sensitized solar cells," *Nanostructured Sol. Cells. InTech*, 2017.

[79] J. Gong, K. Sumathy, Q. Qiao, and Z. Zhou, "Review on dye-sensitized solar cells (DSSCs): Advanced techniques and research trends," *Renew. Sustain. Energy Rev.*, vol. 68, pp. 234-246, 2017.

[80] M. Freitag, J. Teuscher, Y. Saygili, X. Zhang, F. Giordano, P. Liska, and A. Hagfeldt, "Dye-sensitized solar cells for efficient power generation under ambient lighting," *Nat. Phot.*, pp. 372-378, 2017.

[81] P. V. Kamat, "Quantum dot solar cells. Semiconductor nanocrystals as light harvesters," *J. Phys. Chem. C*, vol. 112, no. 48, pp. 18737-18753, 2008.

[82] T. Ibn-Mohammed, S. C. L. Koh, I. M. Reaney, A. Acquaye, G. Schileo, K. B. Mustapha, and R. Greenough, "Perovskite solar cells: An integrated hybrid lifecycle assessment and review in comparison with other photovoltaic technologies," *Renew. Sustain. Energy Rev.*, vol. 80, pp. 1321-1344, 2017.

[83] N. Kour and R. Mehra, "Recent advances in photovoltaic technology based on perovskite solar cell-A review," *Int. Res. J. Eng. Technol.*, vol. 4, no. 7, pp. 1284-1296, 2017.

[84] Y. J. Cheng, S. H. Yang, and C. S. Hsu, "Synthesis of conjugated polymers for

organic solar cell applications," *Chem. Rev.*, vol. 109, no. 11, pp. 5868-5923, 2009.

[85] D. Baran, R. S. Ashraf, D. A. Hanifi, M. Abdelsamie, N. Gasparini, J. A. Rohr, and C. J. Emmott, "Reducing the efficiency-stability-cost gap of organic photovoltaics with highly efficient and stable small molecule acceptor ternary solar cells," *Nat. Mater.*, vol. 16, no. 3, pp. 363-369, 2017.

[86] P. Sonar, J. P. F. Lim, and K. L. Chan, "Organic non-fullerene acceptors for organic photovoltaics," *Energy Environ. Sci.*, vol. 4, no. 5, pp. 1558-1574, 2011.

[87] H. Kim, C. M. Gilmore, J. S. Horwitz, A. Pique, H. Murata, G. P. Kushto, and D. B. Chrisey, "Transparent conducting aluminum-doped zinc oxide thin films for organic light-emitting devices," *Appl. Phys. Lett.*, vol. 76, no. 3, pp. 259-261, 2000.

[88] W. Yue, Y. Zhao, S. Shao, H. Tian, Z. Xie, Y. Geng, and F. Wang, "Novel NIR-absorbing conjugated polymers for efficient polymer solar cells: effect of alkyl chain length on device performance," *J. Mater. Chem.*, vol. 19, no. 15, pp. 2199-2206, 2009.

[89] P. D. Topham, A. J. Parnell, and R. C. Hiorns, "Block copolymer strategies for solar cell technology," *J. Polym. Sci. Part B Polym. Phys.*, vol. 49, no. 16, pp. 1131-1156, 2011.

[90] T. Ameri, G. Dennler, C. Lungenschmied, and C. J. Brabec, "Organic tandem solar cells: A review," *Energy Environ. Sci.*, vol. 2, no. 4, pp. 347-363, 2009.

[91] T. Ameri, P. Khoram, J. Min, and C. J. Brabec, "Organic ternary solar cells: A review," *Adv. Mater.*, vol. 25, no. 31, pp. 4245-4266, 2013.

[92] S. B. Darling, "Block copolymers for photovoltaics," *Energy Environ. Sci.*, vol. 2, no. 12, pp. 1266-1273, 2009.

[93] K. H. Hendriks, W. Li, M. M. Wienk, and R. A. Janssen, "Small-bandgap semiconducting polymers with high near-infrared photoresponse," *J. Am. Chem. Soc.*, vol. 136, no. 34, pp. 12130-12136, 2014.

[94] H. A. Saadeh, L. Lu, F. He, J. E. Bullock, W. Wang, B. Carsten, and L. Yu, "Polyselenopheno[3,4-b]selenophene for highly efficient bulk heterojunction solar cells," *ACS Macro Lett.*, vol. 1, no. 3, pp. 361-365, 2012.

[95] K. R. Graham, Cabanetos, C., J. P. Jahnke, M. N. Idso, A. El Labban, G. O. Ngongang Ndjawa, and A. Amassian, "Importance of the donor:fullerene intermolecular arrangement for high-efficiency organic photovoltaics," *J. Am. Chem. Soc.*, vol. 136, no. 27, pp. 9608-9618, 2014.

[96] A. Saeki, S. Yoshikawa, M. Tsuji, Y. Koizumi, M. Ide, C. Vijayakumar, and S. Seki, "A versatile approach to organic photovoltaics evaluation using white light pulse and microwave conductivity," *J. Am. Chem. Soc.*, vol. 134, no. 46, pp. 19035-19042, 2012.

[97] C. Cabanetos, A. El Labban, J. A. Bartelt, J. D. Douglas, W. R. Mateker, J. M. Fréchet, and P. M. Beaujuge, "Linear side chains in benzo[1,2-b:4,5-b′]dithiophene-thieno[3,4-c]pyrrole-4,6-dione polymers direct self-assembly and solar cell performance," *J. Am. Chem. Soc.*, vol. 135, no. 12, pp. 4656-4659, 2013.

[98] Y. Q. Yang, H. Park, S. H. Lee, D. H. Kim, and Y. S. Lee, "Synthesis of alternating copolymers consisting of N-2-octyldodecyldithieno[2,3-b;7,6-b]carbazole and N-octylthieno[3,4-c]pyrrole-4,6-dione derivative units for photovoltaic applications," *Synth. Met.*, vol. 176, pp. 70-77, 2013.

[99] B. Kim, H. R. Yeom, M. H. Yun, J. Y. Kim, and C. Yang, "A selenophene analogue of PCDTBT: selective fine-tuning of LUMO to lower of the bandgap for efficient polymer solar cells," *Macromolecules*, vol. 45, no. 21, pp. 8658-8664, 2012.

APPENDICES

A. NMR Spectra of Monomers

Each product was analyzed by Bruker Spectrospin Avance DPX-400 Spectrometer with $CDCl_3$ or DMSO as the solvent and TMS as the internal reference.

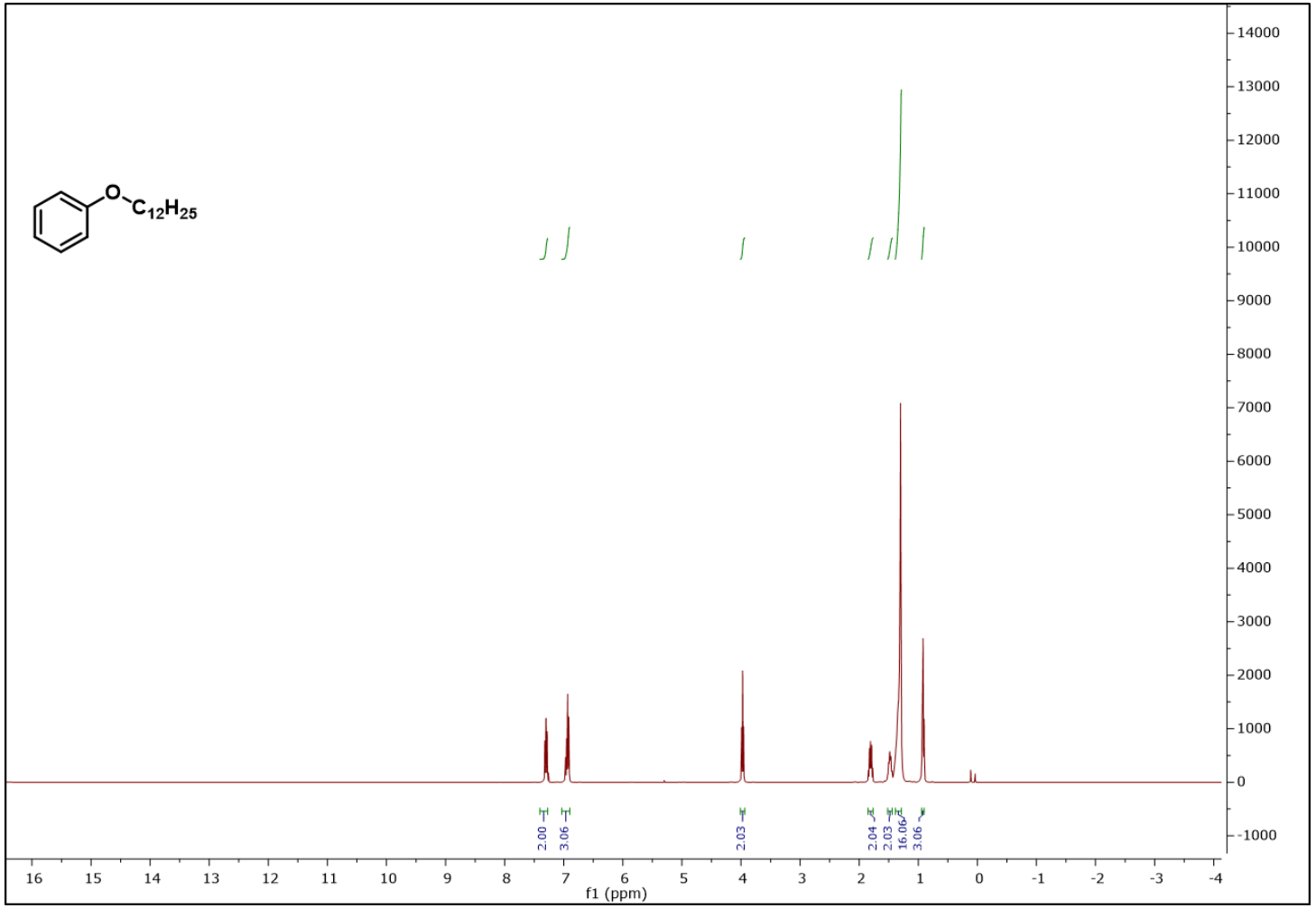

Figure A.1.1. ^{1}H-NMR spectrum of (dodecyloxy)benzene

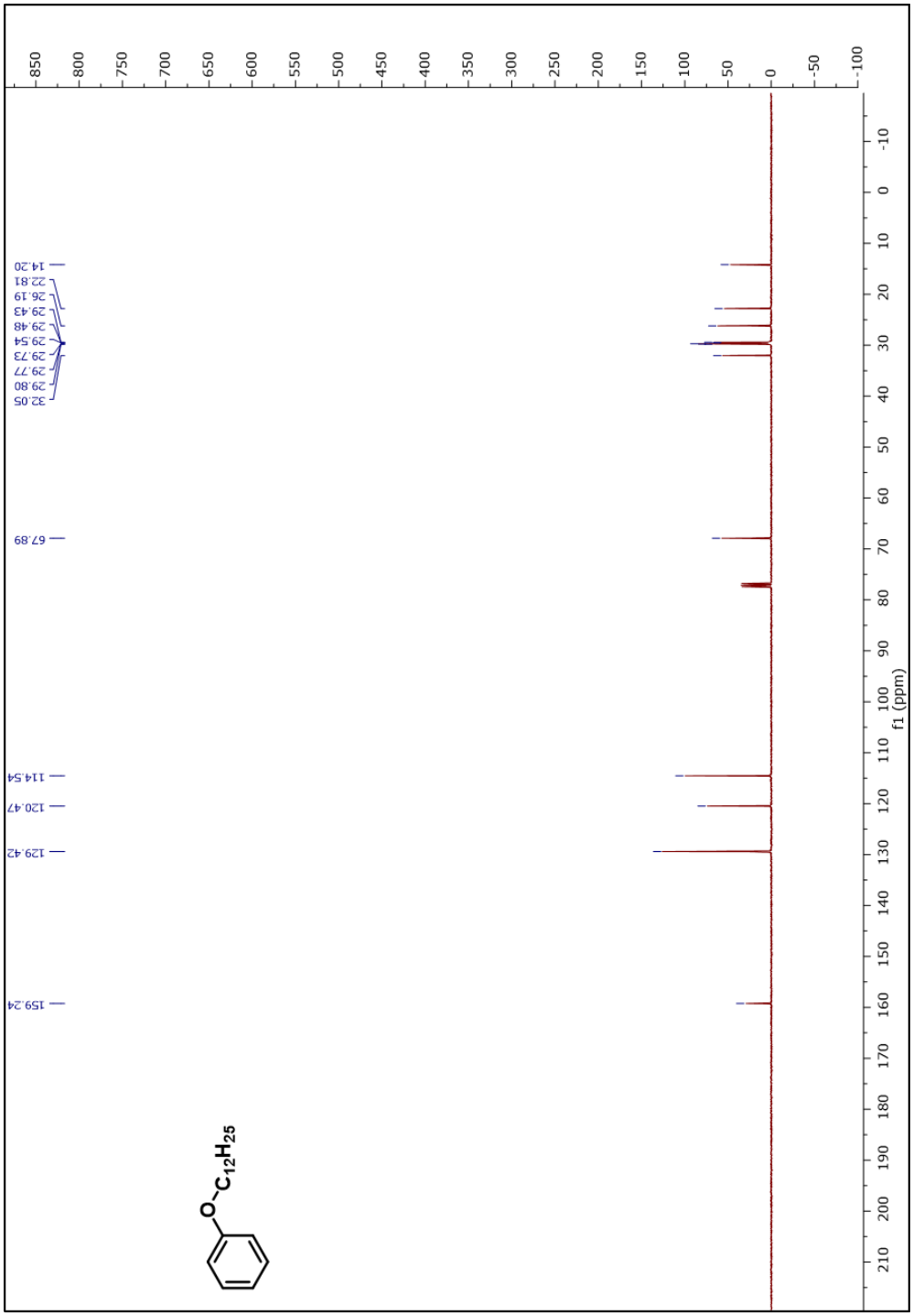

Figure A.1.2. ^{13}C-NMR spectrum of (dodecyloxy)benzene

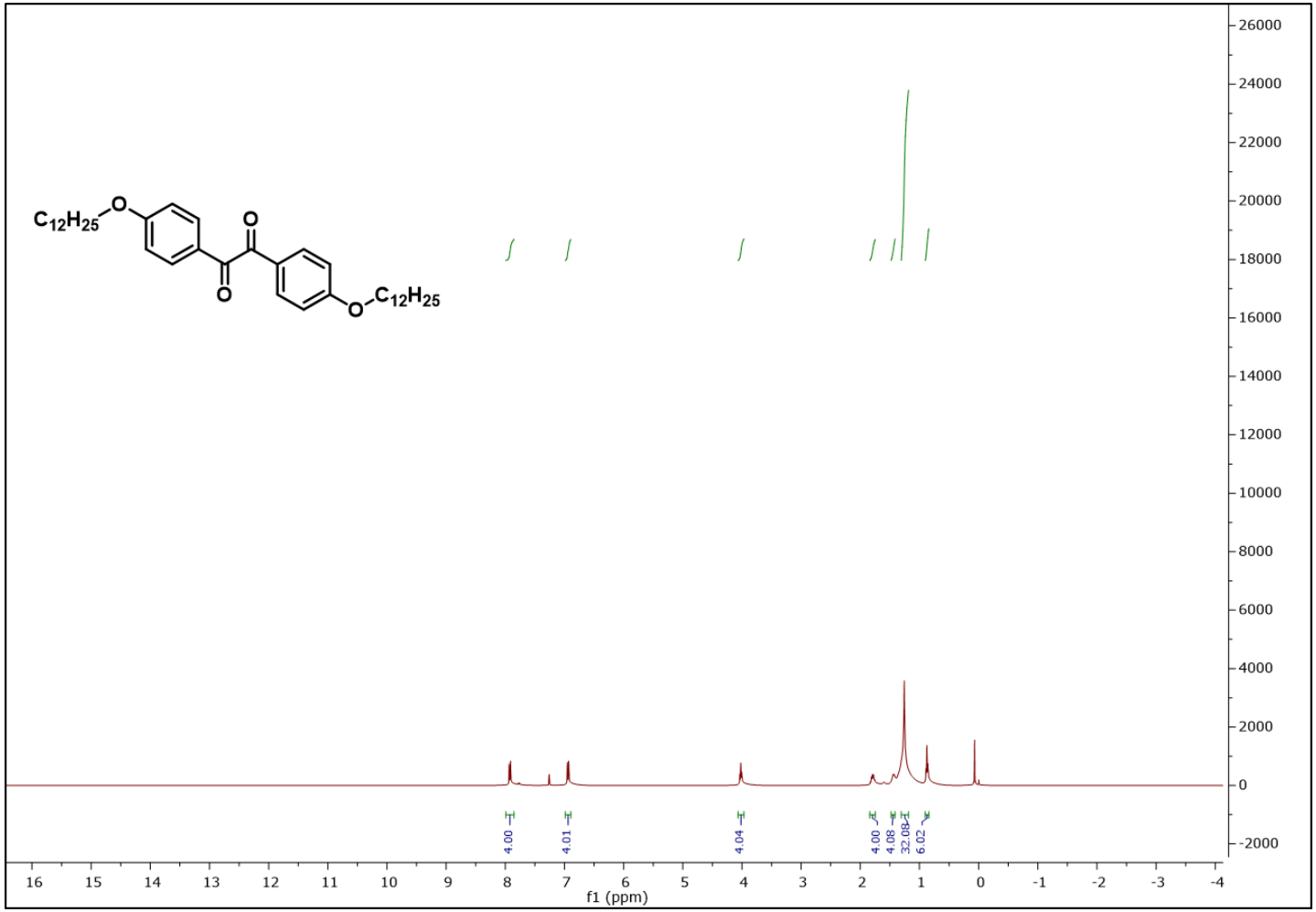

Figure A.2.1. ^{1}H-NMR spectrum of 1,2-bis(4-(dodecyloxy)phenyl)ethane-1,2-dione

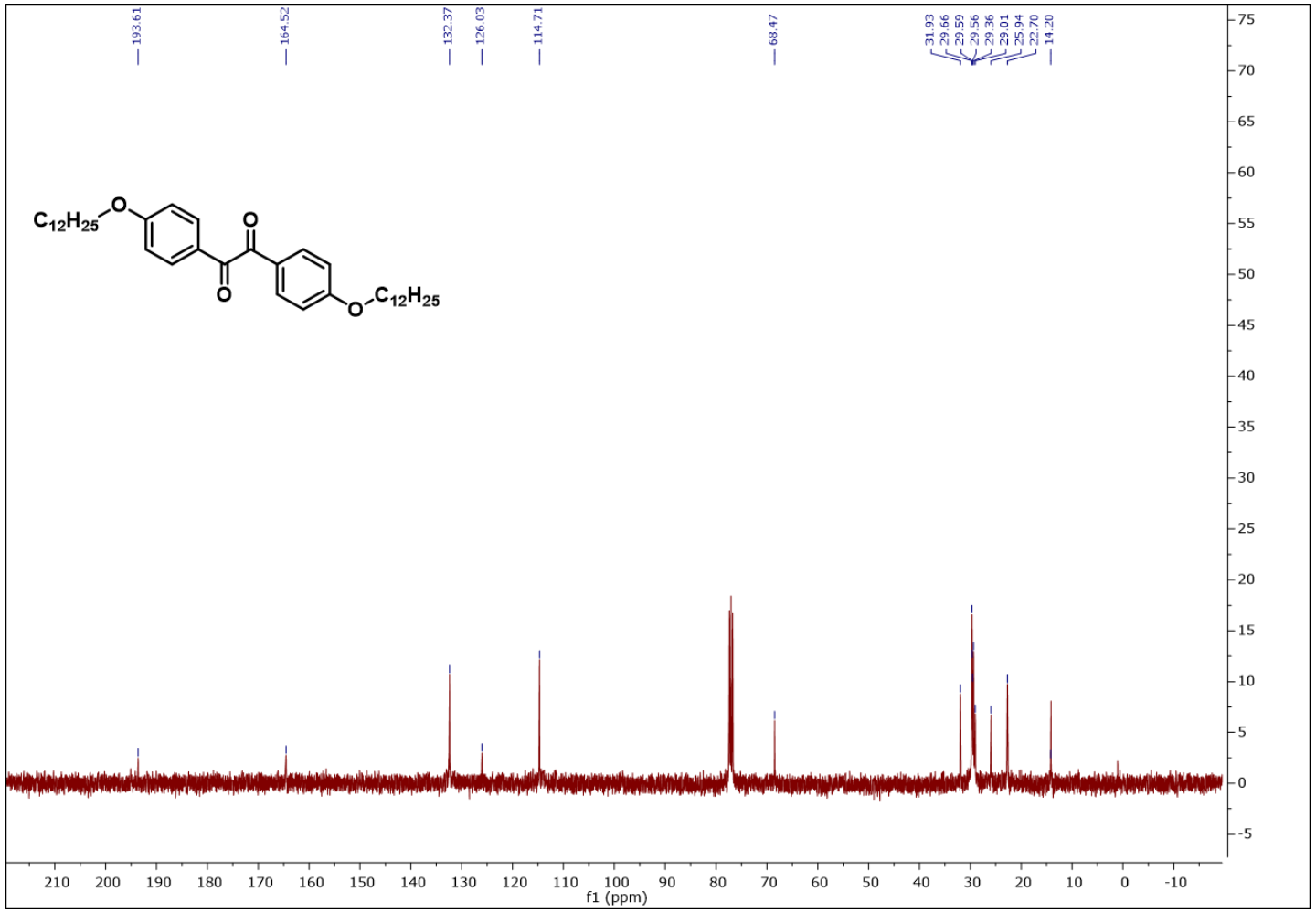

Figure A.2.2. ^{13}C-NMR spectrum of 1,2-bis(4-(dodecyloxy)phenyl)ethane-1,2-dione

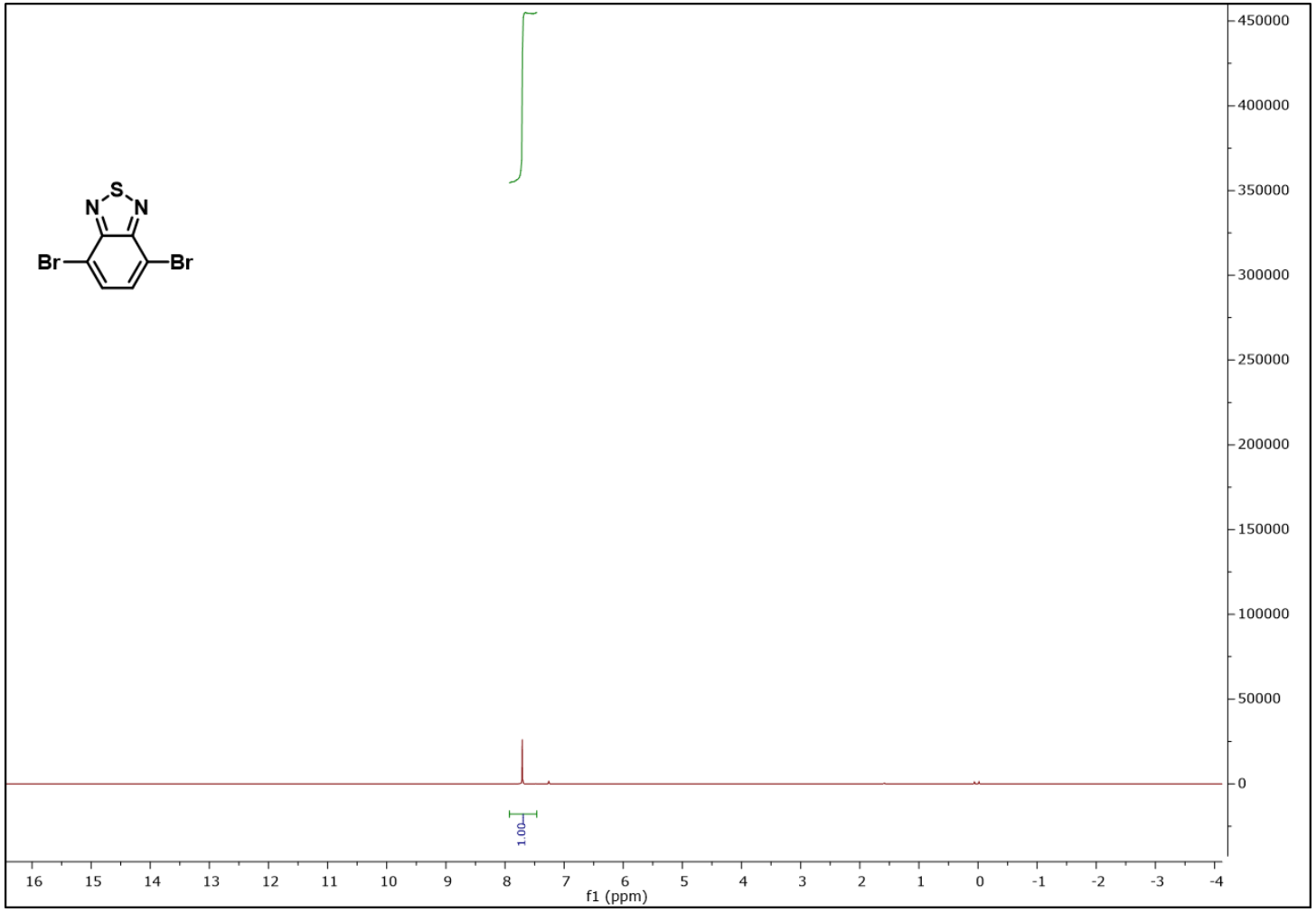

Figure A.3.1. ^{1}H-NMR spectrum of 4,7-dibromobenzo[c][1,2,5]thiadiazole

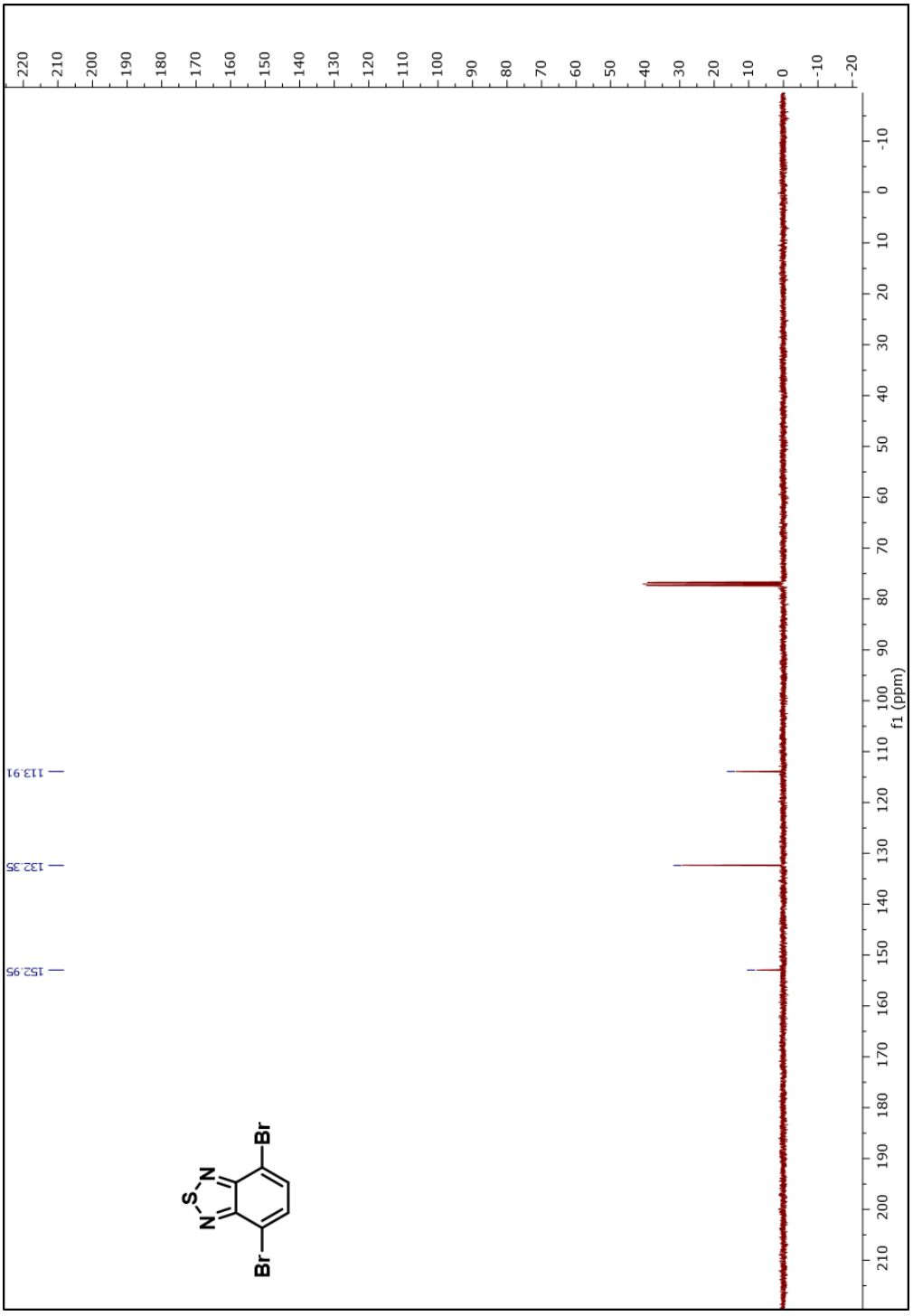

Figure A.3.2. ^{13}C-NMR spectrum of 4,7-dibromobenzo[c][1,2,5]thiadiazole

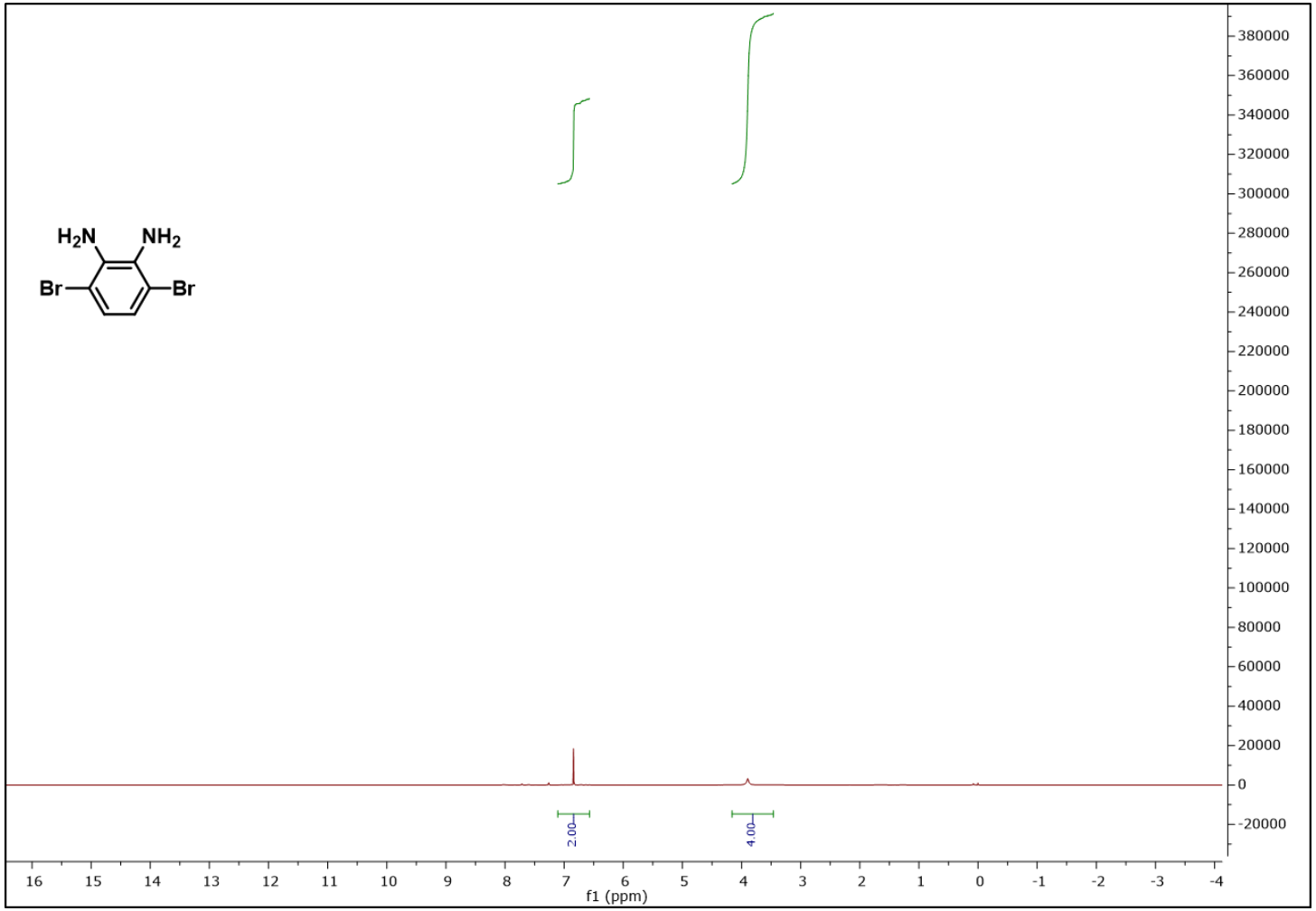

Figure A.4.1. ^{1}H-NMR spectrum of 3,6-dibromobenzene-1,2-diamine

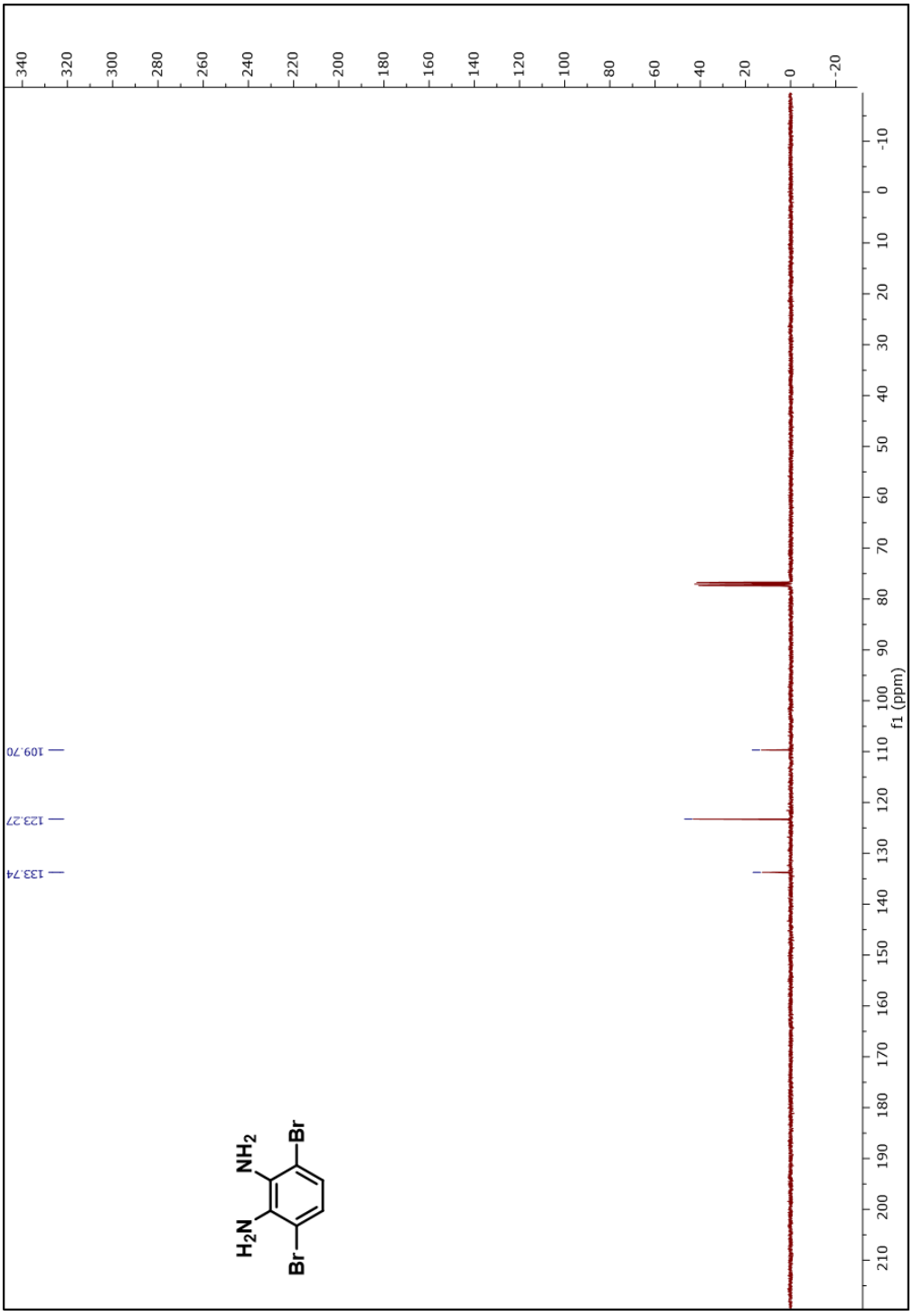

Figure A.4.2. ^{13}C-NMR spectrum of 3,6-dibromobenzene-1,2-diamine

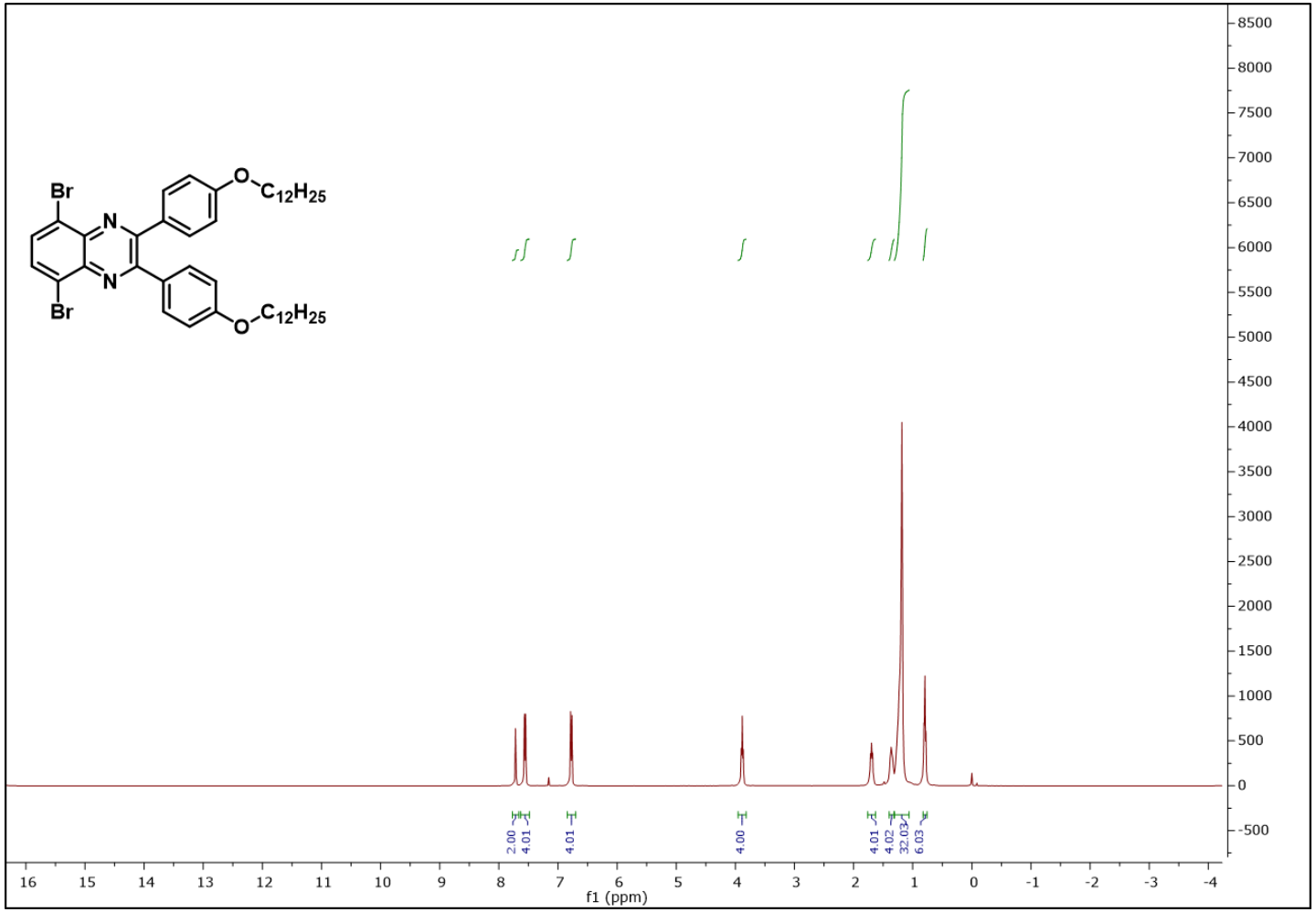

Figure A.5.1. ^{1}H-NMR spectrum of 5,8-dibromo-2,3-bis(4-(dodecyloxy)phenyl)quinoxaline

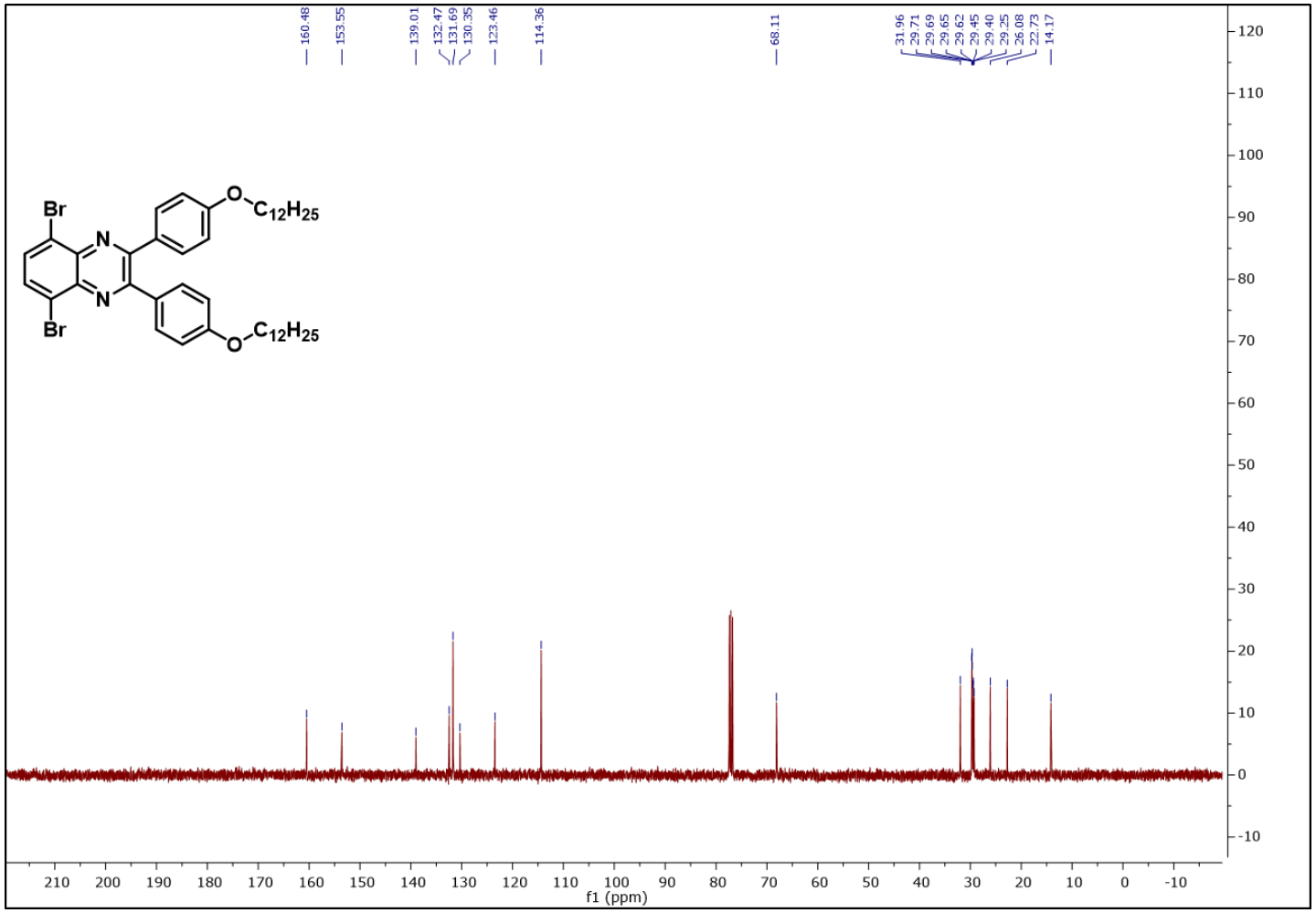

Figure A.5.2. ^{13}C-NMR spectrum of 5,8-dibromo-2,3-bis(4-(dodecyloxy)phenyl)quinoxaline

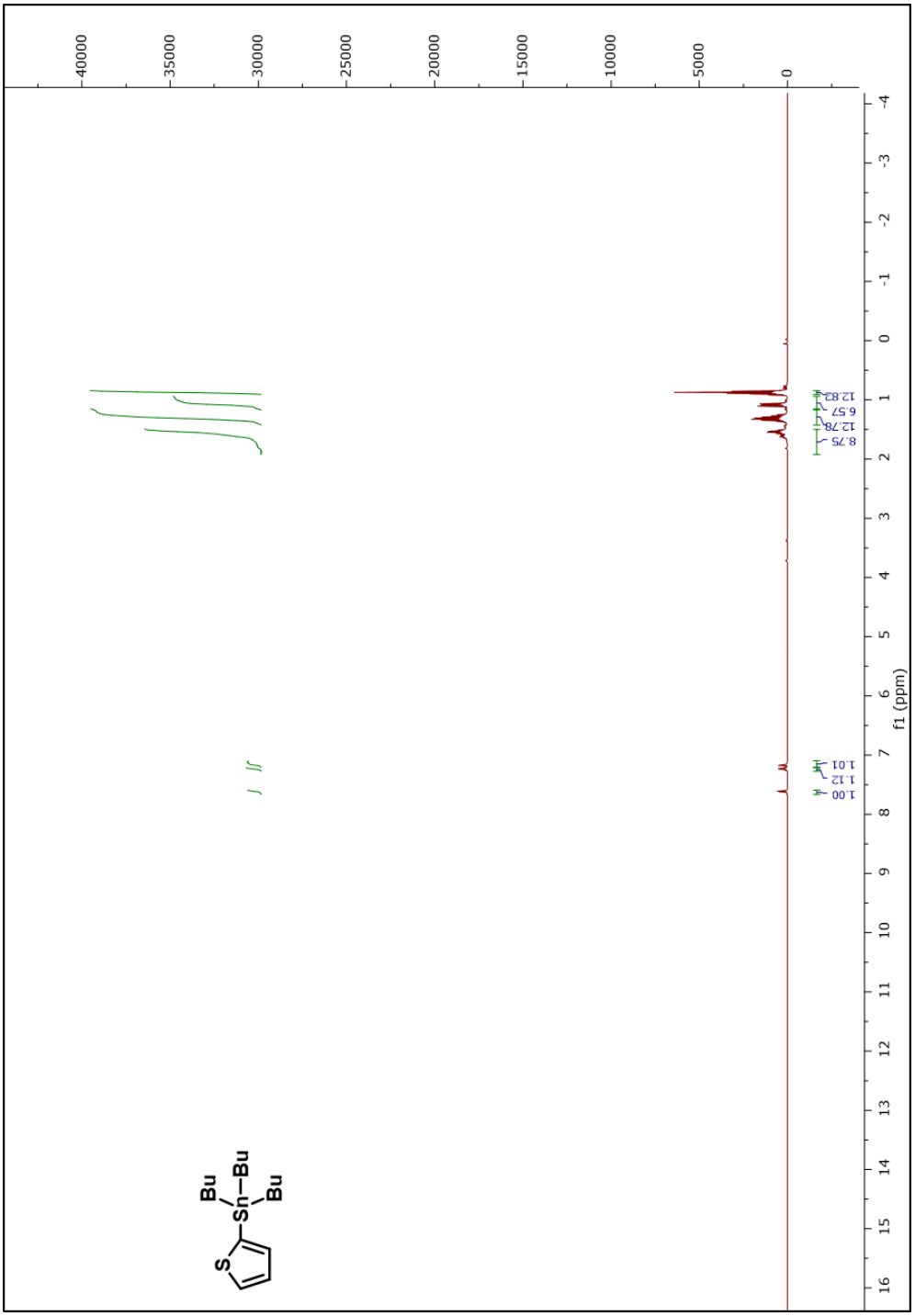

Figure A.6.1. ^{1}H-NMR spectrum of tributyl(thiophen-2-yl)stannane

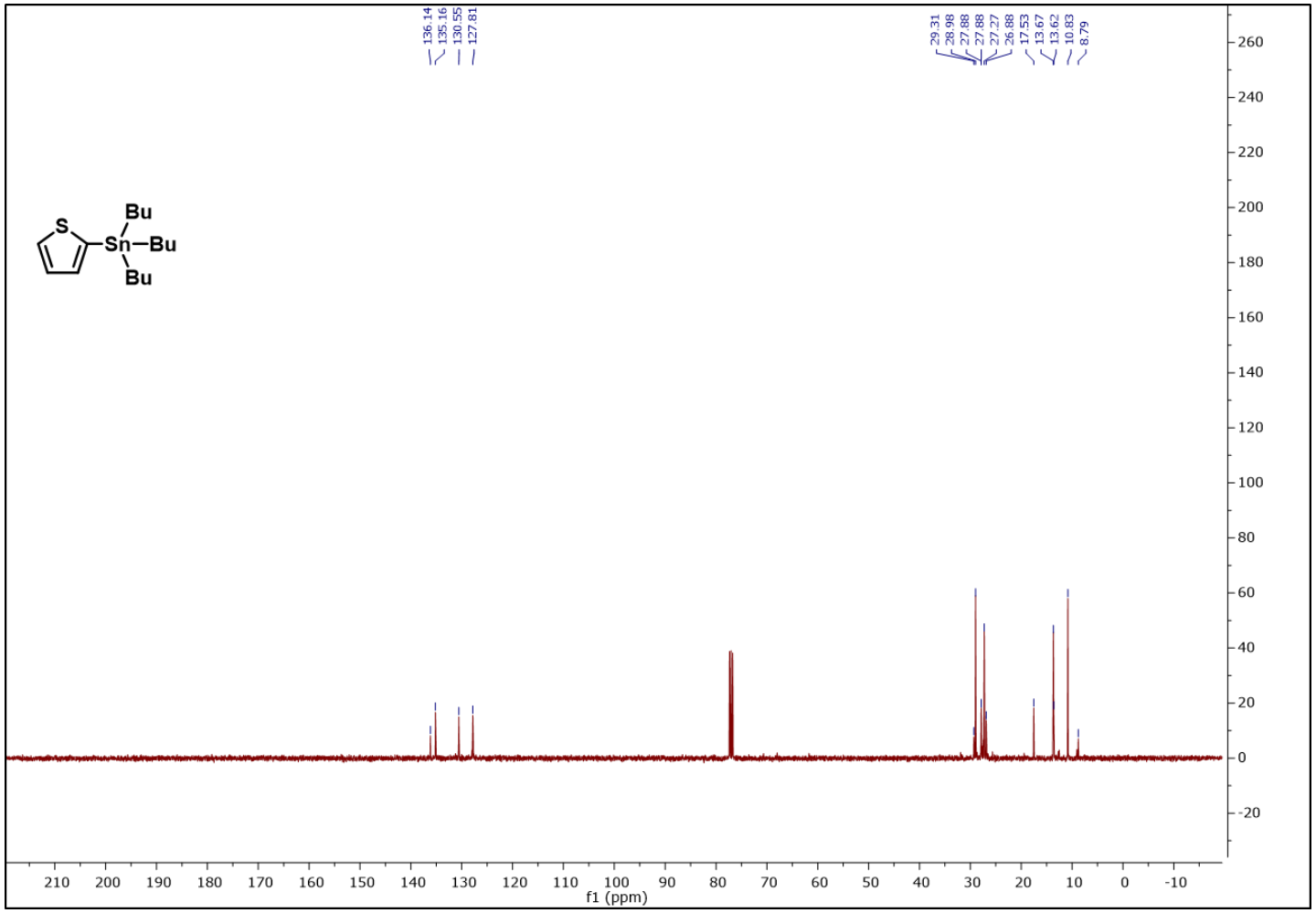

Figure A.6.2. ^{13}C-NMR spectrum of tributyl(thiophen-2-yl)stannane

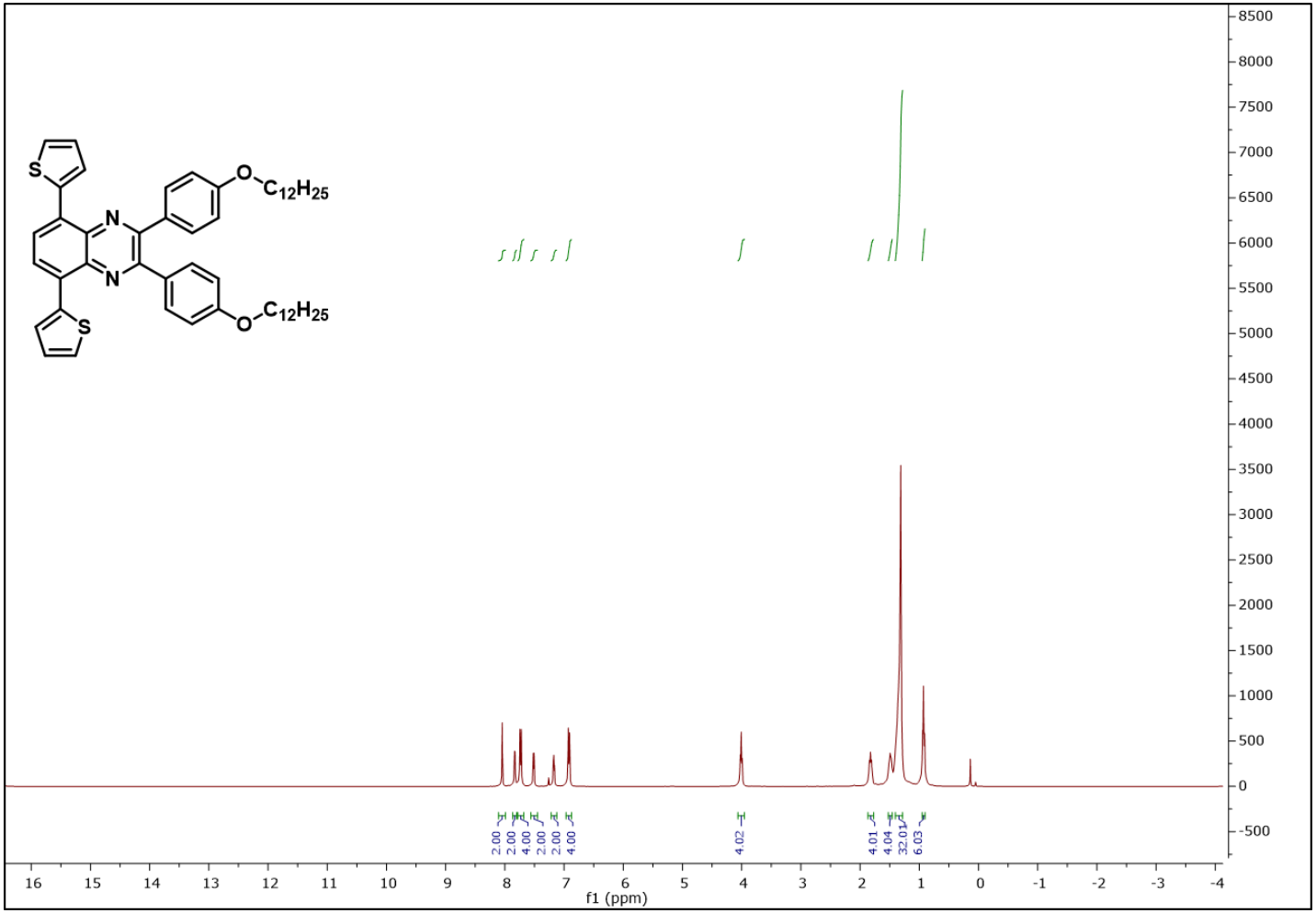

Figure A.7.1. ^{1}H-NMR spectrum of 2,3-bis(4-(dodecyloxy)phenyl)-5,8-di(thiophen-2-yl)quinoxaline

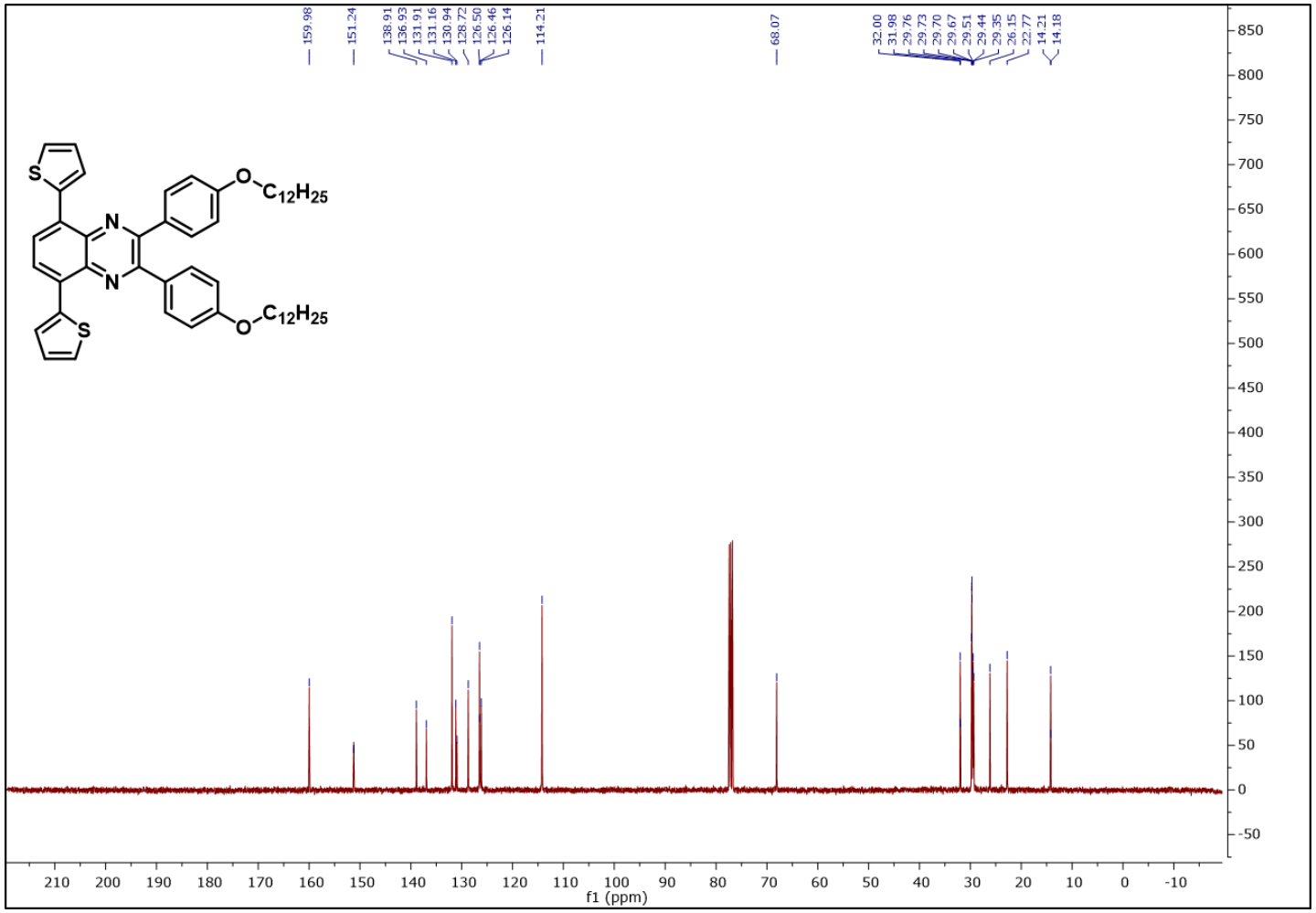

Figure A.7.2. ^{13}C-NMR spectrum of 2,3-bis(4-(dodecyloxy)phenyl)-5,8-di(thiophen-2-yl)quinoxaline

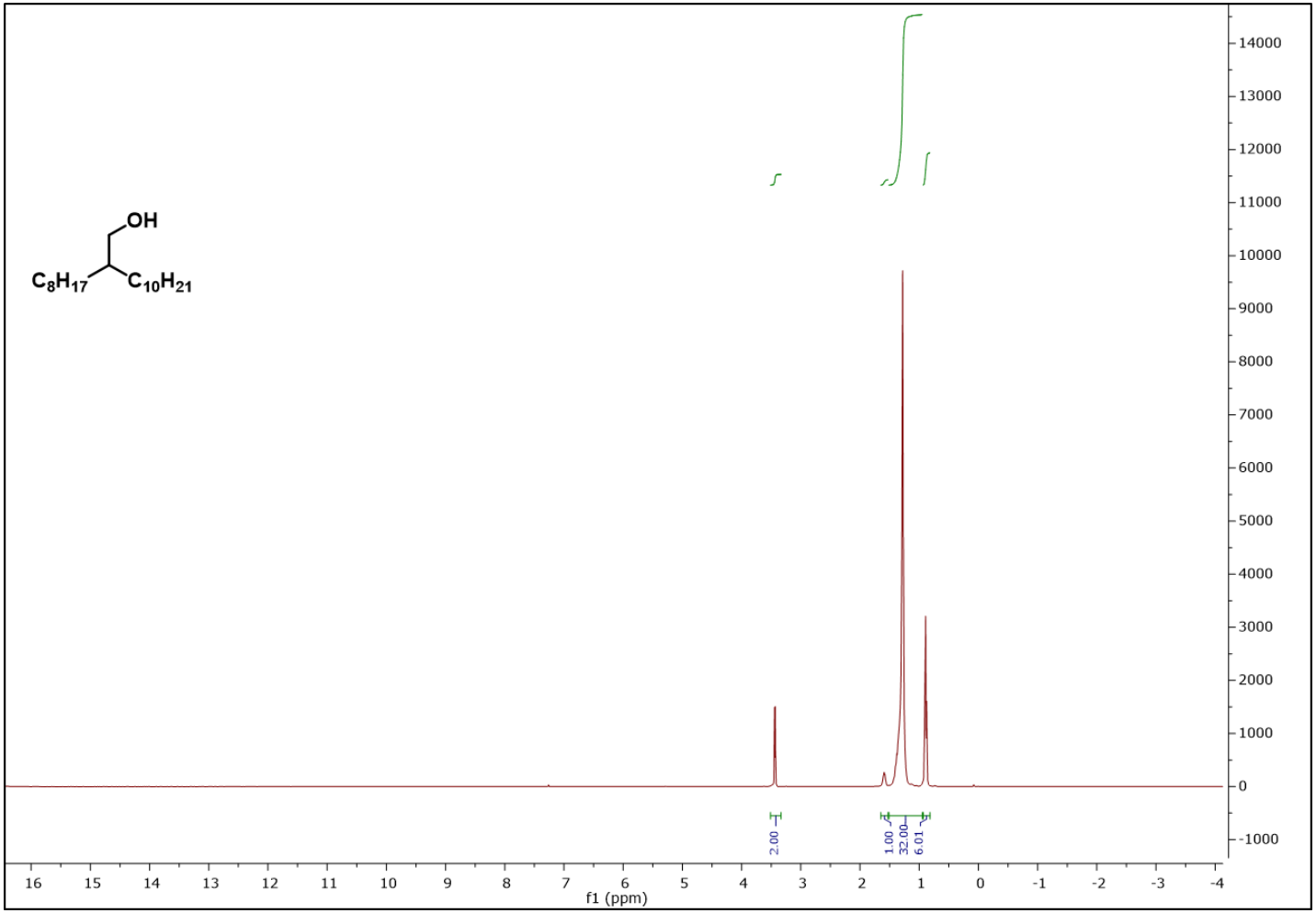

Figure A.8.1. ^{1}H-NMR spectrum of 9-(bromomethyl)nonadecane

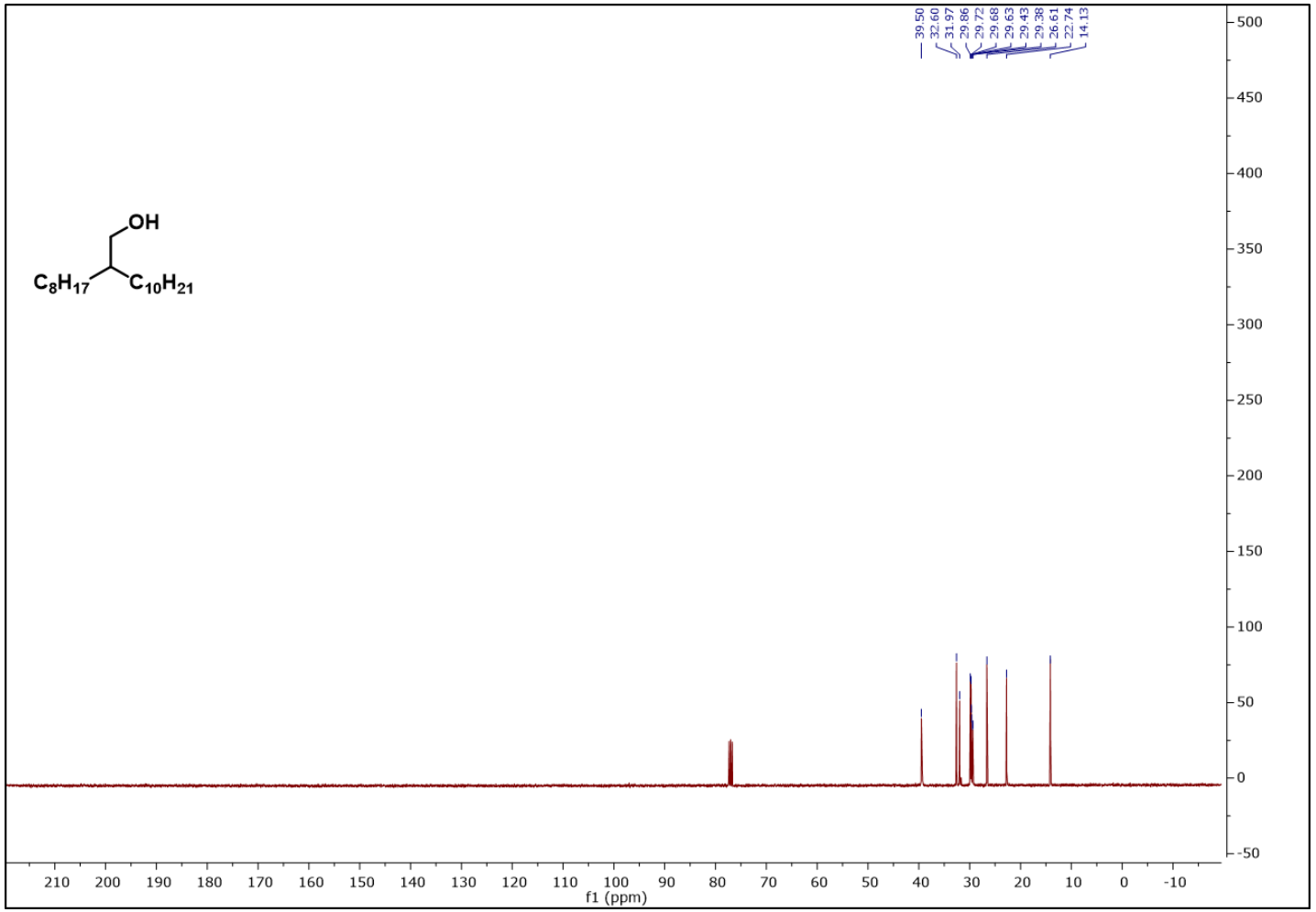

Figure A.8.2. ^{13}C-NMR spectrum of 9-(bromomethyl)nonadecane

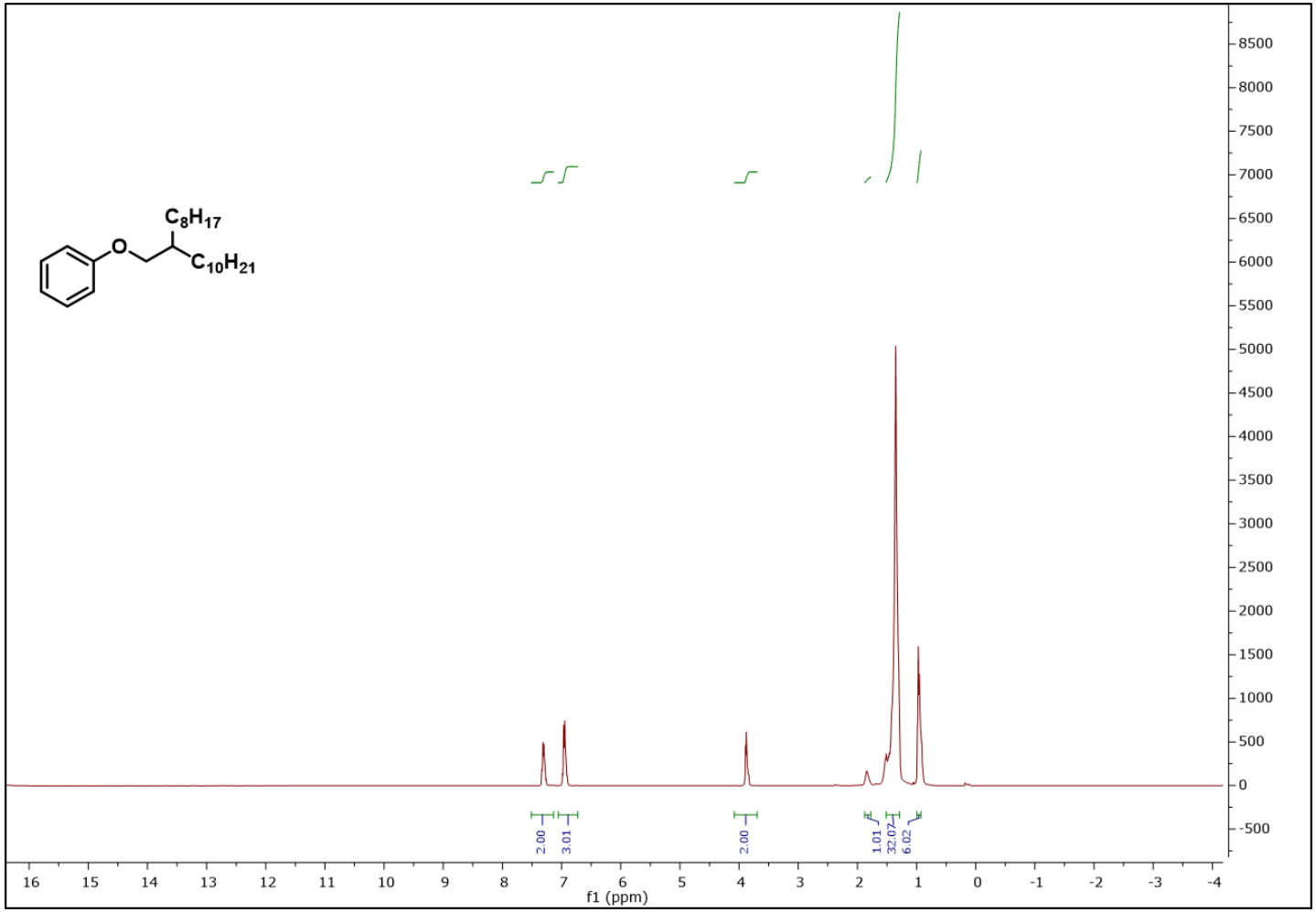

Figure A.9.1. ^{1}H-NMR spectrum of ((2-octyldodecyl)oxy)benzene

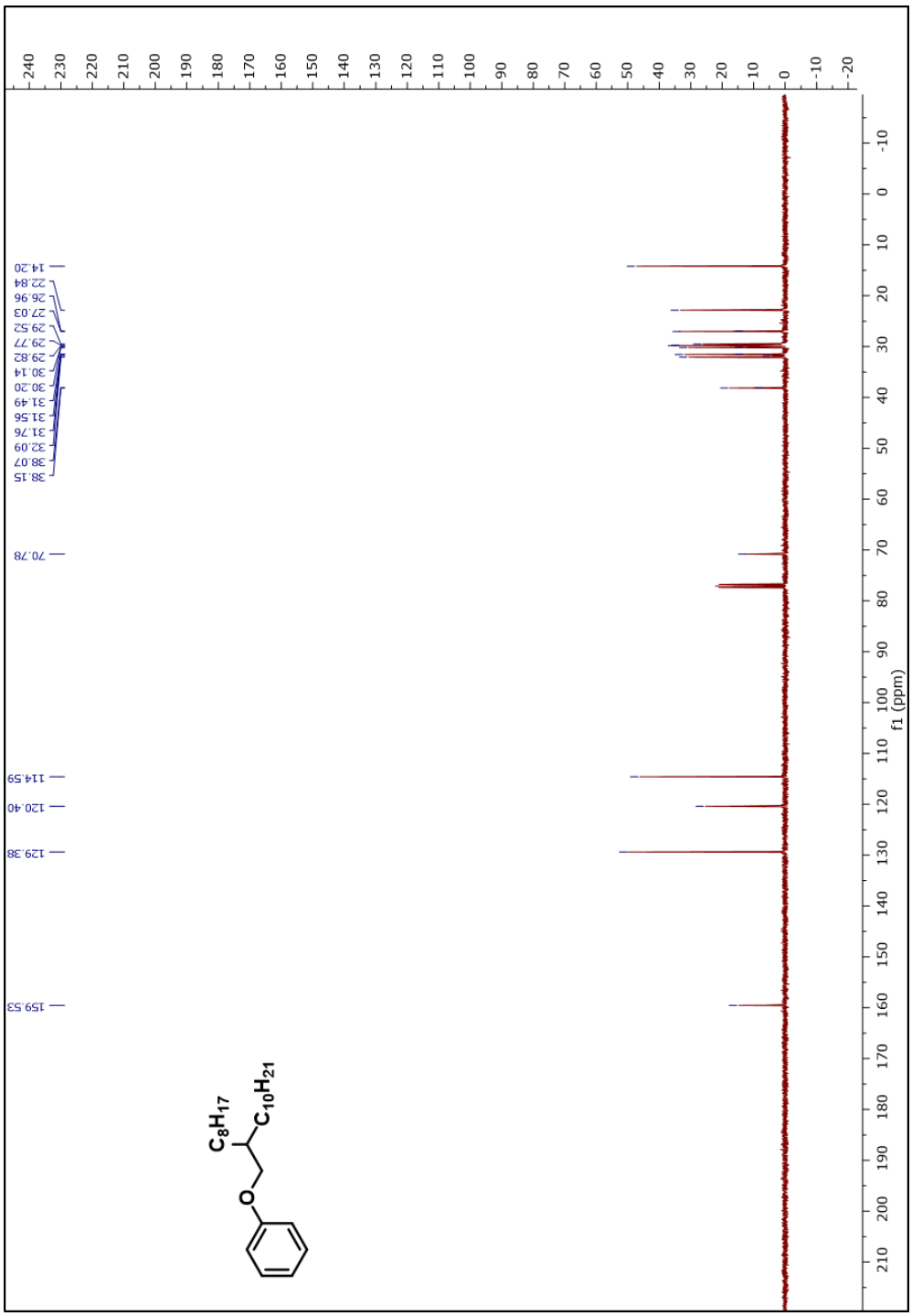

Figure A.9.2. ^{13}C-NMR spectrum of ((2-octyldodecyl)oxy)benzene

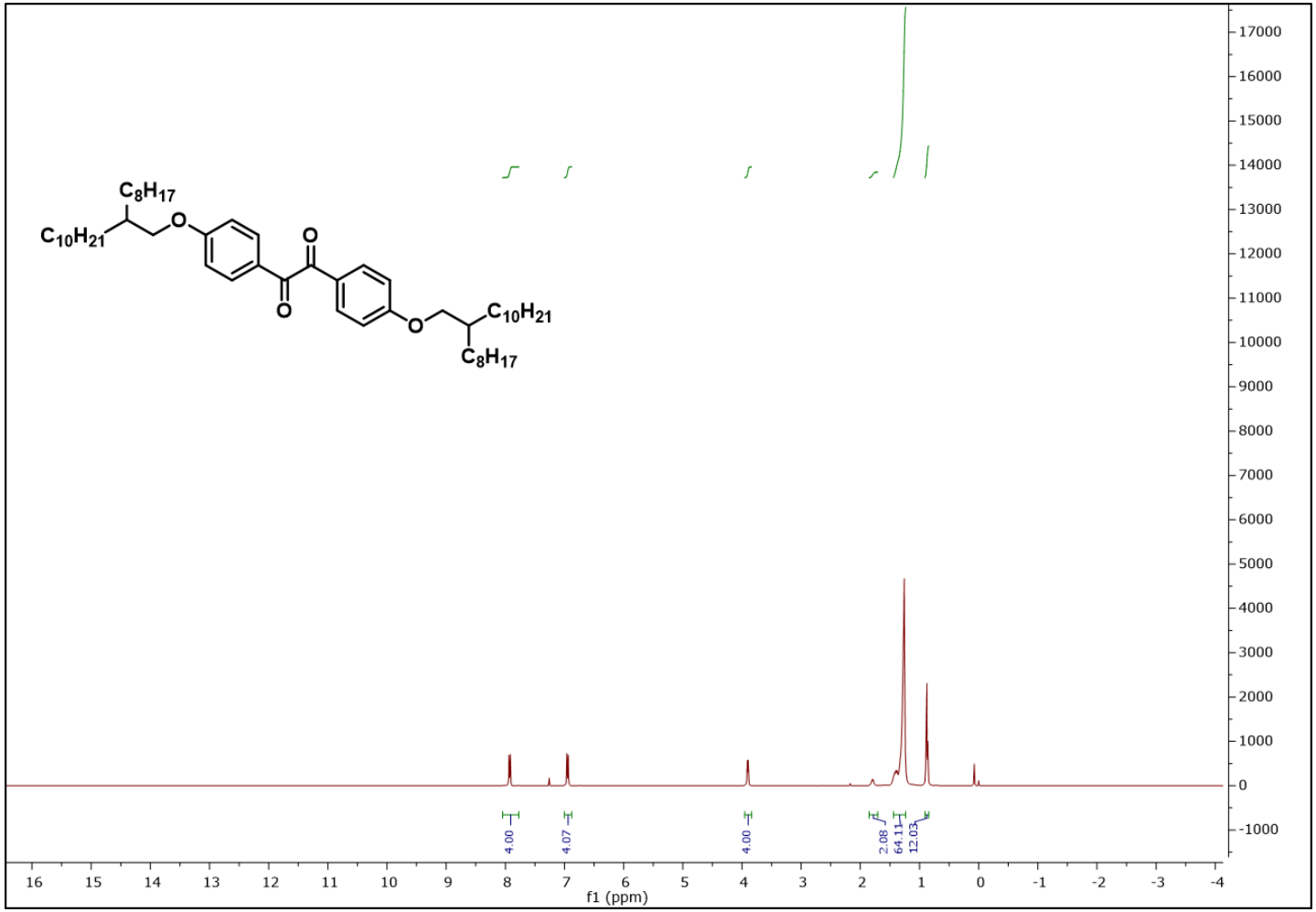

Figure A.10.1. ^{1}H-NMR spectrum of 1,2-bis(4-((2-octyldodecyl)oxy)phenyl)ethane-1,2-dione

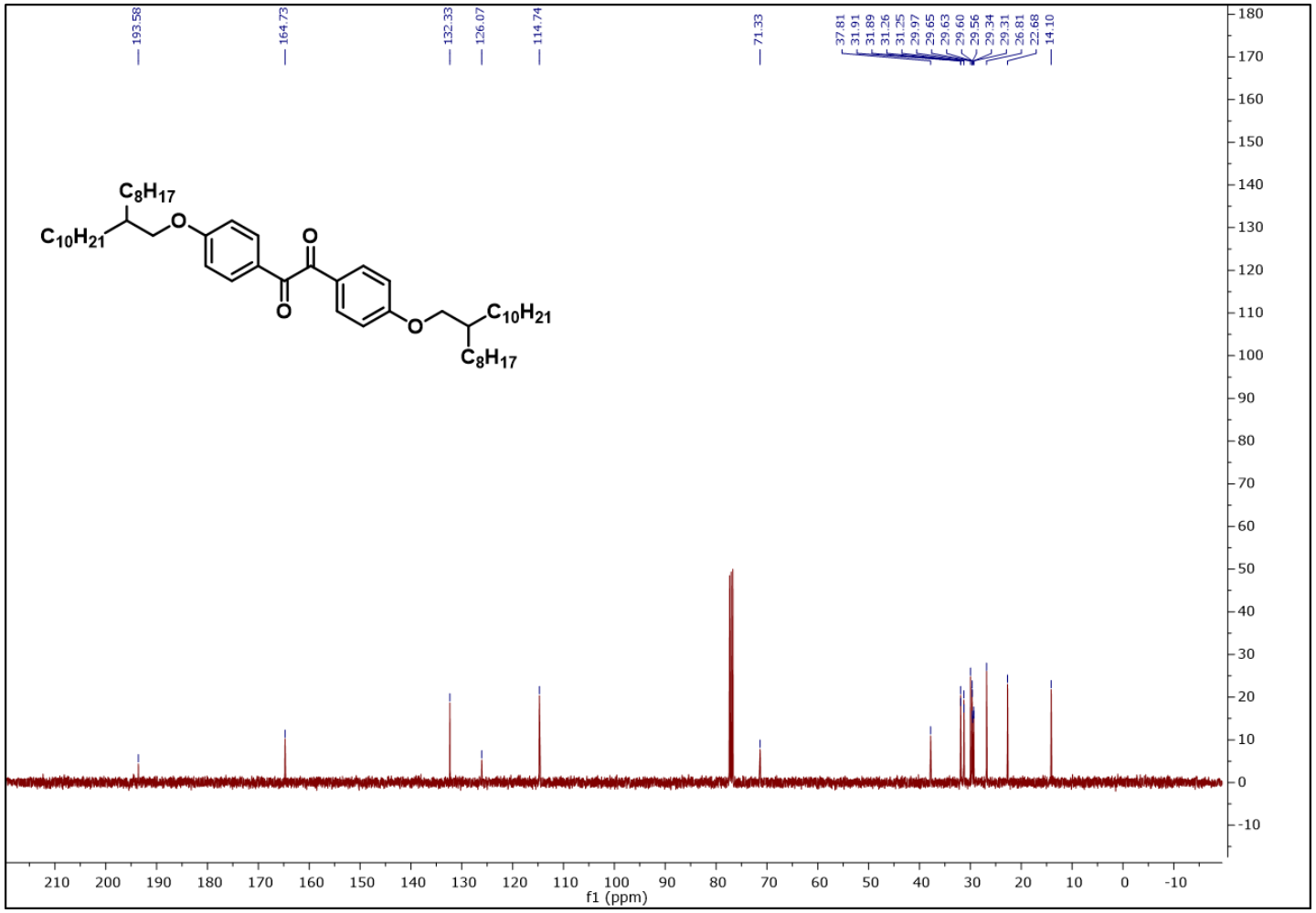

Figure A.10.2. ^{13}C-NMR spectrum of 1,2-bis(4-((2-octyldodecyl)oxy)phenyl)ethane-1,2-dione

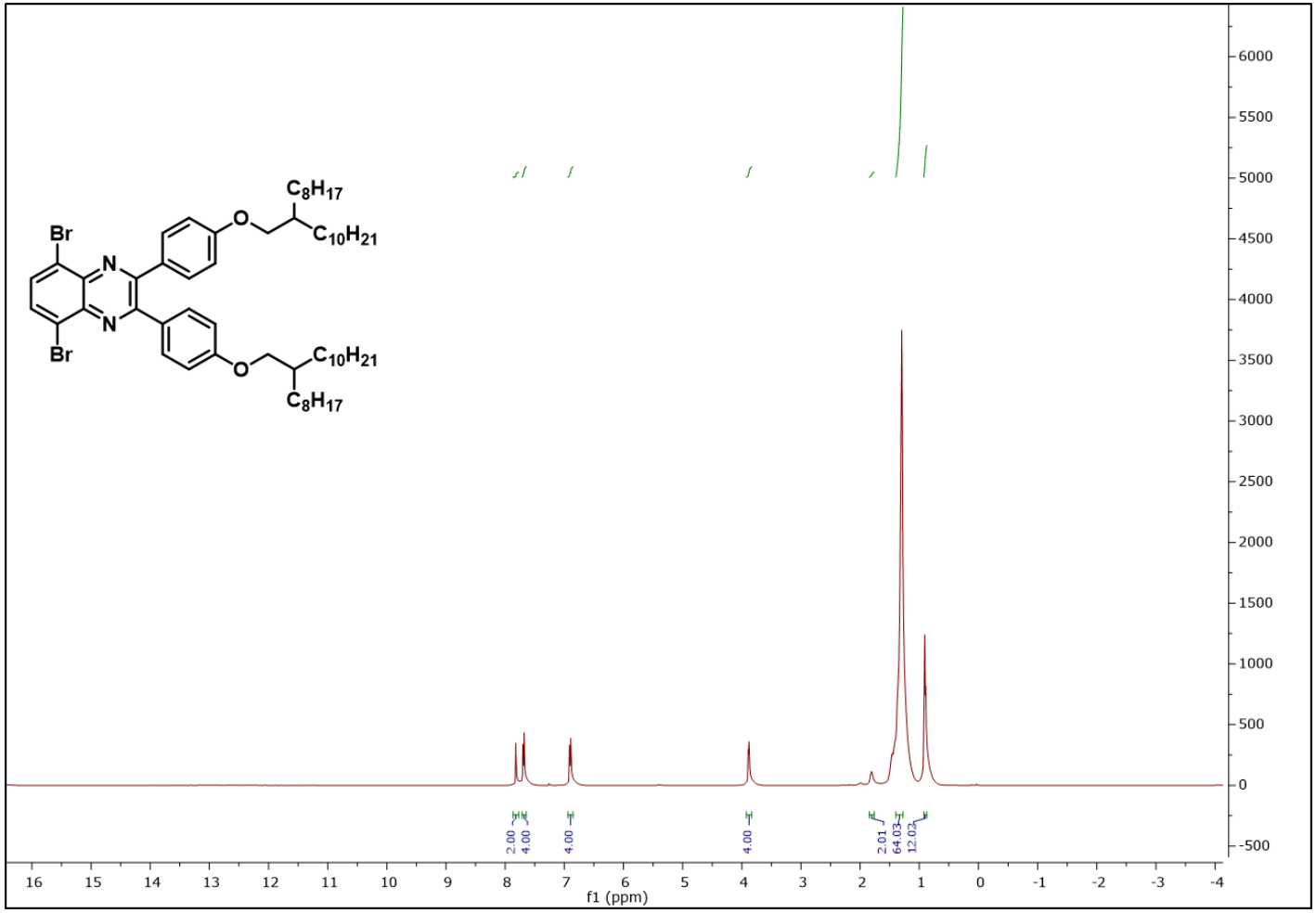

Figure A.11.1. ^{1}H-NMR spectrum of 5,8-dibromo-2,3-bis(4-((2-octyldodecyl)oxy)phenyl)quinoxaline

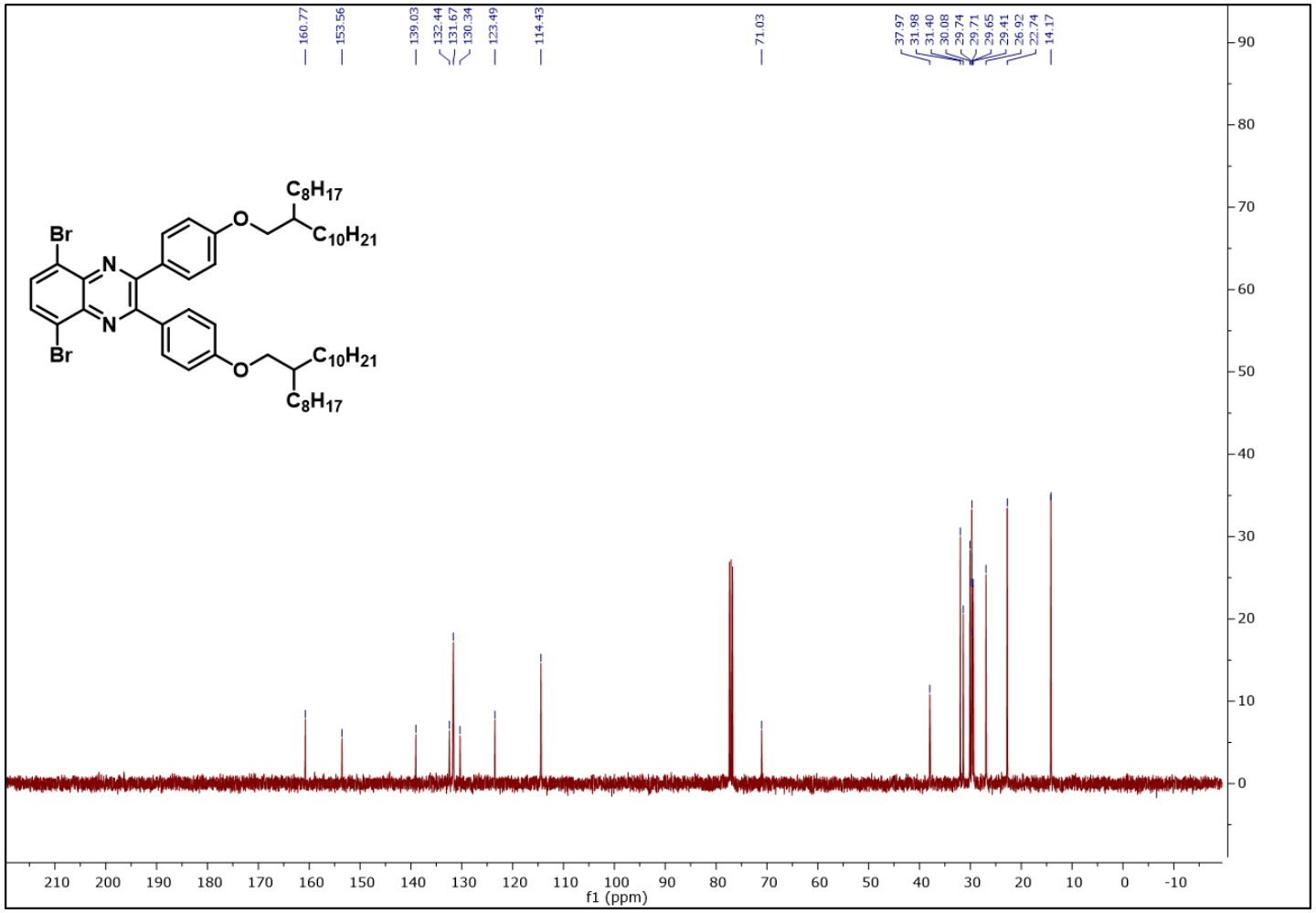

Figure A.11.2. ^{13}C-NMR spectrum of 5,8-dibromo-2,3-bis(4-((2-octyldodecyl)oxy)phenyl)quinoxaline

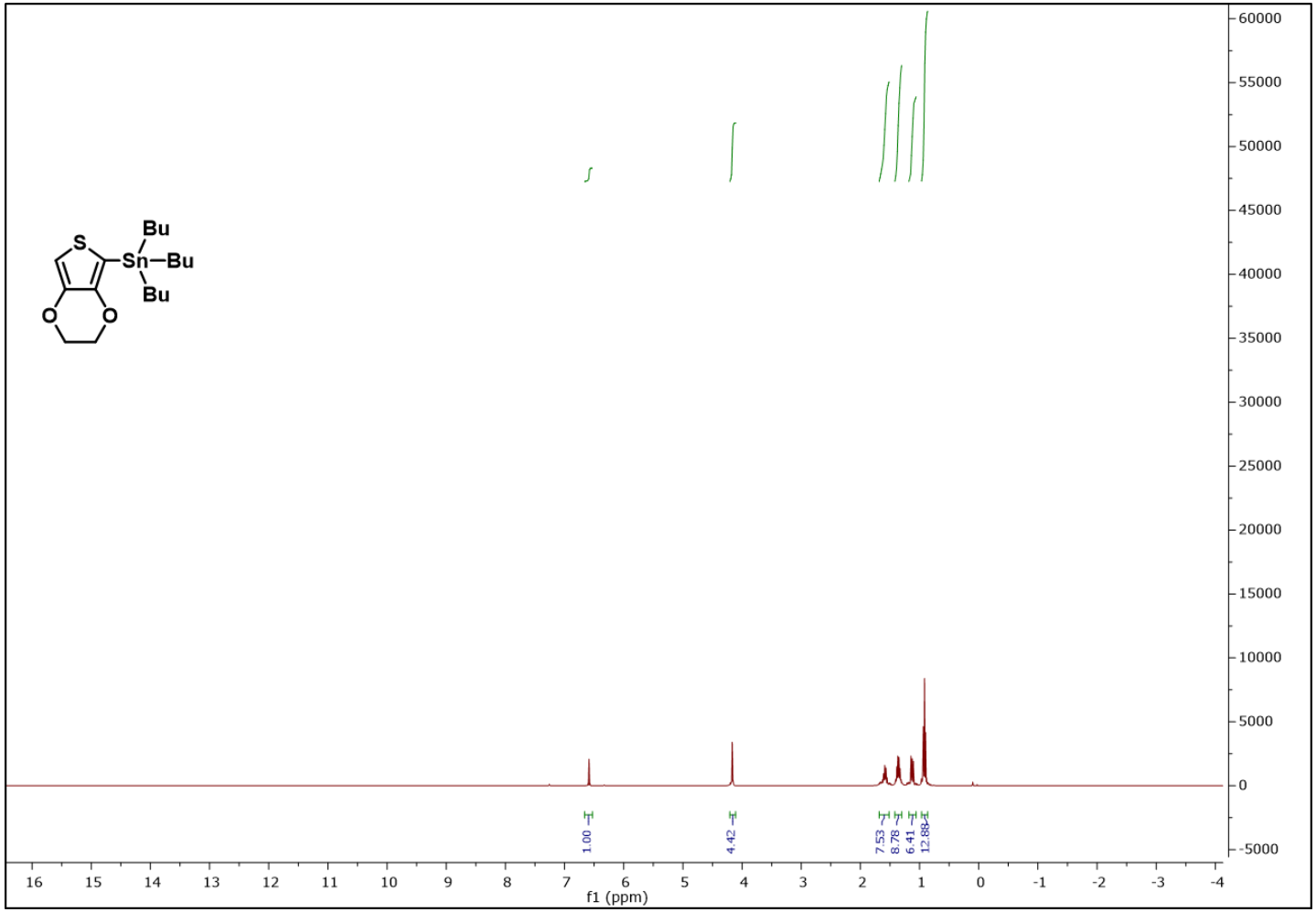

Figure A.12.1. ^{1}H-NMR spectrum of tributyl(2,3-dihydrothieno[3,4-b][1,4]dioxin-5-yl)stannane

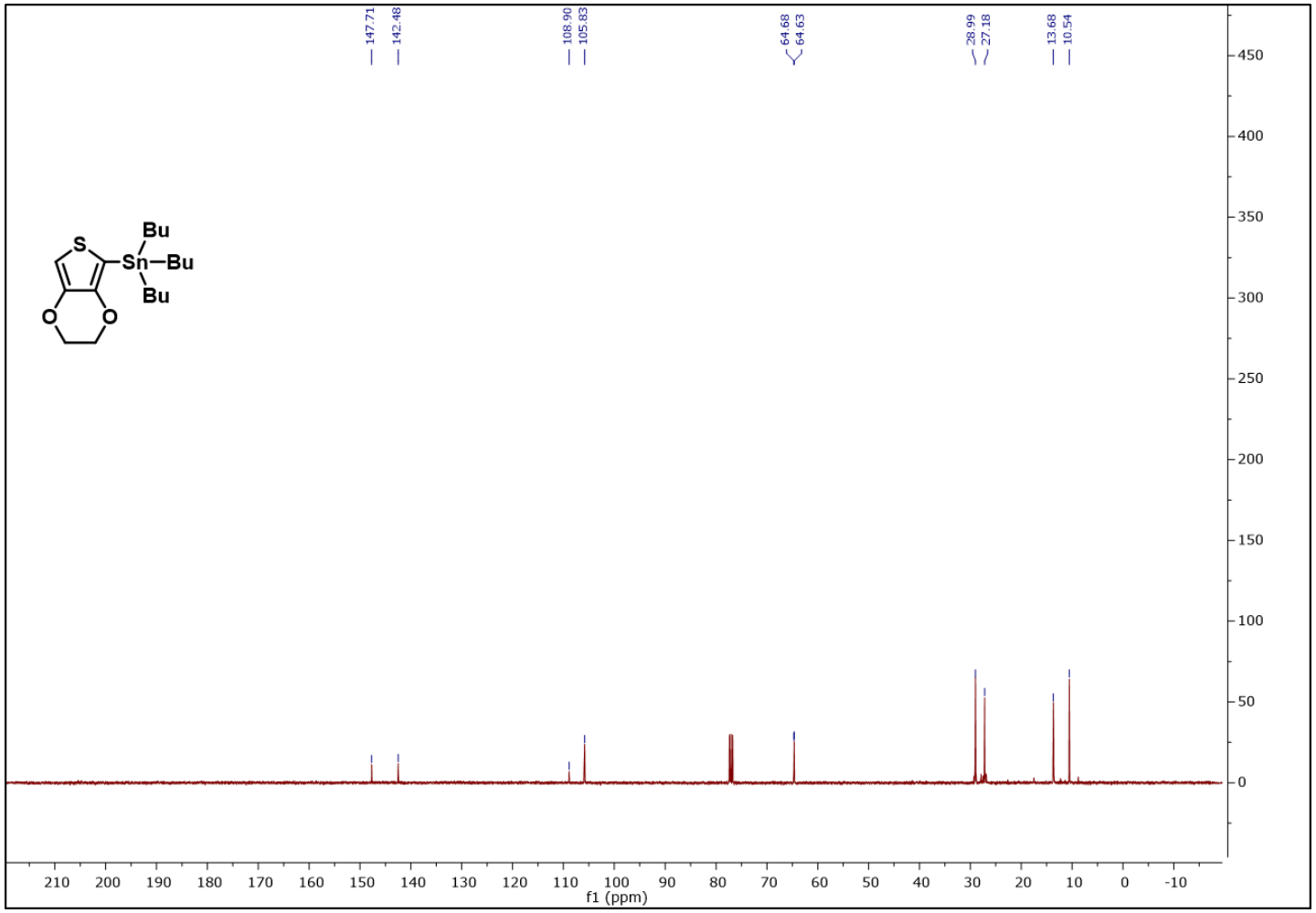

Figure A.12.2. ^{13}C-NMR spectrum of tributyl(2,3-dihydrothieno[3,4-b][1,4]dioxin-5-yl)stannane

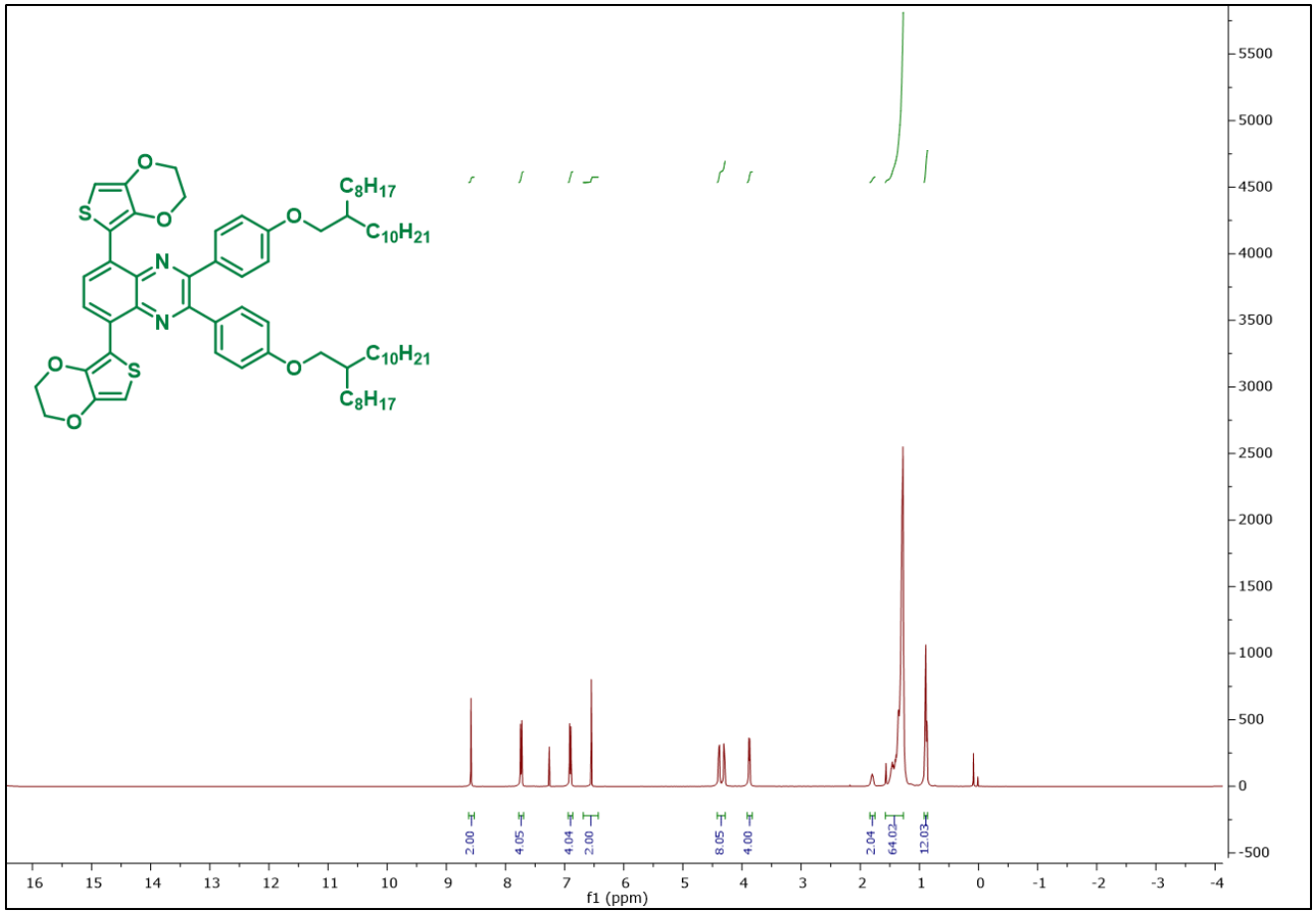

Figure A.13.1. ^{1}H-NMR spectrum of 5,8-bis(2,3-dihydrothieno[3,4-b][1,4]dioxin-5-yl)-2,3-bis(4-((2-octyldodecyl)oxy)phenyl)quinoxaline

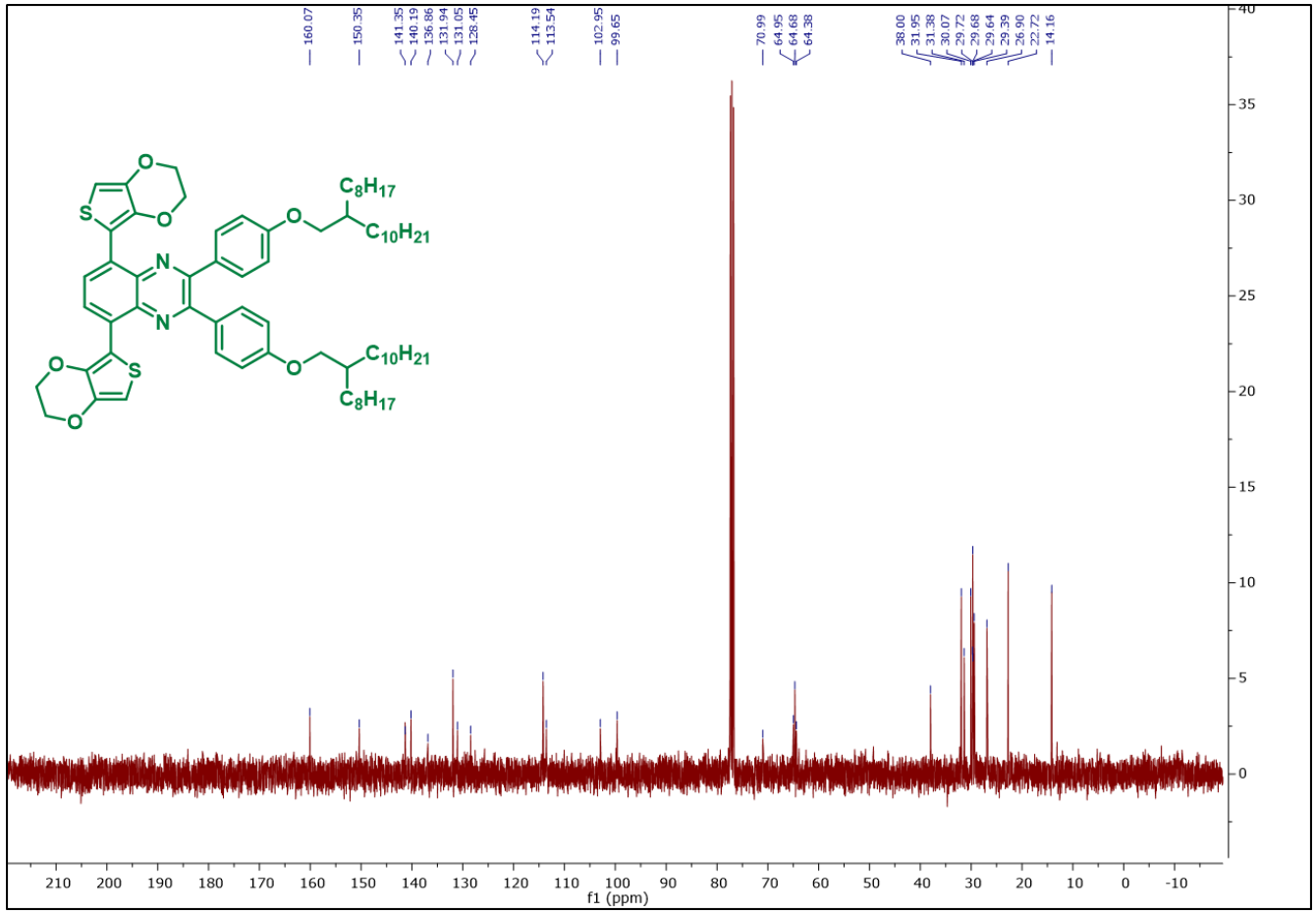

Figure A.13.2. ^{13}C-NMR spectrum of 5,8-bis(2,3-dihydrothieno[3,4-b][1,4]dioxin-5-yl)-2,3-bis(4-((2-octyldodecyl)oxy)phenyl)quinoxaline

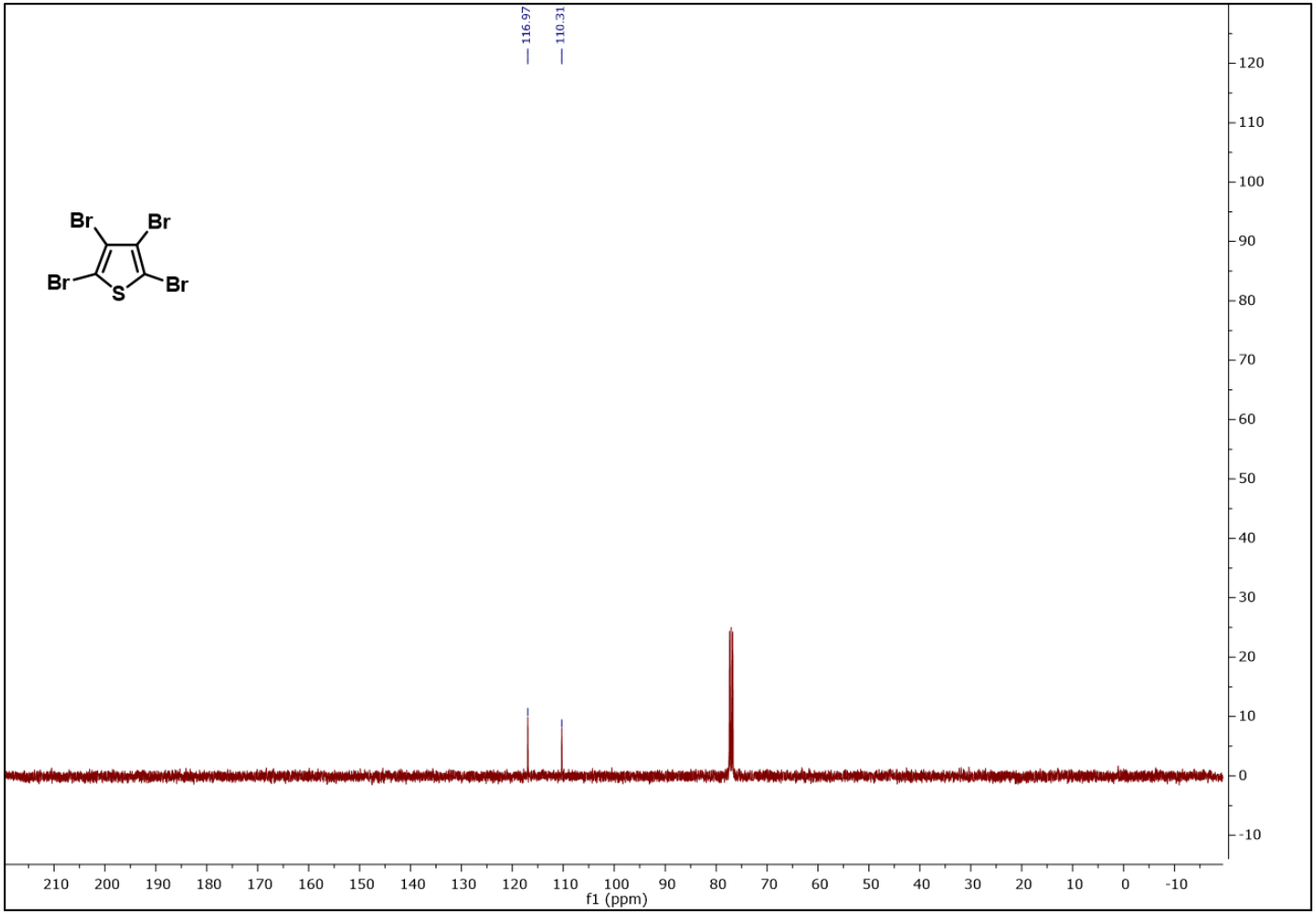

Figure A.14.1. ^{1}H-NMR spectrum of 2,3,4,5-tetrabromothiophene

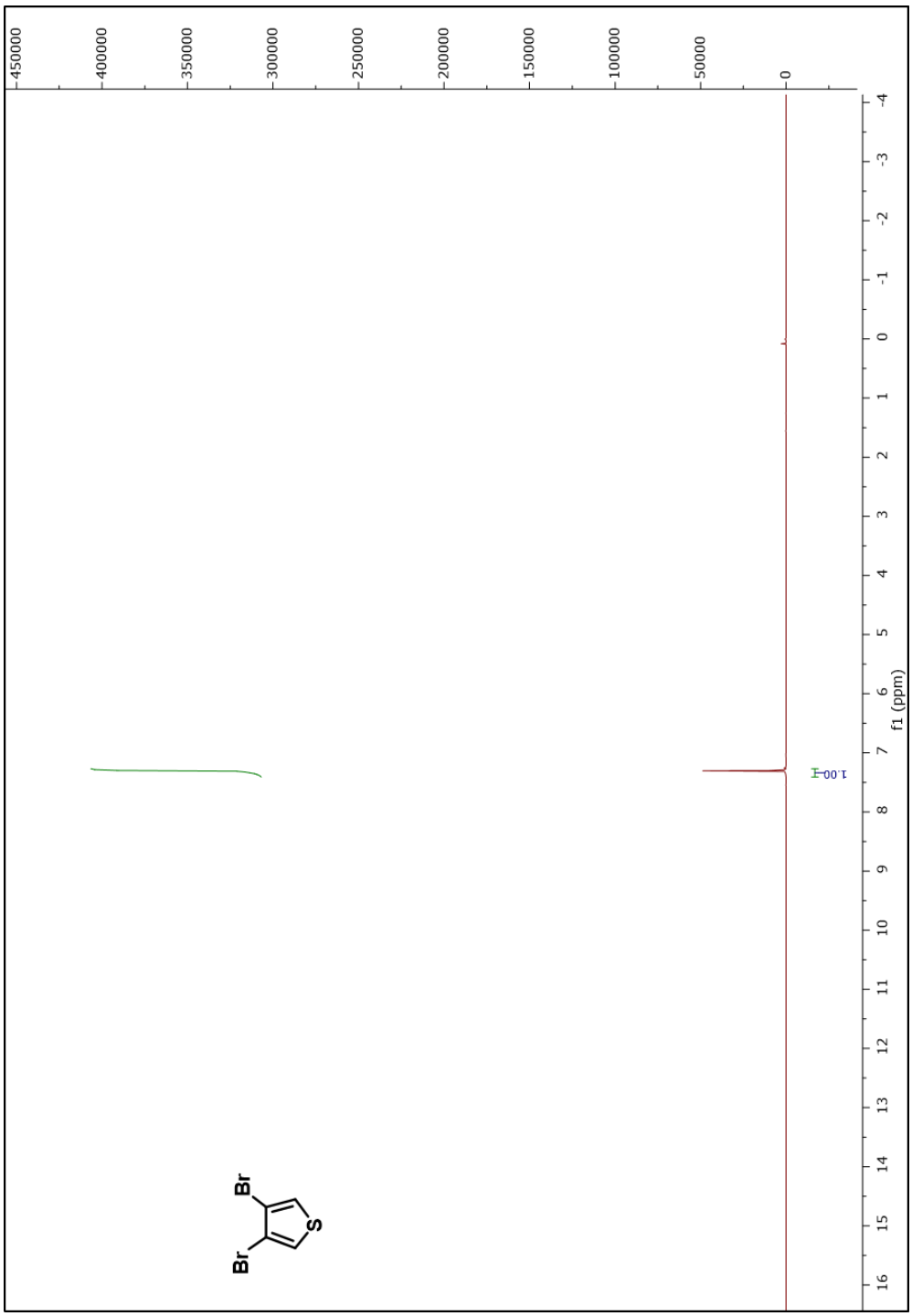

Figure A.15.1. ^{13}H-NMR spectrum of 3,4-dibromothiophene

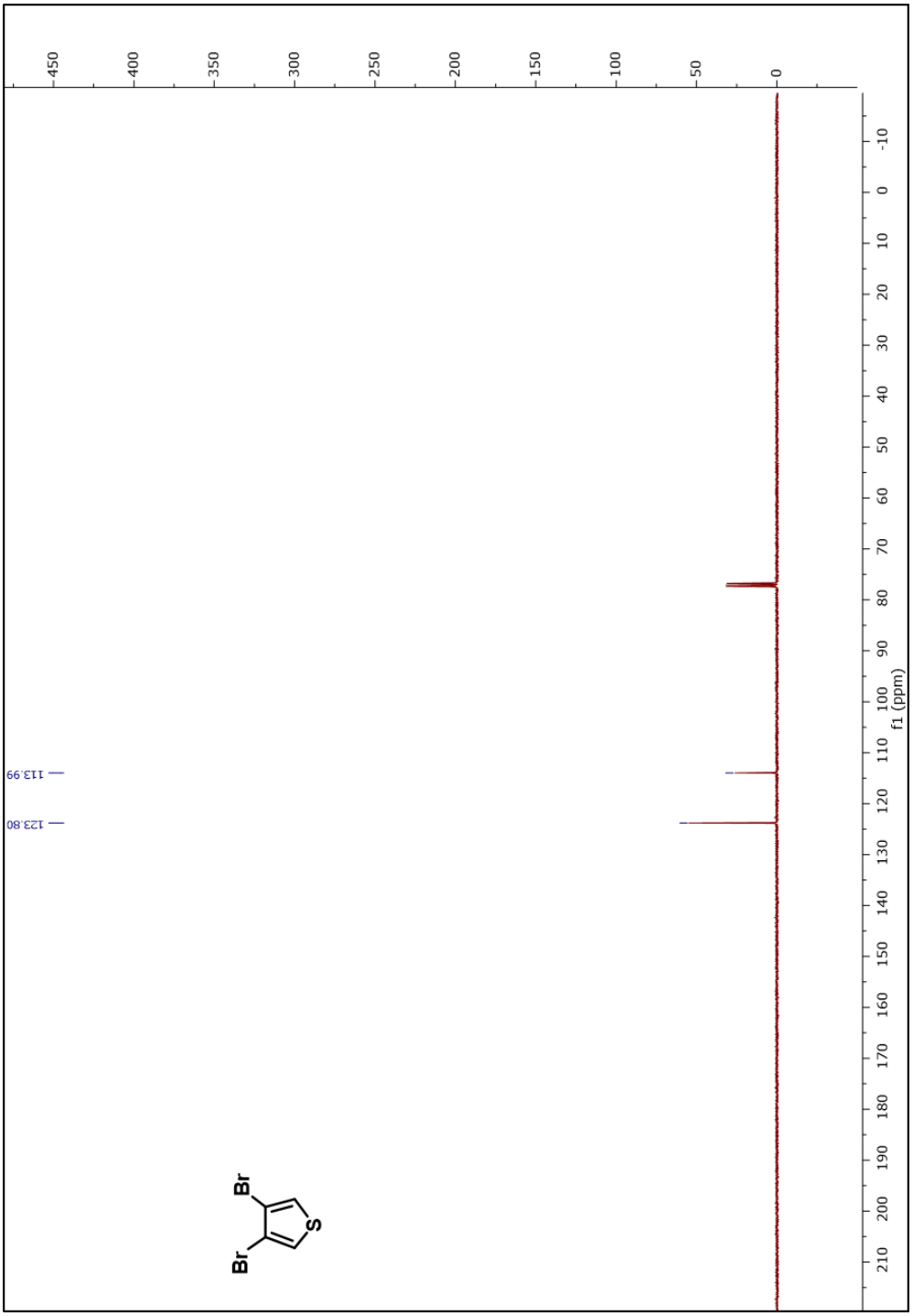

Figure A.15.2. ^{13}C-NMR spectrum of 3,4-dibromothiophene

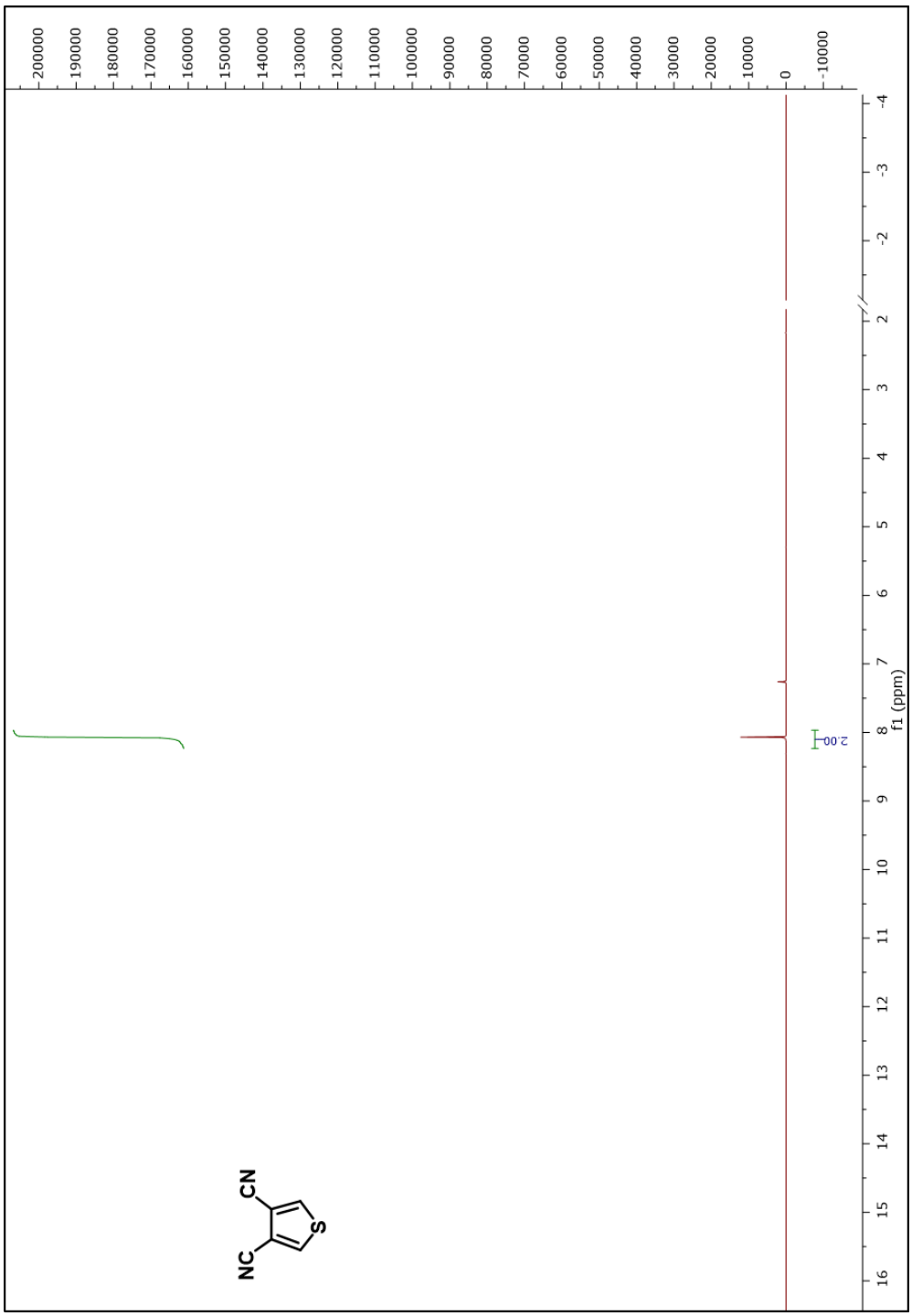

Figure A.16.1. ^{1}H-NMR spectrum of 3,4-dicyanothiophene

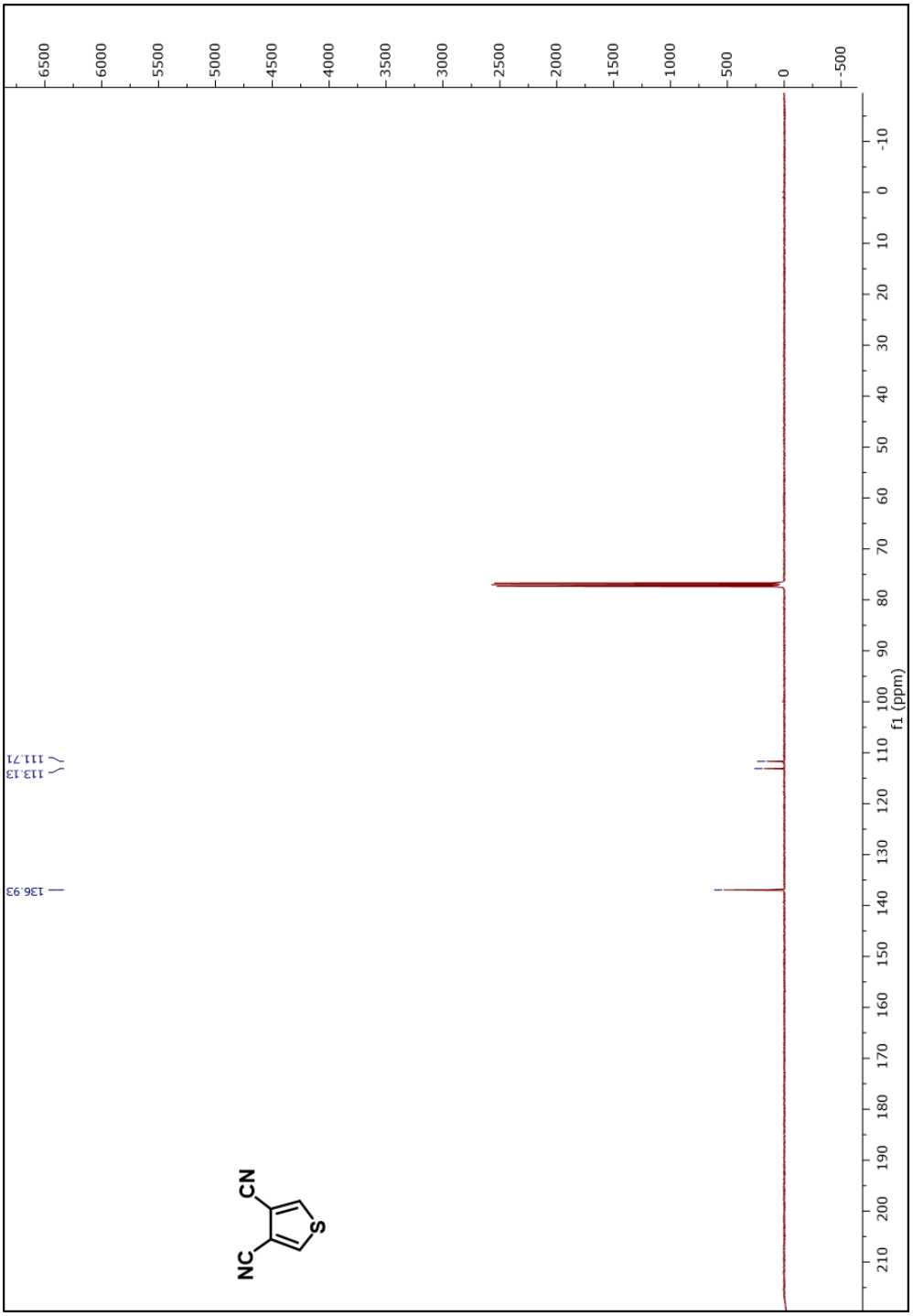

Figure A.16.2. ^{13}C-NMR spectrum of 3,4-dicyanothiophene

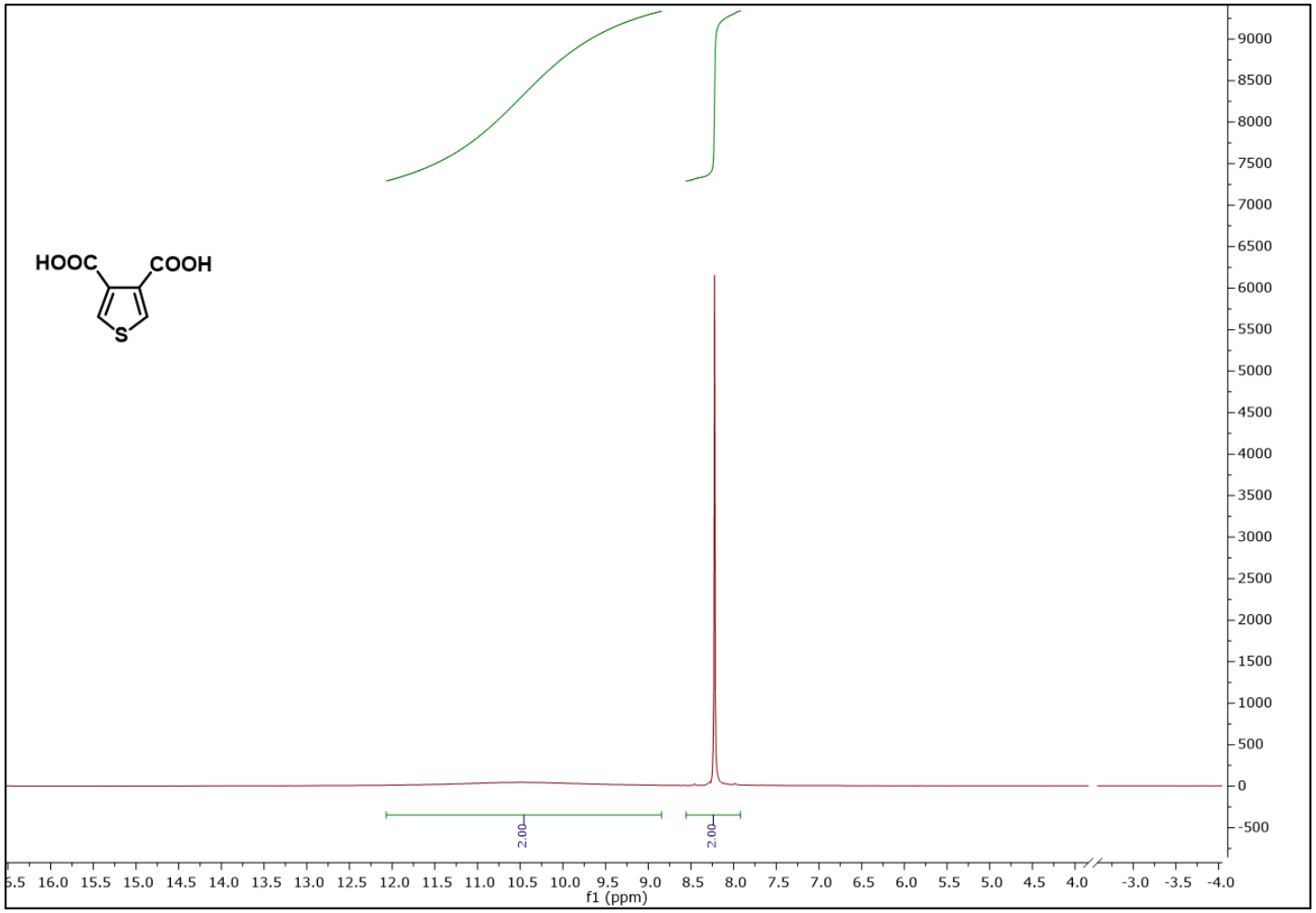

Figure A.17.1. ^{1}H-NMR spectrum of thiophene-3,4-dicarboxylic acid

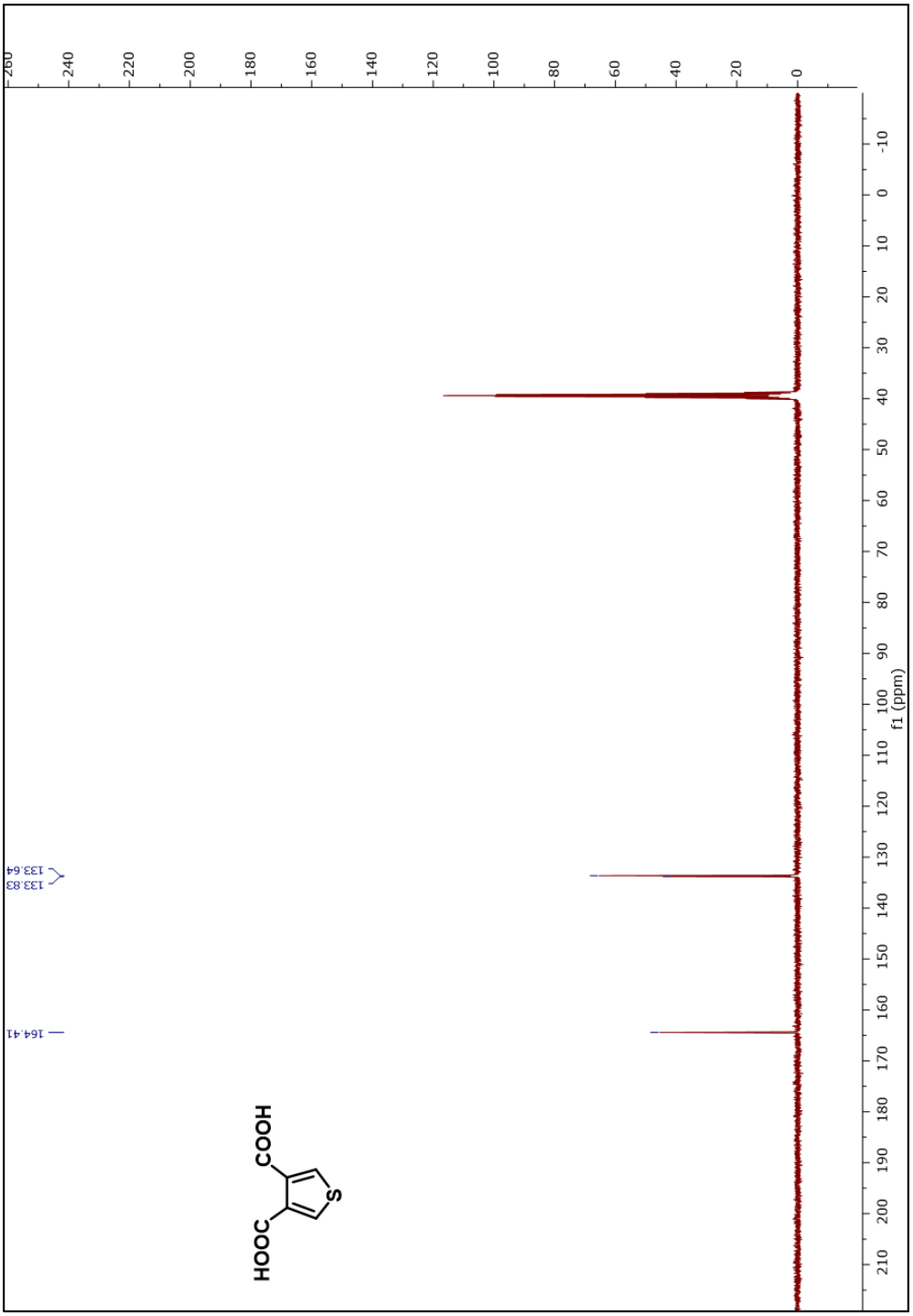

Figure A.17.2. ^{13}C-NMR spectrum of thiophene-3,4-dicarboxylic acid

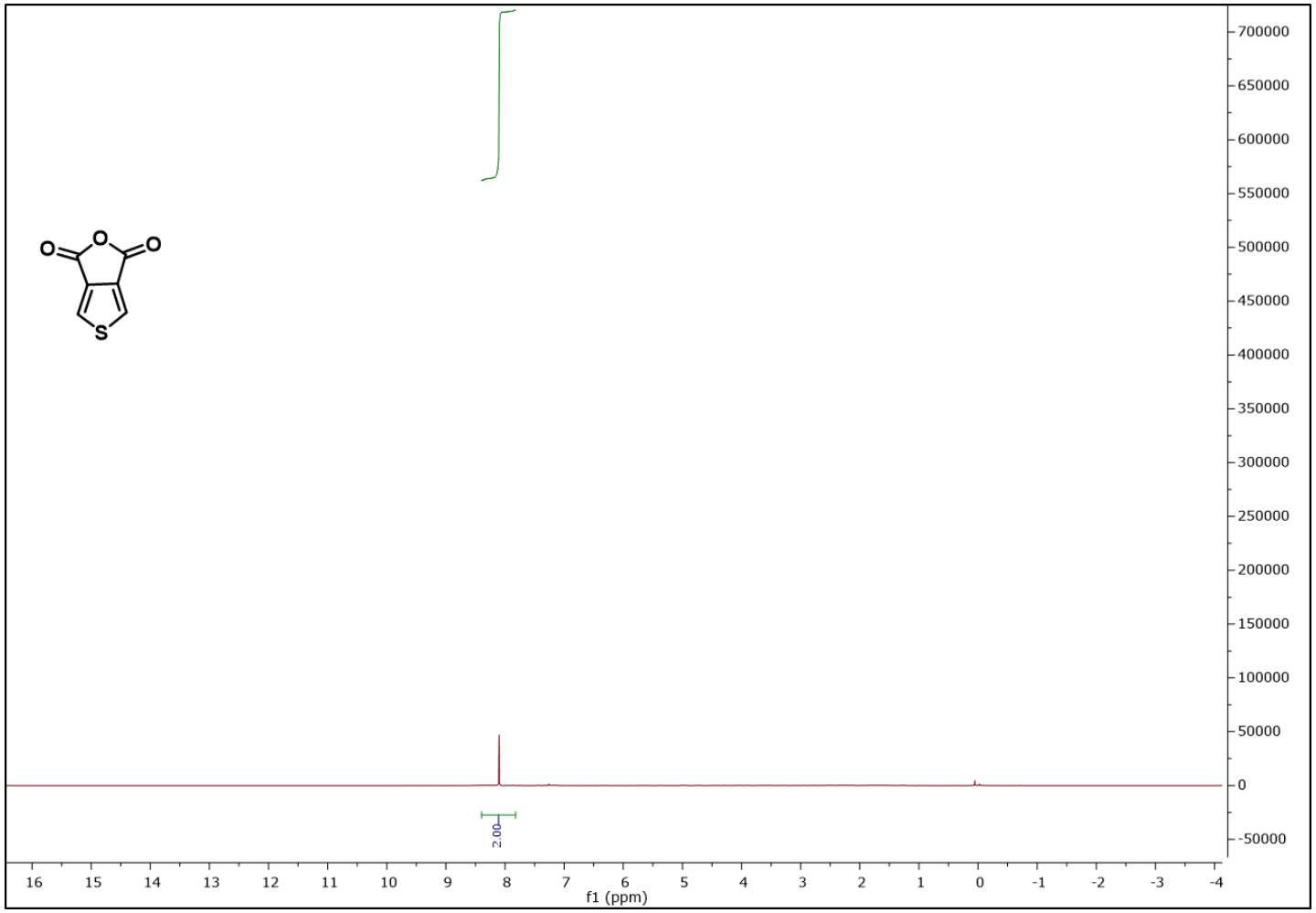

Figure A.18.1. ^{1}H-NMR spectrum of 1H,3H-thieno[3,4-c]furan-1,3-dione

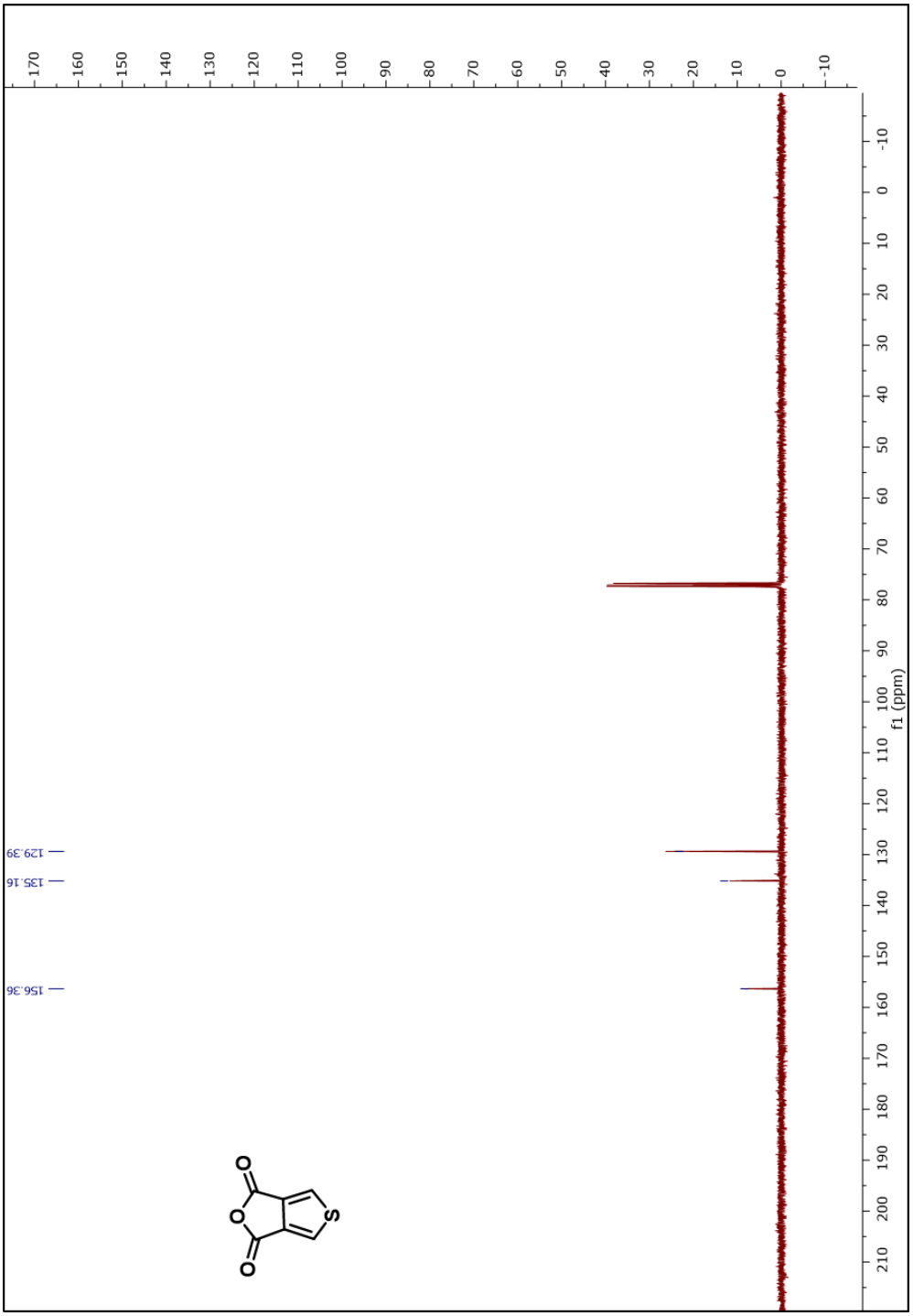

Figure A.18.2. ^{13}C-NMR spectrum of 1H,3H-thieno[3,4-c]furan-1,3-dione

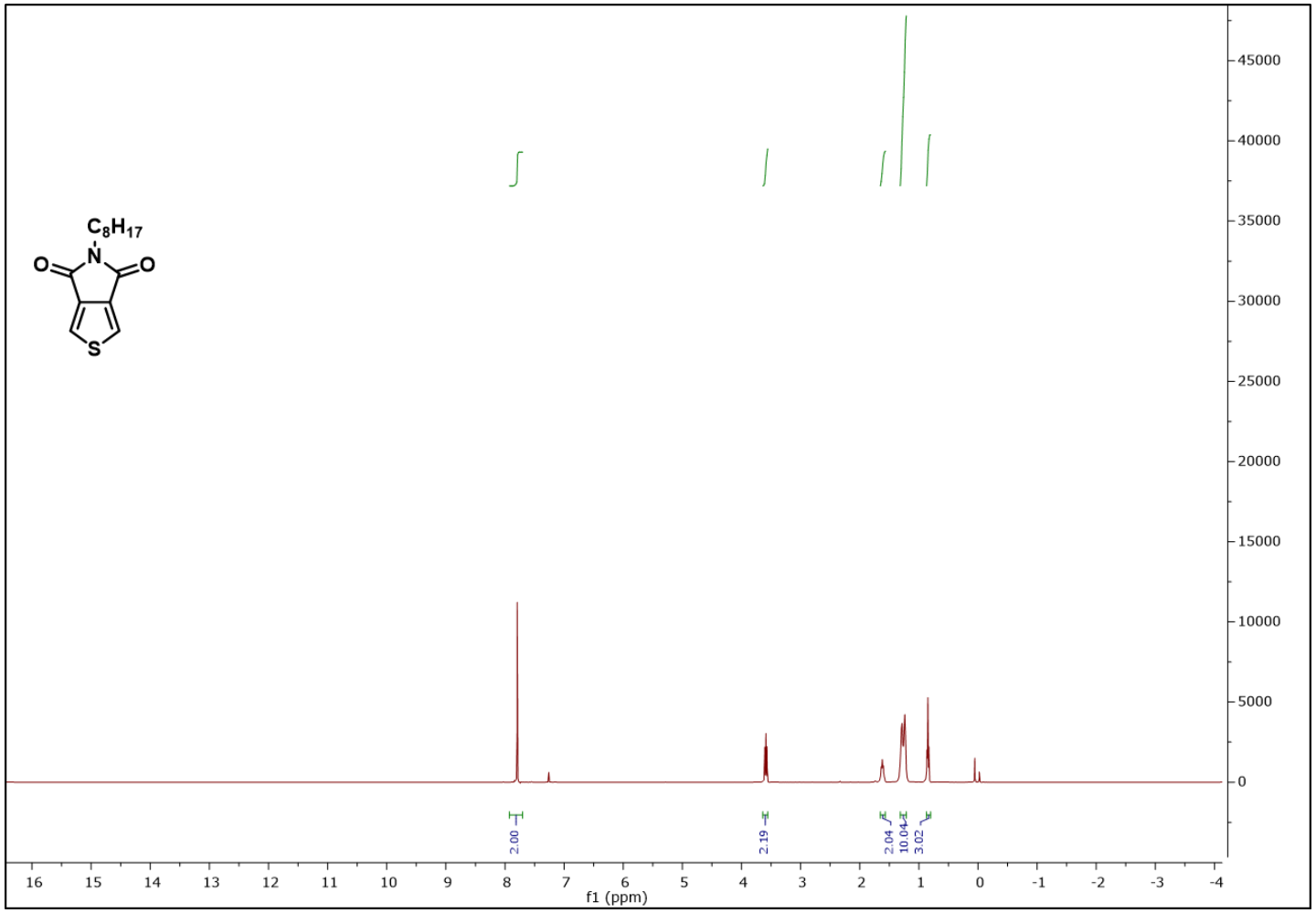

Figure A.19.1. ^{1}H-NMR spectrum of 5-octyl-4H-thieno[3,4-c]pyrrole-4,6(5H)-dione

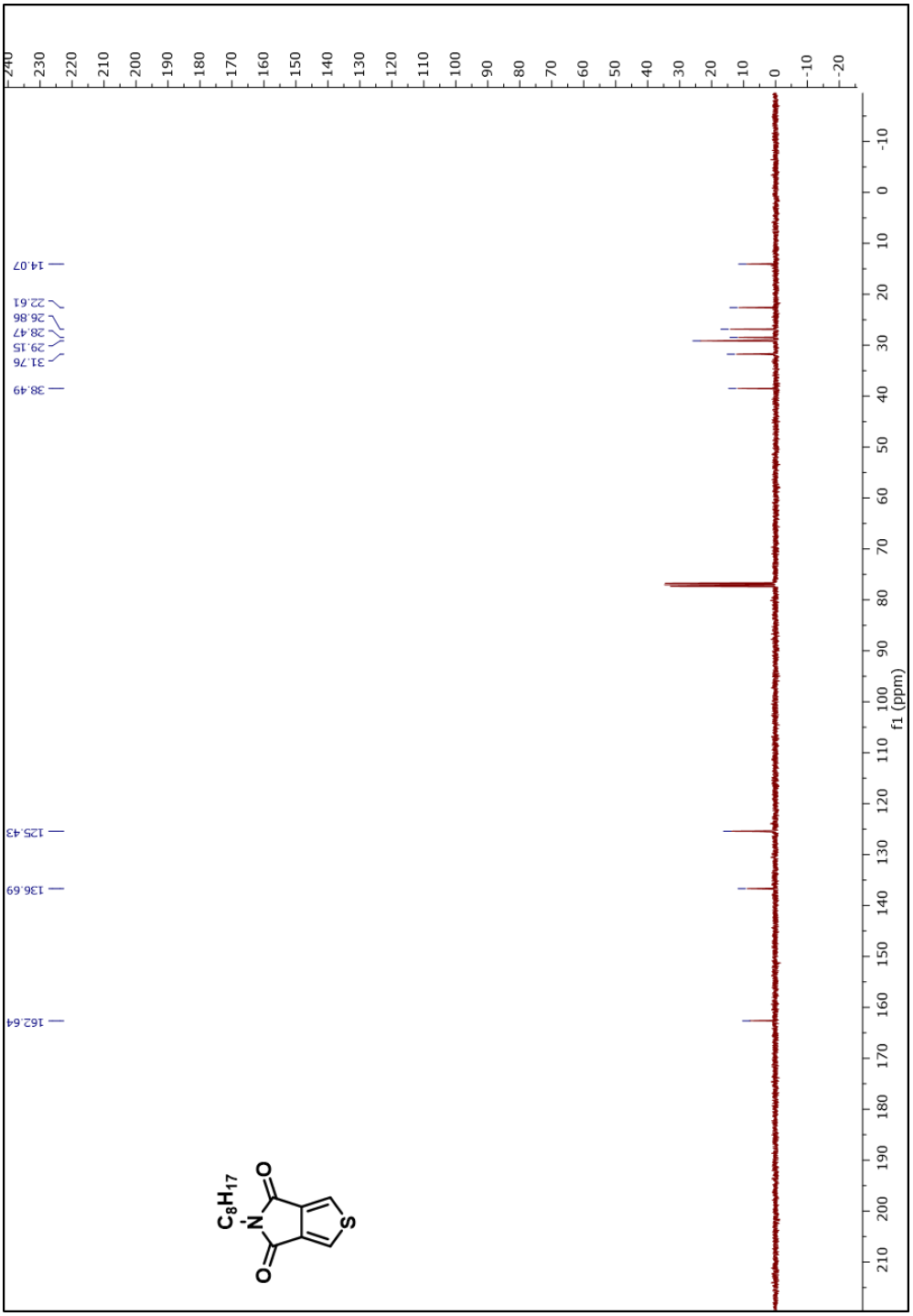

Figure A.19.2. ^{13}C-NMR spectrum of 5-octyl-4H-thieno[3,4-c]pyrrole-4,6(5H)-dione

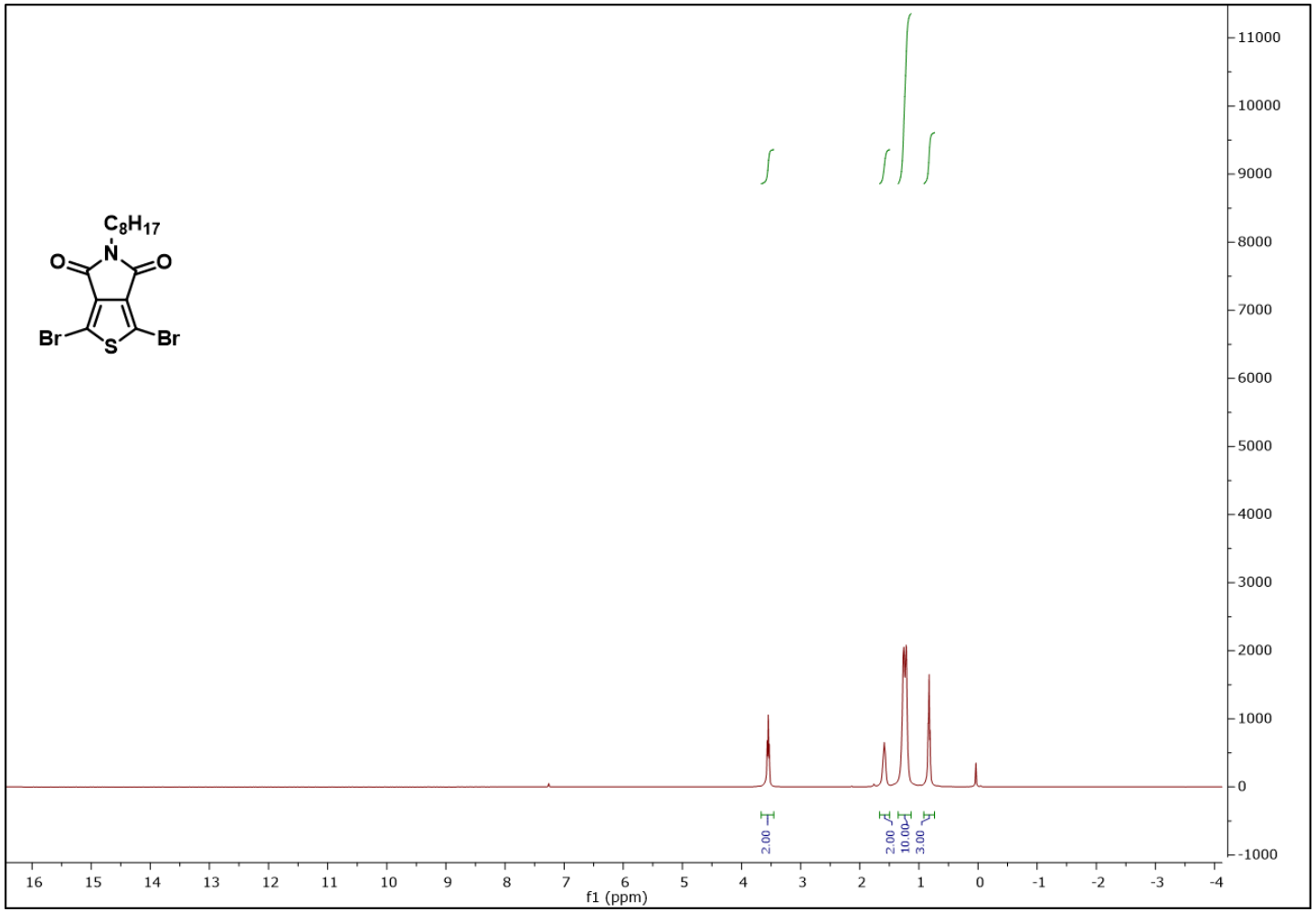

Figure A.20.1. ^{1}H-NMR spectrum of 1,3-dibromo-5-octyl-4H-thieno[3,4-c]pyrrole-4,6(5H)-dione

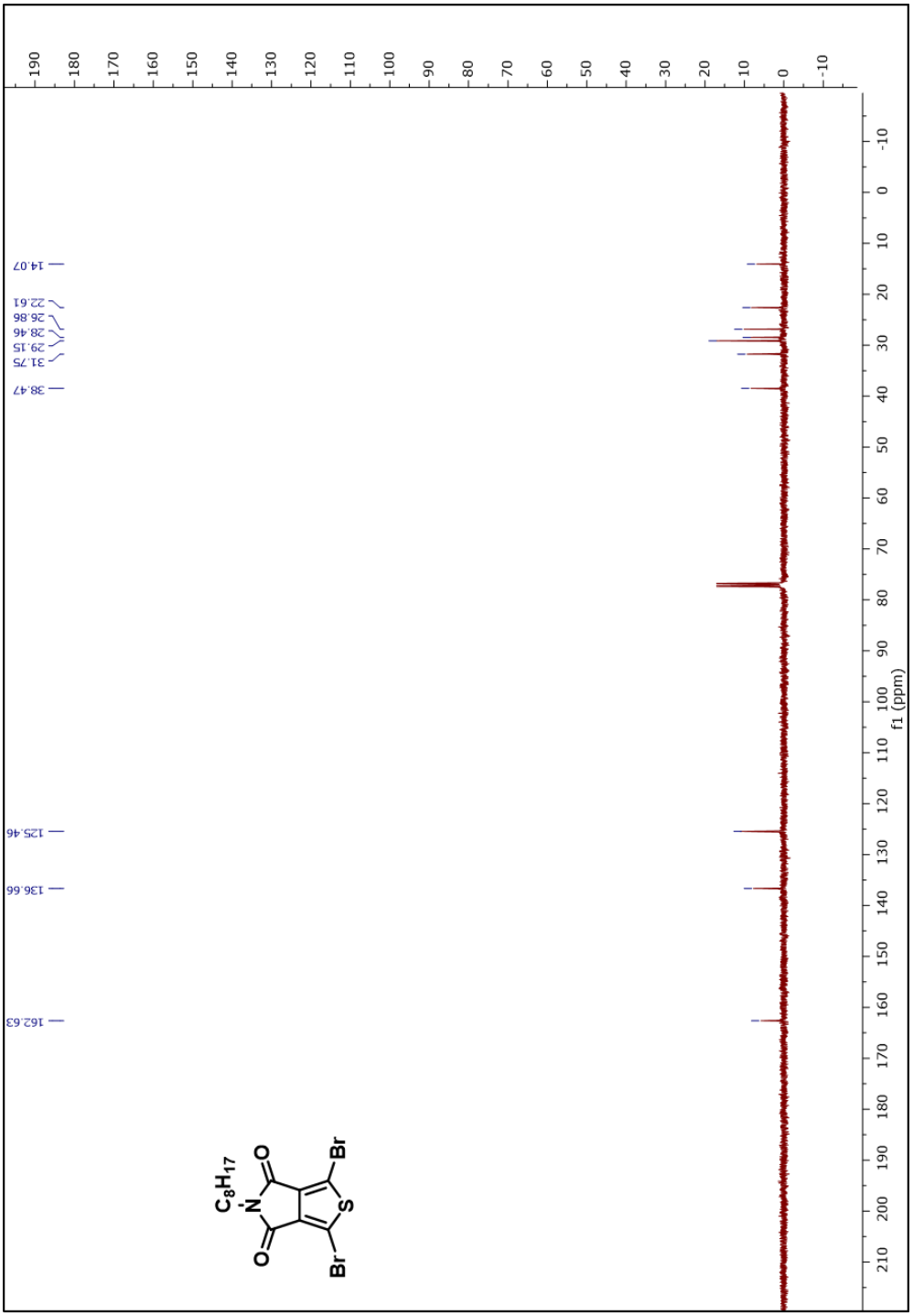

Figure A.20.2. ^{13}C-NMR spectrum of 1,3-dibromo-5-octyl-4H-thieno[3,4-c]pyrrole-4,6(5H)-dione

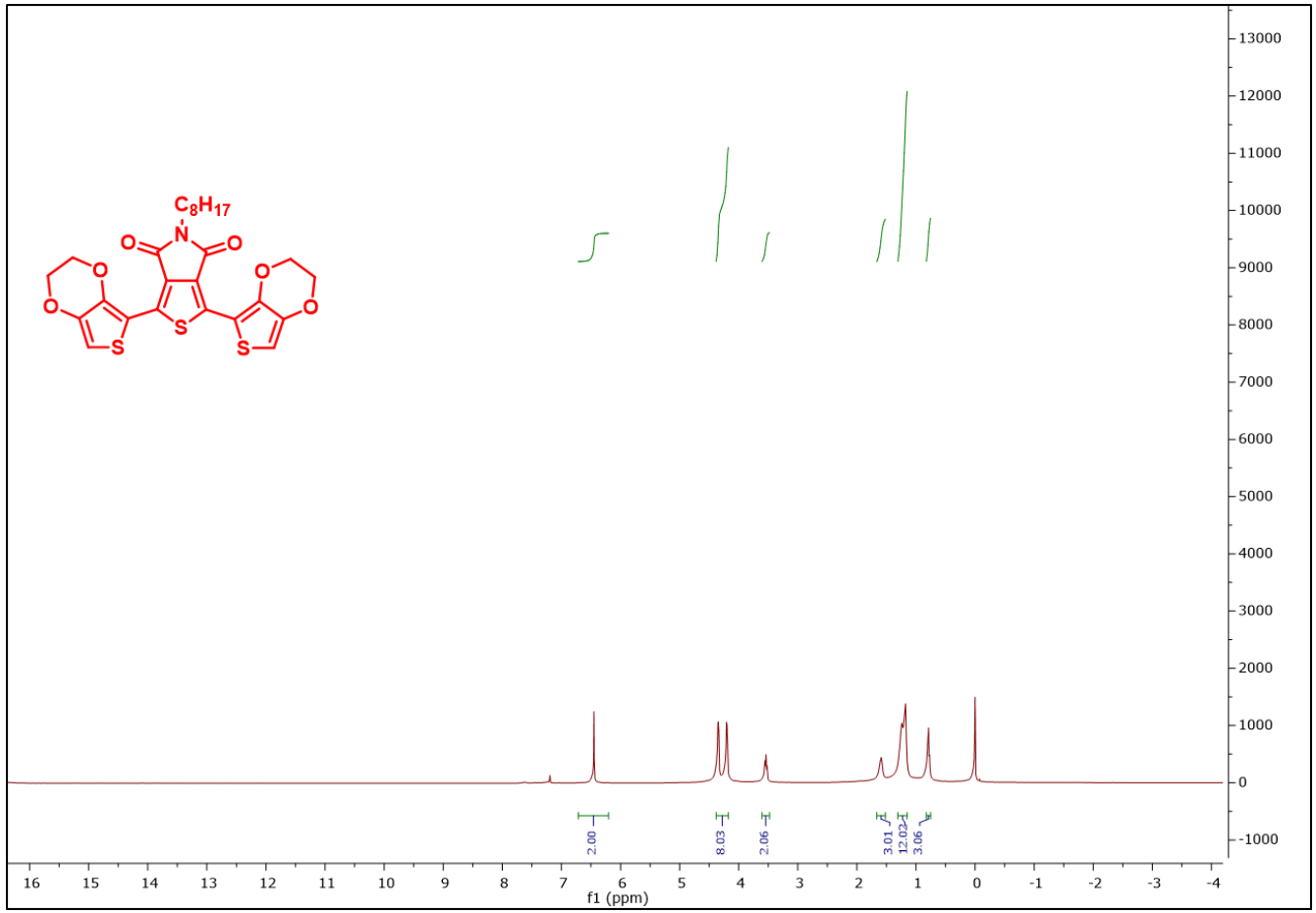

Figure A.21.1. ^{1}H-NMR spectrum of 1,3-bis(2,3-dihydrothieno[3,4-b][1,4]dioxin-5-yl)-5-octyl-4H-thieno[3,4-c]pyrrole-4,6(5H)-dione

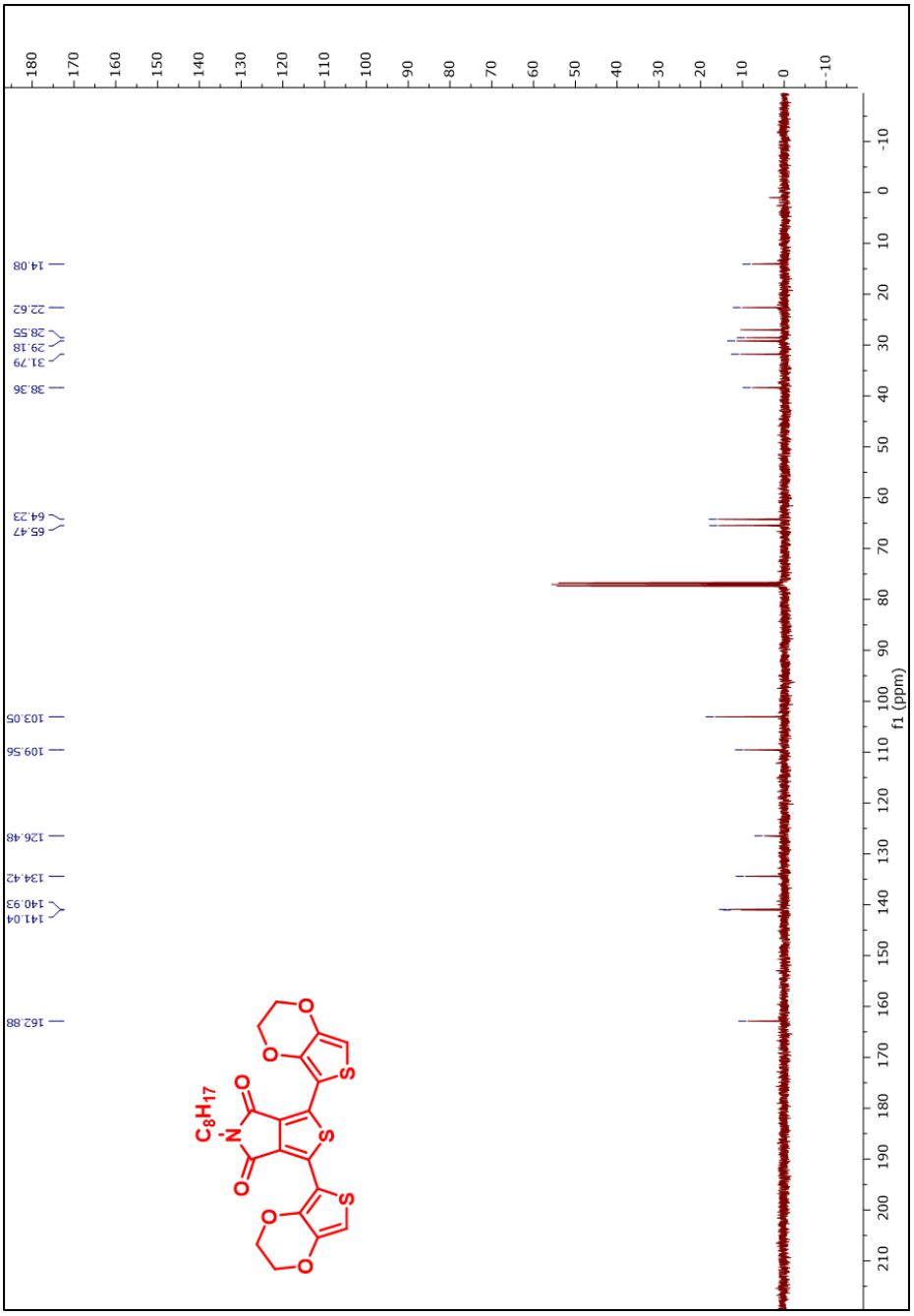

Figure A.21.2. ^{13}C-NMR spectrum of 1,3-bis(2,3-dihydrothieno[3,4-b][1,4]dioxin-5-yl)-5-octyl-4H-thieno[3,4-c]pyrrole-4,6(5H)-dione

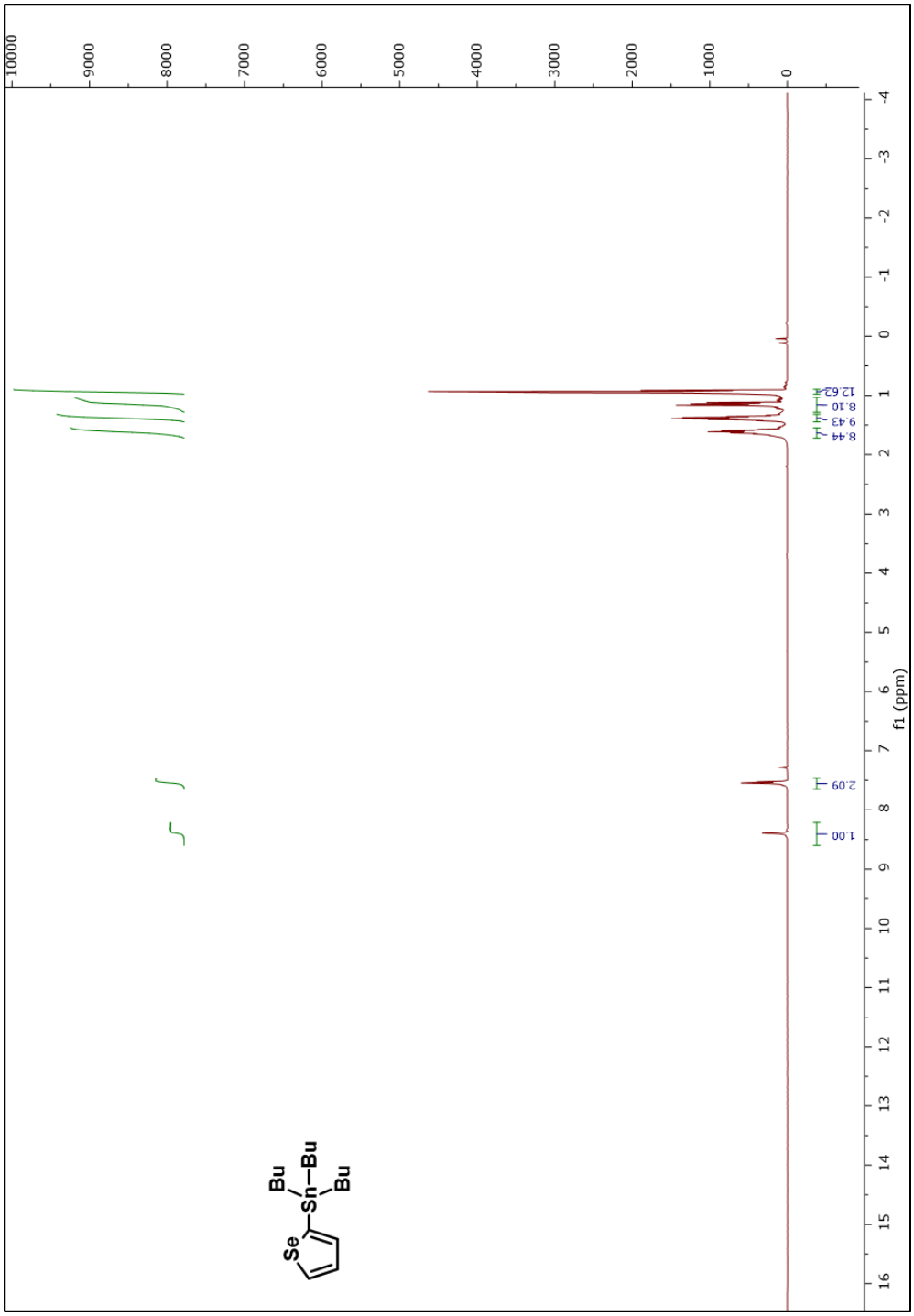

Figure A.22.1. ^{1}H-NMR spectrum of tributyl(selenophen-2-yl)stannane

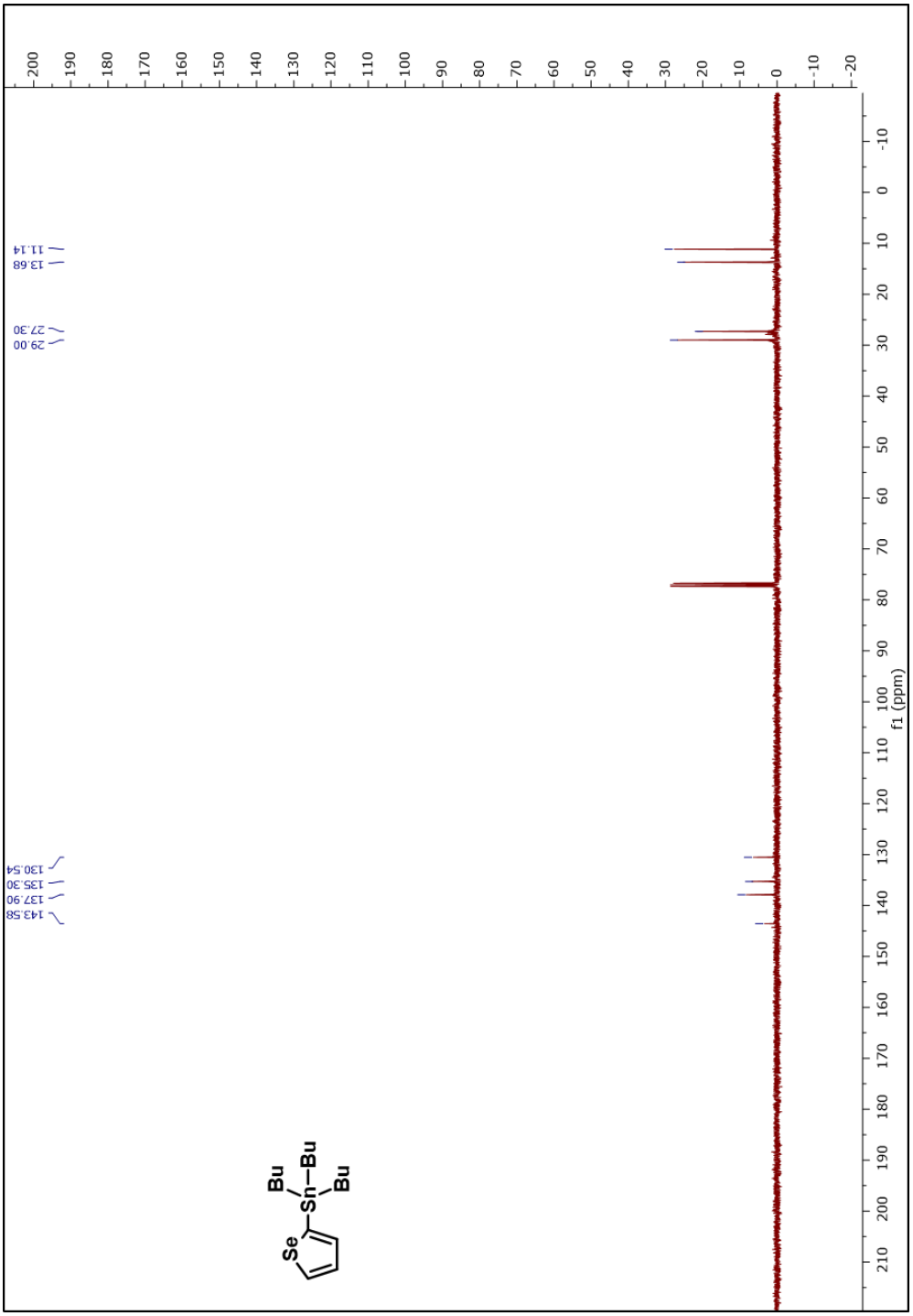

Figure A.22.2. ^{13}C-NMR spectrum of tributyl(selenophen-2-yl)stannane

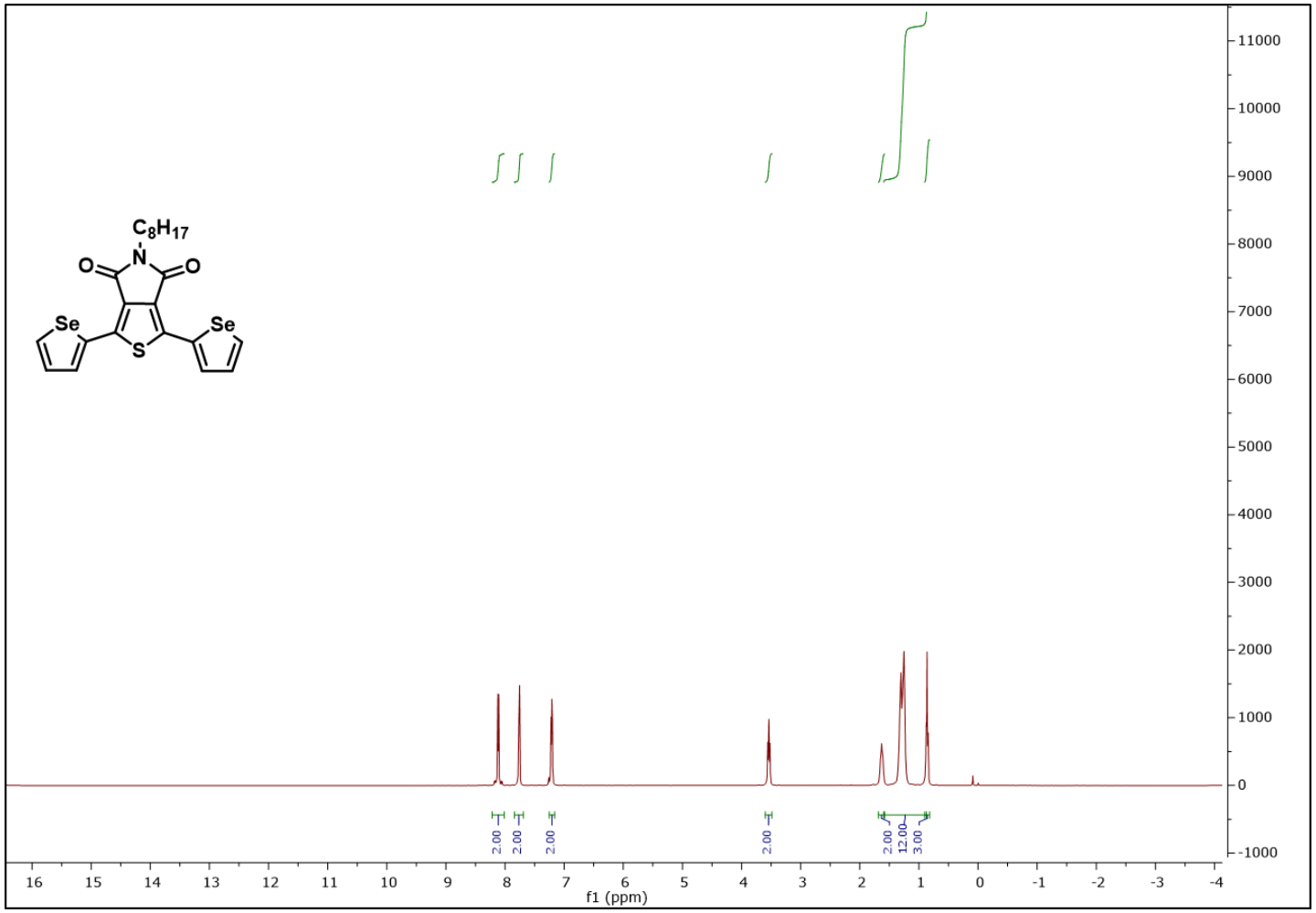

Figure A.23.1. ^{1}H-NMR spectrum of 5-octyl-1,3-di(selenophen-2-yl)-4H-thieno[3,4-c]pyrrole-4,6(5H)-dione

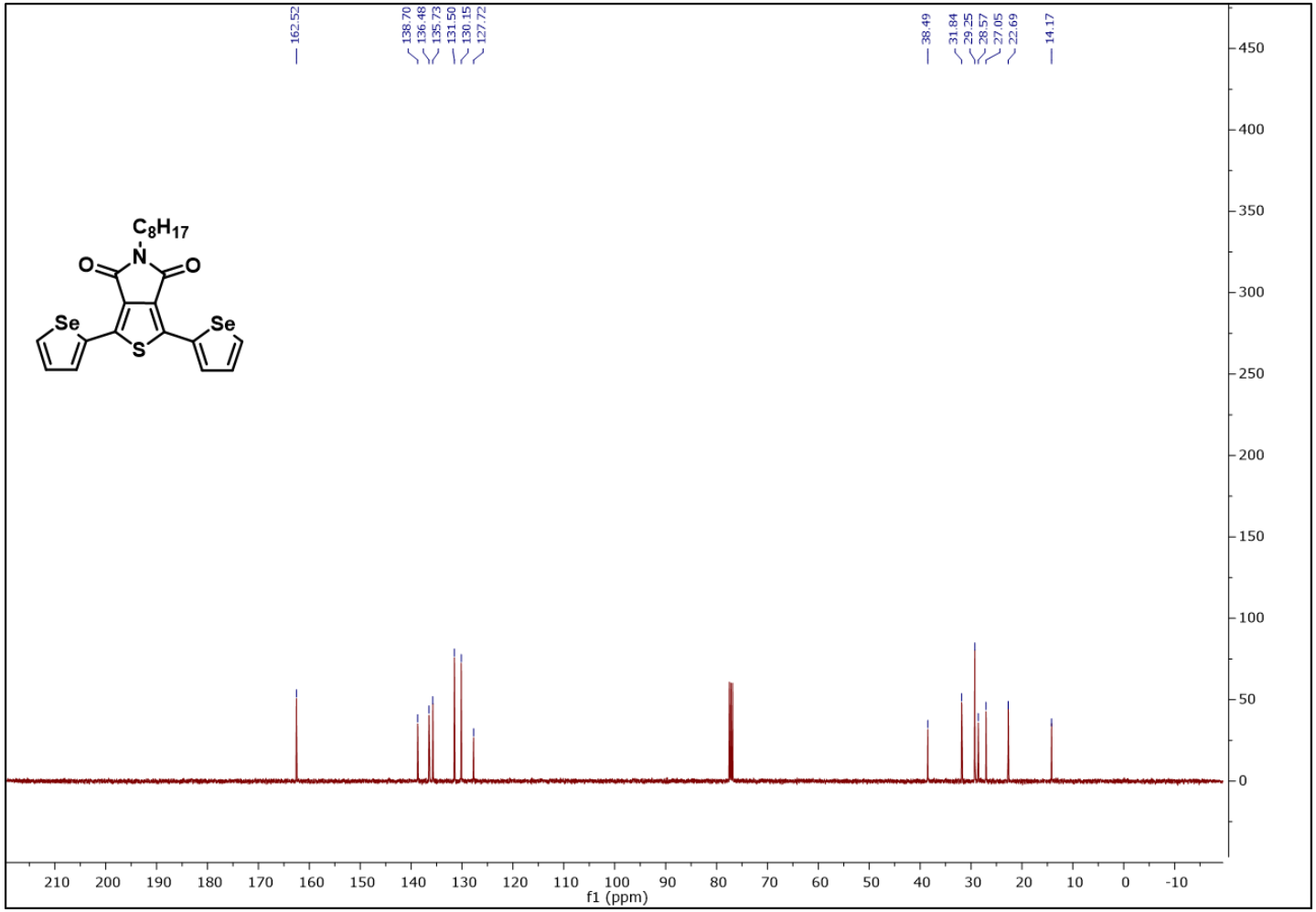

Figure A.23.2. ^{13}C-NMR spectrum of 5-octyl-1,3-di(selenophen-2-yl)-4H-thieno[3,4-c]pyrrole-4,6(5H)-dione

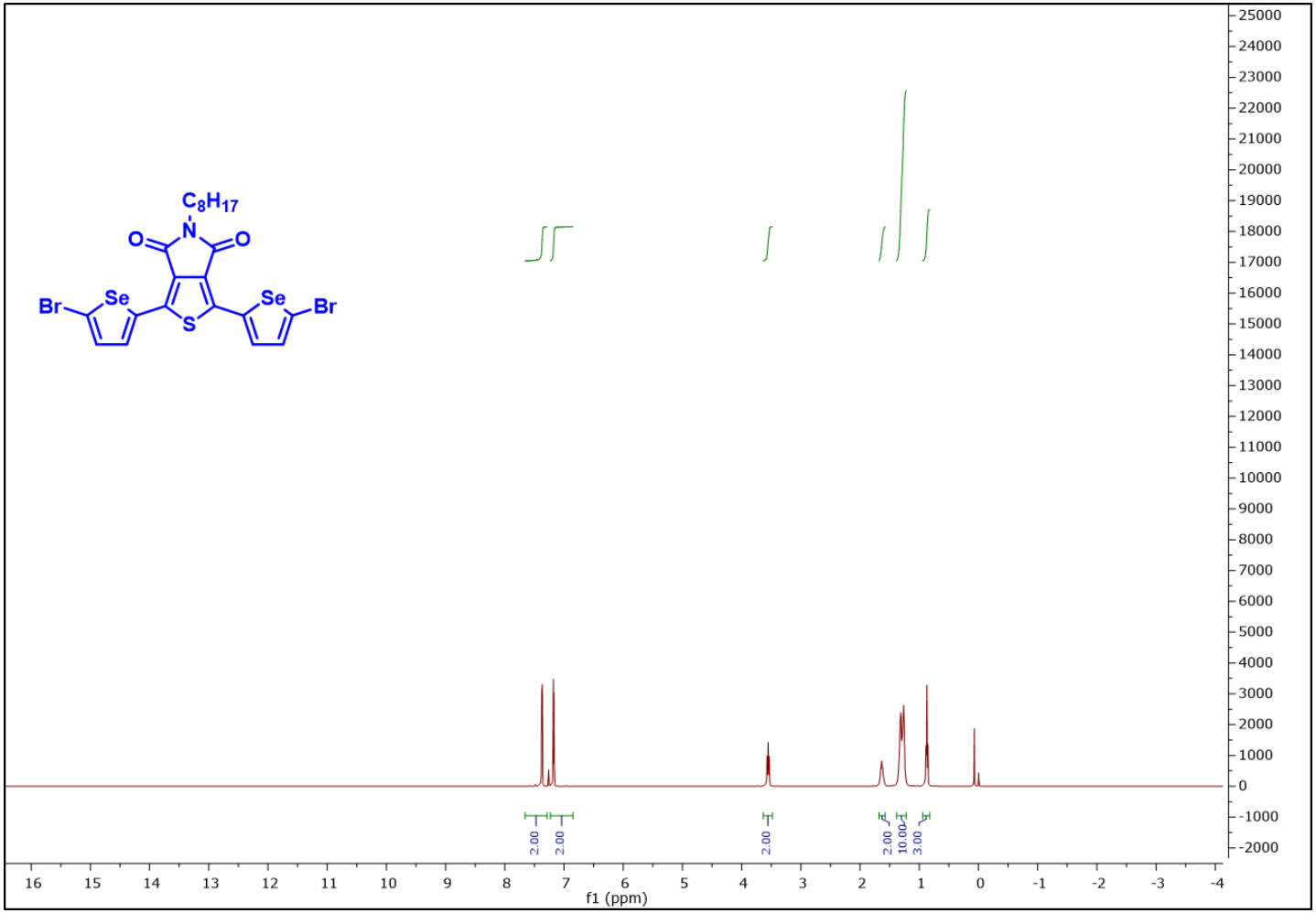

Figure A.24.1. ^{1}H-NMR spectrum of 1,3-bis(5-bromoselenophen-2-yl)-5-octyl-4H-thieno[3,4-c]pyrrole-4,6(5H)-dione

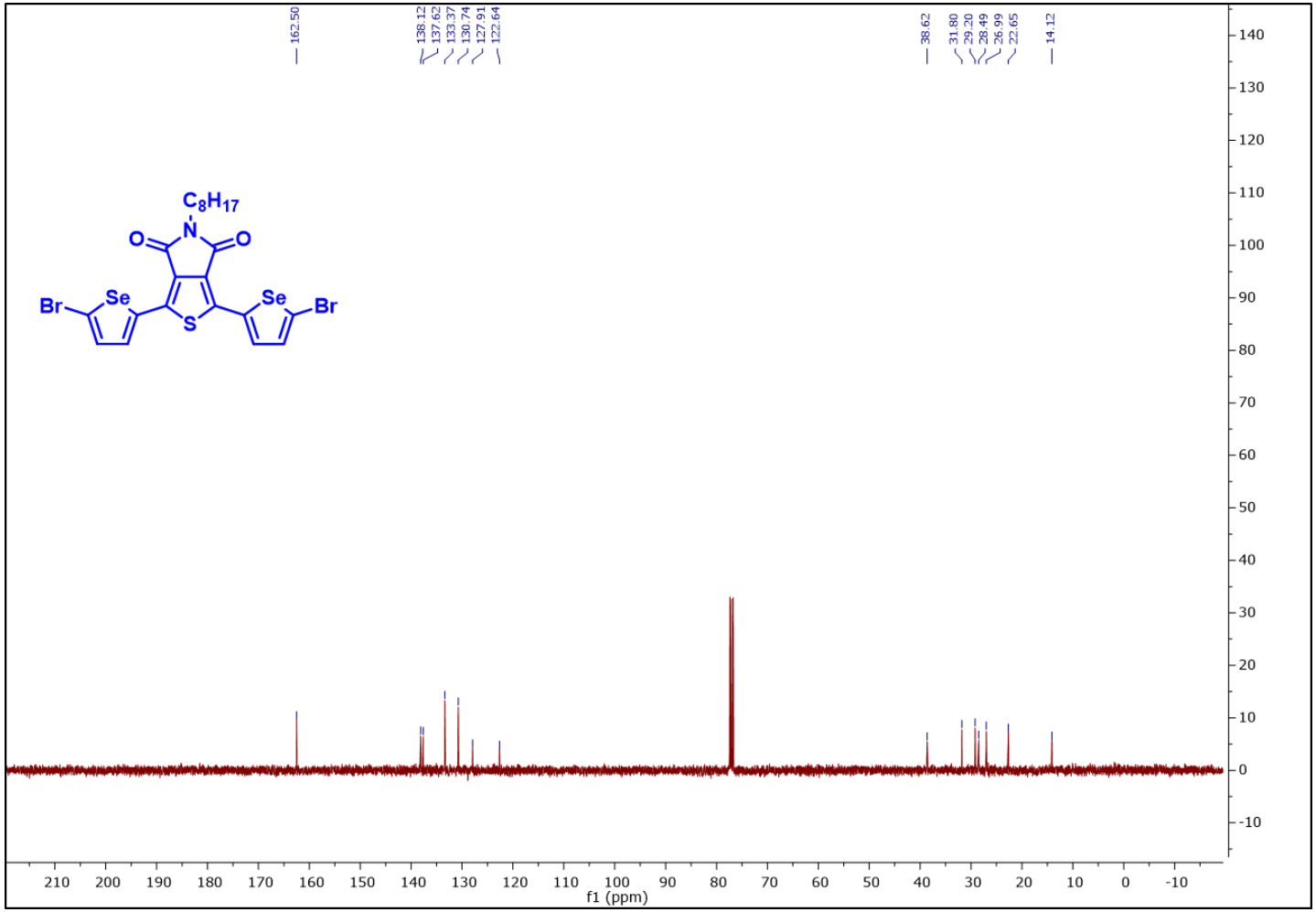

Figure A.24.2. ^{13}C-NMR spectrum of 1,3-bis(5-bromoselenophen**-2-yl)-5-octyl-4H-thieno[3,4-c]pyrrole-4,6(5H)-dione**

A. HRMS Results of Novel Molecules

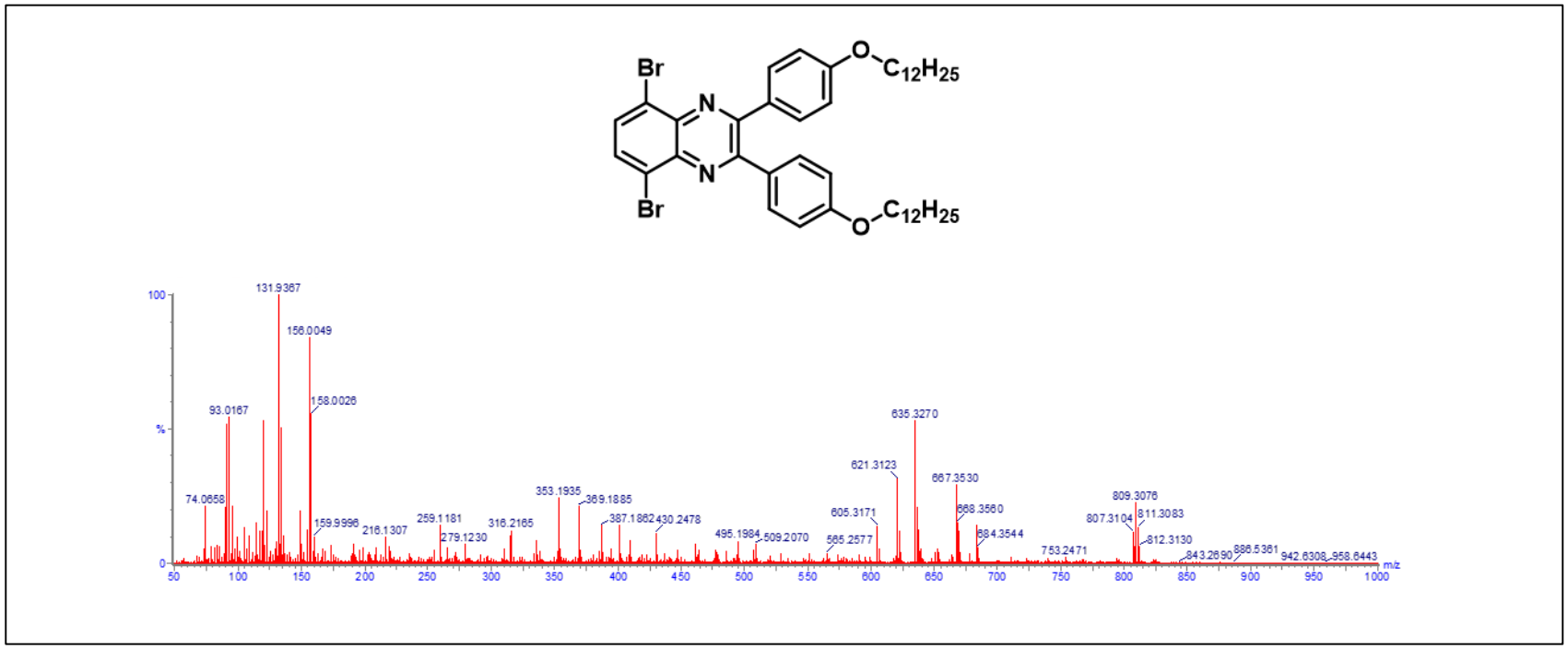

Figure B.1. HRMS data for 5,8-dibromo-2,3-bis(4-(dodecyloxy)phenyl)quinoxaline

Calculated for $C_{44}H_{60}Br_2N_2O_2$: 809.3079; Found: 809.3076

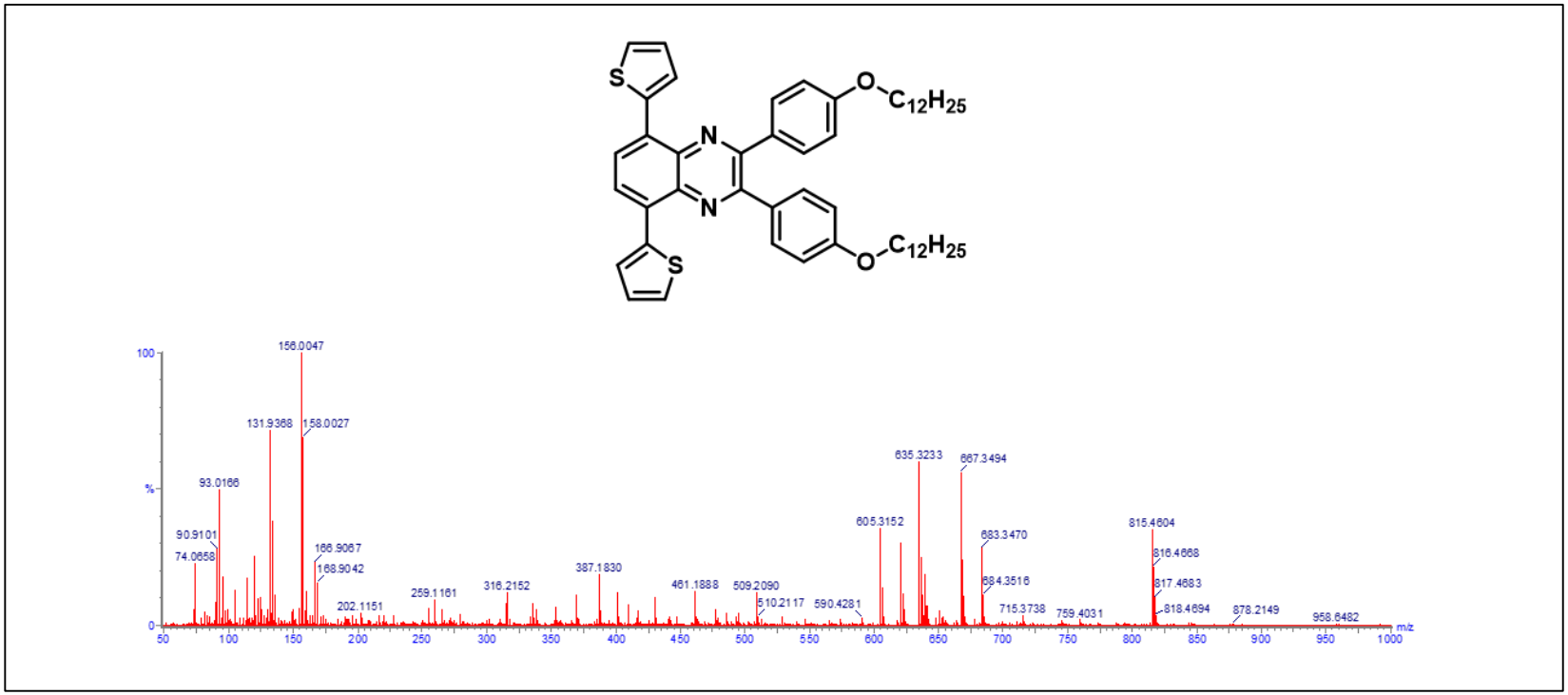

Figure B.2. HRMS data for 2,3-bis(4-(dodecyloxy)phenyl)-5,8-di(thiophen-2-yl)quinoxaline

Calculated for $C_{55}H_{66}N_2O_2S_2$: 815.4644; Found: 815.4604

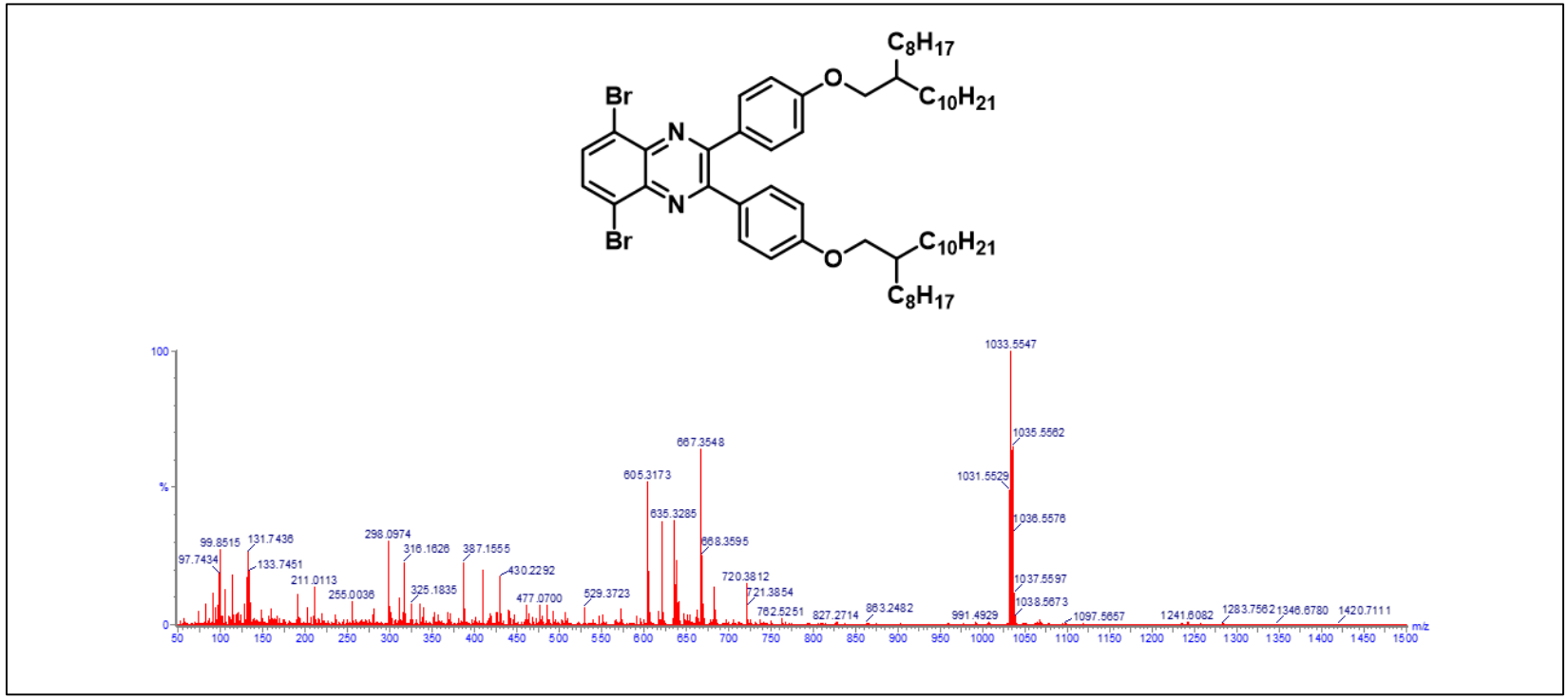

Figure B.3. HRMS data for 5,8-dibromo-2,3-bis(4-((2-octyldodecyl)oxy)phenyl)quinoxaline
Calculated for $C_{60}H_{92}Br_2N_2O_2$: 1033.5583; Found: 1033.5547

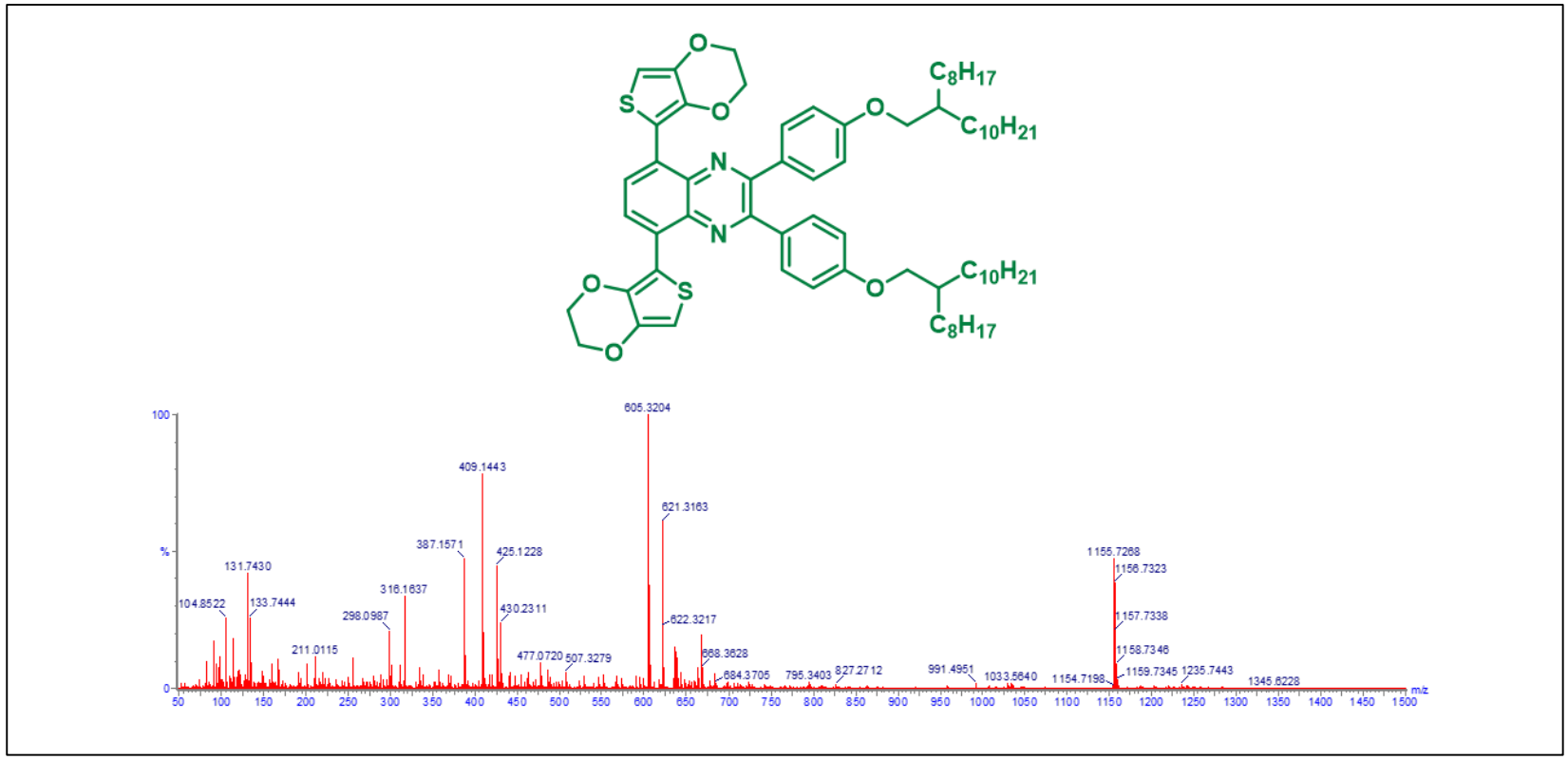

Figure B.4. HRMS data for 5,8-bis(2,3-dihydrothieno[3,4-b][1,4]dioxin-5-yl)-2,3-bis(4-((2-octyldodecyl)oxy)phenyl)quinoxaline

Calculated for $C_{72}H_{102}N_2O_6S_2$: 1155.7258; Found: 1155.7268

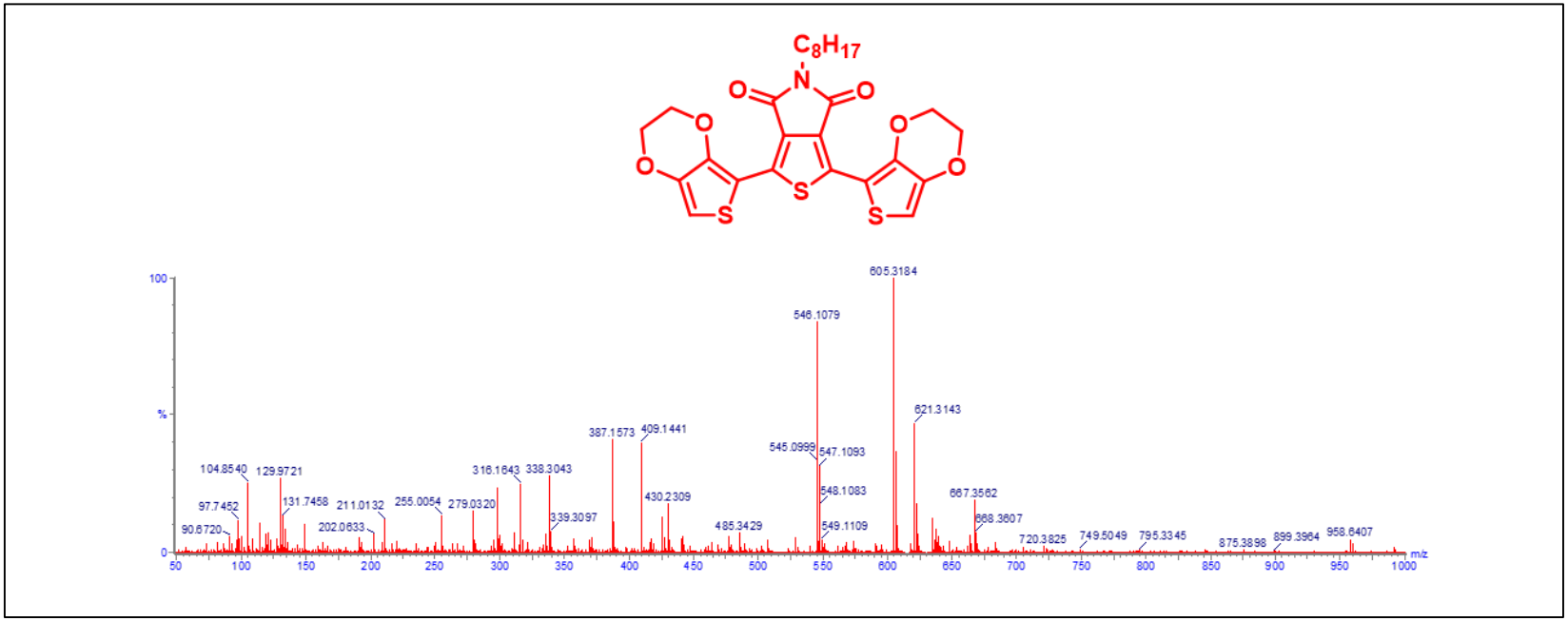

Figure B.5. HRMS data for 1,3-bis(2,3-dihydrothieno[3,4-b][1,4]dioxin-5-yl)-5-octyl-4H-thieno[3,4-c]pyrrole-4,6(5H)-dione

Calculated for $C_{26}H_{27}NO_6S_3$: 546.1079; Found: 546.1079

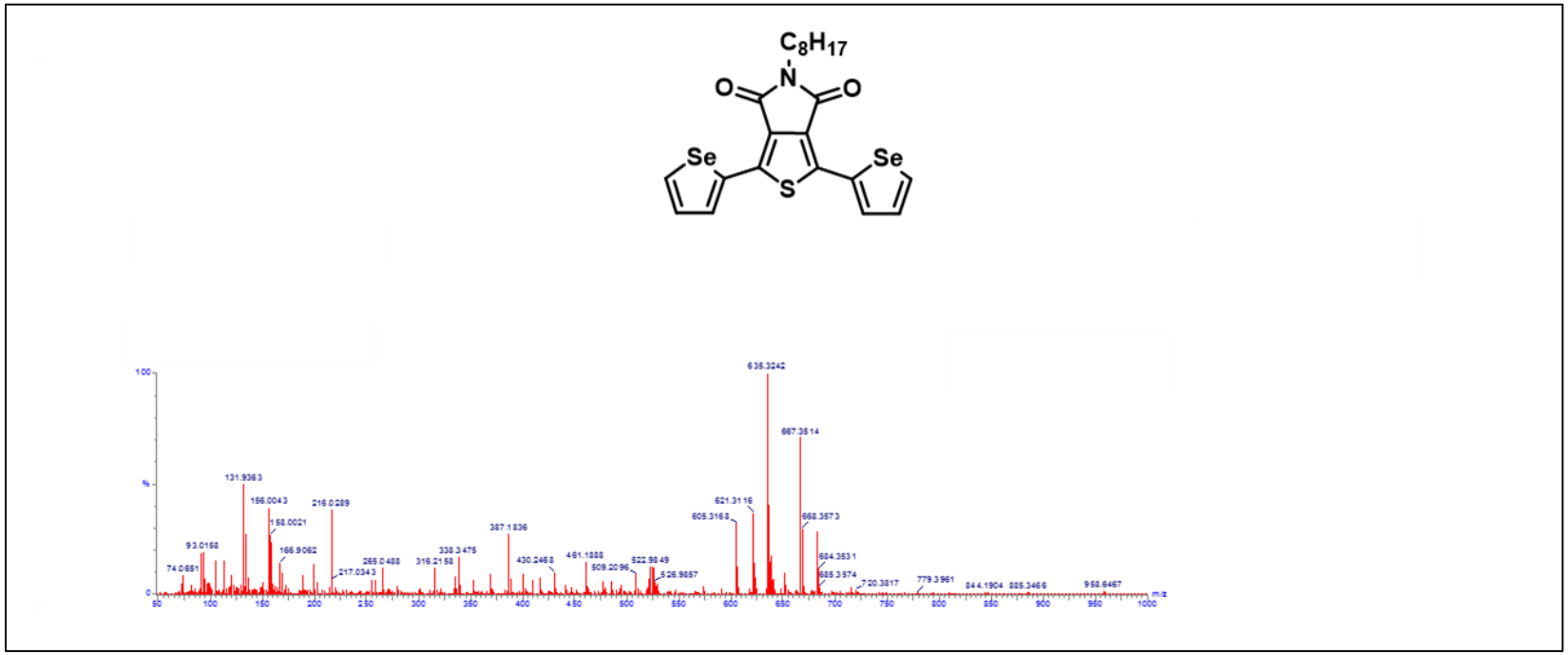

Figure B.6. HRMS data for 5-octyl-1,3-di(selenophen-2-yl)-4H-thieno[3,4-c]pyrrole-4,6(5H)-dione

Calculated for $C_{22}H_{23}NO_2SSe_2$: 524.9790; Found: 524.9835

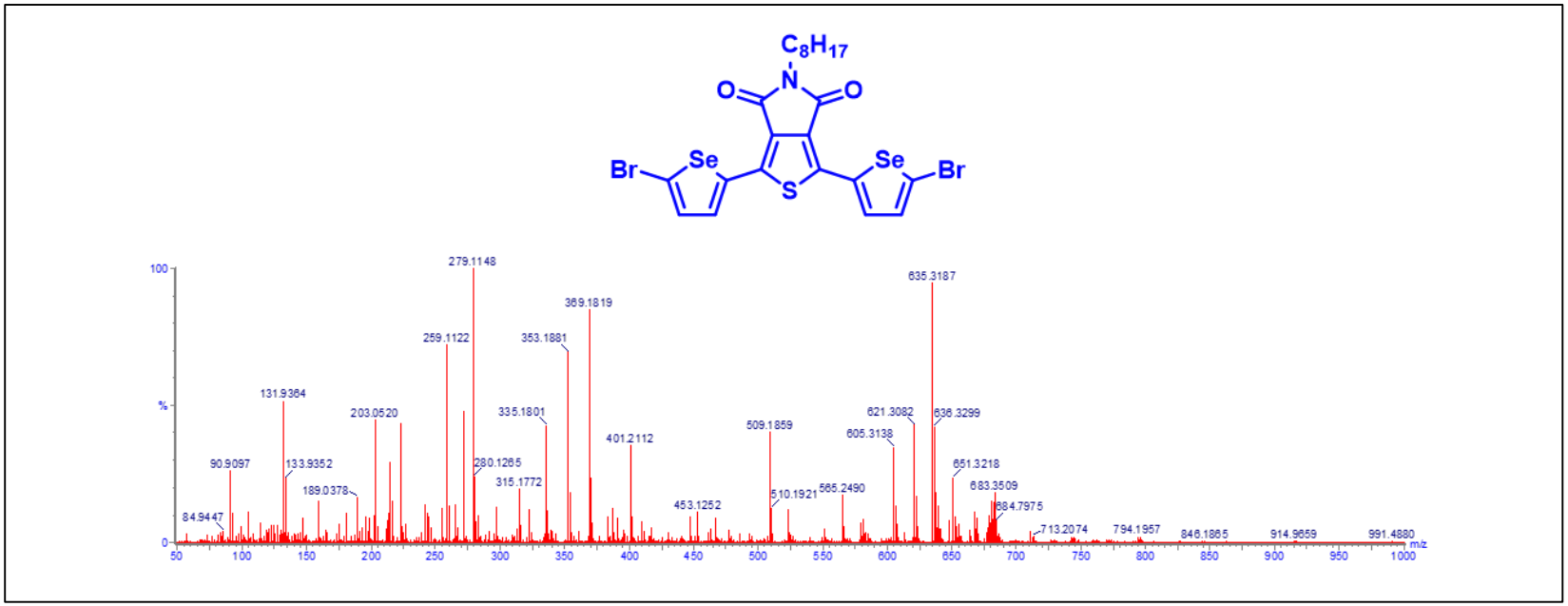

Figure B.7. HRMS data for 1,3-bis(5-bromoselenophen-2-yl)-5-octyl-4H-thieno[3,4-c]pyrrole-4,6(5H)-dione

Calculated for $C_{22}H_{21}NO_2SSe_2$: 682.7992; Found: 682.7977